UNIVERSITÉ DE GRENOBLE

THÈSE

Pour obtenir le grade de

DOCTEUR DE L'UNIVERSITÉ DE GRENOBLE

Spécialité : **Modèles, méthodes et algorithmes en biologie, santé et environnement**

Arrêté ministériel : 7 août 2006

Présentée par

« Mohammad Ali Nazari »

Thèse dirigée par **« Pascal Perrier »** et
codirigée par **« Yohan Payan »**

préparée au sein du **Laboratoire …GIPSA/DPC**
dans **l'École Doctorale …EDISCE**

Modélisation biomécanique du visage: Etude du contrôle des gestes oro-faciaux en production de la parole

Thèse soutenue publiquement le **« 30 Septembre 2011 »**,
devant le jury composé de :

M. Denis Favier
Professeur à l'Université Joseph Fourier (Président)

M. David Ostry
Professeur à McGill University (Rapporteur)

M. Patrick Chabrand
Professeur à l'Université de la Méditerranée (Rapporteur)

M. Rafael Laboissière
Chargé de Recherche au Centre de Recherche en Neurosciences de Lyon (Examinateur)

M. Yohan Payan
Directeur de Recherche au Laboratoire TIMC-IMAG (Codirecteur de Thèse)

M. Pascal Perrier
Professeur à Grenoble INP (Directeur de Thèse)

UNIVERSITÉ DE GRENOBLE

UNIVERSITÉ DE GRENOBLE

Biomechanical Face Modeling:

Control of Orofacial Gestures for Speech Production

By:

Mohammad Ali Nazari

A THESIS

SUBMITTED TO DOCTORAL SCHOOL EDISCE

IN PARTIAL FULFILMENT OF THE REQUIREMENTS

for

The Degree of Doctor of Philosophy (PhD)

GRENOBLE, FRANCE

September, 2011

The undersigned certify that they have read, and recommend to the Faculty of Graduate Studies for acceptance, a thesis entitled "**Biomechanical face modelling: Control of orofacial gestures for speech production** " submitted by **Mohammad Ali Nazari** in partial fulfilment of the requirements of the degree of **Doctor of Philosophy**.

President of Jury, Professor Denis Favier, Université Joseph Fourier

External Examiner and Reviewer, Professor David Ostry, McGill University

External Examinerand Reviewer, Professor Patrick Chabrand, Université de la Méditerranée

External Examiner, Dr. Rafael Laboissière, Centre de Recherche en Neurosciences de Lyon

Co-supervisor, Dr. Yohan Payan, Laboratoire TIMC-IMAG

Supervisor, Professor Pascal Perrier, Grenoble INP

Friday 30th of September, 2011

Date

Abstract

To address motor control issues in speech production a 3D finite element model of the face has been constructed. This model is made of a mesh that consists of hexahedral and wedge elements. The mesh has three distinctive layers and is symmetrical about the mid-sagittal plane. Face muscles are anatomically represented in the mesh as subsets of contiguous elements. The elements of the mesh have elastic properties described by an isotropic nearly incompressible hyperelastic constitutive law. In order to study the global effects of muscles on facial mimics and lips gestures, and more specifically on speech gestures like protrusion and rounding, a simple linear muscle model has been first designed. The impact on facial gestures of stiffness changes in soft tissues is studied. Stiffening in soft tissues is indeed concomitant with muscle activation due to stress stiffening effect. This effect is accounted for in the muscle model through a variation of the hyperelastic constitutive law. Special attention is also devoted to the production of protruded and rounded lips which are required for the production of rounded vowels particularly in French. It is shown that stiffening helps the achievement of an accurate protrusion/rounding gesture thanks to the existence of a saturation effect in the relation between the muscle activations and the acoustically relevant geometrical characteristics of the lips.

The result shows the importance of the dynamical properties of the articulators in the achievement of speech production gestures. Having been incited to improve the modeling of the main source of the force in speech movements, namely the muscles, a more realistic muscle model including a new constitutive law corresponding to a transversely isotropic nearly incompressible hyperelastic material and a Hill-type muscle model is designed in the ANSYS® finite element software thanks to the USERMAT programming facilities of this software. To account for a full Hill-type muscle model a force-velocity characteristic is then included in the new muscle element, thanks to the USERELEM facilities of ANSYS®. The implementation of this force-velocity characteristic introduces a damping effect on muscle movement due to a decrease of the muscle force when muscle compression velocity increases.

The designed structure of the muscle element is general enough to enable studying other muscle models. Hence, Feldman's muscle model, which has been extensively used in former modelling works at Gipsa-lab, is implemented. In a bid to integrate the Feldman's model in a finite element structure a distributed formulation of this model has been proposed. The Hill-type and the Feldman-type muscle element are included in the face model to replace the first simple linear muscle model. The first simulations of lips protrusion/rounding gesture show realistic results. A comparison of the results obtained with the Hill-type model with those obtained with the Feldman's model is also conducted which shows that the final face shapes are very similar to those of these two models.

Résumé

Un modèle tridimensionnel du visage a été élaboré, dans la perspective de contribuer à l'étude de questions importantes sur le contrôle moteur de la production de la parole. Ce modèle est construit sur un maillage constitué d'éléments hexahédraux et de clavettes, qui comporte 3 couches distinctes et est symétrique par rapport au plan medio-sagittal. Les muscles faciaux sont représentés dans le maillage par un sous-ensemble d'éléments contigus. Les propriétés élastiques des éléments du maillage sont décrites par une loi de comportement de type isotrope quasi incompressible et hyperélastique. Dans une première phase de ce travail, pour étudier les conséquences globales de l'activation des muscles oro-faciaux sur les mimiques faciales et les gestes labiaux, et plus particulièrement sur les gestes labiaux en parole, un modèle linéaire de muscle a été élaboré. L'influence des variations de la raideur des tissus mous sur les gestes faciaux a été étudiée. En effet, l'activation des muscles entraîne un raidissement des tissus mous musculaires concernés. Cet effet est pris en compte dans le modèle de muscle par un changement de la loi de comportement hyperélastique avec l'activation musculaire. Une attention particulière a été portée dans cette étude à la production du geste de protrusion/arrondissement des lèvres qui est un geste fondamental dans la production des voyelles arrondies, en particulier en Français. Nous montrons que le raidissement des tissus mous musculaires facilite la production précise de ce geste grâce à l'existence d'un effet de saturation dans la relation entre les activations musculaires et les paramètres géométriques des lèvres qui sont pertinents acoustiquement.

Ce résultat souligne l'importance des propriétés dynamiques des articulateurs dans la production des gestes de la parole, et il nous a incités à améliorer encore la modélisation de la source principale de force en production de la parole, c'est-à-dire les muscles. C'est pourquoi, un modèle de muscles plus réaliste a été élaboré qui se fonde sur une loi de comportement transversalement isotrope quasi incompressible et hyperélastique et sur un modèle de muscle de type Hill. Ce modèle a été implémenté dans le logiciel éléments finis ANSYS® grâce à sa fonction de programmation USERMAT. La prise en compte supplémentaire d'une loi caractéristique force-vitesse a permis la modélisation complète d'un modèle de muscle de type Hill. Ceci a été fait sous ANSYS® grâce à sa fonction de programmation USERELEM. Cette loi caractéristique force-vitesse introduit un effet d'amortissement dans le mouvement du muscle du fait d'une atténuation croissante de la force musculaire lorsque la vitesse de compression du muscle augmente.

Ce nouvel élément de type muscle a été conçu de manière telle qu'il est possible d'implémenter d'autres modèles de muscles que le modèle de type Hill. C'est pourquoi nous avons aussi implémenté le modèle de Feldman, qui a été utilisé de manière importante à Gipsa-lab dans les dernières années. L'intégration du modèle de Feldman dans une structure à éléments finis a nécessité une reformulation de façon à le rendre compatible avec une modélisation distribuée. Les modèles de Hill et de Feldman ont ensuite été incorporés dans le modèle de visage pour remplacer le modèle linéaire initial. Dans ces conditions les premières simulations du geste de protrusion/arrondissement labial ont donné des résultats réalistes. Finalement une comparaison des résultats obtenus avec le modèle de Hill avec ceux qui génère le modèle de Feldman montrent que les formes labiales finales sont très similaires pour les deux modèles.

Acknowledgement

First and foremost, I would like to extend my cordial gratitude to my supervisor, **Professor Pascal Perrier**, for accepting me as a PhD candidate and for his precious continued support during my PhD studies. His criticism and encouragement inspired me all along and showed me how to go through difficulties and leave the obstacles behind. He educated me with the state-of-the-art research methodologies. His insightful courses on speech analysis taught me the fundamentals of speech production and speech signal analysis while his immense knowledge of signal analysis and speech production showed me how to avoid the entanglements of this diverse yet complex domain. And above all, his extremely amicable character established a unique friendship between us which is the most valuable of all.

Furthermore, I would like to thank my co-supervisor, **Dr. Yohan Payan** whose invaluable support and his vast knowledge of both medical and engineering sciences greatly assisted me with my research and showed me how to find my way through the impediments. We worked along like two friends without the slightest feeling of the existing hierarchy.

I would also like to thank the reviewers **Professor David Ostry** and **Professor Patrick Chabrand** for reading and evaluating my work and offering their precious comments.

My special thanks further go the president of the jury, **Professor Denis Favier**, for accepting to read and evaluate my work. His scrupulous comments, especially on the objectivity concept, improved the mechanically oriented material of this work.

I would like to thank the member of the jury, **Dr. Rafael Laboisière**, for reading my work and evaluating it.

I, then, would like to thank **Dr. Matthieu Chabanas** for his invaluable assistance particularly during the first year of my dissertation. His profound knowledge of computer science and programming smoothed the progress of this research particularly the work on face modeling.

My sincere appreciation also goes to the president of the doctoral school, **Professor Jean-Luc Schwarz** for his kind encouragement since the very beginning of the project.

I would like to thank **Professor Abolfazl Masoumi**, the former president of Mechanical Engineering Department in University of Tehran, for his help and encouragement that prompted me to commence my PhD studies.

I would like to thank **Professor Mahmoud Kamarei**, the President of Pardis of Engineering Departments in the University of Tehran, for his precious support in providing a sabbatical period for the first year of my research.

I would like to express my appreciation to **Dr. Reiner Wilhelms-Tricario** for his priceless comments on chapters five and six. It was a great honor for me to see my work reviewed by him.

I would like to thank my dear friend; **Mohammad Ali DinMohammadi,** for his linguistic review of my thesis and the valuable comments he made on the English syntax of the text in spite of his tight schedule.

I would like to cordially thank the **Speech Department in GIPSA-Lab, DPC**, for accepting me extremely warmly and kindly amongst themselves. My very sincere thanks also go to the **Administration of GIPSA-Lab**, its former president, **Professor Jean-Marc Chassery**, its current President, **Professor Jean-Marc Thiriet**, and the secretary, **Madame Isabel Cieren**, for all their influential support and assistance.

I would also like to particularly thank **Professor Christian Jutten**, for all his priceless innumerable favors; he helped me find my supervisor; he took care of all the problems that an expat family might encounter in establishing life in a new environment. I am really grateful to him.
I would like to thank **Tarh-Negasht Company,** especially its directing manager, **Abdolhamid Hannaneh**, who is also my dear friend, for their financial support during my research.
I would like to thank **my mother** but I do not know how. She stood for me and because of her; I managed to find my way; how to live and how to behave.
I would like to thank **my brother, Javad**, who took care of my responsibilities back home such that I could have followed my studies without any worries.
I would like to thank **my father and mother in law** for their sincere support and dedication. In spite of all their own problems, they were more than kind to take the long way journey to France and took care of our son, so that my wife and I could work and progress without any difficulty.
Last but not least, I would like to sincerely thank my precious wife, **Ladan Amini**, for all the unmatched support, encouragement and devotion she displayed throughout this adventurous experience which got off the ground solely due to her whole-hearted assistance. Despite profound involvement in her own PhD studies, she never hesitated to give me relentless support throughout all stages of my research. **I owe this work to her.**

DEDICATION

In memory of *my father* "***Mohammad Hossein Nazari***",

I dedicate this work

To my mother "***Mahindokht Foroutani Yazdi***" for her loving support and unrivalled encouragement throughout my life,

To my wife "***Ladan Amini***" for her sincere love, without her wholehearted support this work wouldn't get started, and

To my beloved son "***Ali Nazari***" whose warm embrace gives me the strength to work and live.

Table of Contents

List of Tables

List of Figures and Illustrations

List of Symbols, Abbreviations and Nomenclature

Symbol	Definition[1]	Type	Dimension[2]
A	Muscle's current cross sectional area	Scalar	m^2
a	1- Acceleration 2- Unit vector along fiber direction in deformed configuration	Vector	1- m/sec^2 2- -
A	Acceleration gradient	2nd order tensor	$1/sec^2$
$\mathbf{a_0}$	Unit vector along fiber direction in undeformed configuration	Vector	-
A_c	Activation level in a muscle model	Scalar	-
A_{ofl}	Muscle's cross sectional area at the optimum fiber length	Scalar	m^2
A_{pcsa}	Physical cross sectional area of a muscle	Scalar	m^2
B	Left Cauchy-Green strain tensor	2nd order tensor	m^2/m^2
b	Body force per unit mass	Vector	N/kg
C	1- Right Cauchy-Green strain tensor 2- Damping Matrix	1- 2nd order tensor 2- Matrix	1-m^2/m^2 2-N.sec/m
$\mathbb{c}$	Truesdell material Jacobian	4th order tensor	Pa
$\mathbb{C}^{\nabla co}$	Green-Naghdi material Jacobian	4th order tensor	Pa
$\mathbb{C}^{\nabla J}$	Jaumann material Jacobian	4th order tensor	Pa
c_i $(i=0,1,2)$	Constants in the passive strain energy density for a transversely isotropic hyperelastic material	Scalar	Pa
$c_{ij}(i,j=0,1)$	Mooney-Rivlin's strain energy density constants	Scalar	Pa
c_j $(j=3,..6)$	Constants in passive force-length characteristic along fiber directions	Scalar	-
$\mathbb{C}^S$	Material Jacobian for second Piola-Kirchhoff stress rate	4th order tensor	Pa
$\mathbb{C}^S_{dev}$	Deviatoric part of $\mathbb{C}^S$	4th order tensor	Pa
$\mathbb{C}^S_{vol}$	Volumetric part of $\mathbb{C}^S$	4th order tensor	Pa
$\mathbf{C_{vir}}$	Virtual damping matrix in a Newton-Raphson iteration method due to velocity dependence of force in fiber direction	Matrix	N.sec/m
$\mathbb{C}^{\mathcal{L}}$	Lie material Jacobian	4th order tensor	Pa
d	1- Maximum ratio of muscle's tension to muscle's maximum voluntary force in eccentric action 2- Mooney-Rivlin's strain energy constant	Scalar	1- - 2- 1/Pa

[1] Some symbols have been used in different places with different meanings.
[2] Dimensions can come with common prefixes such as M (10^6) or m (10^{-3}) or k (10^3).

	corresponding to deformation gradient Jacobian		
$\mathbf{D}$	Symmetric stretching rate tensor	2nd order tensor	1/sec
$\mathbf{D_{co}}$	Corotated stretching rate tensor	2nd order tensor	1/sec
$\mathbf{E}$	Green strain tensor	2nd order tensor	m/m
E	Young's Modulus	Scalar	Pa
$\mathbf{e}$	Almansi strain tensor	2nd order tensor	m^2/m^2
F	Force exerted by or on the muscle	Scalar	N
$\mathbf{F}$	Deformation Gradient	2nd order tensor	m/m
f_{ac}	Activation dynamics	Scalar	-
f_{active}	The ratio of active force in muscle to maximum voluntary force	Scalar	N/N
$\mathbf{F}_{dev}$	Deviatoric or distortional part of deformation gradient	2nd order tensor	m/m
$\mathbf{F_e}$	Element deformation gradient	2nd order tensor	m/m
$\mathbf{f^{ext}}$	Global external force	Vector	N
$f_i\ (i=1,\ldots,5)$	Constants in force-velocity curve in Feldman's Muscle model	Scalar	-
$\mathbf{f_I^{ext}}$	External force at node I	Vector	N
$\mathbf{f_I^{int}}$	Internal force at node I	Vector	N
$\mathbf{f^{int}}$	Global internal force	Vector	N
F_L	Force-length characteristic function of muscle	Scalar	-
F_m	Total force in muscle fibers	Scalar	N
F_{max}	Maximum Voluntary Force (MVF) of a muscle	Scalar	N
$f_{passive}$	The ratio of active force in muscle to maximum voluntary force	Scalar	N/N
F_{PE}	Force in parallel elastic element in muscle model	Scalar	N
F_{SE}	Force in series elastic element in muscle model	Scalar	N
F_v	Force-velocity characteristic function	Scalar	-
$\mathbf{F}_{vol}$	Volumetric or dilatational part of deformation gradient	2nd order tensor	m/m
$\mathbf{H}$	Displacement gradient	2nd order tensor	m/m
$\mathbf{I}$	Identity second order tensor	2nd order tensor	-
I_1	1- First invariant of a second order tensor 2- First Invariant of the right or left Cauchy-Green strain tensor	Scalar	m^2/m^2
I_2	1- Second invariant of a second order tensor 2- Second Invariant of the right or left Cauchy-Green strain tensor	Scalar	m^4/m^4
I_3	1- Third invariant or determinant of a second order tensor 2- Third Invariant or determinant of the right or		m^6/m^6

	left Cauchy-Green strain tensor		
I_4	Fourth invariant (transversely isotropic material)	Scalar	m/m
I_5	Fifth invariant (transversely isotropic material)	Scalar	m^2/m^2
J	Determinant of deformation gradient	Scalar	-
$\mathbf{J_e}$	Jacobian of element in undeformed configuration with respect reference coordinates	2^{nd} order tensor	m/m
$\mathbf{j_e}$	Jacobian of element in deformed configuration with respect reference coordinates	2^{nd} order tensor	m/m
k	Muscle's constant in contraction part of force velocity curve	Scalar	-
$\mathbf{K}$	Stiffness Matrix	Matrix	N/m
K	The coefficient in volumetric part of strain energy density	Scalar	Pa
k_{ec}	Eccentric muscle constant in muscle's force-velocity curve	Scalar	-
$\mathbf{K^{geo}}$	Geometric stiffness matrix	Matrix	N/m
$\mathbf{K^{mat}}$	Material stiffness matrix	Matrix	N/m
$\mathbf{K_T}$	Tangent Stiffness matrix	Matrix	N/m
l	Length	Scalar	m
$\mathbf{L}$	Velocity gradient	2^{nd} order tensor	1/sec
l_0	Muscle's resting length	Scalar	m
l_c	Characteristic length in Feldman's muscle model	Scalar	m
$l_{threshold}$	Starting or threshold length in Feldman's muscle model	Scalar	m
m	Ratio of the slope in eccentric part of force-velocity curve to concentric part at zero velocity	Scalar	-
$\mathbf{M}$	Mass matrix	Matrix	Kg
$\mathbf{M_{vir}}$	Virtual inertia matrix in a Newton-Raphson iteration method due to acceleration dependence of force in fiber direction	Matrix	Kg
N_I	Shape function corresponding to node I	Scalar	-
$\mathbf{P}$	First Piola-Kirchhoff stress tensor	2^{nd} order tensor	Pa
$\mathbf{R}$	Rotation tensor	2^{nd} order tensor	-
$\mathbf{r}$	Position vector of a point inside an element in reference coordinates	Vector	m
$\mathbf{S}$	Second Piola-Kirchhoff stress tensor	2^{nd} order tensor	Pa
$\mathbf{S}_{dev}$	Deviatoric part of second Piola-Kirchhoff stress tensor	2nd order tensor	Pa
$\mathbf{S}_{vol}$	Volumetric part of second Piola-Kirchhoff stress tensor	2nd order tensor	Pa
$\mathbf{t}$	Traction force vector	Vector	Pa
t_d	Time delay	Scalar	sec

$\mathbf{U}$	Right stretch tensor	2nd order tensor	m/m
$\mathbf{u}$	Displacement vector	Vector	m
$\mathbf{u}^h$	Approximate displacement for body	Vector	m
$\mathbf{u}_I$	Displacement vector for node I	Vector	m
$\mathbf{u}^{i+1}{}_{n+1}$	Displacement at time $t+\Delta t$ in (i+1)th iteration in Newton-Raphson method	Vector	m
$\mathbf{u}^{i}{}_{n+1}$	Displacement at time $t+\Delta t$ in ith iteration in Newton-Raphson method	Vector	m
$\mathbf{u}_n$	Displacement at time t	Vector	m
$\mathbf{u}_{n+1}$	Displacement at time $t+\Delta t$	Vector	m
v	Velocity of a muscle along its fibers	Scalar	m/sec
$\mathbf{V}$	Left stretch tensor	2nd order tensor	m/m
$\mathbf{v}$	Velocity vector	Vector	m/sec
v_{max}	Maximum shortening velocity of muscle	Scalar	m/sec
W	Strain energy density	Scalar	Nm/m^3 (N/m^2=Pa)
$\mathbf{w}$	weight vector	Vector	-
$\mathbf{w_e}$	Weight vector of an element	Vector	-
$W_{passive}$	Strain energy density for passive tissues in muscle	Scalar	Nm/m^3
W_{vol}	Volumetric part of strain energy density for passive tissues	Scalar	Nm/m^3
$\mathbf{X}$	Position vector in undeformed configuration	2nd order tensor	m
$\mathbf{x}$	Position vector in deformed configuration	2nd order tensor	m
$\mathbf{x_{co}}$	Corotated position vector	2nd order tensor	m
$\mathbf{x}_e$	Position vector of a point inside an element in deformed position	Vector	m
$\mathbf{X_e}$	Position vector of a point in an element in undeformed configuration	Vector	m
$\mathbf{x}_I$	Position vector of node I	Vector	m
α	1- Thermal expansion coefficient 2- Rayleigh's damping mass matrix coefficient	Scalar	1- $1/^oC$ 2- 1/sec
β	Rayleigh's damping stiffness matrix coefficient	Scalar	Sec
β_i $(i=1,\ldots,4)$	Transversely Isotropic material invariants	Scalar	-
Δt	Time increment	Scalar	sec
$\Delta\mathbf{u}^{i+1}{}_{n+1}$	Increment in displacement at ith iteration in Newton-Raphson method	Vector	m
$\boldsymbol{\epsilon}$	Small deformation strain tensor	2nd order tensor	m/m
λ	Stretch along the muscle's fibers	Scalar	m/m
λ^*	Fiber stretch ratio at which the force-length characteristic become linear	Scalar	m/m
λ_{ofl}	Fiber stretch ratio at the optimum fiber length of muscle	Scalar	m/m
$\lambda_{threshold}$	Threshold stretch ratio of a muscle in Feldman's	Scalar	m/m

	muscle model		
μ	Damping coefficient	Scalar	Sec
v	Poisson's ratio	Scalar	-
ρ	Density in current or deformed configuration	Scalar	kg/m^3
ρ_0	Density at undeformed configuration	Scalar	$kg/m^{3=}$
$\boldsymbol{\sigma}$	Cauchy stress tensor	2^{nd} order tensor	Pa
$\boldsymbol{\sigma}^{\nabla co}$	Corotational or Green-Naghdi Cauchy stress rate	2^{nd} order tensor	Pa/sec
$\boldsymbol{\sigma}^{\nabla J}$	Jaumann rate of Cauchy stress tensor	2^{nd} order tensor	Pa/sec
σ_{active}	Active stress in muscle	Scalar	Pa
$\boldsymbol{\sigma}_{\mathbf{c}}$	Cauchy stress vector	Vector	Pa
$\boldsymbol{\sigma}_{\mathbf{co}}$	Corotated Cauchy stress tensor	2^{nd} order tensor	Pa
$\dot{\boldsymbol{\sigma}}_{\mathbf{co}}$	Corotated Cauchy stress rate	4^{th} order tensor	Pa/sec
σ_{max}	Maximum voluntary stress in muscle	Scalar	Pa
$\sigma_{passive}$	Passive stress in muscle	Scalar	Pa
$\boldsymbol{\tau}$	Kirchhoff stress tensor	2^{nd} order tensor	Pa
$\boldsymbol{\Omega}$	Spin tensor	2^{nd} order tensor	1/sec
$\boldsymbol{\omega}$	Skew tensor	2^{nd} order tensor	1/sec
Ω_0	Element volume in reference coordinates	Scalar	m^3
ω_e	Element volume in deformed configuration	Scalar	m^3
Ω_e	Element volume in undeformed configuration	Scalar	m^3
$\pounds_v(\ )$	Lie derivative	Operator	-

Chapter One: Introduction: Speech Production, Motor Control and Biomechanics

"A director makes only one movie in his life."
"Then he breaks it into pieces and makes it again."
Jean Renoir

1.1 General scientific context, goals and challenges

Human motor effectors, fingers, hands, arms, legs, eyes, the jaw or the tongue, have physical properties such as mass, inertia, damping factor, stiffness, elasticity or degrees of freedom, which determine their behaviours in response to external or internal stresses. These behaviours can be very different across motor effectors. Inertia is for instance very low for eyes and very significant for the legs; the tongue or the lips are highly deformable structures in which elastic characteristics are determining factors of movements, while arms, legs or jaw are rigid bodies articulated at joints that specify and limit their degrees of freedom. In the context of the study of motor control of human skilled movements, this statement raises the issue of the way the Central Nervous System takes into account these specific physical properties of the motor effectors, in order to achieve the intended movements, with the desired spatial accuracy and the desired timing. Two main classes of hypotheses exist in the literature to study this issue.

The first class of hypotheses, defended amongst others by Kawato et al. (1990), Shadmehr & Moussavi (2000), Hinder & Millner (2003) or Ahmed & Wolpert (2009), suggests that the brain stores a comprehensive description of the physical behaviours of the motor effectors in the so called "*internal models*". It is hypothesized that the Central Nervous System would use these models to compute *inverse dynamics*, and determine the time variation of the motor commands that are appropriate to a correct achievement of the motor goals with the required timing. This is done in the context of a so-called *feedforward* motor control scheme. In sum, according to this first class of hypotheses the time courses of movements are determined by a procedure that anticipates or predicts the consequences on movements of the physical properties of the motor effectors, in order to counteract them and to reach the motor goals in any case.

The second class of hypotheses, mainly defended by Feldman (1986), Gribble et al. (1998), or Perrier et al. (2003), suggests that only global representations of the physical system would be stored in the brain. These representations would be used by the Central Nervous System to determine a global setting of the motor commands as for example the co-contraction level, in order to deal with timing and accuracy constraints. However, these representations would be not accurate and comprehensive enough to allow any inverse dynamics procedure. Thus, the actual movements would be the results of a combination of influences, namely the one of the centrally specified motor commands and the one of the physical properties of the motor effectors. In this context, the variability of the physical characteristics of motor effectors would result in an equivalent variability of movement patterns.

The aim of this thesis is not to provide direct support to any of these hypotheses in the context of speech motor control rather to elaborate a sophisticated biomechanical model of the face, in order to provide a thorough full and realistic account of the physical characteristics of the orofacial region. This should allow evaluating very precisely and quantitatively to which extent these physical properties are likely to significantly influence movements. In the line of the works of Payan & Perrier (1997), Gerard

et al. (2006) and Buchaillard et al. (2009), this work is an additional step toward the elaboration of a powerful modeling context that will enable quantitative testing all these different hypotheses, by confronting simulated and experimental movements.
This approach is in line with the one of Gribble, Ostry and colleagues (Gribble & Ostry, 1996, Gribble et al. 1998), who used biomechanical models to evaluate basic hypotheses about motor control. In their controversy with Gomi & Kawato (1996) about the complexity of the control signals in human arm movements, Gribble et al (1998) suggested that the differences between their own results (i.e. control signals are simple) and those of Gomi & Kawato (1998) (i.e. control signals are complex in shape) would "*arise from their* (Gomi & Kawato's) *use of a simplified model of force-generation*" (p. 1413). This example illustrates well the central challenge of the present work, namely achieving a high degree of accuracy and realism in the description of face biomechanics in the model, in order to ensure the validity and the generality of the conclusions of future works that will be carried out with this model. Since face is mainly made of soft tissues and muscles, soft tissues properties, muscle force generation mechanisms and their influence on muscle tissues mechanics are at the core of the present work. If it is considered that leaving human soft tissues have a negligible plasticity and are nearly incompressible, their mechanical behavior is described by the relation between stress and strain, also called "*constitutive law*". The derivative of the stress with respect to strain is the "*Young Modulus*", which described the sensitivity of the tissue's size to local variations of stress in the direction of the applied force. It is an expression of the common concept of stiffness. Muscle activation generates an increase of the stiffness of muscles soft tissues in the directions orthogonal to the muscle fibers direction. This phenomenon is known as the "stress-stiffening" effect. Its amplitude increases with the so-called *co-activation* of antagonist muscle pairs. Stiffness is classically considered as an important parameter in motor control studies, and from different perspectives (see below section 1.2). However, the "stress-stiffening" effect is generally ignored in these studies that are mainly concerned by articulated rigid motor effectors. Hence, a significant part of the present work has been devoted to the study of the potential impact of this biomechanical effect on oro-facial gestures and more specifically on gestures underlying speech production. This has been done first with a muscle model in which stress-stiffening effect is accounted for in a functional manner and isotropically, in the continuity of the proposals made for the tongue by Gerard et al (2006) and Buchaillard et al (2009). In a second stage, a more sophisticated model has been elaborated that models physically the muscle generation mechanisms in transversally isotropic tissues, in which the muscle fiber direction has a specific status. In this model stress-stiffening effect arises naturally from muscle mechanics when muscle is activated. Rationales for these two main achievements of the present work are summarized below in sections 1.2 and 1.3

1.2 Stiffness: biomechanical and motor control perspectives

Stiffness properties of the human motor system depend on various physiological influences, such as passive elastic properties of muscle tissues, muscle activations, and neural feedback (McMahon, 1984). Thus muscle activations in motor systems not only induce changes in position but also changes in stiffness. Stiffness changes and position changes intrinsically co-occur as the consequences of muscle activation, but to a certain extent they can also be controlled separately. Evidence supporting the hypothesis of these separate controls has been well documented in different studies that have shown the existence of (1) isometric motor tasks (change in muscle activations and stiffening, but no

change in position), (2) isotonic motor tasks (change in position and in individual muscle activations, but without change in global muscle activation), and (3) unconstrained motor tasks (change in position and in muscle activations and stiffening) (see for example Feldman, 1986, for an account of these separate controls in the context of the Equilibrium Point Hypothesis). According to the literature, a specific control of stiffness is useful in motor control mainly for two reasons: increasing stiffness has an impact on movement speed and duration, and it is an efficient way to control movement accuracy, especially in the context of external perturbations.

A number of experimental (Bennett, 1993; Suzuki et al., 2001) and modelling studies (Gribble & Ostry, 1998; Perrier et al., 1996) of speech production have shown that high stiffness levels of the motor system are associated with rapid movements. Controlling the stiffness of the motor system allows the global movement duration for a given movement amplitude to be influenced. In a pure dynamical representation of motor systems (Kelso, 1995) the motor system is represented as sets of coupled oscillators. In the framework of coupled oscillators it has been proposed that modulating stiffness would be the means to control time, in the form of individual movement durations as well as of interlimb (or, for speech, interarticulator) time coordination (phasing) (Kelso et al., 1981; Kelso, 1995, p.104-106; for speech production see also Saltzman, 1986). For speech research this proposal is grounded in the intrinsic speech timing theory proposed by Fowler (1980) (but see Fuchs et al., 2011).

So far, the majority of recent studies on stiffness control in movement production are related to the question of movement accuracy control. It has been shown that, for postural control, increasing the co-activation of agonist and antagonist muscles would minimize the consequences of perturbing external loads by increasing joint stiffness (see for example Milner & Cloutier, 1998, and Milner, 2002 for the wrist joint). Similar findings have been obtained for movement control in perturbed conditions. For example, Burdet et al. (2001) observed that, in a motor task where the subjects had to follow with their arm a straight line connecting two targets, the subjects adapted to an unstable velocity-dependent perturbing force field imposed by a robot by increasing the stiffness of their arm in the direction of a perturbing field. However, as suggested by Milner (2002), increasing the stiffness is “metabolically costly” (p. 406). Hence, it can be expected that under normal movement execution, i.e. in the absence of a perturbing field, subjects could favour alternative and less costly motor strategies to ensure accuracy. Milner & Franklin (2005) indeed found that, in the presence of a perturbing force field, subjects would increase stiffness only during the first trial. According to these authors, for the other trials, other strategies were elaborated based on the acquisition of a crude internal model of the dynamics in the perturbed conditions. Assuming the acquisition and the use of internal dynamical representations, similar results were observed by Davidson & Wolpert (2003) for subjects performing a single task in a predictably varying environment. A number of studies confirm, though, that even under normal, unperturbed conditions, stiffness is used to control accuracy. Studying jaw movements in speech production with respect to relations between positioning accuracy and stiffness ellipses, Shiller et al. (2002) found that accuracy is better in the direction of the major axes of the ellipses, i.e. movements are more precise in the directions along which stiffness is larger. Osu et al. (2004) observed that in tasks where subjects were asked to reach targets of different sizes, they stiffened their arm when the targets were small. These authors also noticed that movements intentionally produced with increased co-contraction were more accurate. Similarly, Wong et al. (2009) measured the variation in limb stiffness when subjects were asked to move their arm from a start target to an end target, in the absence of any perturbing external force field, with various requirements in terms of end

target accuracy. The authors observed that stiffness increased when the size of the end target decreased.

Hence, the relation between stiffness of the limb, the jaw or the arm and movement accuracy seems to be well established. However, all motor effectors studied so far are rigid bodies articulated at joints. Stiffening these effectors actually means stiffening the joints, by increasing the forces of the agonist-antagonist sets of muscles (a coordinated muscle activation also called *co-activation*) around these joints. In the case of speech production, the articulators that are responsible for the fine shaping of the vocal tract, which determines the properties of the acoustic signals, are soft bodies such as the tongue, lips, and velum. The impact of stiffening on soft bodies is likely to be quite different from that observed for rigid bodies. Indeed, stiffening a joint changes the stability of the motor system around this joint, without modifying in any way the range of the configurations that are likely to be achieved by the motor system. In the case of rigid bodies a change in stiffness modifies the dynamical characteristics of the task space, but it does not alter the shape or the size of the task space. For soft bodies, the situation is different because different stiffness values may affect the required shape of motor system. Consequently, it can be expected that controlling stiffness could be used in speech movements for other purposes than in limb or arm movements.

There is only one study on the role of stiffening in the control of soft body motor systems which was proposed by Hooper (2006) and concerns the octopus. Hooper (2006) explains the observation that octopuses stiffen their tentacles when they grasp at food by the fact that this strategy allows a reduction in the number of degrees of freedom of the tentacle. This reduction simplifies the selection of the motor commands that enable a precise achievement of a particular gesture. However, to our knowledge, there has so far been no study on the role of stiffening in soft body motor control for humans.

1.3 Biomechanical face model: modelling issues and goals

Numerous biomechanical models of the face have been developed in the last 10-15 years. Many of them were developed in the framework of computer graphics facial animation (Lee et al. 1995; Sifakis et al. 2005) or computer aided surgery (Chabanas et al. 2003; Gladilin et al. 2004; Beldie et al. 2010), but only a few were used in studies about speech production and speech perception (Lucero and Munhall 1999; Piterman & Munhall, Gomi et al. 2006).

The pioneer work of Lee et al. (1995) has made popular a discrete modelling framework, with sparse mass-spring entities regularly assembled inside facial tissues. This approach allows fast computations with a simple algorithmic implementation. However, in addition to the lack of accuracy of such models and to their numerical instabilities, it seems to be very difficult to set their elastic parameters (the stiffness of springs) in order to fit the constitutive law that is observed and measured on living tissues. Recently Kim & Gomi (2007) have improved Gomi et al.'s (2006) discrete model by implementing a so-called "continuum compatible" mass-spring model with stiffness parameters that can be adjusted in order to follow a simple linear continuum constitutive law. Although this model is interesting in computational terms, especially for dynamic simulations, it is limited to correctly reproduce the behaviour of highly non-linear material such as facial tissues (Fung 1993; Gerard et al. 2005).

In continuity with the works of Chabanas et al. (2003) the finite element framework is used here to model the continuous tissues of the human face. Although computationally less efficient than the discrete modelling framework, it enables in particular the use of non linear mechanical modelling such as hyperelastic laws to better approximate the tissues behaviour (Fung 1993).
The total force generated in a muscle is the sum of two components: an active one (F_{ac}) and a passive one (F_{pc}). Due to α-motoneurons depolarization, muscle fibres generate force, which in turn causes change in muscle length. The force generated through the actin-myosin cross-bridges is the active component of muscle force. According to this basic model a contractile element generates force as a function of muscle length (F versus L curve) and its velocity (F versus V curve). These curves are assumed to be scaled up or down as a function of the level of activation (Zajac 1989). Due to their stiffness the surrounding tissues will resist to the active component thus defining a passive component of muscle force. In real muscles this passive component is not isotropic since the mechanical properties in the direction of muscle collagen fibres are different from the embedding matrix (McMahon 1984). Hence, the passive material behaviour should ideally be modelled with a transversely isotropic material (Humphrey and Yin 1989; Weiss et al. 1996). As mentioned in section 1.1, our approach consisted in two stages: in the first one, to limit the complexity of the modelling approach, we did not consider this transversally isotropic characteristic, and worked with a face model made of isotropic elements. In the second stage, after a first evaluation that has demonstrated the potential impact of muscle stiffening on facial shaping and speech production gestures, a detailed and physically advanced modelling work was initiated, that aimed at accounting as realistically as possible for muscle forces generation mechanisms and their associated muscle tissues stiffening.
Some authors working with finite element modelling have implemented muscle force generation mechanisms by designing new elements which include both active stress stiffening effect and passive transversal isotropy (see among others Wilhelms-Tricario 1995; Johansson et al., 2000;Yucesoy et al. 2002; Blemker et al. 2005;Martins et al., 2006; Rohrle and Pullan, 2007; Tang et al., 2009). These elements need to be oriented along the axis orthogonal to the direction of isotropy (Ng-Thow-Hing and Fiume 2002) in order to define fibre and cross fibre directions. These elements also should obviously be distinguished from the surrounding tissues (Teran et al. 2005). This method has been implemented by Sifakis et al. (2006) for modelling face muscles and speech behaviours quasi-statically.
In order to increase the realism of model we have developed a transversely isotropic constitutive law together with muscle activation function via a user-defined element in finite element. This work has required a long mathematical study that is based on advanced mathematical formulations of soft tissue mechanics. This element has been included in the face model, to replace the functional model used in the first stage of the work. This provides more realism to the model for further assessments of motor control hypotheses in the context of orofacial gestures. In addition this muscle element can be in the future integrated in finite elements models of other soft tissues articulators such as tongue, velum or pharyngeal constrictors.

1.4 Structure of the manuscript

This manuscript can be divided in three parts. In the first part (chapters 2 and 3) states of the art are presented that served as foundations for the whole work. . In the second part (chapter 4) a study of the impact of stiffening of lips gestures is presented. It is based on the use of the first face model, which

integrates the functional modelling of muscle force generation mechanisms and stress-stiffening. In the last part (chapters 5 and 6) mathematical formulations of the new muscle element are presented and a first evaluation is proposed in the context of the face model. Some of the new horizons that this new implementation provides are also presented.

1.4.1 First part

Muscles in face are interwoven and their tracks are complex and object specific. A short study of orofacial muscles anatomy and their innervating nerves is presented in chapter 2.
Muscles are main driving elements of face model hence a good understanding of muscle behaviour is essential. A literature survey regarding muscle mechanics are presented in chapter 3. In this chapter macroscopic muscle models are revisited. Two types of muscle models are more specifically studied which are at the core of important debates in motor control studies: Hill-type models (Hill, 1938; Siebert et al, 2008), also called adjustable stiffness models, and Feldman's like model (Feldman, 1986; Gribble et al., 1998), also called adjustable starting length models. These models differ basically in the way motor control parameters are defined and influence muscle force. The chapter is closed with an original mathematical reformulation of Feldman's model which is suitable for finite element modelling.

1.4.2 Second part

A simple version of an adjustable starting length model (sliding spring model) is used to produce orofacial gesture. The implementation of this model is presented in chapter 4. The stress-stiffening effect due to activation is presented in this chapter. The effect of this muscle modeling and its consequence on face model regarding speech production and motor control studies conclude this part.

1.4.3 Third part

This third part deals with the description of the new muscle model that account physically for muscle force generation mechanisms and stress-stiffening. It accounts precisely for the complexity of the Due to fiber-like structure of muscle a transversely isotropic incompressible hyperelastic constitutive law can model the behaviour of the passive property of the muscle. This constitutive law also should include the force generating mechanism of the muscle (active force). The mathematics required to implement this model in a finite element model are presented. A quantitative comparison between a Hill-type muscle models and Feldman muscle model in producing voluntary movements of face model are presented in the last part of chapter 6.

Chapter Two: Anatomical review of orofacial muscles

"I'm not ugly, but my beauty is a total creation."
Georg Wilhelm Friedrich Hegel

In this chapter a summary of the orofacial muscles' anatomy is presented with a focus on characteristics that are related to speech production. After a general introduction, twelve different orofacial muscles are classified into five functional groups considering their effects on oral fissure. Then each group is discussed functionally. Two special muscles that have an indirect effect on oral fissure shaping are then introduced. Finally this chapter ends with a short discussion of fiber types of orofacial muscles and their innervations.

2.1 Orofacial Muscles: Generalities

Orofacial muscles are those face muscles that are located around the lips to produce different shapes of mouth opening. Their main role is to produce the shape and movements necessary for speech and for the emotional expressions like sadness and happiness. Fibers of these muscles are interdigitated and interwoven with each other in conjunction points (*modioli*). At these points the muscles cannot be distinguished from one another. It means that they together behave like a tent-like network around the mouth orifice. This network is attached to the skull at some points. This network is embedded in two layers of face, namely the *dermis* (middle layer) and the *hypodermis* (the inner layer). The outer layer of the face, the *epidermis*, covers that sandwiched structure. This tent-like structure can behave in stretch only but because of contacts with the teeth and jaws, the muscles can generate complex lip shapes such as protrusion and rounding. Ivancevic & Ivancevic (2006) adhere to this idea and consider this structure as a 2D Riemannian manifold which is driven by internal muscles.
There are 24 orofacial muscles appearing symmetrically with respect to the sagittal plane (Figure 2.1). These muscles are: 1- Levator Labii Superioris Alaeque Nasi (LLSAN) 2- Levator Labii Superioris (LLS) 3- Levator Anguli Oris (LAO) 4- Zygomaticus Minor (ZYG_MIN) 5- Zygomaticus Major (ZYG_MAJ) 6- Risorius (RIS) 7- Buccinator (BUC) 8- Depressor Anguli Oris (DAO) 9- Depressor Labii Inferioris (DLI) 10- Mentalis (MENT) 11- Orbicularis Oris Peripheralis (OOP) 12- Orbicularis Oris Marginalis (OOM). Each orbicularis oris muscle is composed of two upper and lower parts which are called superioris and inferioris, respectively. Muscle attachments on the skull are shown in Figure 2.2. Innervation of these muscles is done through the facial part of cranial nerves. The motor branches of facial nerves are shown in Figure 2.3. A summary of both end attachment points of these muscles is presented in Table 2.1. Interindividual variability of these muscles can be significantly reduced with spatial normalization of their positions with respect to individual and average facial dimensions (Lapatki et al., 2006).
These orofacial muscles can be categorized functionally in five different groups:

1- Upper lip levators: LLSAN, LLS,ZYG_MIN
2- Mouth angle (lip corner) mobilizers: in upward direction by LAO, upward and laterally by ZYG_MAJ, laterally by RIS and downward by DAO
3- Lower lip mobilizers: in upward direction by MENT and downward by DLI

4- Oral fissure constrictors: OOP and OOM
5- Specific muscle: BUC

In the following each muscle group is explained.

2.2 Upper Lip Levators

This group of muscles elevates the upper lip and controls the shape of the nasolabial furrow. This shaping mostly happens in facial expressions like sadness, happiness or mockery. Zygomaticus minor is not common in all people (Pessa et al., 1998b).

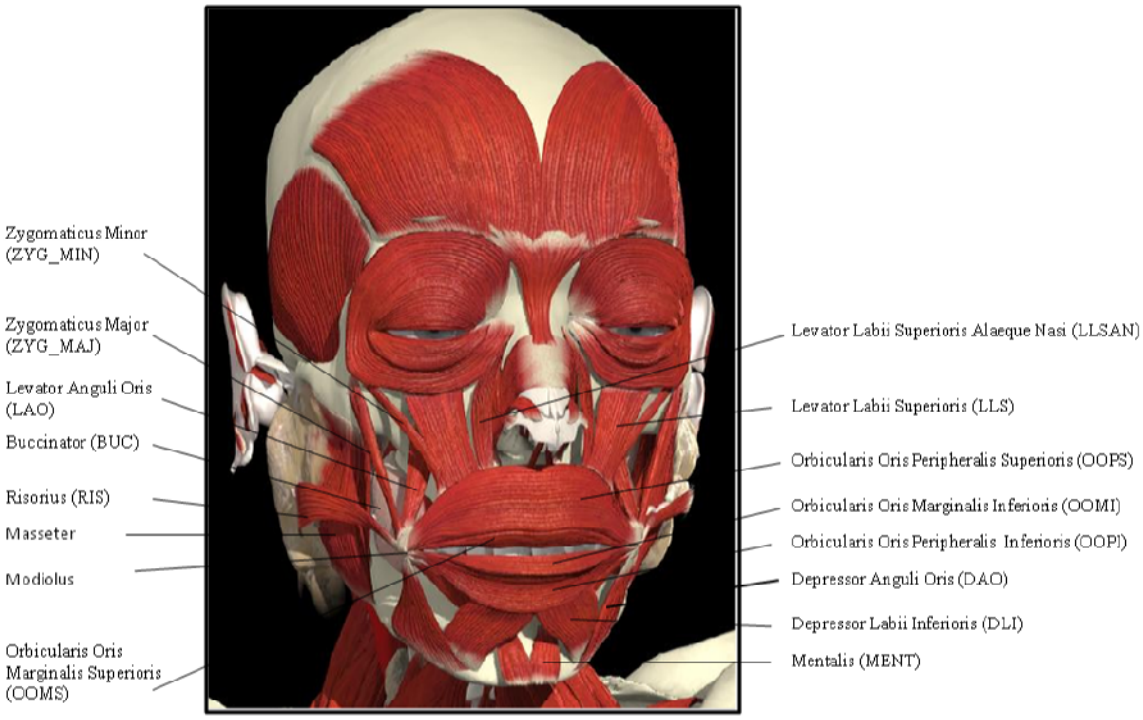

Figure 2.1 Orofacial muscles of the face (original picture taken from www.anatomy.tv)

2.3 Mouth Angle Mobilizers

These muscles move lip corner in different directions. Zygomaticus major moves the lip corner upwards and laterally. This muscle has two morphologies: single or double (bifid) type (Pessa et al. 1998a). The bifid zygomaticus is more common in females. This muscle is responsible for cheek dimples. It plays an important role in smiling and laughing. This action can be augmented by levator anguli oris and risorius muscles. Risorius muscle is also used in grinning action. This muscle is not well developed in all people (Pessa et al. 1998b). Depressor anguli oris muscle moves the mouth corner downward in actions like mockery and contempt.

2.4 Lower Lip Mobilizers

Depressor labii inferioris muscle moves the lower lip downwards as for instance in irony speaking. Mentalis helps upward motion of lower lip in lips protrusion initiated by orbicularis oris muscles. This upward motion also helps in the act of drinking and while expressing doubt (Standring, 2005).

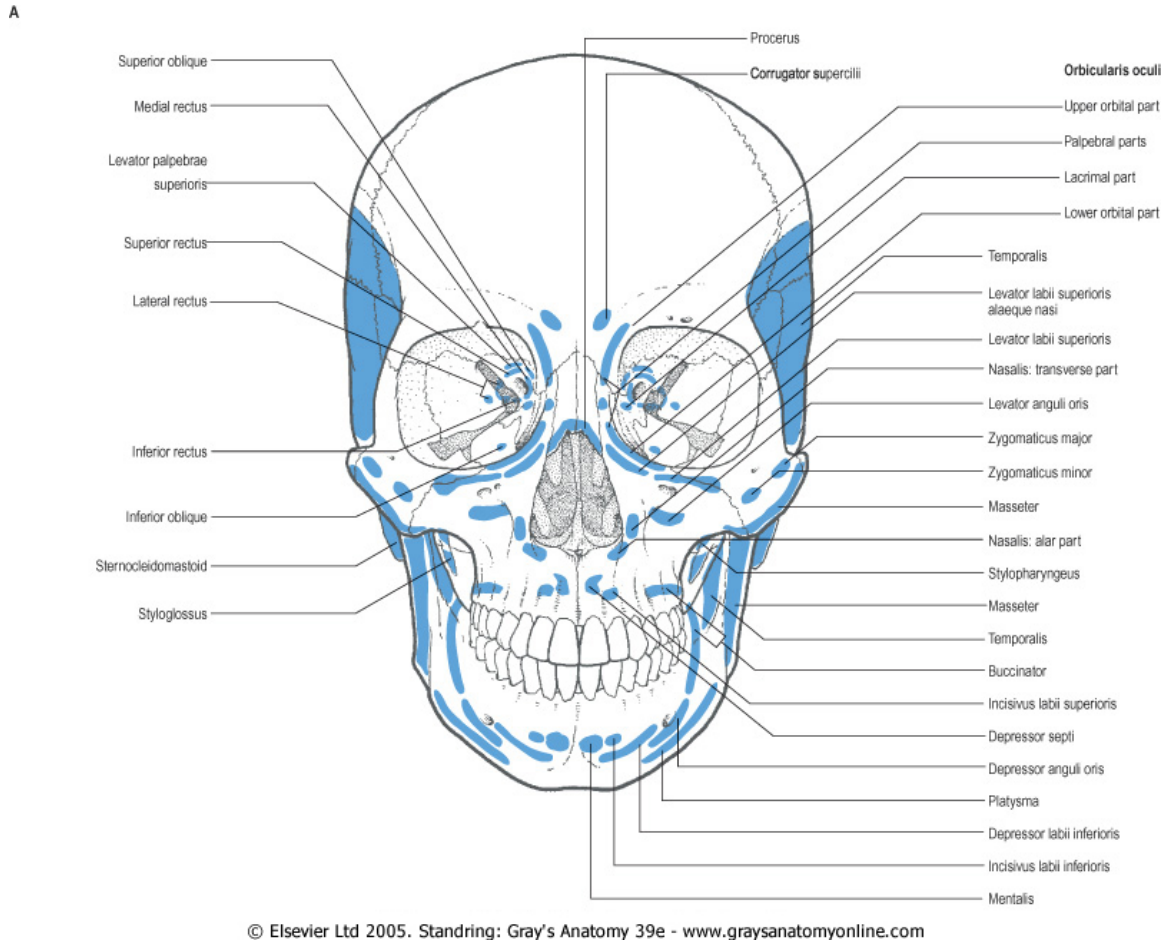

Figure 2.2 Skull attachments of face muscles (Standring, 2005)

Table 2.1 Summary of orofacial muscles' starting and ending positions with the corresponding innervation branches

Group No.	Muscle Name	Abbreviation	Muscle's Starting Position	Muscle's Ending Position	Innervation
1	Levator Labii Superioris Alaeque Nasi	LLSAN	Upper frontal process of maxilla	Skin of the lateral parts of the nostril and upper lip (OOPS)	Zygomatic and buccal branches of facial nerve
1	Levator Labii Superioris	LLS	Lower margin of the orbit immediately above the infraorbital	OOPS (between zygomaticus and LLSAN)	Zygomatic and buccal branches of facial nerve

			foramen(maxilla and zygomatic bone)		
1	Zygomaticus Minor	ZYG_MIN	Malar surface of the zygomatic arc or bone	Corners of the mouth and the upper lip (OOPS)	Zygomatic and buccal branches of the facial nerve
2	Zygomaticus Major	ZYG_MAJ	Malar surface of the zygomatic arc or bone	OOPS	Buccal and zygomatic branches of the facial nerve
2	Levator Anguli Oris (Caninus)	LAO	Canin fossa on the skull	OOPS	Buccal and zygomatic branches of the facial nerve
2	Risorius	RIS	Fascia over the patoid gland	Insert to the skin of the angle of mouth	Buccal branches of the facial nerve
2	Depressor Anguli Oris(Triangularis)	DAO	Oblique line of mandible	OOPI & RIS & LAO	Mandibular and buccal branches of the facial nerve
3	Depressor Labii Inferioris	DLI	Oblique line of mandible	Skin of lower lip (OOPI)	Mandibular branches of the facial nerve
3	Mentalis	MENT	Mentalis on the skull	OOPI	Mandibular branches of the facial nerve
4	Orbicularis Oris Peripheralis Superioris	OOPS	It is derived from the other facial muscles which are inserted into the lips and partly of fibers proper to the lips.	1-Buccinator: from maxilla to the lower lip and from the mandible to the upper lip but from the uppermost and lowermost without intersection 2- LAO to OOPS 3- DAO to OOPI 4- LLS, ZYG_MIN, ZYG_MAJ, DLI (all with oblique	Buccal and mandibular branches of facial nerve
4	Orbicularis Oris Peripheralis Inferioris	OOPI			
4	Orbicularis Oris Marginalis Superioris	OOMS			
4	Orbicularis Oris Marginalis Inferioris	OOMI			

				direction)	
5	Buccinator	BUC	It arises from the alveolar processes of the maxilla and mandible corresponding to the molar teeth	Toward the angle of the mouth where the fibers intersect each other (OOPS & OOPI)	Buccal branches of the facial nerve

2.5 Oral Fissure Constrictors

Four orbicularis oris muscles control the orbital shape of the mouth. These muscles produce lip protrusion and rounding (Standring, 2005). They are also used in pursing of the lips. These muscles are the main muscles in speech gestures. Peripheralis muscle is the main component in lip shaping while the marginalis helps better shaping of the lips especially in rounding. Since the muscles act in tension only the protrusion gesture is accompanied by an increase in transversal resistance while the contact between the peripheralis and teeth/jaws provide part of this transversal motion. The marginalis part is more involved in speech gestures.

2.6 Specific Muscle: Buccinator

This muscle draws the corner of the lips laterally. Its main effect as its name stands for (Latin buccinator means trumpeter) is for compressing the cheeks against jaws and teeth as in sucking or blowing. It helps to hold food between the teeth during chewing.

2.7 Masseter and Platysma

Masseter (Figure 2.1) is a mastication muscle. It attaches to mandible and maxilla and elevates the mandible for chewing action. It has little effect on side by side motion. Fibers in masseter are pennated which allows the increase of number of fibers in its body and hence in its cross sectional area. It can produce forces up to 1kN (Miles and Nordstrom, 1995). In fact jaw movements due to masseter affect the lip shaping.

Platysma (Figure 2.3) is a sheet-like muscle in the neck region. It arises from the clavicle and ascends through the neck towards the face. Most of its fibers are attached to the mandible. Some of its fibers join with muscles around the mouth. It can draw down the lower lip and the corners of the mouth during facial expressions like surprise. In some cases it attaches the lateral cheek which causes a furrow (Schmidt and Cohn, 2001).

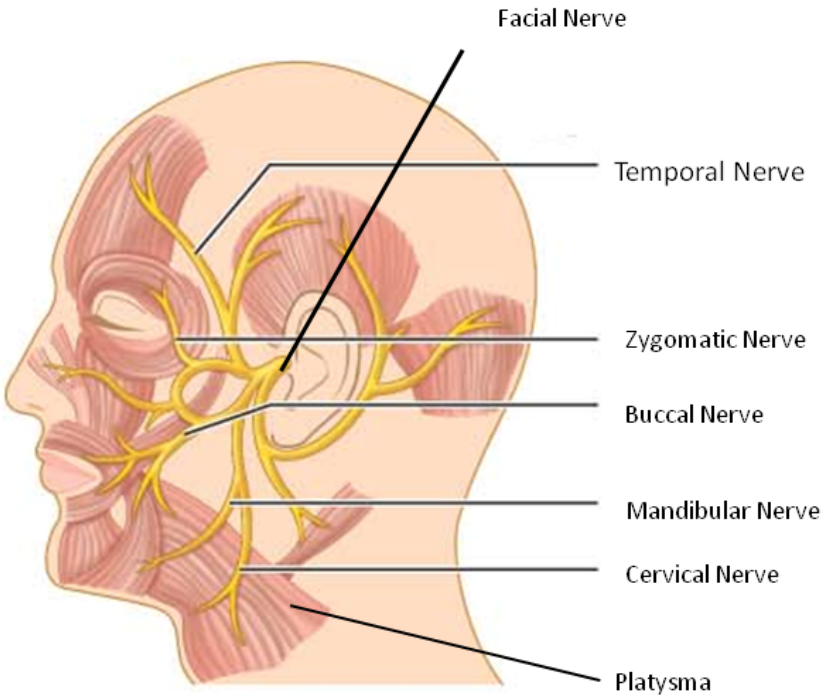

Figure 2.3 Motor branches of the facial nerve for the muscles of facial gestures; these branches are classified into five groups: temporal, zygomatic, buccal, mandibular, and cervical (Marieb & Hoehn, 2007); (platysma muscle also is shown)

2.8 Orofacial fibers characteristics and their motor units

In contrast to masseter the other orofacial muscles (and even tongue muscles) are not expected to develop large forces. Orofacial muscle fibers, because of their moving attachment points develop passive stretching, but the magnitude of this passive stretch is low (McComas, 1998). Muscle fibers from contraction speed can be categorized into three groups (Wise and Shadmehr, 2002): *slow non-fatiguing* (type I or S), *fast and quickly fatiguing* (type IIB or FF) and *fast and fatigue resistant* (type IIA or FR). Fiber types in orofacial muscles are of FF type except in masseter and buccinator where a percentage of fibers of S type exist. The domination of type IIB in orbicularis oris muscle shows that it is for high velocity and acceleration movements during intermittent motions like speech. But the dominance of fibers of type S in buccinator show it is built for slow and continuous work under low level of forces (Stal et al., 1990).

There is little data on orofacial muscles but it is likely that these muscles have smaller motor units than limb muscles. Consistent with this assumption the number of motor units in orofacial muscles and especially in masseter is much higher than limb muscles. This provides a safety margin for these muscles against neuropathy diseases (McComas, 1998). Afferent cell bodies for masticatory muscles are located in brainstem. Muscle spindles do not exist in orofacial muscles (Stal et al., 1990) except in masseter where spindles are larger and more complex than for limb muscles (with type II afferents) (Appenteng et al., 1978). The short distance between muscle fibers and motoneurons in the brainstem (pons) enable activation signals with a small delay to arrive to these muscles. Histological examinations show that most of orofacial muscles have a small number of innervating terminals;

exceptions are orbicularis oris and buccinator in which motor endplates were found to be spread over the whole of muscle resulting in a smaller motor unit zone for these muscles (Happak et al., 1997).

2.9 Synergies and antagonism in orofacial muscles for lips movements; the role of the modiolus

A number of muscles converge towards the lip corner where they form a dense mass that is called the modiolus (Figure 2.1). At least nine muscles (orbicularis oris is regarded as four muscles, see Table 2.1) are attached at this point (there are even 10 muscles if risorius included). In the modiolus, on the basis of orientation of their fibers, the muscles can be grouped into four bundles (Standring, 2005). The main factor influencing the positioning and the displacement of the modiolus, and then of the lip corner is the equilibrium between the forces exerted by these bundles of muscles. When the lips and teeth are in closed position, the modiolus mobility is at its minimum. But as soon as mouth opening reaches 2 to 3 millimeters, this mobility becomes maximal. Most activities take place in three steps (Standring, 2005). First a particular group of modiolar muscles become dominant over its antagonist group and relocate modiolus rapidly. At the second phase the modiolus is fixed transiently in this position by simultaneous contraction of ZYG_MAJ, LAO, DAO and platysma (and RIS). This provides a fixed basis from which the other orofacial muscles attached to this point, i.e. OO or BUC, can perform their actions. These actions are integrated with partial jaw movements.
On the basis of the origin of their innervations from the facial nerve (see Table 2.1) orofacial can be classified into five groups:

1- Zygomatic and buccal branch innervation: LLSAN, LLS, LAO, ZYG_MIN and ZYG_MAJ
2- Buccal branch innervation: RIS, BUC
3- Mandibular and buccal branch innervation: DAO, OO
4- Mandibular branch innervation: DLI, MENT
5- Cervical branch innervation: platysma

As it can be seen muscles in groups 2, 4 and 5 can operate independently from the other muscles. But muscles in groups 1 and 3 should perform a coordinated action with other muscles. Positioning muscles of modiolus have a connection from all branches, which is an interesting fact. This allows how keeping the lip corner in position is possible, since this requires the simultaneous activations of a large number of muscles, which is made possible thanks to an innervation from all branches.

Chapter Three: Biomechanics of Striated Muscles: A Literature Survey and Distributed Feldman Model (DFM)

"Never mistake motion for action."
Ernest Hemingway

Muscles are the main end effectors of moving body parts in directions that are decided and controlled by the Central Nervous System (CNS). After receiving a command from the CNS, a muscle generates a force that is transmitted to the muscle's attachment points. These attachment points can be on bony structure (as in the masseter), on surrounding tissues (like for one end of the mentalis), or on the extremity of another muscle (like the attachment of the corner of orbicularis oris to zygomaticus). If the attachment points are free to move, muscle length starts to decrease with activation which then moves the tissues attached to the muscle (e.g. the jaw during the mastication process through masseter activation, or the lower lip that moves upwards in the process of lip protrusion with orbicularis oris muscles helped by the mentalis). The force generated in the muscle is due to links (the "crossbridges") between actin and myosin filaments and depends on the rate at which these linking mechanism works. These features give rise to two important properties of the force generated in the muscle and its resulting motion: the force-length and the force-velocity characteristics. The arrangement of these filaments structurally classifies muscles into striated ones, like *skeletal* and *cardiac* muscles, and non-striated ones which are *smooth* muscles. Since all the orofacial muscles used in speech are of striated type, our emphasis will be on the characteristics of these muscles. They are reviewed in detail in this chapter which will conclude with the proposal for a distributed version of Feldman muscle model (Feldman 1966; 1986).

3.1 Crossbridge theory

Striated muscles are composed of fibers (Figure 3.1). These fibers are composed of thousands of smaller myofibrils (muscle cells). The myofibrils are in turn composed of a series of sarcomeres. Each sarcomere is located between two Z-discs and is a combination of parallel bands of actin (thin) and myosin (thick) proteins filaments. Following a motor command, calcium ions in the sacs surrounding the myofilaments are released and cause the hydrolization of myosin heads. The hydrolysis of ATP in the myosin heads makes them ready to be attached to the actin filaments, and therefore muscle starts to contract. The degree of overlap between myosin and actin filaments limits the level of force generation capacity of a sarcomere. With increasing overlap, the number of crossbridges between myosin heads and actin molecules increases. Hence the force generated by the muscle can be higher. This mechanism of force generation in a single sarcomere is the sole basis of the sliding filament theory as proposed by H.E. Huxley and A.F. Huxley at the same time (1954), yet separately without knowing each other and it was published in the same issue of *Nature*. Acquaintance of this mechanism is needed to understand the behavior of a muscle macroscopically. This mechanism is described in detail in next section.

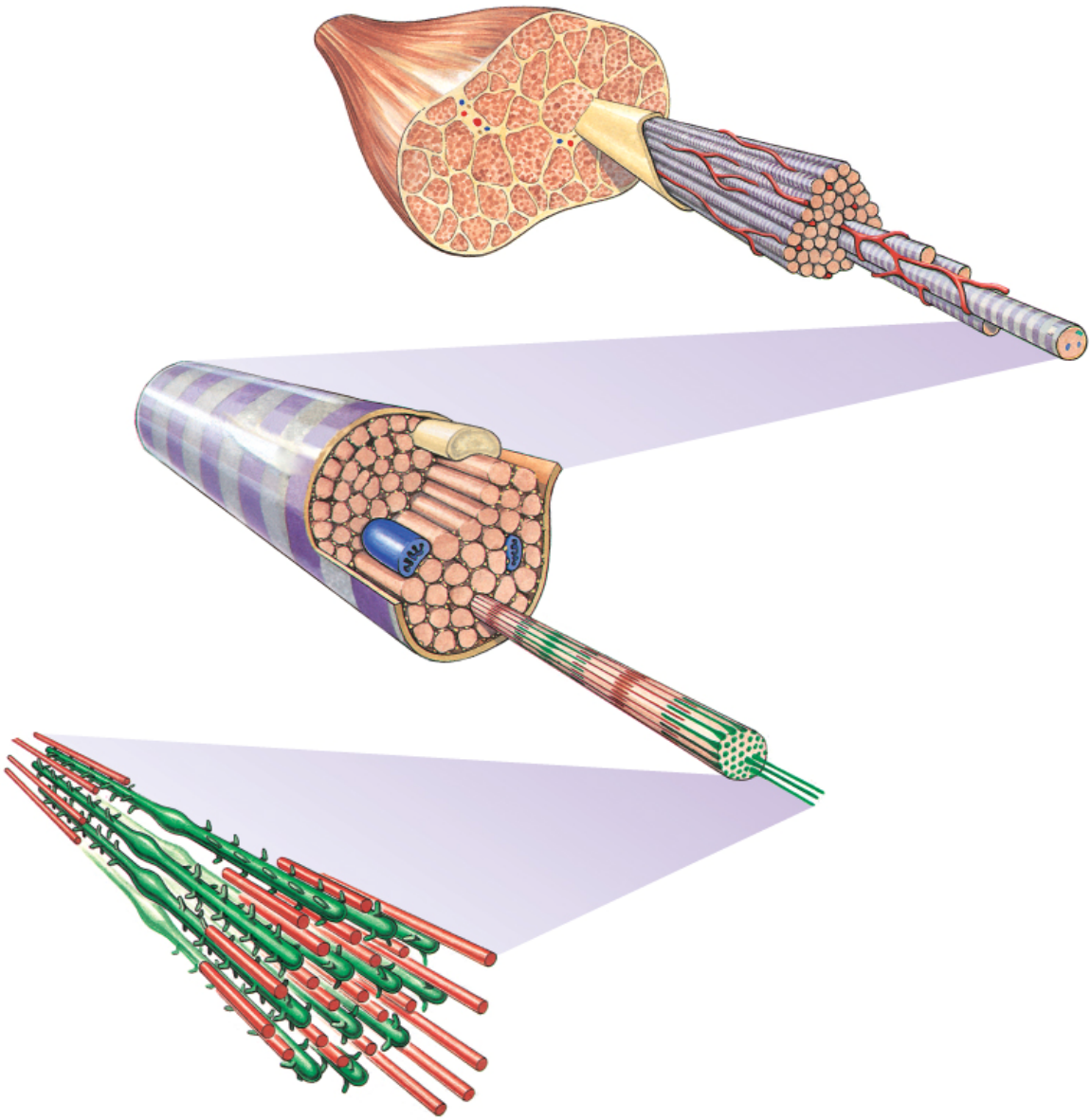

Figure 3.1 Muscle structure in striated muscles; Top panel: A striated muscle composed of fibers; Middle panel: Each fiber consists of myofibrils; Bottom panel: Myofibrils are a sequence of Z-discs and sarcomeres and each sarcomere consists of parallel bands of actin (shown in red in bottom panel) and myosin (shown in green in bottom panel) protein filaments (from Standring, 2005).

Figure 3.2 (McMahon, 1984) shows the tension produced in a single muscle fiber as a function of the length between two consecutive Z-discs (so-called striation spacing). The interval between points 2 and 3, where there is maximum overlap between myosin and actin fibers, corresponds to the maximum force that a sarcomere can generate. Toward point 1, with more elongation due to the separation of actin and myosin filaments, the force drops. This part is called *descending limb*. With more contraction, between the points 3 and 5, the actin filaments overlap each other and therefore the total number of crossbridges is reduced. Hence the force decreases as well. After point 5, the myosin filaments collide with the Z-discs and the force reduces sharply. This part of the curve is called the

ascending limb. This behavior is reproduced at a macroscopic level (Zajac, 1989), which is described in the next section.

3.2 Force-length characteristics of a muscle

All the elements that generate force in a muscle are referred to as contractile element (CE). When all myofibrils in a striated muscle are activated, they produce the same sort of behavior as a single sarcomere. This property is described in the active force-length characteristics of a muscle (Figure 3.3, active part shown in red). Each point on this curve shows the maximum voluntary force (MVF) that a muscle can generate at the corresponding length. The curve describes the envelope of normal active muscle behavior, excluding the stretch reflex case.

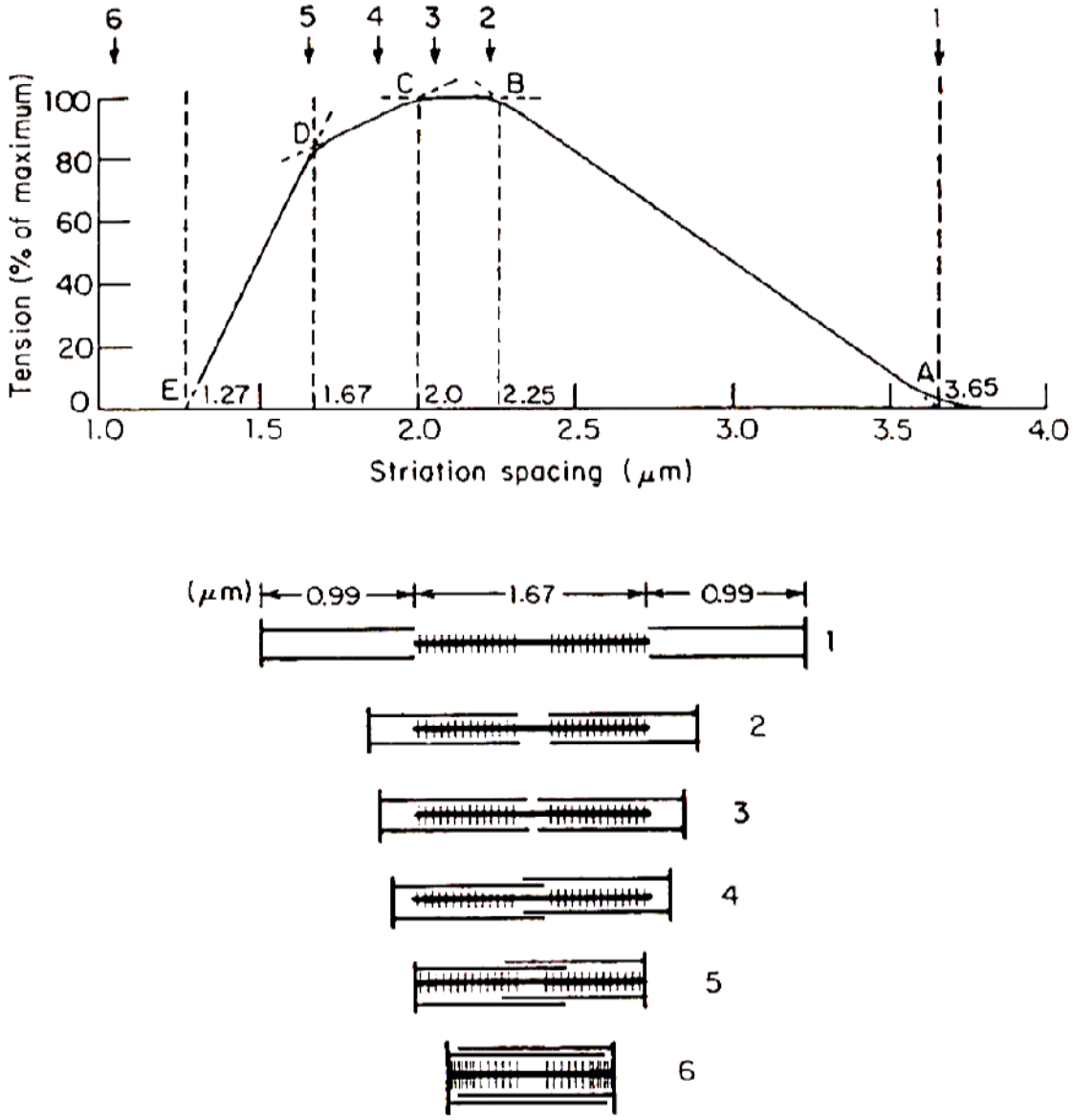

Figure 3.2 Force as a function of length in a single sarcomere; Point 1: fully extended sarcomere; no force is generated by muscle (1-2 is called descending limb part); Point 2&3: maximum overlap between actin and myosin and maximum force generation capacity of sarcomere; Point

4: decreasing overlap between actin and myosin during contraction; Point 5: collision of myosin heads with end Z-discs and fast decrease of force (4-6 is called ascending limb part); Point 6: fully contracted sarcomere with no overlap between actin and myosin heads(from McMahon, 1984).

In fact, each point of this curve is obtained when a muscle isometrically (muscle length kept constant) generates the maximum force. There is also a passive resistance to extension when an external force is applied to the muscle. This resistance comes from elastic properties of fibers when they are extended beyond their rest length. This elastic property is different across muscles, and it mainly depends on the proportion of connective tissues of muscle fibers (passive blue part in Figure 3.3). A high proportion of connective tissues leads to important resistance as in masseter (Figure 3.3b) while a low proportion generates small resistance as in zygomaticus (Figure 3.3a). The actual behavior of an active muscle fiber in response to an external force (described with the black curve in Figures 3.3a, b) is the sum of the red and blue curves. The corresponding black curve can show a local maximum when the muscle has less connective tissues (Figure 3.3a).
There are controversies concerning the shape of the force-length characteristic of a muscle when the level of activation is below the maximum voluntary force (MVF). It is assumed (Zajac, 1989; Winters, 1990; Shapiro & Kenyon, 2000) either that the active part is scaled multiplicatively (Figure 3.4a) or it is scaled additively (Figure 3.4b).

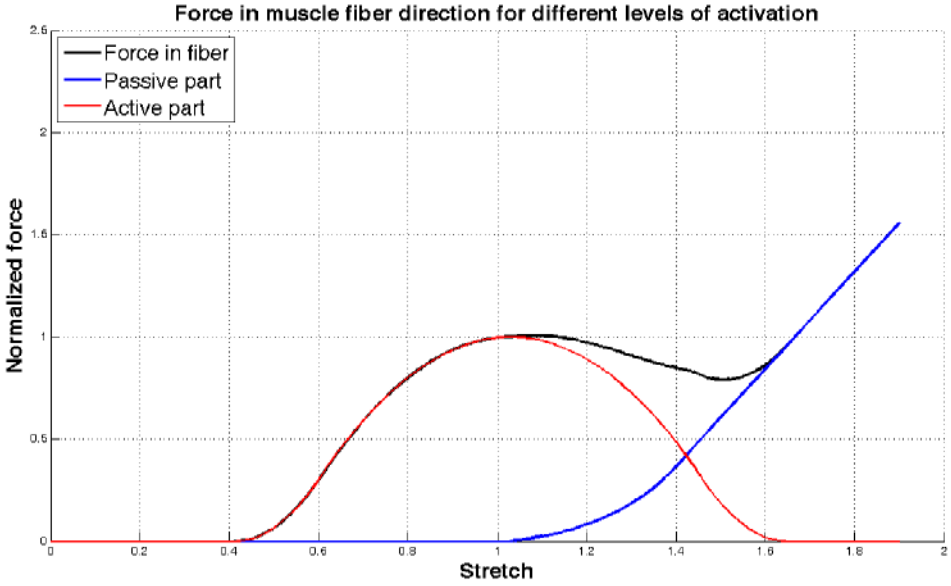

(a)

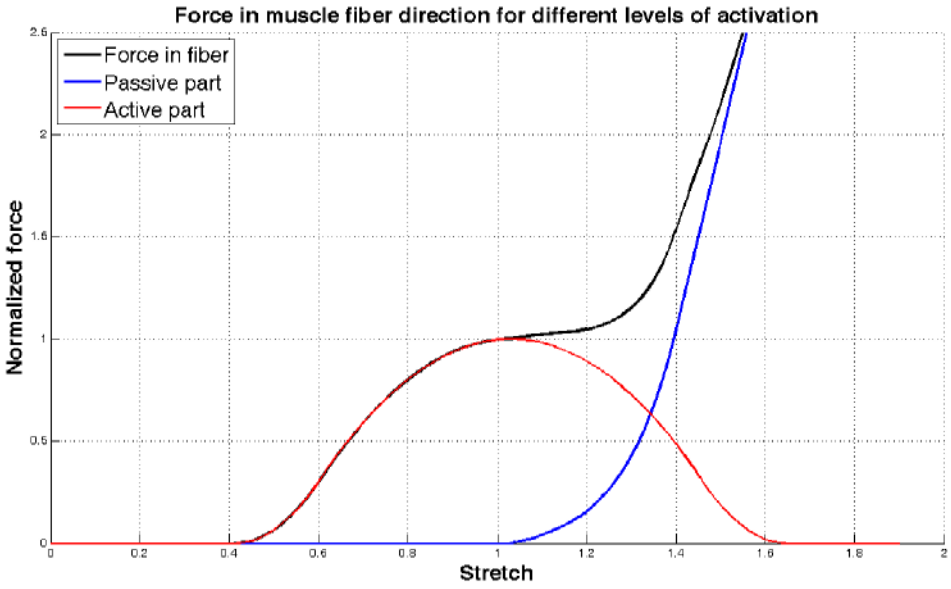

(b)

Figure 3.3- Force-length characteristics of a muscle with (a) weak passive part or (b) strong passive part (Blue curve shows the passive part; Red curve shows the force in the contractile element; Black curve is total force in the muscle).

There are three passive elastic elements within the muscle. The first one behaves as an exponential function and is shown in the figures 3.3 and 3.4 (blue curve). This corresponds to the passive property of connective tissues and membranes which is part of elastic properties in series with fibers. This behavior manifests itself in the extension phase only. For measuring this property the standard universal tension test can be used. The second elastic property comes from tissues surrounding the muscle fibers. This property is referred to as parallel elastic (PE) elements since it acts in parallel fibers. Surrounding tissues resist in both directions. It means they can also withstand while the muscle fibers shorten. This property is not shown in figures 3.3 and 3.4.

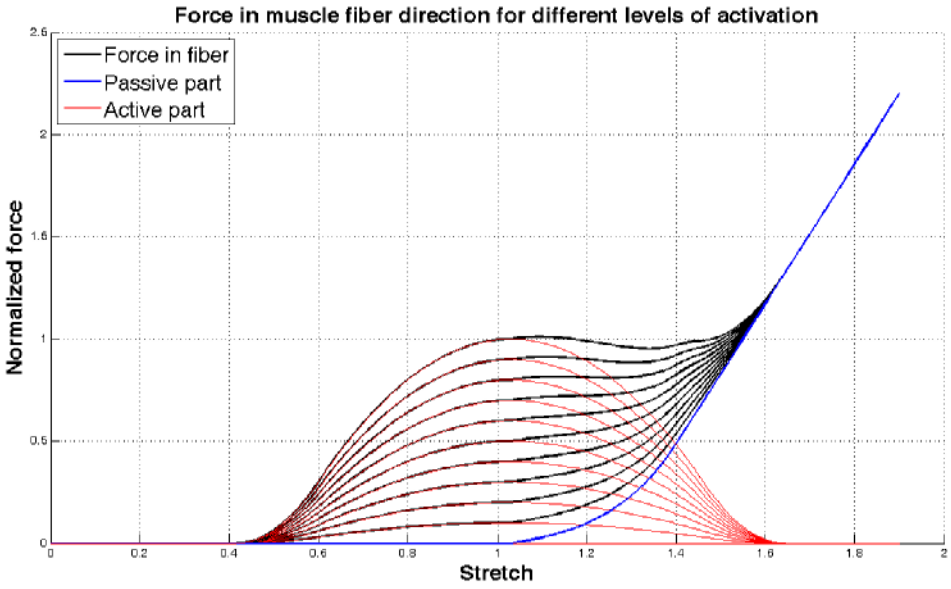

(a)

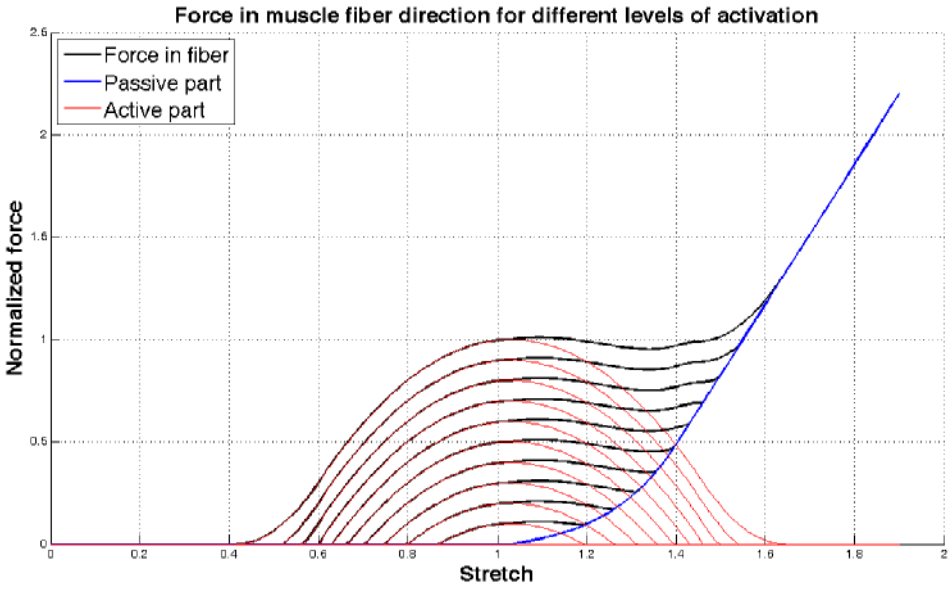

(b)

Figure 3.4 Force-length characteristics for different levels of activations (a) multiplicative scaling or (b) additive scaling (the passive part (blue curve) is fixed).

The third elastic element accounts for the intrinsic elasticity of myofibrils and crossbridges (Fung, 1993). This element acts in series with contractile elements and is designated as series element (SE). In fact the series element has been included in Figures 3.3 and 3.4 implicitly. Indeed this series element works like a conveying media between the contractile element (CE) and the extremities of the muscle (Winters, 1990). It can be said that this element plays the role of a low stiffness tendon. This means that it transfers muscle action to the attachment points. The effect of this series element is shown in Figure 3.5. If the contractile element force is shown by red curve, then it means that this series elastic

property implicitly has been taken into account. If the green curve shows the output of contractile element then the series elastic stiffness should be augmented with this series element.

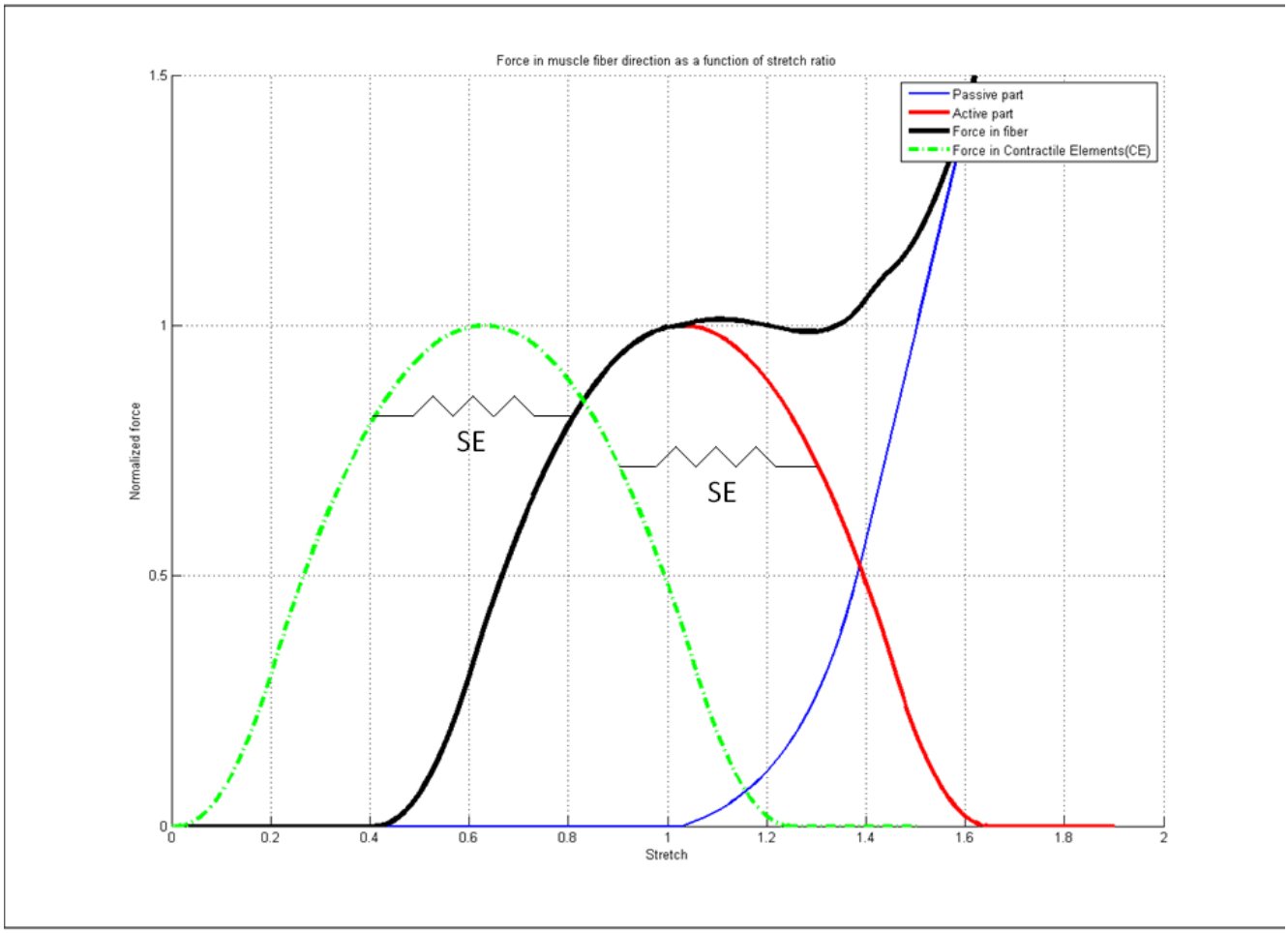

Figure 3.5 Series elastic effect on output of contractile elements. This series elastic element is due to intrinsic elasticity of crossbridges.

The first functional model for these three elements has been presented by Hill (1938) and illustrated in Figure 3.6 in two forms. A recent study (Siebert et al, 2008) has shown that the model with PE in parallel with the contractile element (Figure 3.6b) better matches experimental results. However the model with PE in parallel to both CE and SE can be better justified with physiological characteristics of muscle alone (Figure 3.6a) without considering the effect of tendons.

During motion the behavior of a muscle is different from the above properties since the generated force depends on muscle velocity. The effect of kinetics of the muscle is discussed in next section.

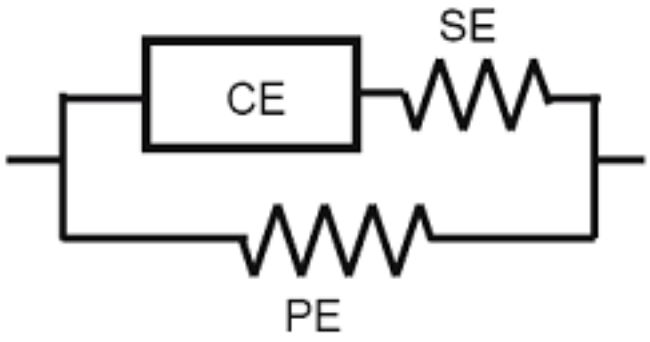

(a)

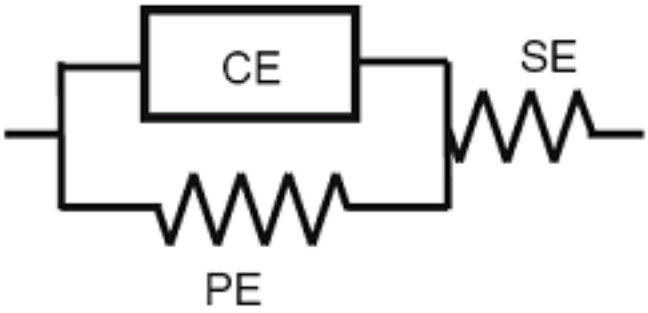

(b)

Figure 3.6 Two different Hill-type muscle models (a) the force in series elastic element is equal to force in contractile element (b) the force transferred to series elastic element is attenuated by parallel elastic element.

3.3 Force-velocity characteristics of a muscle

When a muscle shortens quickly, it generates less force than when it moves slowly. This is explained by the fact that the force output of contractile element is damped by the viscosity property of the muscle. This phenomenon was studied for the first time by Hill (1938). He studied the effect of shortening velocity on the force produced by a muscle. He proposed that the force varies with respect to velocity of shortening as a hyperbolic function (eq. 3.1).

$$F/F_{max}=(1-v/v_{max})/(1+(1/k)(v/v_{max})) \quad if\ v_{max}<v<0 \qquad (3.1)$$

In this equation v_{min} is the maximum shortening velocity (negative velocity). Constant k for all vertebrate muscles lies in the range $0.15<k<0.25$. The shortening of the muscle is called *concentric contraction*, since in that case, the crossbridges between myosin and actin filaments are oriented towards the z-discs (or centers). When the muscle lengthens, it is an *eccentric contraction*. In this case the crossbridges are moving away from the center. In an eccentric contraction, when the velocity of lengthening increases the force is also increasing in a first stage. Katz (1939) found that the behavior in extension cannot be extrapolated from the Hill's equation and that at velocities close to zero, the slope

of the force-velocity curve is about six times (m=6) greater for concentric contraction. Katz also discovered that, above a certain level of tension, muscle yields when the elongation rate increases. It means that after a threshold (the yield point), the muscle loses its ability to withstand more elongation. Katz found that this threshold is about $d=1.8$ times the maximum isometric tension at a specified length. The equation governing this behavior according to Leeuwen & Kier (1997) is:

$$F/F_{max}=d-(d-1)((1+v/v_{max})/(1+(k_{ec}/k)(v/v_{max}))) \qquad if\ v>0 \qquad (3.2)$$

where k_{ec} is an eccentric muscle constant and which can be computed from the difference between the slopes of the force velocity curves on both sides of the zero velocity. If the slope in eccentric section is m times the slope in concentric section, k_{ec} becomes:

$$k_{ec}=(m(k+1)/(d-1))-k \qquad (3.3)$$

The curves corresponding to the combination of equations (3.2) and (3.3) are shown in Figure 3.7 with $k=0.25$ and $m=5$.

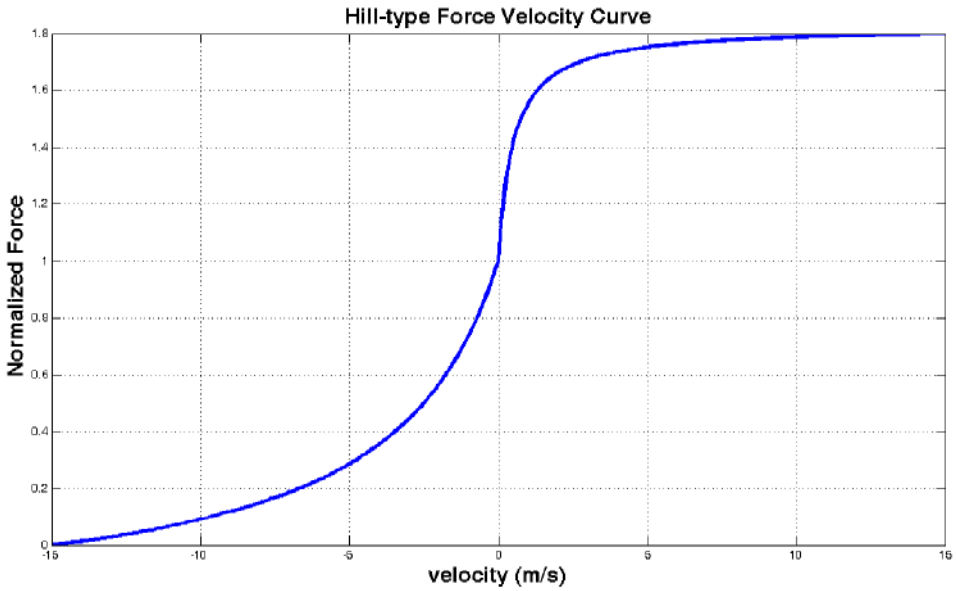

Figure 3.7 Hill-type force-velocity curve; negative velocity shows the concentric motion and positive velocity eccentric motion; at zero velocity the curve is not smooth (not C^1 continuous).

The inclusion of force-velocity characteristics of a muscle in Hill's functional model is shown as a damper element in parallel to contractile element and with a damping constant (B) which is a nonlinear function of velocity (Figure 3.8).

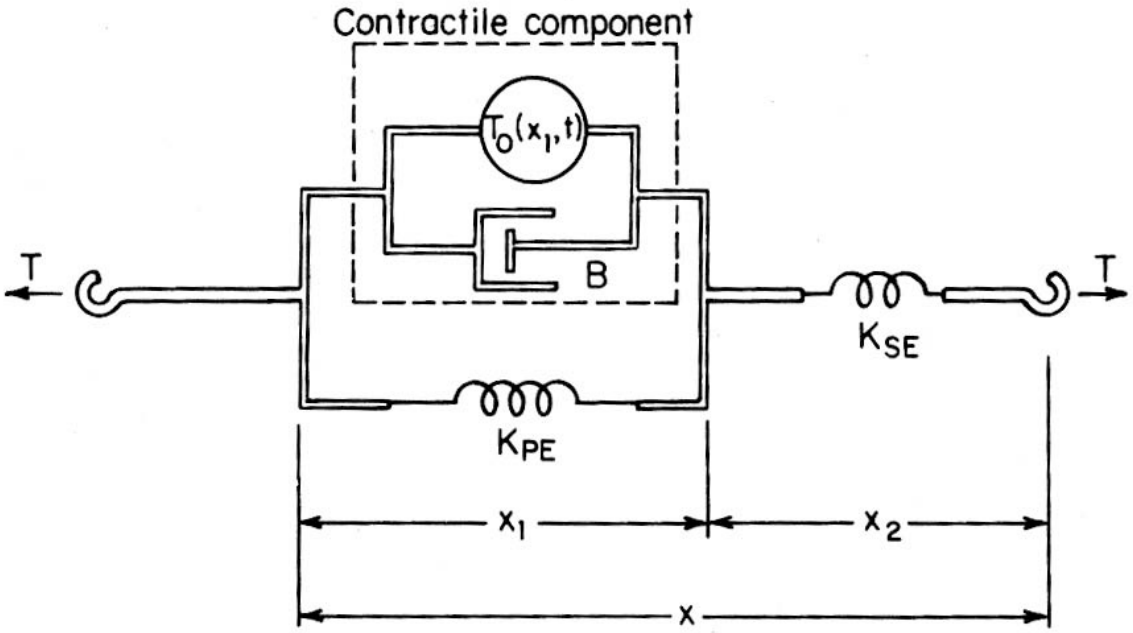

Figure 3.8 Functional model of a muscle; damper B is added to take care of damping property of the muscle (from McMahon, 1984).

The combined effect of force-velocity and force-length characteristics is shown in three dimensions in Figure 3.9.

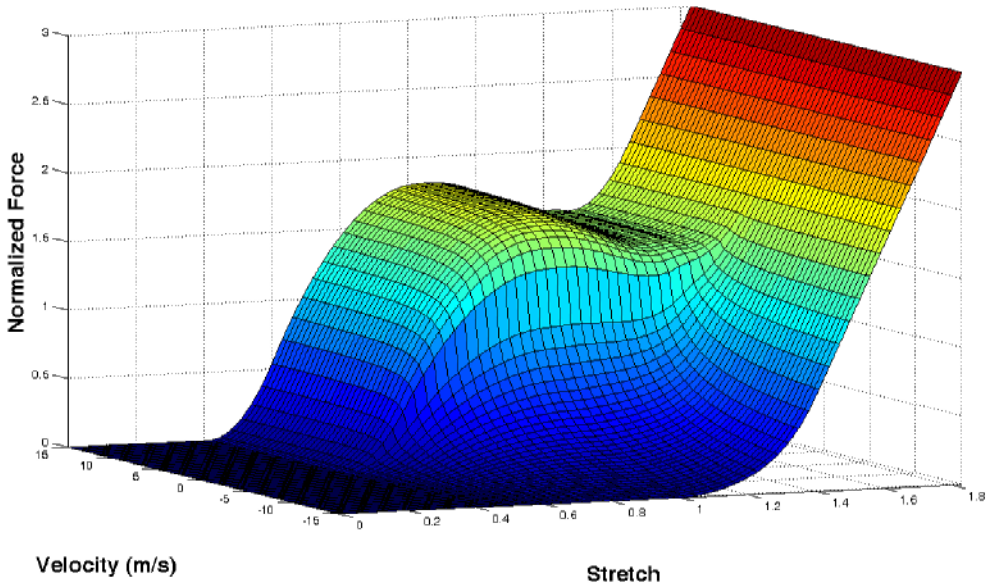

Figure 3.9 Total effect of the behavior of a muscle (Hill-type muscle); with more negative velocity the force generated by muscle decreases strongly.

In the next section discuss different functional models of muscle, other than Hill's basic model is studied.

3.4 Functional models of muscle

In general two types of functional models were provided in the literature. In one type, the muscle behaves as a black box, assuming a macroscopic description of the input/output relationships. Basic Hill model belongs to this group. The force output of muscle (F_m) can be expressed as the sum of a force in the parallel elastic element (F_{PE}) and a force in the contractile element (F_{CE}):

$$F_m=F_{PE}+F_{CE}=F_{SE} \qquad (3.4a)$$

$$F_{CE}=f(L,v,A_c) \qquad (3.4b)$$

Force in the contractile element is a function of muscle length (L), muscle velocity (v) and activation (A_c). This force is usually expressed in a multiplicative way (like in Figure 3.4a) as a product of three distinct functions: force-length (F_L), force-velocity (F_v) and time transition function of the activation (called henceforth *activation dynamics*) (f_{ac}) (Zajac 1989; Cheng et al., 2000):

$$F_{CE}=F_L\times F_v\times f_{ac} \qquad (3.5)$$

The activation dynamics (f_A) can be either taken as a function of the firing frequency or recruitment of muscle fibers (for example filtered EMG) or the level of activation. This multiplicative account of contractile force is called *adjustable stiffness* because the contractile element behaves like a nonlinear spring whose stiffness varies as a linear function of force (Shadmehr & Arbib, 1992).
In other approaches, the contractile force is expressed as a general nonlinear function of activation level and velocity as in equation (3.4a) (Feldman, 1986) or in a multiplicative way (Shapiro & Kenyon, 2000; Laboissière et al., 1996):

$$F_{CE}=f(A_c,L)\times g(v) \qquad (3.6)$$

In this subgroup, models that indicate the activation as a length quantity, like Feldman's model (1966), are called *adjustable starting length* models (Shadmehr & Arbib, 1992). In these models, muscle stiffness changes as a nonlinear function of force.
In the second type of models, muscles are considered microscopically. These models are based on Huxley's sliding filament theory and take into account physiological mechanisms of force generation in the muscle (Zahalak, 1990; Murtada et al., 2010a and 2010b). In the macroscopic models the muscle velocity is uniquely related to muscle length and to the level of muscle activation, which is generally not true. On the other hand the microscopic models can better predict the viscoelasticity behavior of muscles than the Hill-type models. However these microscopic models suffer from lack of simplicity requirement of a model. That's the reason why we have chosen to focus on the first group of models in the rest of this chapter.
The activation mechanism in the muscle completely limits the domain of applicability of models and their competency. In the next section, this mechanism is reviewed. After this review adjustable stiffness and adjustable starting length models will be compared in detail.

3.5 Activation Mechanism

The nerve cells (neurons) that innervate the muscles are called motoneurons. Their activity varies with their membrane potential. Hence innervation signals are called action potentials. A motor unit consists of a set of muscle fibers activated by a motoneuron plus the motoneuron itself. The motor units responsible for force generation and associated with the main muscle fibers (also called *extrafusal fibers*) are called *α-motors*. The associated motoneurons are known as *α-motoneurons*. Motor units involving fine movements have a small number of fibers. Those motor units which correspond to a large number of fibers have larger motoneurons. Depending on the speed of contraction, the motor units may be classified into *fast* or *slow* motor units (Wise and Shadmehr, 2002).
In most muscles, there are some stretch receptors in parallel with extrafusal fibers. These receptors are called *spindle organs* or *intrafusal fibers*. These receptors act as a strain gauge in the muscle. The functional model of the spindle organs can be represented as the model of Figure 3.8. The spindle organs with their driving motoneurons are called *γ-motor units*. Another receptor known as *Golgi tendon organ,* is located inside the tendon. It provides information about the force acting on the tendons. The arrangement of these two types of receptors is shown in Figure 3.10. As it can be seen, these receptors send their signals to the spinal cord (or, in case of orofacial muscles, brainstem), where motoneurons reside. Since these signals carry information from the peripheral motor systems back to spinal cord/brainstem, they are called *afferents*. Signals sent from the motoneurons to the motor system are going away from spinal cord/brainstem; these signals are called *efferents*. Afferents Ia and II are provided from the spindle organs while Ib afferents come from Golgi tendon organs. Efferents α and γ are activation signals to the extrafusal and intrafusal fibers respectively. The afferents reside on dorsal root of spinal cord and efferents in ventral root. The path of the descending commands down from the central nervous system (CNS) to motoneurons is shown in Figure 3.11 for hand movements.
There are four activation mechanisms that influence the behavior of a muscle: 1-α-γ co-activation, 2-stretch reflex, 3- Golgi tendon organ inhibition (reflex stiffness), and 4- inhibition (feedforward and feedback).

3.5.1 α-γ Co-activation

This mechanism governs voluntary muscle activation (Figure 3.11). When a command from CNS is sent to α motoneurons, the muscle starts to be shortened. Accordingly the parallel spindle organs get slackened. This causes the afferents from spindle organs (Ia and II) to reduce the activation in α motoneurons. In fact the change in signal from a spindle organ (ΔS) is proportional to its length change ($\Delta L=L_{spindle}-L^{0}_{spindle}$): $\Delta S=k_s\Delta L$. The signal to the muscle fibers from α motoneurons is: $\alpha=\alpha_m+\Delta S$, where α_m is the reference signal set by the CNS. Because of the spindle organs slackening ($\Delta L<0$), a negative signal is added to the α activation signals which reduces the muscle activation level. To avoid this problem, the CNS sends two simultaneous signals to α and γ motoneurons: the muscle contraction is accompanied by spindle contraction (from γ motoneurons) which means that the spindle slackening won't occur ($\Delta L=0$). This co-activation process therefore solves the inhibitory action of slackening. Of course in presence of external loads, if a load causes extra lengthening or shortening of muscle fibers, as for stretch reflex (see § 1.5.2), the activation level changes accordingly to compensate the muscle force. In fact the spindle organ acts as a model reference for muscle (Houk & Rymer, 1981). This mechanism is shown in the Figure 3.12.

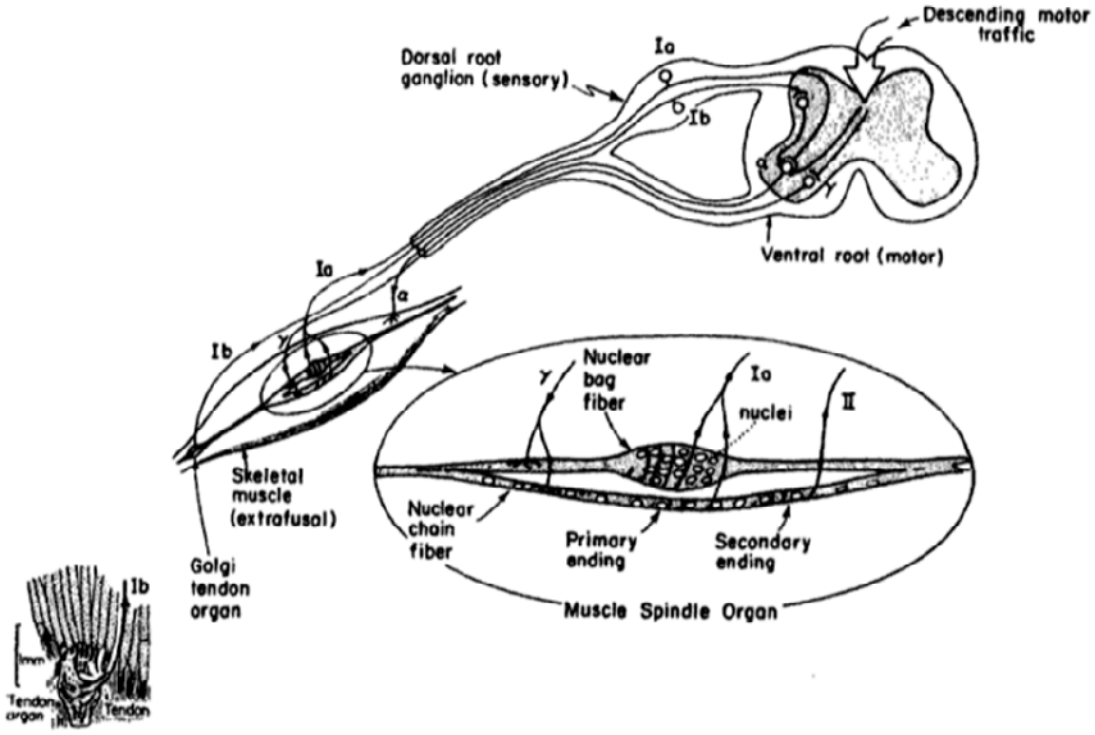

Figure 3.10- Signal paths of muscle spindle and Golgi tendon organs to spinal cord; Afferent signals from muscle spindle: Ia and II and from tendon organ: Ib; Efferent signals from motoneurons: α and γ (from McMahon 1984).

3.5.2 Stretch Reflex

A reflex is an involuntary response to an outside disturbance. When a muscle is stretched involuntarily by an external force, it reacts to regain its current length. This phenomenon is called the *stretch reflex* and is due to spindle organs. Since spindle organs are located in parallel to the main direction of muscle fibers, they are stretched with muscle extension. They therefore send their afferent signals (Ia and II) to α motoneurons which causes the motoneurons to fire more (α efferents) thus inducing higher contraction in muscle fibers ($\Delta L>0$). Consequently, the muscle produces more resisting force than before: this is the stretch reflex.

3.5.3 Golgi tendon organ inhibition (reflex stiffness)

Tendon organs send an afferent signal (Ib) that is proportional to the force level in the tendon. With increase of force the charging rate increases. This charging rate is sent to α motoneuron. Due to the linear relationship between charging rate and change in muscle force we can assume the feedback signal is proportional to change in muscle force level (ΔF): $\Delta T_g = k_g \Delta F$. This is an inhibitory signal that protects the muscle from extra tension. This signal is therefore subtracted from α motoneuron output:

$\alpha=\alpha_m - \Delta T_g$. If the external load induces an increase in muscle force ($\Delta F>0$) the Golgi receptors will decrease the force.

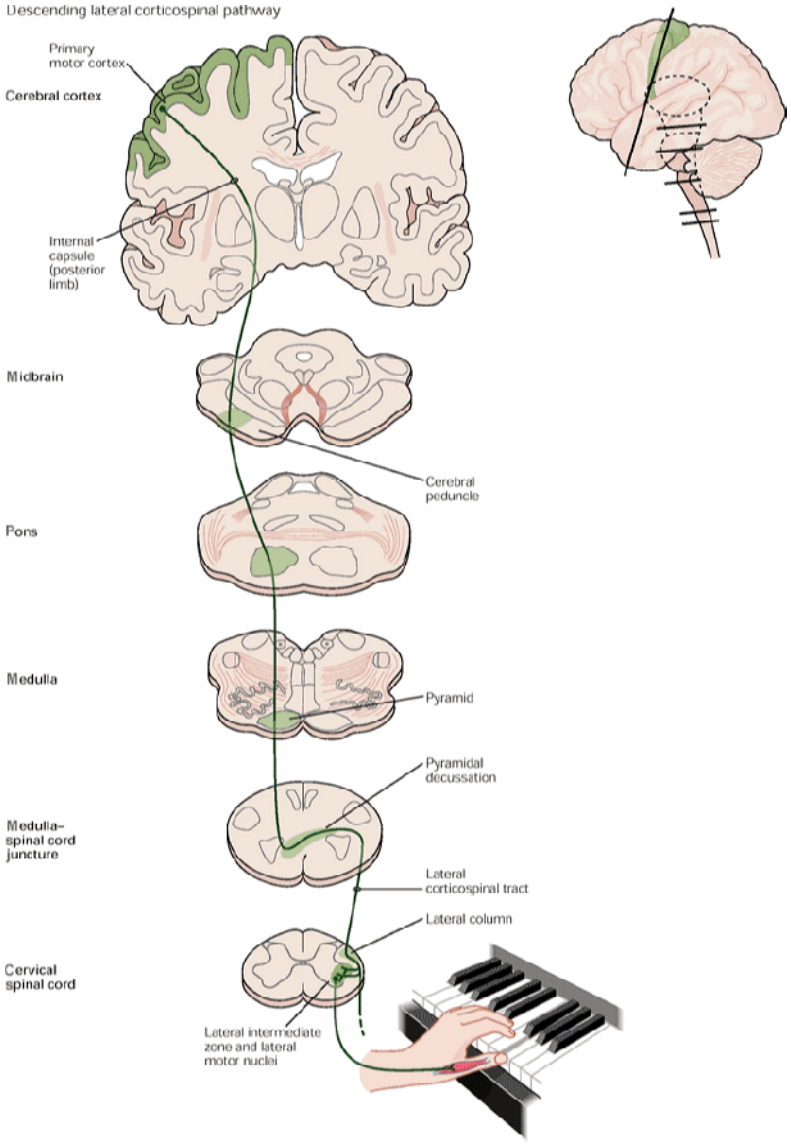

Figure 3.11 Descending tract of motor system from central nervous system to motoneurons and then to corresponding muscle fibers (extrafusal and intrafusal fibers) (from Kandel et al., 2000).

Thus with more tension in the tendons less activation is sent to the muscle fibers. This, in turn, increases muscle length. However, since the γ activation level has not changed, the length of spindle organs increases which causes a higher α signal. This dual mechanism keeps constant the change of force with respect to the change in length. Actually this can be seen as a control mechanism to maintain the *reflex stiffness* at a constant level (Figure 3.13). The reflex stiffness is the slope (K) of the force-length characteristics at a given level of muscle activation ($\alpha=\alpha_m$). Therefore corresponding to a change of length (ΔL) the change in force is: $\Delta F=K\Delta L$. In presence of a load that does not induce a need for change in the reference activation (α_m), the combined action of spindle organs and Golgi tendon organs compensate each other: $k_g\Delta F=k_s\Delta L$. Hence $K=k_s/k_g$, which means that reflex stiffness remains constant.

3.5.4 Inhibition (feedforward and feedback)

In addition to Golgi tendon inhibition, there are two inhibitory mechanisms that regulate muscle action: the *feed-forward inhibition* due to inhibitory interneuron cells and the *feedback inhibition* due to Renshaw cells (figure 3.14). The feedforward mechanism happens in agonist and antagonist muscle pairs (flexor and extensor). When a flexor (or extensor) muscle is innervated through signals from CNS or from receptors, the afferent signals to α motoneurons have a branch on intermediary neurons called interneurons (figure 3.14). These interneurons inhibit the activation of antagonist muscle which means that the agonist muscle moves independently. The only resistance comes from passive properties of the antagonist muscle.
In the feedback inhibition, the activation signal from motoneurons goes through an intermediate cell called Renshaw cell. This neuron cell produces a short-lived inhibitory effect on α motoneurons. This feedback mechanism around a motoneuron controls the sensitivity of the motoneuron to a given change of afferent signal and produces a non-oscillatory transient response in mechanisms like stretch reflex. In fact this feedback loop attenuates the gain of afferent signals and this in turn controls the level of outgoing efferent signals. This attenuation inhibits the occurrence of muscle spasm.

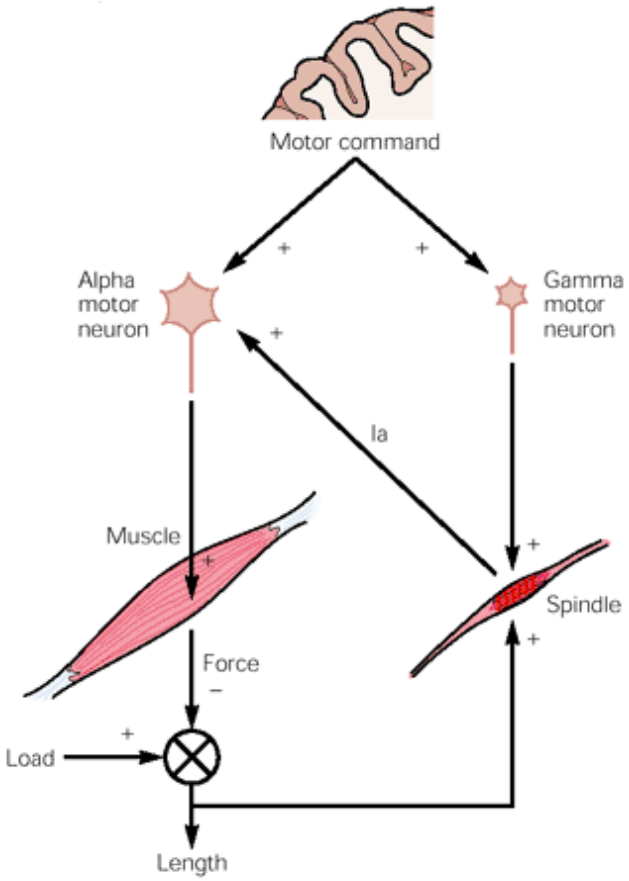

Figure 3.12 α-γ coactivation; simultaneous signals from CNS to α and γ stops the inhibitory action of muscle spindles and voluntary muscle movement occurs (from Kandel et al., 2000)

3.6 Comparison between adjustable stiffness and adjustable starting length models

Adjustable starting length or reflexive models (eq. 3.6) refer to models that better simulate the behavior of the muscle active part in the presence of a high level of descending commands. In contrast to these models are the *adjustable stiffness* models or areflexive models (eq. 3.5) that better simulate muscle active behavior when the muscle acts only through its stretch reflex mechanism (Shadmehr & Arbib, 1992). The very first adjustable starting length models go back to Feldman's muscle model (1966). Feldman's model states that the muscle starting length (or zero-force point length) is the activation command from CNS. For a given activation command, muscle behaves through its stretch reflex mechanism and its force-length characteristics will stay on an exponential curve called the invariant characteristic (IC) (Feldman, 1986):

$$F_{active\_Feldman}=F_{max}(exp([l(t-t_d)-l_{threshold}+\mu v(t-t_d)]^{+}/l_c)-1) \qquad (3.7)$$

where F_{max} is the maximum force generation capacity of a muscle and is a function of the physical cross sectional area (PCSA) of the muscle, $l_{threshold}$ it the starting or threshold length, l_c is a characteristic length, v is muscle velocity and μ is a damping coefficient. Both muscle length and velocity in this equation are delayed values at time $t- t_d$. $[]^{+}$ means that the force is equal to zero if the expression within $[]^{+}$ is negative.

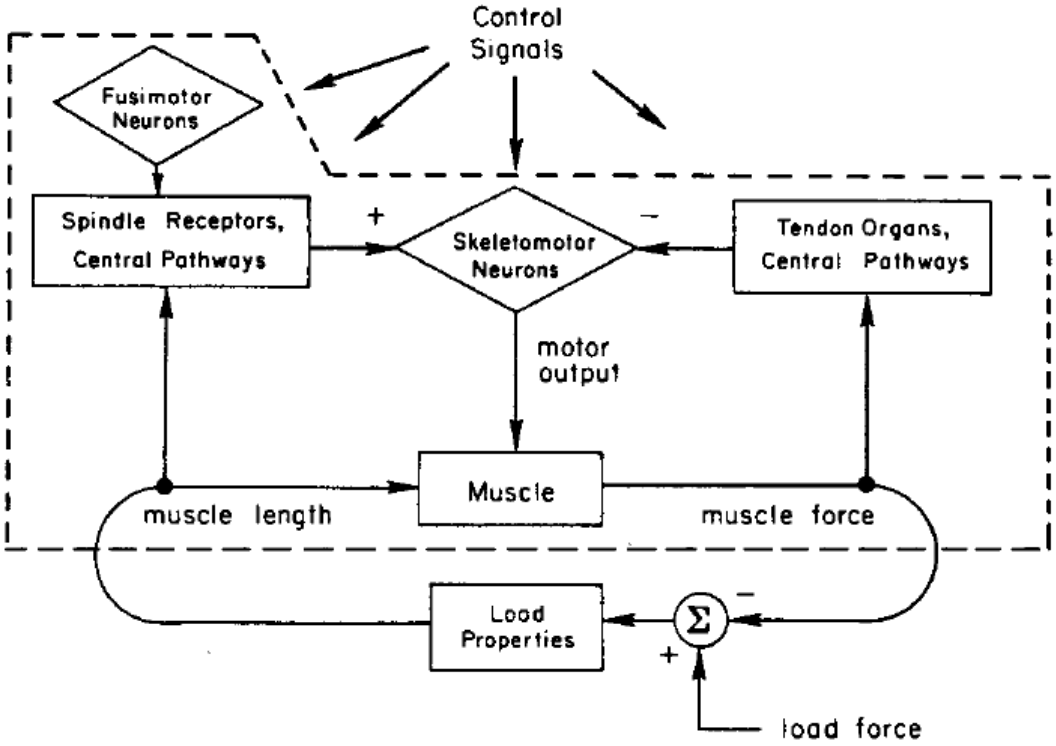

Figure 3.13 Structural plan of reflex system on muscle; the feedback signals (afferents) provided from spindle receptors (positive) and tendon organs (negative) to move a load adjust the output of motoneurons to keep the muscle stiffness at a fixed level (from Houk and Rymer, 1981).

A passive force should be added to this active force to take into account the passive mechanical property of the muscle. Examples of these IC curves at zero velocity are plots in figure 3.15. The

difference between these curves comes from their starting point or threshold length. If no voluntary movement is involved, the stretch reflex mechanism will maintain the movement on one of these IC. The force-length variation of a muscle which is moving voluntarily against an external load is shown with the red path in the figure. This path is generated with changing threshold length while the muscle tries to move against an external load.

In a more recent version of this model the force was scaled multiplicatively by a hyperbolic force-velocity term (Laboissière et al., 1996; Payan & Perrier, 1997). This term enhances the damping characteristics of the model:

$$F=F_{passive}+F_{active\_Feldman}*(f_1+f_2 tan^{-1}(f_3+f_4 v/l_0)+f_5 v/l_0) \qquad (3.8)$$

where l_0 is the resting length i.e. the length at which the muscle can generate its maximum voluntary force, and f_1 to f_5 are constants used to fit the force-velocity characteristics of the muscle. In this model the velocity in hyperbolic term is the current value of the velocity and not a delayed value as in equation (3.7). A 3D (force-length-velocity) comparison between the original Feldman model and this new version is provided in figure 3.16a. In the left panel (Figure 3.16b) the classic Feldman model is plotted without the velocity effect on threshold length as well as the new version. As it can be seen there are few differences between the two cases (Figures 16a and b) in the range of values reported for damping coefficient μ. As it can be seen for the new version of the model, the effect of the velocity term in displacing the threshold length can be neglected, since this effect is taken into account by the hyperbolic force term. Another comparison between the original Feldman model (with a high damping coefficient value μ) and the new version reveals that the damping effect added by the hyperbolic force-velocity term can be removed since this damping effect is already included in the original version (Figure 3.17). For this reason, it should be better to keep only one damping term.

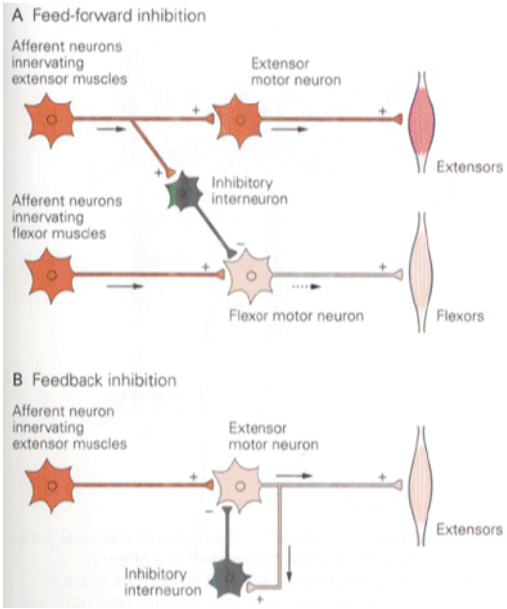

(a)

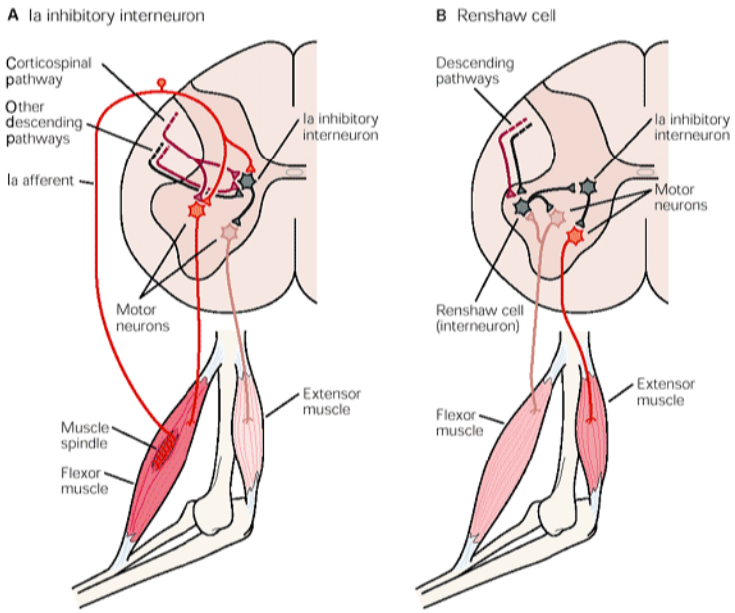

(b)

Figure 3.14 Feed-forward inhibition provided through inhibitory interneurons release the antagonist muscle and agonist muscle moves freely except against the passive property of antagonist muscle (part A in both figures); feedback inhibition through Renshaw cells controls the oscillatory movement of a muscle and protects the muscle from spasm (part B in both figures) (from Kandel et al., 2000)

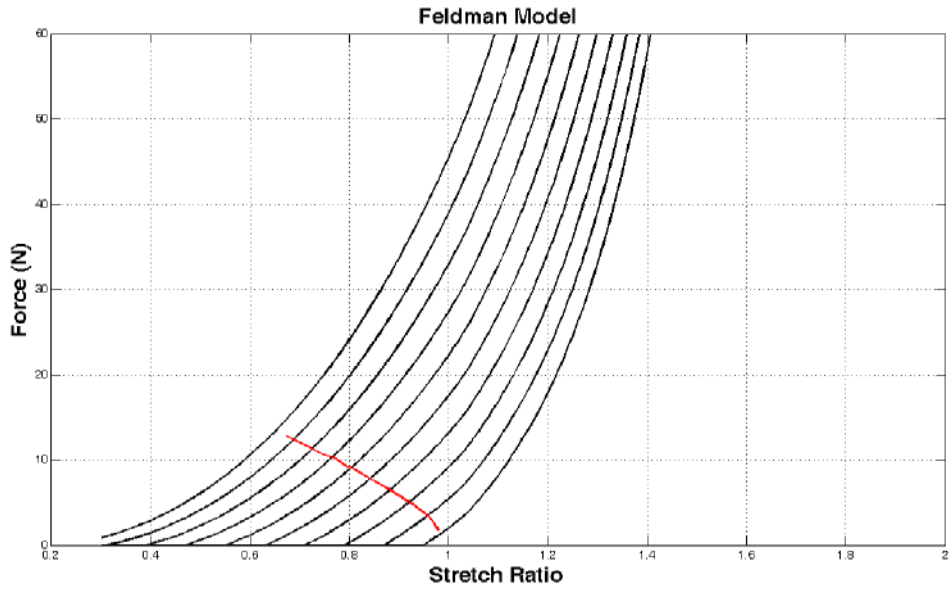

Figure 3.15 Feldman muscle invariant characteristics (IC) at a given velocity; Red path shows an example of a voluntary contraction of muscle when motor commands (starting lengths) are decreased.

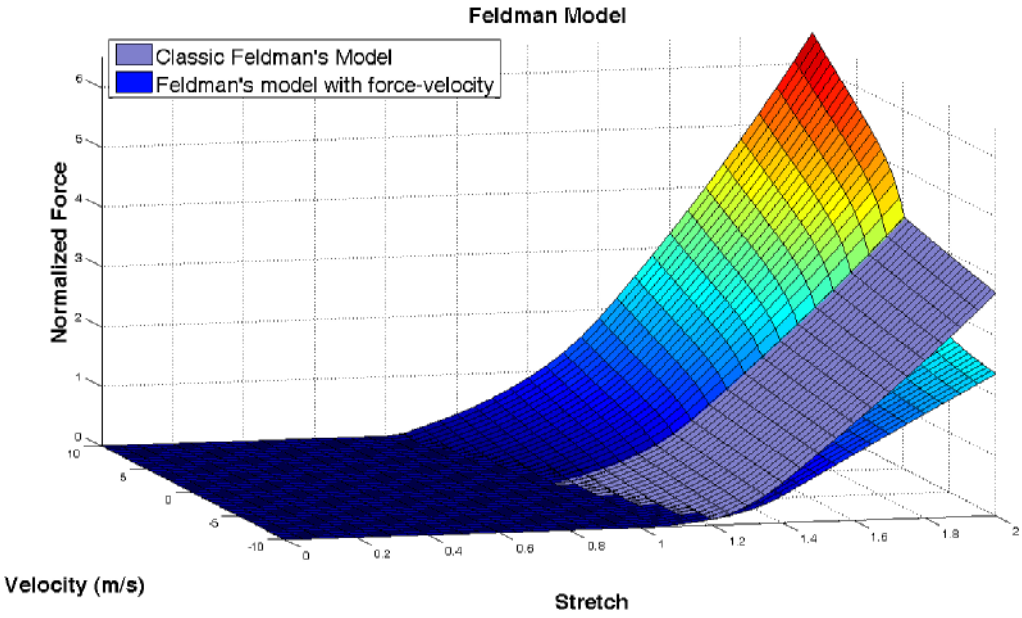

(a)

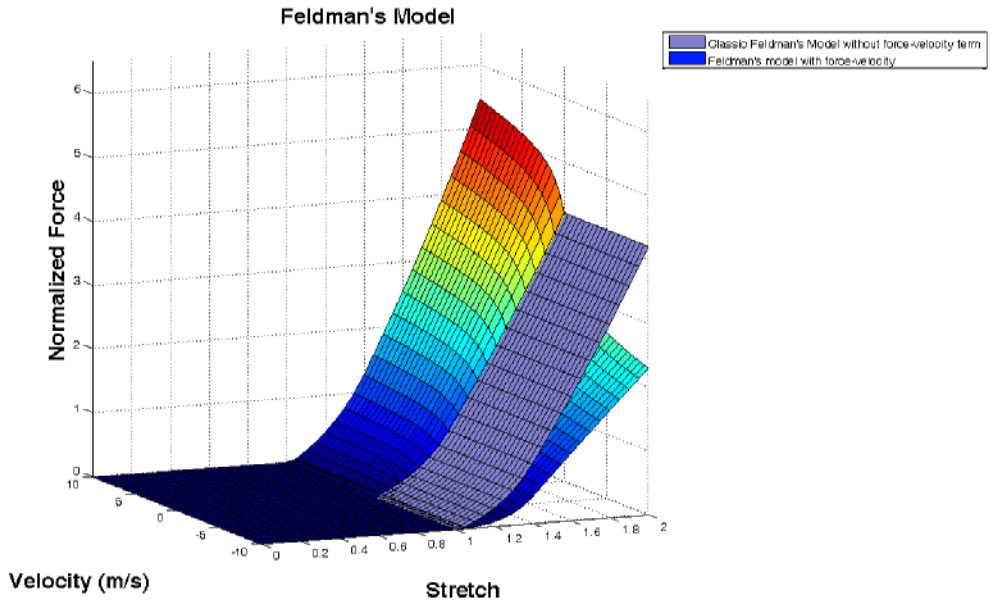

(b)

Figure 3.16 Comparison of classic Feldman model with the new version proposed by Laboissière et al. (1996) (a) new model which takes into account the effect of velocity on both starting length (b) a Feldman model without velocity effect on threshold length.

The comparison between Feldman muscle model and a Hill type muscle model (Figures 3.4a and b) is shown in Figure 3.18. As can be seen the interpretation of voluntary movement between a Feldman model and an additive hill model, especially in the concentric part, is not very different.

In the next section a distributed version of Feldman muscle model is introduced which is more suitable for the use in a discretized modeling framework such as finite element method (FEM).

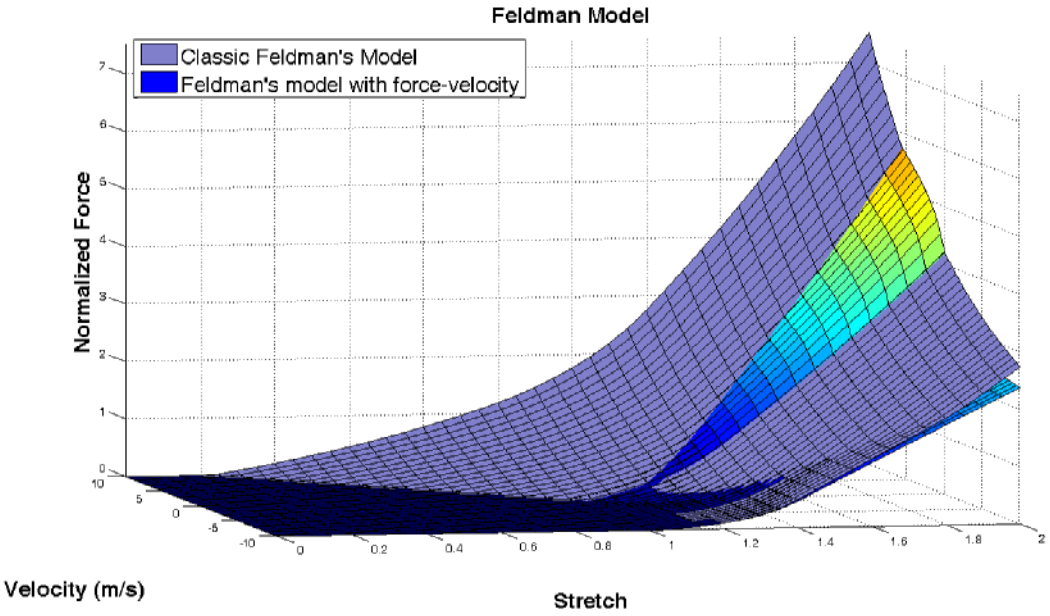

Figure 3.17 Comparison between new Feldman model with highly damped classic model; few differences are observed between a highly damped classic model and the new version introduced by Laboissière et al. (1996).

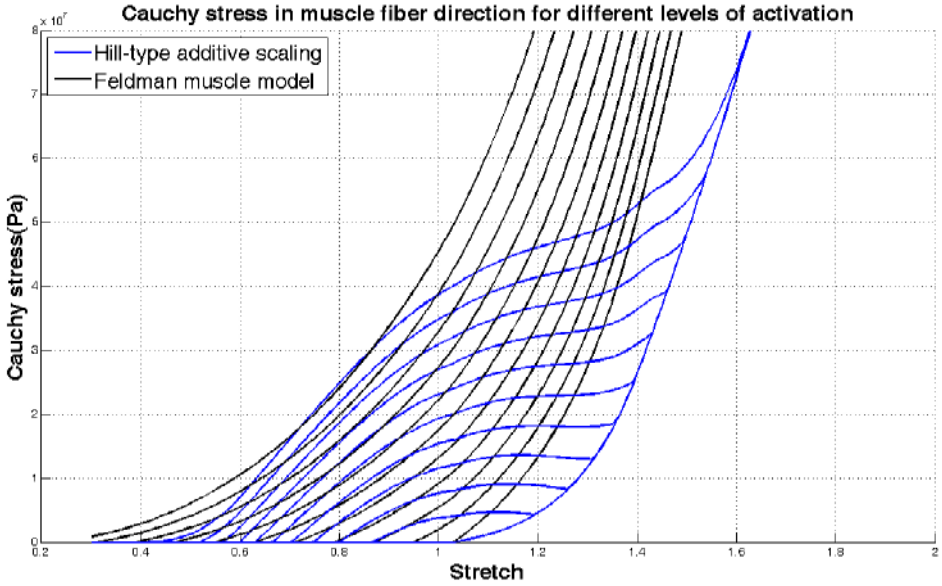

(a)

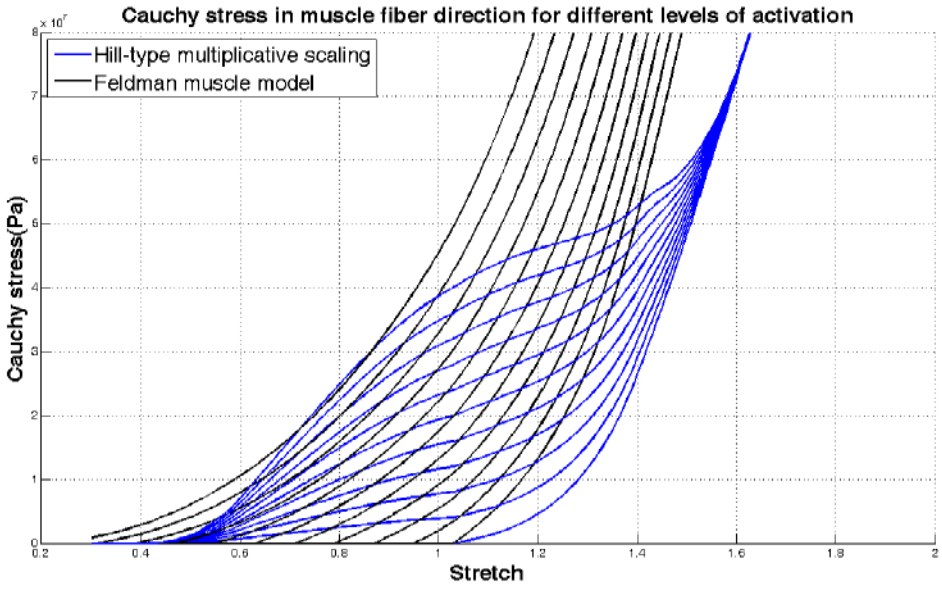

(b)

Figure 3.18 Comparison between Feldman and Hill-type model (a) multiplicative scaling Hill-type model and (b) additive scaling Hill-type model.

3.7 A Distributed Feldman Model (DFM)

Extension of a one dimensional muscle model spatially to three dimensions necessitates the design of a distributed version of that model. In a distributed model all lumped quantities are replaced with their distributions:

- force terms are replaced with Cauchy stresses which are the ratio of force in muscle fibers to their current cross sectional area ($\sigma = lim(\Delta F/\Delta A)_{\Delta A \to 0}$) ;
- length quantities are replaced with stretch values which are the ratio of current muscle lengths to their initial lengths ($\lambda = l/l_0$).

Starting from equation 3.7, the active Cauchy stress in the so-called Distributed Feldman Model (DFM) becomes:

$$\sigma_{active\_Feldman} = \sigma_{max}\,(A_{pcsa}/A)(exp([\lambda(t-t_d)-\lambda_{threshold}+\mu v(t-t_d)]^{+}\,(l_0/l_c))-1) \qquad (3.9)$$

In this relation $\sigma_{max}=F_{max}/A_{pcsa}$ is the maximum stress generation capacity of the muscle. As said above, the threshold length is replaced with threshold stretch ratio ($\lambda_{threshold}=l_{threshold}/l_0$) and the velocity term becomes the strain rate ($1/sec$).

In this form the ratio l_0/l_c shows that how many characteristic lengths are incorporated in the initial or resting length. In the literature the characteristic length varies between 9 mm (Laboissière et al., 1996) and 25 mm (Buchaillard et al., 2010) with a role that is to stabilize the model. Since this ratio l_0/l_c also influences the stiffness of the muscle during the stretch reflex action (gradient of the invariant characteristic), the ratio implicitly takes into account the type of the muscle from the speed of

contraction point of view (fast or slow muscle). It can be enunciated that when a muscle rest length contains more characteristic lengths it reacts faster.

Chapter Four: Face Model: Shaping and Dynamics[3]

"One often makes a remark and only later sees how true it is."
Ludwig Wittgenstein

In this chapter the face mesh and its properties are introduced. Following that the finite element model features is presented. The muscle modelling through cable elements and how they behave is the subject of next section. The stress stiffening effect of muscle behaviour and modelling the stiffness change of muscles due to activation is introduced next. Then the effect of dynamics on face movement and its consequence in comparison to a quasi-static one is studied. The chapter will conclude with a discussion of shaping by stiffening and its impact on lip movements during protrusion and rounding.

4.1 Face Mesh

The main mesh is a Finite Element (FE) discretization of the volume defined by the facial tissues located between the skull and the external skin surface of the face. It is based on a previous continuous face model developed by Chabanas et al. (2003) in the context of computer aided maxillo-facial surgery. The outer and inner surfaces of the mesh were extracted from a CT scan of a female adult subject. The volume delimitated by these two surfaces was then manually meshed, as regularly as possible, with hexahedral and wedge elements (Figure 4.1). Anatomically, the face can be considered as the superposition of three distinct layers of tissues, namely (from the internal to the external layer) the hypodermis, dermis and epidermis (Stranding 2005). The mesh is thus also built in three discrete layers of elements. The external one corresponds to the epidermis (very thin) and dermis parts while the two internal layers model the hypodermis, which will later include the facial musculature. The mesh is composed of 6342 brick elements (6024 hexahedrals and 318 wedges) based on 8720 nodes. In order to reduce the number of DOF during simulation the mesh was assumed to be symmetrical along the sagittal plane, which seems reasonable in the context of speech production.

4.2 Finite element model

To produce facial gestures the mesh introduced in last section is used in a finite element solver (ANSYS® software). The different parts of finite element model are explained in the following.

4.2.1 Elements and their mechanical property

A 3D solid element (SOLID185) which is an isoparametric element is assigned to elements of face. This element is a linear Lagrangian element. Nodes in this element type have three displacement degrees of freedom (translations). Element material properties are assumed to follow a hyperelastic law (Fung 1993) and to behave isotropically. A simplified 5 parameters Mooney-Rivlin model (Mooney, 1940; Rivlin, 1948) is used, which is based on a strain-energy function W defined by:

$$W=c_{10}(I_1-3)+c_{01}(I_2-3)+c_{20}(I_1-3)^2+c_{11}(I_1-3)(I_2-3)+c_{02}(I_2-3)^2+((J-1)^2/d) \qquad (4.1)$$

[3] This chapter has been published in a slightly different form in two different papers, namely Nazari et al., (2010) that focused on biomechanical aspects and general assessment of facial mimics, and Nazari et al. (2011) that focused mainly on the influence of stiffening on lip protrusion shaping and on its control for speech production.

where I_1 and I_2 are respectively the first and second invariants of the right Cauchy-Green strain tensor, Jacobian J is the determinant of the elastic deformation gradient, and $d=(1-2v)/(c_{10}+c_{01})$ with v the Poisson's ratio.

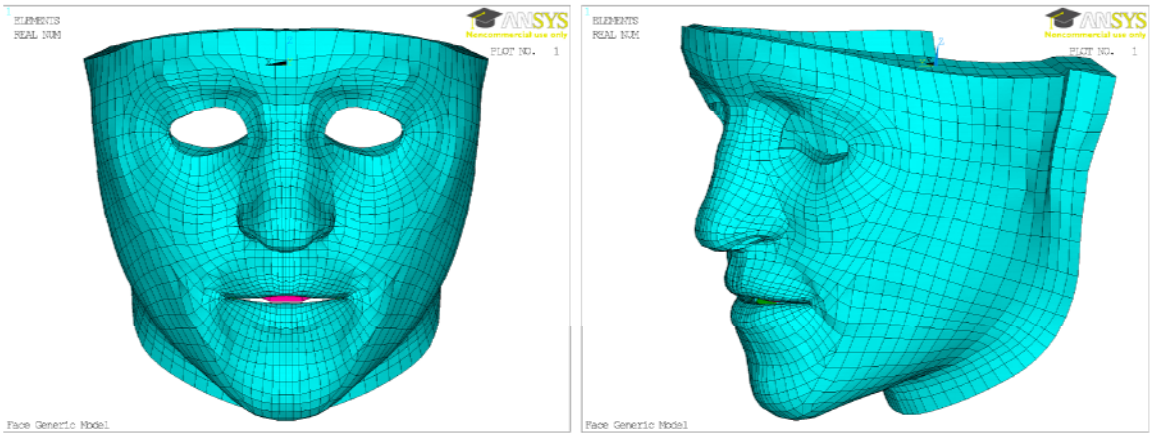

(a) (b)

Figure 4.1 Face mesh (rest position); mesh has three layers and is symmetrical with respect to mid-sagittal plane and consists of 6342 hexahedral elements and 8720 nodes, (a) front view (b) profile view.

The derivatives of W with respect to strain give stress:

$$S_{ij}=2\partial W/\partial C_{ij} \qquad (4.2)$$

S_{ij} are the components of the second Piola-Kirchhoff stress tensor and C_{ij} the components of the right Cauchy-Green deformation tensor. (A complete discussion about the related theory can be found in chapter 5).

In this model a simplified version of the strain-energy function W is used with only two constants, c_{10} and c_{20}, different from zero (Gerard et al. 2005; Buchaillard et al. 2009). According to Tracqui and Ohayon (2004), linearization of strain energy gives: $c_{10}\approx E/6$ where E is the equivalent Young's modulus. The two coefficients c_{10} and d have been calculated from the values reported in Payan and Perrier (1997), with the assumption of mechanical linearity and incompressibility of tissues, namely $E=15$ kPa and v=0.499. The c_{20} coefficient has been adapted from the values proposed for tongue tissues by Buchaillard et al. (2009) based on indentation measures from a cadaver's tongue (Gerard et al., 2005). The computed constants are shown in table 4.1.

Table 4.1 Constants of the simplified 5-parameter Mooney-Rivlin model for passive tissues

c_{10} (MPa)	c_{20} (MPa)	d (1/MPa)
2.5e-3	1.175e-3	0.8

The density of face tissues is set to $\rho=1.04E^{-6}$ kg/mm^3 (Buchaillard et al. 2006). The effect of gravity has not been considered. In fact the effect of the gravity on the body appears as a pretension effect on tissues, hence not considering the effect of gravity is equivalent to neglecting the effects of pretension.

4.2.2 Boundary conditions and contact surfaces

Nodes of the internal layer of the mesh corresponding to the face tissue attachments to the skull are fixed. The other nodes are free.
During speech and facial mimics, many contacts regions created. These regions are between the upper and lower lip, and between the lips and the teeth. They are extremely important in lips shaping. The teeth surfaces on mandible and maxilla, segmented on CT images, have been approximated with spline surfaces, and then meshed with quadrilateral undeformable elements (Figure 4.2). Contacts are handled using surface to surface contact elements which provide collision detection and sliding reaction, considered here without friction (MU=0). There is no initial interpenetration between all the contact surfaces.

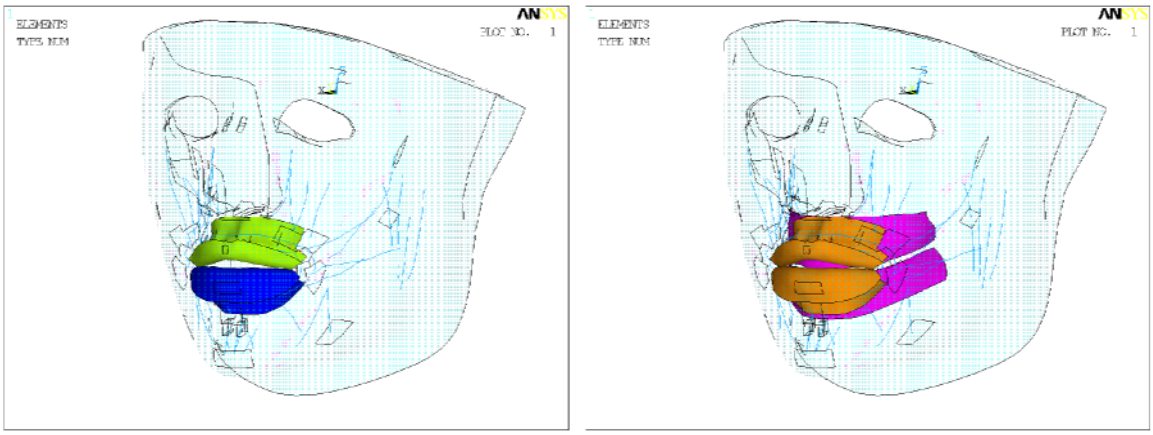

(a) (b)

Figure 4.2 Contact surfaces: (a) lip-lip contact (b) lip-teeth contact.

4.2.3 Muscle contractile fibers

The muscular structure of the face enables huge possibilities of movements, in speech, eating and facial expressions, with a great dexterity. Its complex structure can be divided in two groups of muscles (Stranding 2005). Muscles of mastication are the deep, strong muscles that generate the movement of the mandible. Since the mandible is not handled yet in our modelling, we have only focused on the other group, the muscles of the lip region, namely the superficial muscles involved in facial mimics (Hardcastle 1976). Most of them are bilateral, symmetrical, gathered around the lips with one bony insertion and the other within the facial tissues. A notable exception is the orbicularis oris, a specific constrictor muscle embedded in the lips without bony insertions.
In order to ensure anatomical and physical reliability, muscles courses and insertions were directly defined from medical images and anatomical charts, with the help of a maxillofacial surgeon.

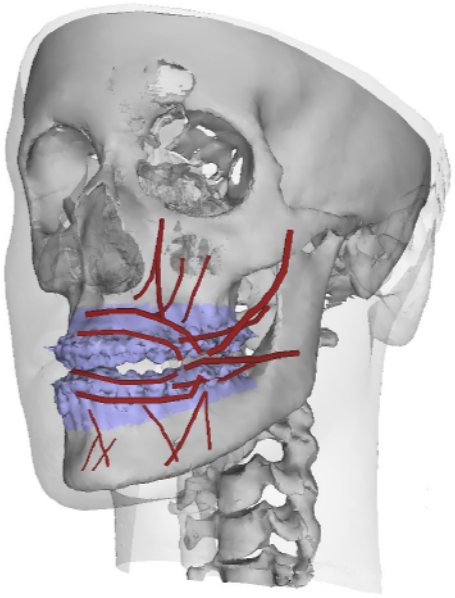

(a)

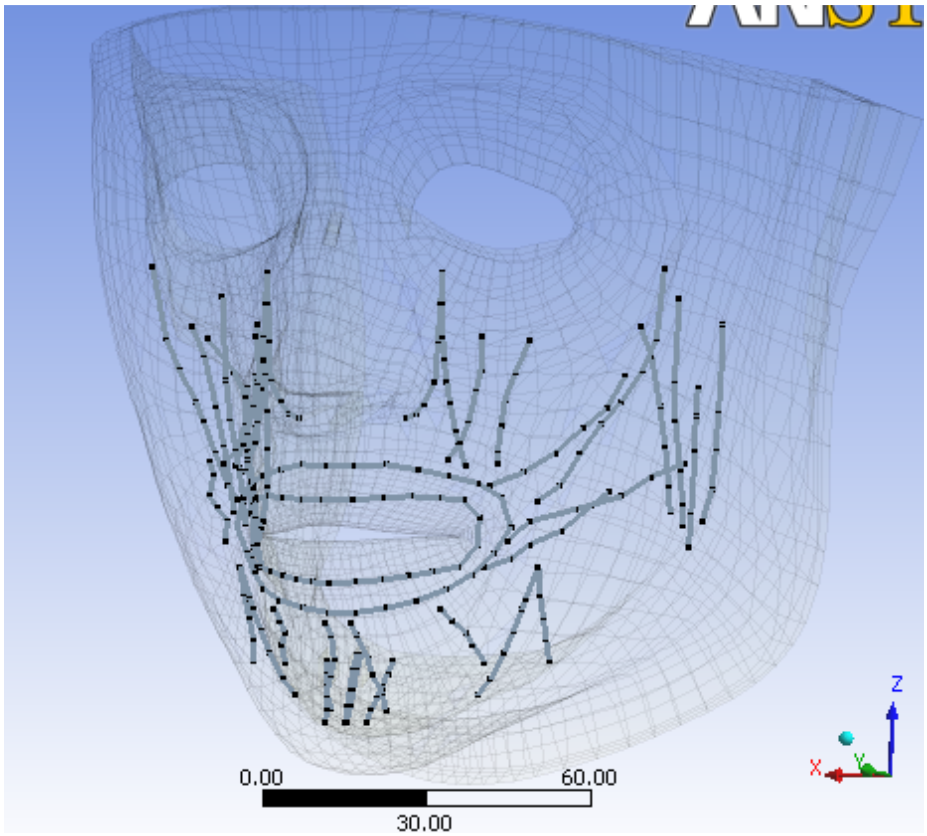

(b)

Figure 4.3 Macrofibers of orofacial muscles extracted from CT data shown on (a) CT scan (b) face mesh.

Table 4.2 Orofacial Muscle fibers for half of the face

Muscle Name	Abbreviation	Number of Fibres	Total Number of Cable Elements
Levator Labii Superioris Alaeque Nasi	LLSAN	2	12
Levator Anguli Oris	LAO	1	9
Zygomaticus (major and minor)	ZYG	2	15
Risorius	RIS	1	6
Buccinator	BUC	2	12
Depressor Anguli Oris	DAO	2	12
Depressor Labii Inferioris	DLI	2	11
Mentalis	MENT	2	11
Orbicularis Oris Peripheralis (Inferioris and Superioris)	OOP	2	14
Orbicularis Oris Marginalis (Inferioris and Superioris)	OOM	2	14

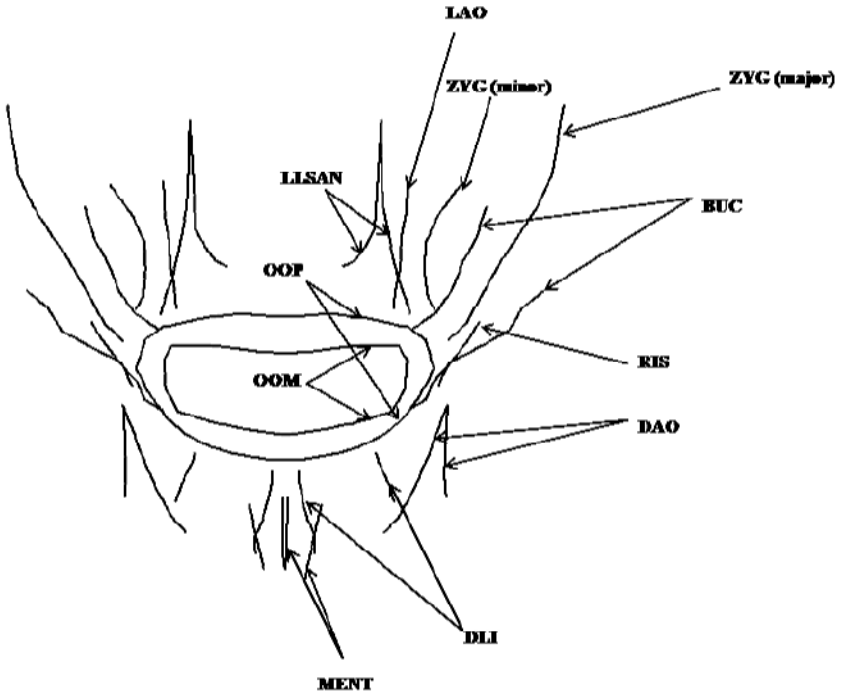

Figure 4.4 Naming of orofacial muscle fibers.

The locations of points describing the muscle fibres were measured in the different CT scan slices. The number of fibres per muscle depends on its extent and size. Figure 4.3 and table 4.2 show the ten orofacial muscles that are modelled. In figure 4.4 naming of the muscle tracks is shown.

Muscle fibres are embedded in the facial mesh as continuous sets of uniaxial cable elements. Since each cable is a line in 3D space, their number per fibre increases as a function of the muscle fibre curvature, to model this curvature smoothly. These cable elements (LINK10 in ANSYS®) act in tension only and will become slack under compression. Such properties are consistent with the

observations that in the fibre direction a muscle can resist only tensile forces and not compressive forces (Loocke et al. 2006).
End points of the cable elements are defined independently of the level of refinement of the main mesh. They correspond to anatomical landmarks located in reference to the skull. This approach enables to refine or modify the mesh without requiring any change in the definition of muscle courses. To couple the fibres with the main mesh, *point to surface* contact elements are used. The *points* (pilot nodes) are the extremities of the cable elements. They are bilaterally linked to the *surfaces* of the mesh elements which their centroids are the closest to the cable extremity. Figure 4.5 displays the cable elements and the corresponding coupling elements for the muscles in half of the face. The no-displacement boundary condition is also applied to the ends of cable elements that correspond to the muscles insertions on the skull.

4.2.4 Loading: Muscle activation

The cable elements generate the active force F_{active} of each muscle, following the relation:

$$F_{active}=AE_{cable}(\varepsilon-\alpha\Delta T) \qquad (4.3)$$

where A is the cable cross sectional area, ε its strain, and E_{cable} its Young's modulus. In standard ANSYS ® use, parameter T is equivalent to the temperature of the element, and α to the thermal coefficient of expansion of the cable. In our case, we have used parameters T and E_{cable} to specify the *level of activation*. Parameter E_{cable} is a scaling factor specifying the gradient of muscle force. E_{cable} is increasing in parallel to activation to simulate the muscle behaviour as close as it possible.

Figure 4.5 Coupling elements between the piece-wise fibres of cable elements and the main mesh.

Parameter T is used to control the *level of activation* within the muscle specific maximal range of variation. Thus, parameter T can be considered as a *normalized control parameter of muscle activation*. Decreasing T leads to a shortening of the cables lengths, which therefore exert forces on the main mesh through the coupling elements. The activation level is then a decreasing function of parameter T. The value of α is arbitrarily set to 0.001. This muscle model is a type of adjustable starting length (see chapter 3) model. The force in the muscle varies linearly with respect to length and it can be called a sliding spring model (Shapiro & Kenyon, 2000) (Figure 4.6). Setting the parameter T specify the starting point on horizontal axis or zero-force length of muscle. The final force in muscle in a pseudo-static analysis is equal to the force generated in surrounding tissues due to their passive mechanical property. The intersection of blue curves and red curve shows the stress-stretch relation that the muscle produces in a voluntary action. Of course this path in a dynamical process, including inertia and damping, won't be like that. Since in a dynamical process muscle force should overcome both surrounding tissues resistance and dynamical loadings.

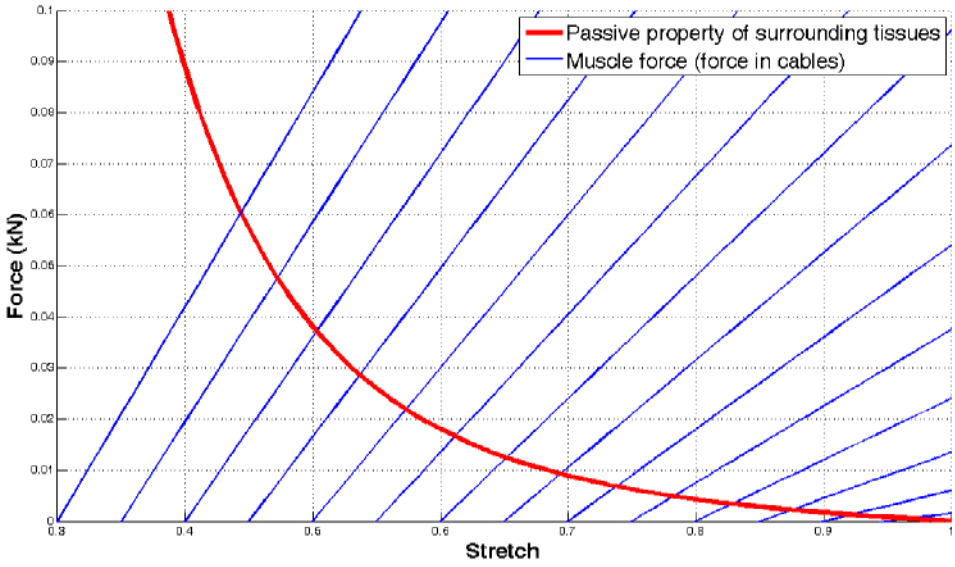

Figure 4.6 Muscle model; the force in the muscle varies along straight lines (blue lines) and the final muscle force in a pseudo-static analysis is equal to force in surrounding tissues (intersection of blue lines with red curve).

4.3 Stress stiffness effect and its implementation in muscle model

Muscles behave like a transversely isotropic material, with an isotropic behaviour in the directions orthogonal to the muscle fibres. This means that mechanical properties in the direction of muscle fibres are different from the ones in the cross-fibre direction. Due to force generation in the fibres direction and to the fibres tensile characteristics, the transversal bending stiffness increases with the tensile force (similarly to the stress stiffening phenomenon in cable members or membranes).
This is illustrated in Figure (4.7) with a simple example of a virtual point P inside a muscle fibre originally at equilibrium under constant muscle activation (force F_1) and then displaced (by δ) because of the action of a force F applied in the muscle transversal direction. Once the new equilibrium is reached (Figure 6 lower panel), assuming a linear relationship between force and displacement, we have:

$$F=2F_1(\delta/l_1)(1/\sqrt{(1+(\delta/l_1)^2}) \qquad (4.4)$$

This means that, when δ is negligible as compared to l_1 the muscle transversal stiffness $dF/d\delta$ is proportional to muscle force F_1.
When a muscle is activated, its fibres generate forces that resist to elongation, according to a certain tension-length relation (see chapter 3), and in a way that increases when activation increases. In real muscle the fibres distribution is so dense, that the resistance to elongation of the whole muscle body increases with elongation in the fibres direction. In our model, muscle fibres are not represented in all their details. They are modelled by a limited number of *localized* macrofibers (typically from one to three). When the muscle is activated, each of these macrofibers generates a force and resists to the

elongation, but since the fibres are localized, this resistance does not apply to the whole body of the muscle.

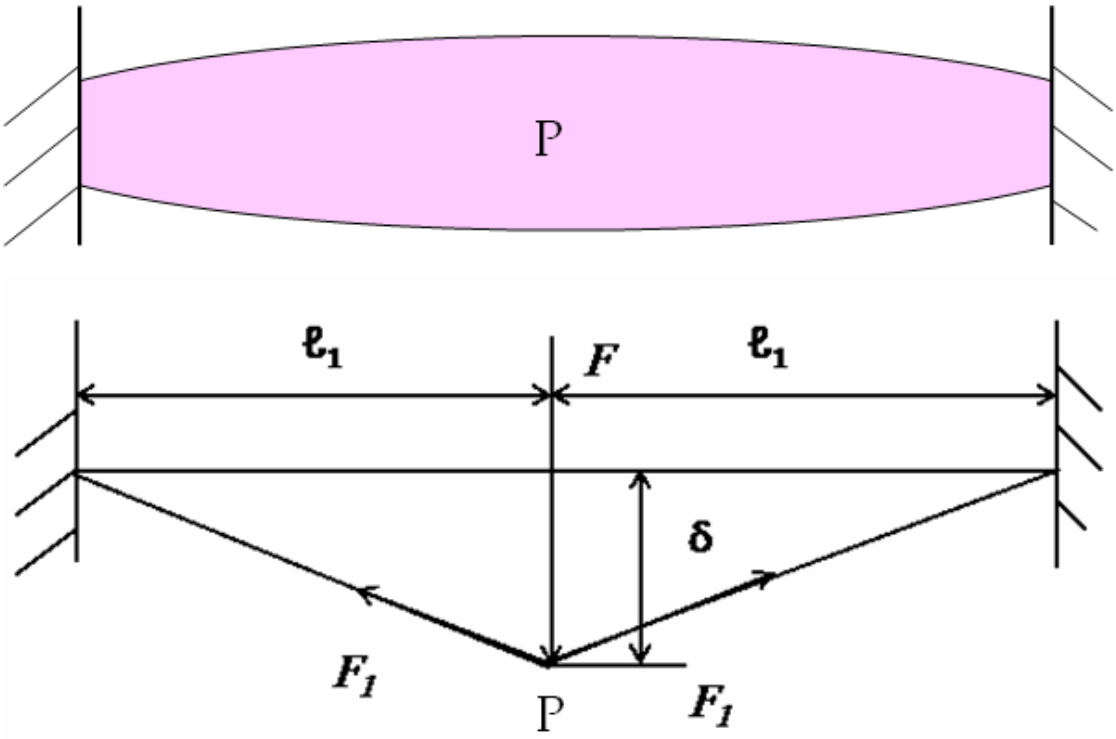

Figure 4.7 Stress stiffening effect; the horizontal tension F_1 in the member increases its stiffness in transverse direction.

This would not be a realistic behaviour. In order to compensate for this drawback, the stiffness in the body elements of the muscles increases with muscle activation in the fibres directions. Hence, muscle activation is associated both with a resistance to stress in the direction orthogonal to the fibre direction (the stress stiffening effect) and with a resistance to elongation in the fibre direction. Consequently, it is modelled by an isotropic increase of the tissues stiffness, implemented by modifying the parameters of the passive constitutive law (equation (4.1)).

4.3.1 Muscle region: neighbourhood algorithm

Once the fibres are set, the body of the muscles can be defined in the main mesh. A neighbourhood is determined around each fibre by an algorithm considering a sphere, which radius is equal to an estimation of the muscle cross-sectional dimension, running along the cable elements lines. Each element of the main mesh intersecting the sphere is then labelled as a part of the muscle body. The resulting bodies of the muscles in the mesh are displayed in Figure 4.8 for the left half of the face. Although this definition of the muscle body is a rough approximation, it is enough so far for our use, which is to account for the stress stiffening effect.

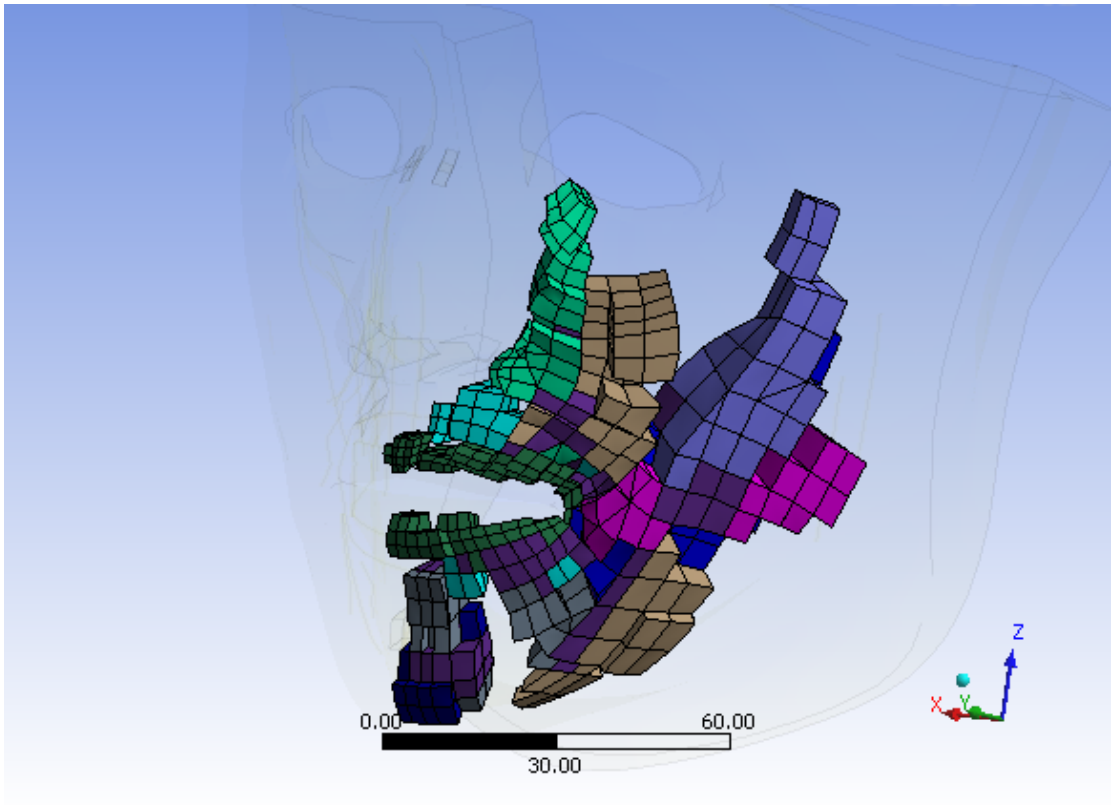

Figure 4.8 Muscle regions (half of face); the elements surrounding a cable in a spherical neighbourhood are assigned as corresponding muscle region.

4.3.2 Modelling muscle's stress stiffening effect

To account for the stress stiffening effect, the constitutive law of the elements of a muscle body varies with the level of muscle activation specified with T. In agreement with Buchaillard et al. (2009), parameters c_{10} and c_{20} of the passive hyperelastic law are hence linearly scaled as an increasing function of the activation, which is a decreasing function of T (Figure 4.9). When different muscles are activated simultaneously, the stiffness of the main mesh elements which are common to these muscles' bodies change as a function of the most activated muscle, and not as the result of an accumulation of the stiffness changes associated with each individual muscle activation. The proposed stress stiffening modelling is functionally correct, except for the resistance to compression in the fibres direction. Indeed, it is known that this resistance varies with the strain rate and is close to zero when this rate is low (Loocke et al. 2006). Further improvements will be provided along this line in future works.

The muscle activation varies in time as a ramp function. In further works that we will develop in the context of speech production, these commands will be handled by a motor control mechanism integrating voluntary commands and low-level feedback information sent by the muscles (Feldman 1986; Buchaillard et al. 2006).

This mechanism of modelling muscle activation is shown in Figure 4.10. As muscle cables are activated they introduce compressive stress in surrounding tissues. In Figure 4.10 the red curves show the compressive part of curves shown in Figure 4.9. In a pseudo-static problem the muscle force is equilibrated with force in surrounding tissues. The intersection of blue and red curves shows the path of a voluntary action (compare with Figure 3.15). In this case the intersection of these curves does not

stay on one red curve because the mechanical property of surrounding tissues increases when activation increases (going to the left).

In the presented simulations, the activation parameter T is incremented as a staircase function of the time, so approximates a linear variation. Since we want to focus on orofacial gestures at the end of the movement and not on its time variation during the movement, this simple approach of staircase activation seems appropriate. Different amplitudes of the T variation were tested in the simulations: c_{10} and c_{20} are multiplied by a factor ranging from 1 (no change in stiffness) to 10 (strong increase in stiffness). Hence, in our simulations two degrees of freedom are manipulated independently: the amplitude of the global change in T and the global increase in stiffening. This approach enables the influence of two factors to be determined independently: the amplitude of the activation and the amplitude of the associated stiffening. It is important to clarify that this approach was set up in order to study the response of the model to different activation/stiffening conditions, and not in order to account for any physiological process in which stiffening and activation would be decoupled.

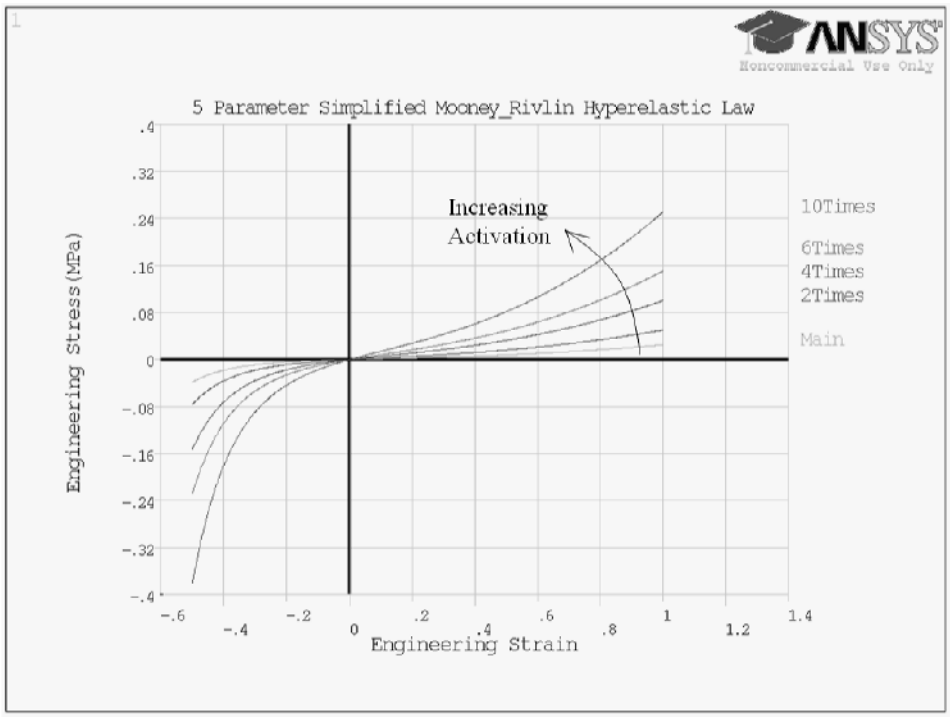

Figure 4.9 With increasing the activation (starting length of muscles) the mechanical properties of surrounding elements of muscle region increase.

4.4 Damping model: proportional damping

For dynamic transient analysis, viscosity is modelled using proportional damping:

$$\boldsymbol{C}=\alpha\boldsymbol{M}+\beta\boldsymbol{K} \qquad (4.5)$$

To determine α and β coefficients the first 7000 modes of the main mesh (about a third of the total number of free degrees of freedom) were calculated. Simulations were run twice, first with the material stiffness used in the absence of muscle activation and then for a high material stiffness level (10 times

more). The corresponding natural frequencies vary from 0.5 Hz up to 15 Hz. Within this interval, parameters α and β have been tuned such that the damping ratio (ratio of viscous damping factor to critical damping) is larger than and near to one. The computed values are $\alpha=19\ sec^{-1}$ and $\beta=0.055\ sec$.

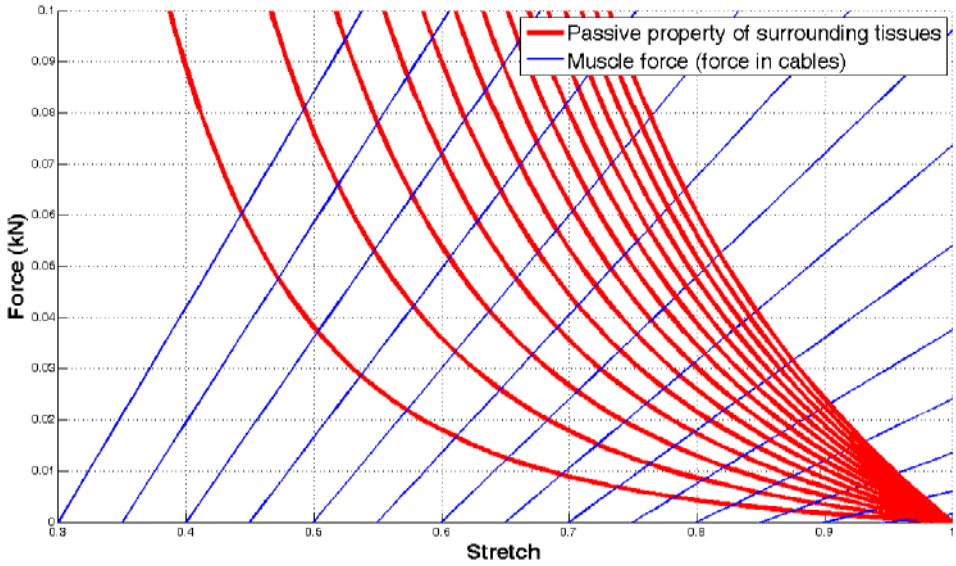

Figure 4.10 Muscle model with stress stiffening effect; with increase of activation in muscle (muscle starting length) the passive property of surrounding tissues (red curves) increases to model the stress stiffness effect.

4.5 Simulations and results

Different muscle activation patterns have been used and their influences on facial gestures and mimics evaluated. Both static and transient analyses have been performed. In addition to the static analysis that takes into account only the stiffness matrix, dynamic simulations obtained with full transient analysis also takes into account the effect of inertia and viscosity.

4.5.1 Simulation of facial mimics[4]

Activation of muscles taken individually and in coordination has been investigated. In this section, only the final shapes of the mesh resulting from these activations are shown. They are the same for the static and the full transient analysis. These results well comply with the anatomical predictions in the related literature (Standring 2005).
The result of activating zygomaticus draws the angle of the mouth upwards and laterally (Figure 4.11).

[4] Results in this section have been published in Nazari et al. (2010).

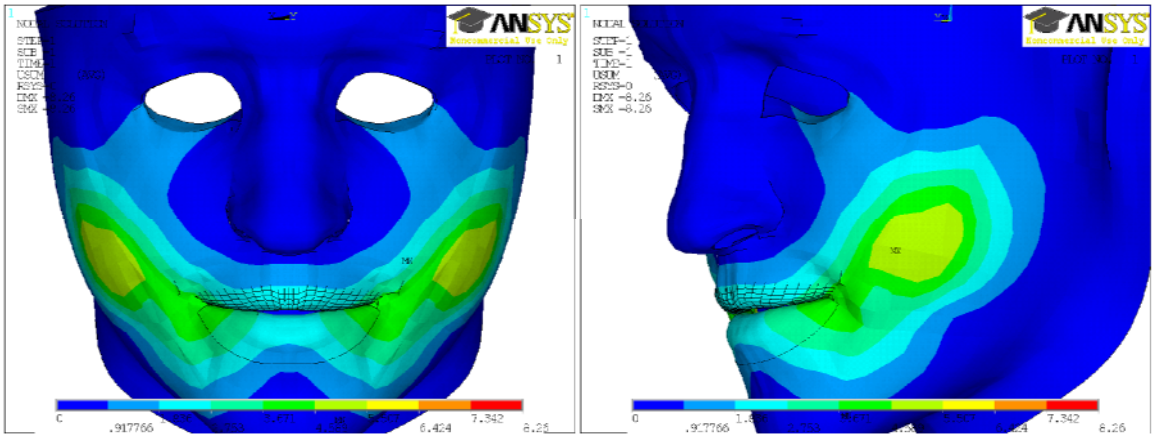

(a) (b)

Figure 4.11 Face shaping after activation of the zygomaticus muscle.

Levator labii superioris elevates the upper lip. Acting with other muscles, it modifies the nasolabial furrow. In some faces, this furrow is a highly characteristic feature often deepened in expressions of sadness or seriousness. The activation of the levator labii superioris with zygomaticus and levator labii superioris alaeque nasi in Figure 4.12 well satisfies that hypothesis.

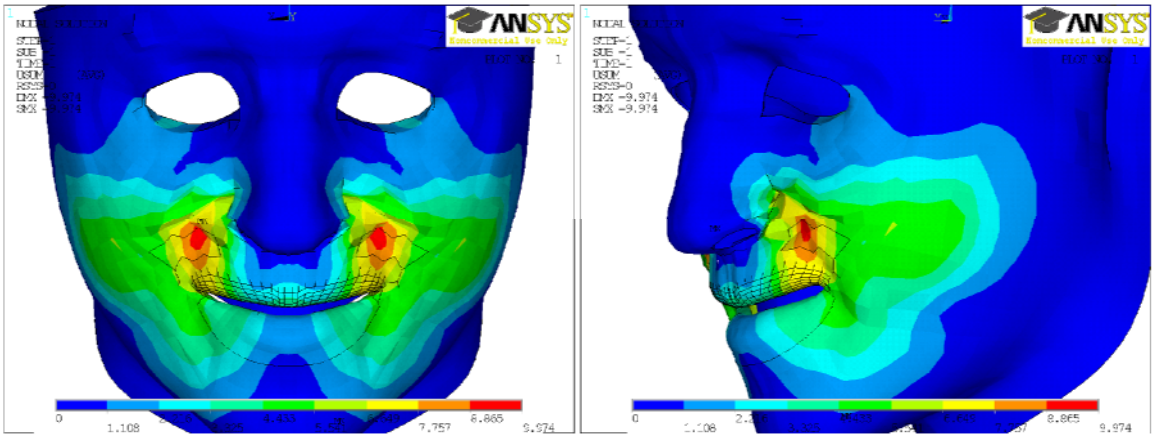

(a) (b)

Figure 4.12 Face shaping from coordinate activation of the zygomaticus, levator labii superioris alaeque nasi and levator anguli oris muscles.

The effect of orbicularis oris peripheralis (OOP) in protruding and rounding the lips has been shown (Figure 4.13). The effect of stiffening in producing rounding with protrusion will be discussed in section *4.5.3 shaping by stiffening.* Without the stiffening, lips are protruded but the amount of lip opening is too large.

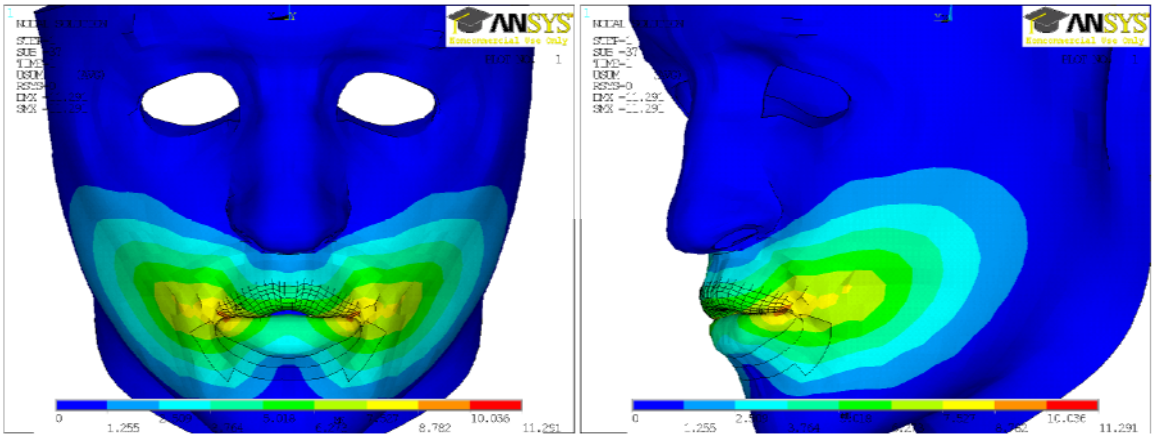

(a) (b)

Figure 4.13 Face shaping resulting from the orbicularis oris peripheralis activation.

Figure 4.14 shows the consequence of the activation of the risorius and Figure 4.15 the impact of activation of the buccinator (BUC). In Figure 4.16 the mimic associated with the coordinated action of OOP and BUC is illustrated. In all these figures these actions are qualitatively consistent with predictions made from anatomical knowledge.

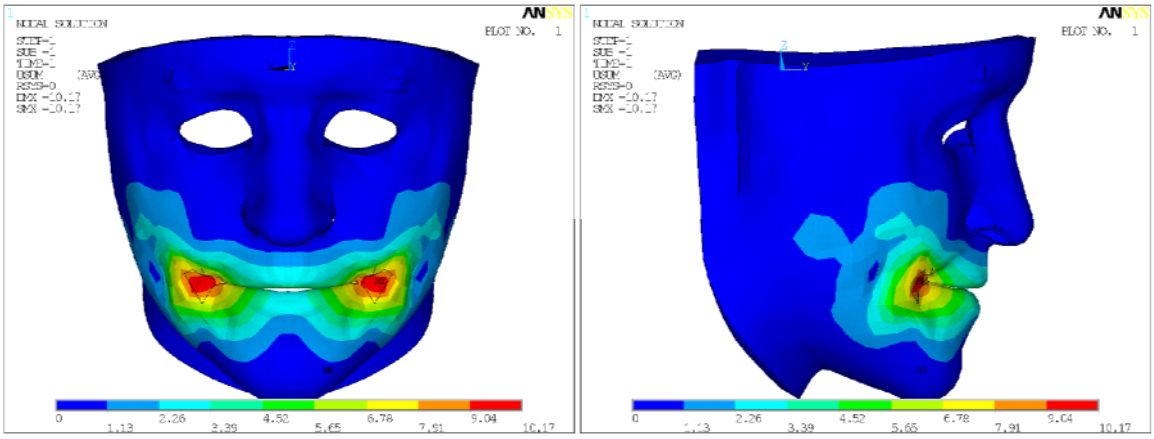

(a) (b)

Figure 4.14 Face shaping resulting from the risorius activation.

The risorius is known to stretch the mouth laterally and to retract the corners of the mouth. This is consistent with the strain depicted in Figure 4.14.The buccinator has no or little influence on the lips, and essentially compresses the cheeks against the teeth (Blanton et al. 1970). Our simulation matches quite well these expectations (Figure 4.15): the lips have the same shape as in our model at rest, while the strain essentially affects the lower part of the face.

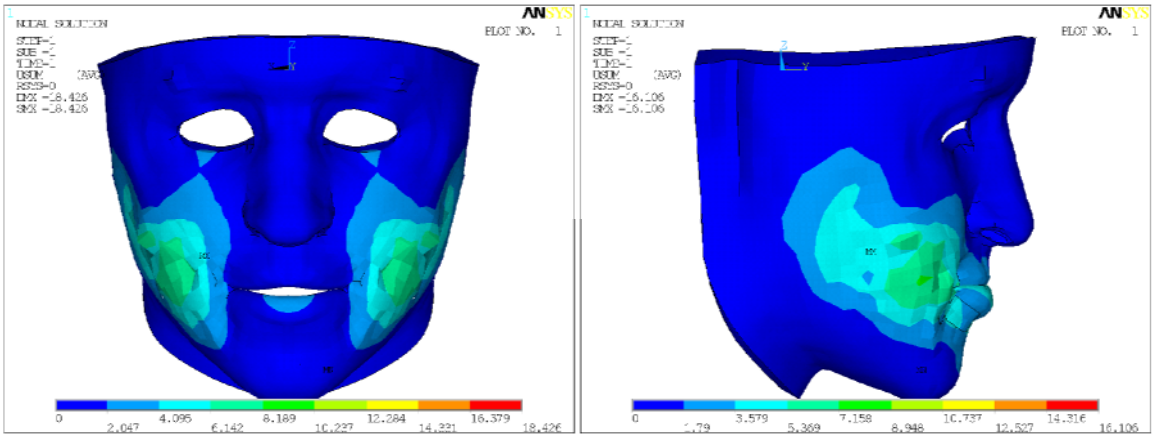

(a) (b)

Figure 4.15 Face shaping resulting from the buccinator activation.

The OOP has been shown in our model to generate a protrusion and a closing of the lips which is consistent with usual hypotheses in the literature (Gomi et. al 2006; Nazari et. al 2008). Meanwhile, the coordinated action of the buccinator and the OOP generates a closing of the lips only. It can be assumed that the stiffening of the cheeks due to the buccinator activation limits the amplitude of the lip protrusion, which would explain that mainly closure is observed.

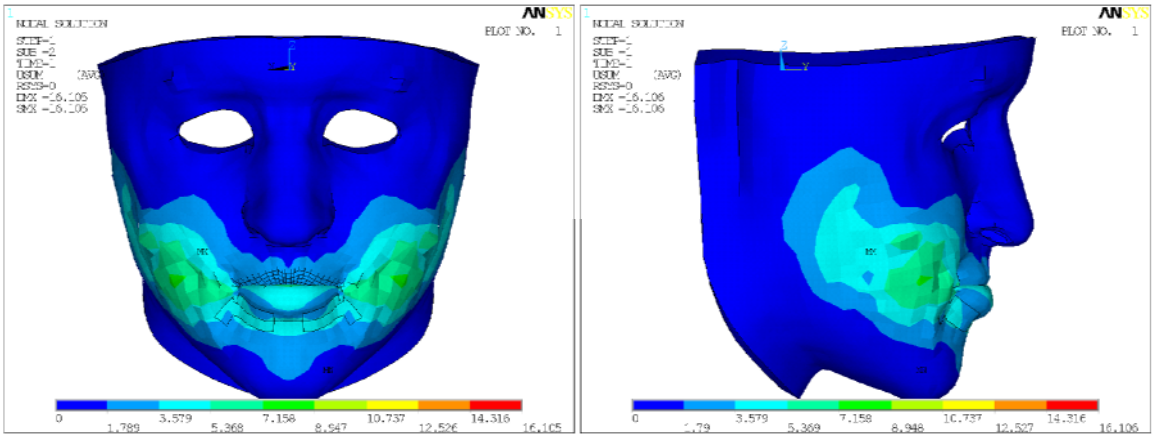

(a) (b)

Figure 4.16 Face shaping resulting from the orbicularis oris peripheralis and buccinator co-activation.

4.5.2 Dynamics versus Quasi-static simulations[5]

We have studied the effect of dynamic versus quasi-static analysis on the lip protrusion. For this purpose both OOP and mentalis (MENT) muscles are activated. The same activation level in both dynamic and static analyses is assumed. Figure 4.17 shows the trajectories, for both conditions, of a node located on the lower lip in the midsagittal plane.

[5] Results in this section have been published in Nazari et al. (2010).

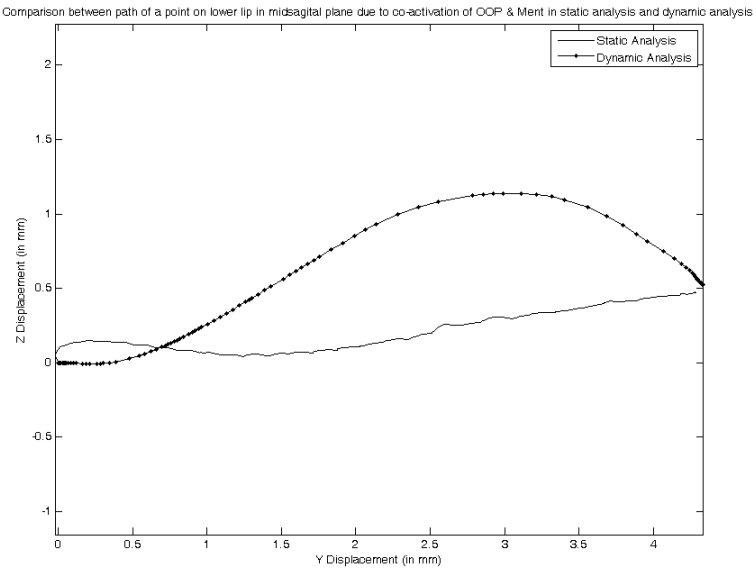

Figure 4.17 Comparison between the trajectories of a point on the lower lip in the mid-sagittal plane in static and dynamic analysis resulting from an orbicularis oris peripheralis and mentalis co-activation (with E_{cable}=0.3 and T=-500 with spherical neighbourhood radius for OOP 3mm and for MENT 2 mm).

While starting and ending points are the same in static and dynamic analysis, the trajectories are clearly different. The trajectory obtained with the static analysis is close to a straight line while the dynamic trajectory is noticeably curved. This difference is large enough to generate significant differences in lip shape variation from the starting point to the ending point, and then to significantly influence the acoustic signal. In addition, a large number of human skilled movements have been shown to follow curved path (Morasso, 1981). Figure 4.18 shows the tangential velocity profile for the same point together with the corresponding activation signal. An asymmetrical bell-shaped velocity pattern is generated. This kinematic pattern is typical for lip movements as shown for example by Shaiman et al. (1997) for several American English speakers. An asymmetrical bell-shaped velocity pattern is generated. This kinematic pattern is typical for lip movements as shown for example by Shaiman et al. (1997) for several American English speakers. Both properties, the curved path and the bell-shaped velocity profiles, observed in experimental studies and accounted for in dynamic analysis and not in quasi-static analysis demonstrates the necessity to integrate dynamic factors, such as inertia and damping, to obtain realistic simulations of lip shape variations in speech production.

To assess more precisely the realism of the trajectories produced by our model, they can be compared to lips trajectories measured with video processing (Abry et al. 1996) from a native speaker of French. As an illustration, let us consider the sequence /iRy/ embedded in the carrier sentence‘Tu dis “ruise” (/tydiRyiz/, you’re saying “ruise”, /). These data was processed with a low-pass linear phase filter (cut-off frequency 6 Hz). The trajectory of a point located on the lower lip in the mid-sagittal plane has been extracted in the temporal section corresponding to lip protrusion from /i/ to /y/ (Figure 4.19). It can be observed that the path of this point is qualitatively similar to the path simulated with dynamic analysis (Figure 4.17). More specifically, the path is curved, a key feature that could not be predicted from the pseudo-static analysis.

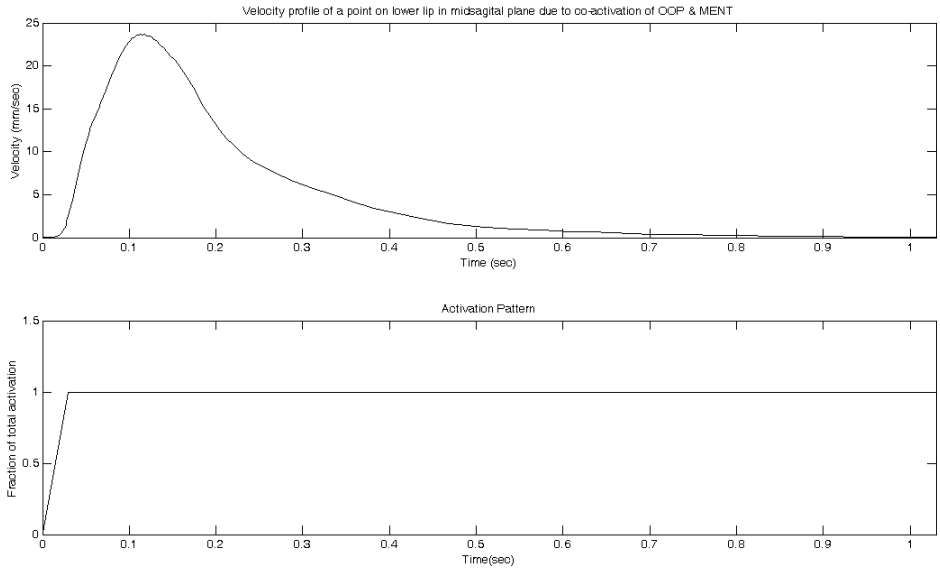

Figure 4.18 Upper panel: Velocity profile of a point on the lower lip in the mid-sagittal plane resulting from the co-activation of orbicularis oris peripheralis and mentalis in dynamic analysis. Lower panel: Time patterns of the corresponding activations. (with E_{cable}=0.3 and T=-500 with spherical neighbourhood radius for OOP 3mm and for MENT 2 mm).

Figure 4.20 shows the experimental velocity profile: it has, like our simulation, an asymmetrical bell-shape in agreement with Shaiman et al.'s (1997) data collected from speakers of American English.
This example of a comparison between simulations and real data confirms the general observation made above: contrary to those obtained in the quasi-static analysis framework, the simulations obtained in the dynamic analysis framework generate curved paths and bell-shaped velocity profiles similar to those observed in experimental lips protrusion movements collected during speech production
The experimental movement and the simulation in dynamic analysis have also similar ranges of velocity (maximum velocity 3.9cm/s *versus* 2.4cm/s), durations (200ms *versus* 270ms at 20% of the peak velocity), and movement amplitudes (4.5mm versus 4mm for the horizontal protrusion). Some discrepancies can be noticed between simulations and experimental data. In the experimental data, the curved path includes a rising part followed by a short decline. In the simulation this rising/declining sequence is also observed, but it is preceded by a horizontal part. It is important to state that these differences are not intrinsically due to the characteristics of the model but more factually, to differences between the conditions of simulation and the conditions of real speech production. In the simulations the movement starts from a zero velocity position and ends at a zero velocity position, while experimental data were extracted from a longer speech continuum (Figure 4.19) in which the observed section does not start or end with a zero velocity position.

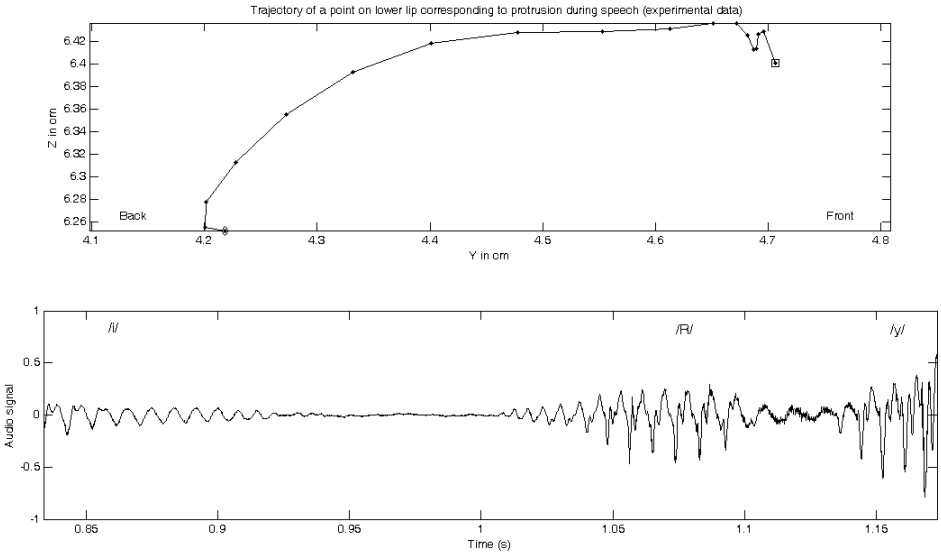

Figure 4.19 Experimental data. Top panel: trajectory of a point on the lower lip in the mid-sagittal plane in /iRy/ sequence; diamond mark is for the starting point and square mark for the ending point. Bottom panel: corresponding acoustic signal with phonetic labelling.

This phenomenon can be clearly seen in the experimental velocity profile (Figure 4.20), in which velocity curve never crosses zero.

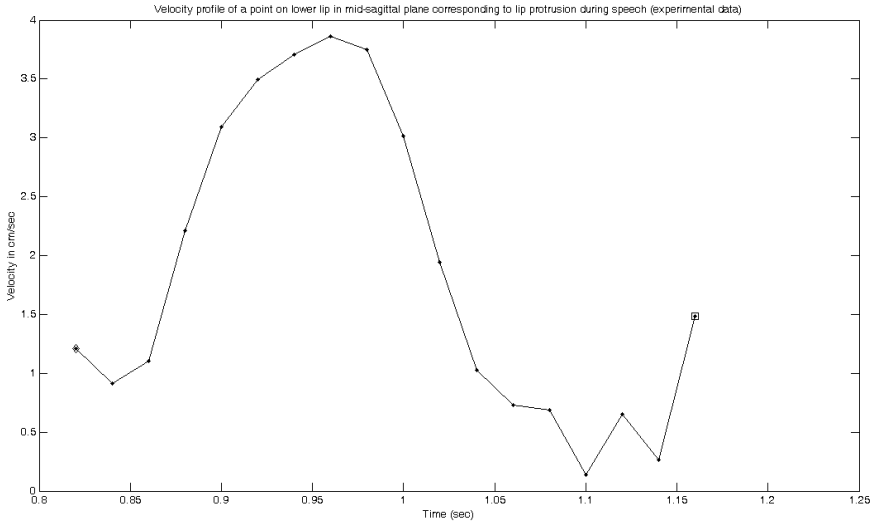

Figure 4.20 Experimental data. Tangential velocity profile corresponding to trajectory and the acoustic signal displayed in Figure 4.19.

4.5.3 Shaping by stiffening[6]

Static and full transient analyses were carried out in order to test the realism of the model's behaviour in response to various muscle activation patterns. In addition to the impact of tissue elasticity, the transient analysis takes into account the effect of inertia and gravity as well as the effect of viscosity. Special attention is devoted in this paper to lip protrusion and lip rounding gestures, which are basic speech gestures associated with the phonetic characteristics "rounded" *versus* "spread" lips (IPA *Handbook,* IPA, 1999). Classically these gestures are analysed in the literature as being generated mainly with the activation of the Orbicularis Oris (OO) (Delaire, 1977; Abry et al., 1980; Standring, 2005). So far, to our knowledge, biomechanical models have not been successful in modelling lip rounding in a realistic way. To study the potential contribution of muscle stiffening to the achievement of this gesture, simulations were run with and without the changes in the constitutive law associated with muscle activation.

Figure 4.21 shows the final lip shape obtained without accounting for the stress stiffening effect (multiplication factor of c_{10} and c_{20} is equal to 1).

To observe the effect of stiffening the same simulation was run with the same activation level and the same timing on face model for the activation of the OOP associated with the largest stiffening value (multiplication factor of c_{10} and c_{20} is equal to 10) (Figure 4.22). As compared to Figure 4.1 (rest position), both figures show a clear protrusion and a reduction in lip area. This reduction is less strong though without stiffening, mainly because the lip height is significantly larger. The lip shape achieved without stiffening does not correspond to a prototypical protruded/rounded shape, mainly because of this large lip height value.

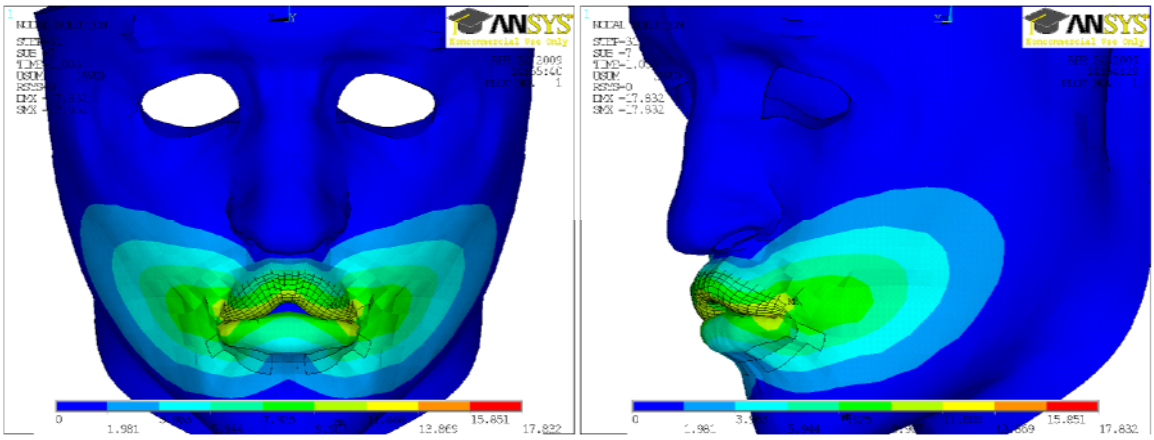

(a) (b)

Figure 4.21 OOP activation without stiffening (a) front view, (b) profile view.

[6] Results in this section has been published in Nazari et al., 2011

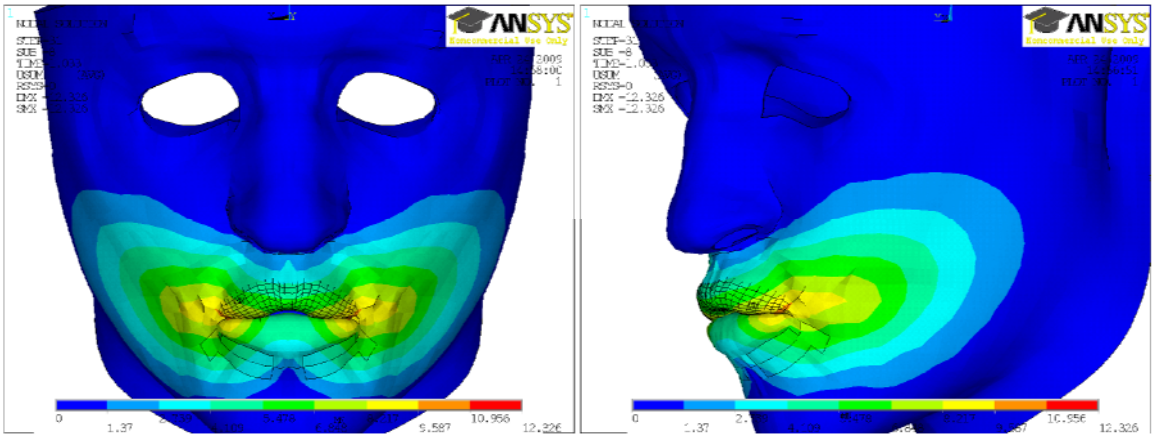

(a) (b)

Figure 4.22 Activation with maximal stiffening (same activation as in Figure 4.21) (a) front view, (b) profile view.

Variability of lip shaping due to the different simulated conditions is measured using the parameters proposed by Abry & Boë (1986). A description of these parameters in profile view and frontal view is shown in Figures 4.23 and 4.24 respectively. They measure the amplitude of the protrusion (lip horn depth, lip corner protrusion, upper lip protrusion and lower lip protrusion), the aperture (lip opening, lip height, lip area) and the rounding (ratio between lip height and lip width). These three geometrical features are basic means to characterize labial speech gestures. They are measured between the rest position and the stable shape attained at the end of the movement simulation.

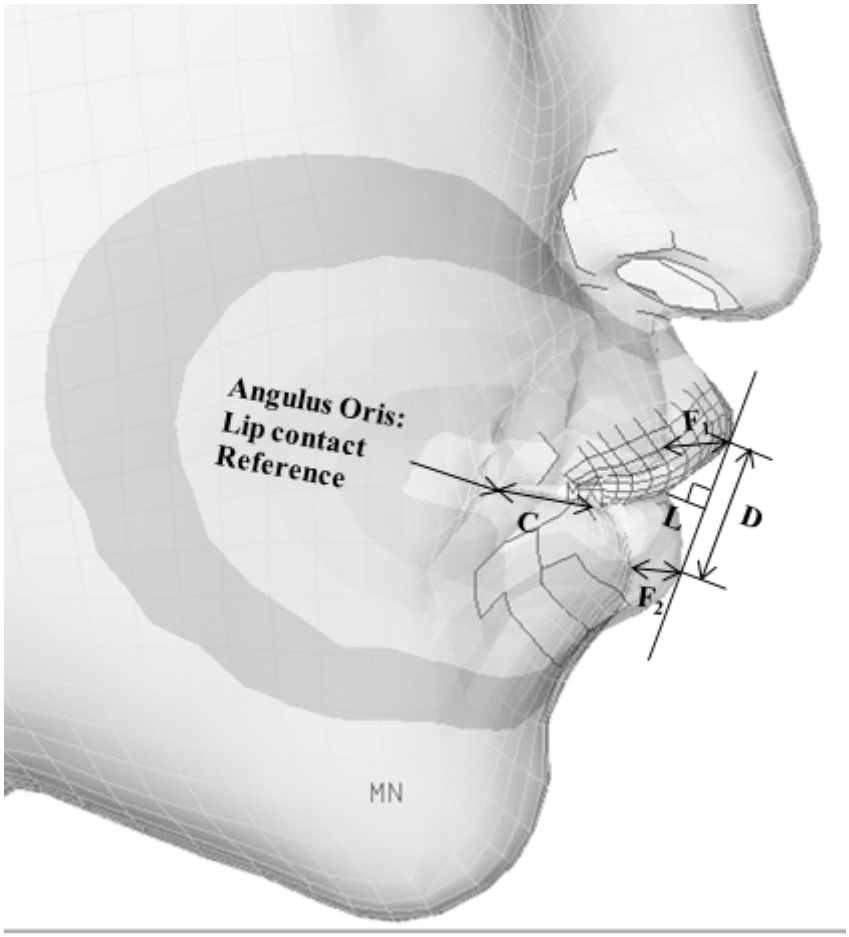

Figure 4.23 Lip shape parameters (profile view): lip opening (D), lip horn depth (L), lip corner protrusion (C), upper lip protrusion (F_1), lower lip protrusion (F_2) (Abry & Boë, 1986).

As stated above, the presentation of the results focuses on the role of stress stiffening in the achievement of rounded lips. The production of some vowels (called *rounded* vowels, as opposed to *spread* vowels) requires a small lip area. Classic examples of this vowel category are the French vowels /u/, /y/ or /O/. For a large majority of subjects, this small area is achieved by protruding the lips, in spite of the fact that the protrusion gesture is not the only way to achieve a small lip area. This regularity across speakers is interpreted as evidence for the fact that protrusion is an efficient way to achieve small lip areas. Our simulations, in the context of the effect of stiffening on shaping, aim at further understanding this strategy. The impact of the Orbicularis Oris (OO) activation is analyzed with and without the stress stiffening effect.

The presentation of the results is organized in two main subsections. First we study the impact of the OO activation and of the stress stiffening on the lip shape based on the parameters proposed by Abry & Boë (1986). Second, an evaluation of the impact of the different simulated lip shapes on the spectral properties of the associated acoustic speech signal is performed on the French vowel /u/. In both studies, the role of the stress stiffening effect is at the core of the analysis.

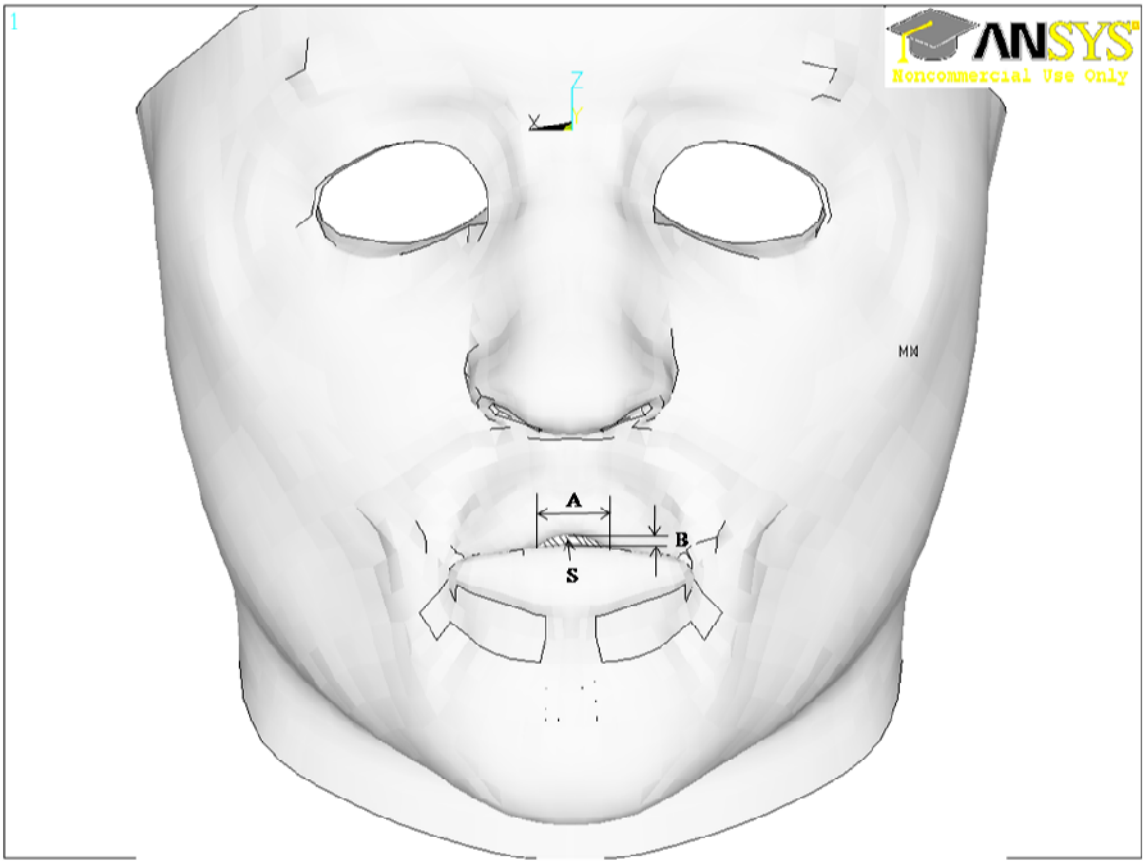

Figure 4.24 Lip shape parameters (frontal view): lip area (S), lip width (A), lip height (B) (Abry & Boë, 1986).

4.5.3.1 Lip protrusion and rounding gesture

Two preliminary conclusions can be drawn from these first qualitative observations: (1) in our model the Orbicularis Oris Peripheralis simultaneously generates a protrusion and a narrowing of the lips; (2) accounting for the stress stiffening effect significantly influences lip shaping and it reinforces the efficiency of the protrusion gesture in achieving a small lip area, which are the key characteristics of rounded lips. In order to further assess these preliminary conclusions and to do so quantitatively, four sets of simulations were run. In two sets (Table 4.3) the stress stiffening level varied in 10 regular steps from its minimum (factor equal to 1) to its maximum (factor equal to 10) while the activation level was set either to its minimum (Table 4.3a) or to its maximum (Table 4.3b). In two other sets of simulations (Table 4.4), the activation level varied in twelve regular steps from its minimum (0.1) to its maximum (0.4) while the stress stiffening level was set either to its minimum (Table 4.4a) or to its maximum (Table 4.4b). The results of Tables 4.3a and 4.3b are depicted in Figures 4.25 and 4.26 respectively. These figures show that for both levels of muscle activation, while the majority of the geometrical lip parameters tend to globally vary linearly with the increase in stress stiffening, the lip area and the lip height follow a clear non-linear variation.

Table 4.3a Different lip parameters with respect to different stiffness levels at minimum activation

Stiffness	CORNER LIP PROTRUSION (mm)	LIP HORN DEPTH (mm)	LIP AREA (mm^2)	LIP HEIGHT (mm)	LIP WIDTH (mm)	LIP OPENING (mm)	LOWER LIP PROTRUSION (mm)	UPPER LIP PROTRUSION (mm)	Maximum Force (N)
1	7.08	8.29	23.98	2.52	14.00	16.93	3.35	4.30	2.39
2	6.61	8.55	20.23	2.15	13.77	15.73	3.07	3.58	2.79
3	6.22	8.73	19.19	1.96	14.10	15.09	2.87	3.20	3.16
4	5.84	8.17	18.85	1.87	14.44	14.64	2.70	3.03	3.41
5	5.51	8.32	18.75	1.82	14.66	14.32	2.56	2.76	3.57
6	5.21	8.72	19.39	1.83	15.61	14.10	2.48	2.57	3.75
7	4.94	8.88	19.31	1.81	15.65	13.92	2.38	2.44	3.88
8	4.69	9.04	19.36	1.80	15.88	13.76	2.29	2.34	3.95
9	4.47	9.19	19.36	1.76	15.84	13.62	2.22	2.27	4.04
10	4.30	9.31	19.46	1.75	15.96	13.51	2.15	2.21	3.91

Table 4.3b Different lip parameters with respect to different stiffness levels at maximum activation

Stiffness	CORNER LIP PROTRUSION (mm)	LIP HORN DEPTH (mm)	LIP AREA (mm^2)	LIP HEIGHT (mm)	LIP WIDTH (mm)	LIP OPENING (mm)	LOWER LIP PROTRUSION (mm)	UPPER LIP PROTRUSION (mm)	Maximum Force (N)
1	9.77	6.58	20.39	3.07	10.78	18.99	5.33	7.38	4.65
2	10.19	7.32	17.70	2.59	10.52	17.90	5.25	6.97	5.67
3	10.17	7.63	15.27	2.14	10.59	17.09	5.12	6.53	6.40
4	10.07	7.58	13.47	1.84	10.76	16.48	4.98	6.24	6.95
5	9.97	7.59	12.06	1.62	10.89	16.07	4.85	5.88	7.53
6	9.85	7.61	11.13	1.46	11.00	15.73	4.75	5.71	8.13
7	9.79	7.63	11.23	1.44	11.07	15.58	4.63	5.59	8.61
8	9.64	7.67	10.65	1.35	11.16	15.32	4.53	5.40	9.20
9	9.48	7.73	10.38	1.29	11.21	15.13	4.43	5.25	9.64
10	9.35	7.78	10.23	1.25	11.28	14.96	4.34	5.12	10.00

This non-linearity is characterized by a rapid decrease for low stress stiffening levels followed by quasi-stabilization above a certain stress stiffening level (around 4 for low activation and 6 for high activation). This corresponds to a saturation effect. For the high activation level, lip horn also shows such a saturation effect, but this is not true for the low activation level. Interestingly the two parameters that depict a saturation effect independently of the activation level, namely the lip area and the lip height, are considered to be crucial for the geometrical characterization of lip shapes in the protrusion/rounding condition (Abry & Boë, 1986). In terms of motor control, this saturation effect is interesting since it enables the same values for crucial lip shape parameters to be reached over a wide range of motor commands.

Table 4.4a Different lip parameters with respect to different activation levels at minimum stiffness

Activation	CORNER LIP PROTRUSION (mm)	LIP HORN DEPTH (mm)	LIP AREA (mm^2)	LIP HEIGHT (mm)	LIP WIDTH (mm)	LIP OPENING (mm)	LOWER LIP PROTRUSION (mm)	UPPER LIP PROTRUSION (mm)	Maximum Force (N)
0.1	7.08	8.29	23.98	2.52	14.00	16.93	3.35	4.30	2.39
0.125	7.67	8.14	23.55	2.58	13.62	17.29	3.68	4.86	2.72
0.15	8.20	7.97	23.11	2.62	13.44	17.58	3.94	5.38	3.05
0.175	8.72	7.82	22.76	2.69	13.10	17.89	4.25	5.93	3.42
0.2	9.06	7.70	22.39	2.72	13.06	18.06	4.39	6.23	3.67
0.225	9.34	7.66	22.57	2.89	12.50	18.38	4.64	6.53	3.90
0.25	9.45	7.64	22.21	2.95	12.53	18.46	4.75	6.67	4.03
0.275	9.70	7.57	21.43	2.98	11.93	18.64	4.93	6.96	4.28
0.3	9.59	7.09	20.65	3.04	11.45	18.86	5.18	7.19	4.42
0.325	9.85	6.96	21.34	3.06	11.78	18.83	5.08	7.16	4.42
0.35	9.90	6.93	21.51	3.12	11.66	18.87	5.12	7.22	4.47
0.38	9.77	6.58	20.39	3.07	10.78	18.99	5.33	7.38	4.65
0.4	10.25	6.57	18.97	3.15	10.82	19.37	5.69	7.96	5.22

Table 4.4b Different lip parameters with respect to different activation levels at maximum stiffness

Activation	CORNER LIP PROTRUSION (mm)	LIP HORN DEPTH (mm)	LIP AREA (mm^2)	LIP HEIGHT (mm)	LIP WIDTH (mm)	LIP OPENING (mm)	LOWER LIP PROTRUSION (mm)	UPPER LIP PROTRUSION (mm)	Maximum Force (N)
0.1	4.30	9.31	19.46	1.75	15.96	13.51	2.15	2.21	3.91
0.125	5.05	9.63	17.37	1.65	15.61	13.63	2.47	2.58	4.68
0.15	5.73	8.68	15.54	1.52	14.48	13.74	2.76	2.86	5.54
0.175	6.46	8.36	13.66	1.43	13.50	13.88	3.06	3.26	6.37
0.2	6.90	8.19	12.47	1.31	13.32	13.99	3.26	3.53	6.92
0.225	7.48	7.94	11.49	1.26	11.88	14.16	3.51	3.91	7.58
0.25	7.80	7.78	10.92	1.22	11.78	14.25	3.65	4.12	8.02
0.275	8.25	7.53	10.33	1.19	11.65	14.42	3.86	4.47	8.60
0.3	8.68	7.97	9.93	1.19	11.49	14.60	4.06	4.78	9.09
0.325	8.73	7.94	9.75	1.17	11.47	14.61	4.09	4.81	9.27
0.35	9.01	7.86	10.50	1.26	11.40	14.82	4.16	5.08	9.52
0.38	9.35	7.78	10.23	1.25	11.28	14.96	4.34	5.12	10.00
0.4	9.89	7.59	9.83	1.24	11.09	15.18	4.64	5.53	10.89

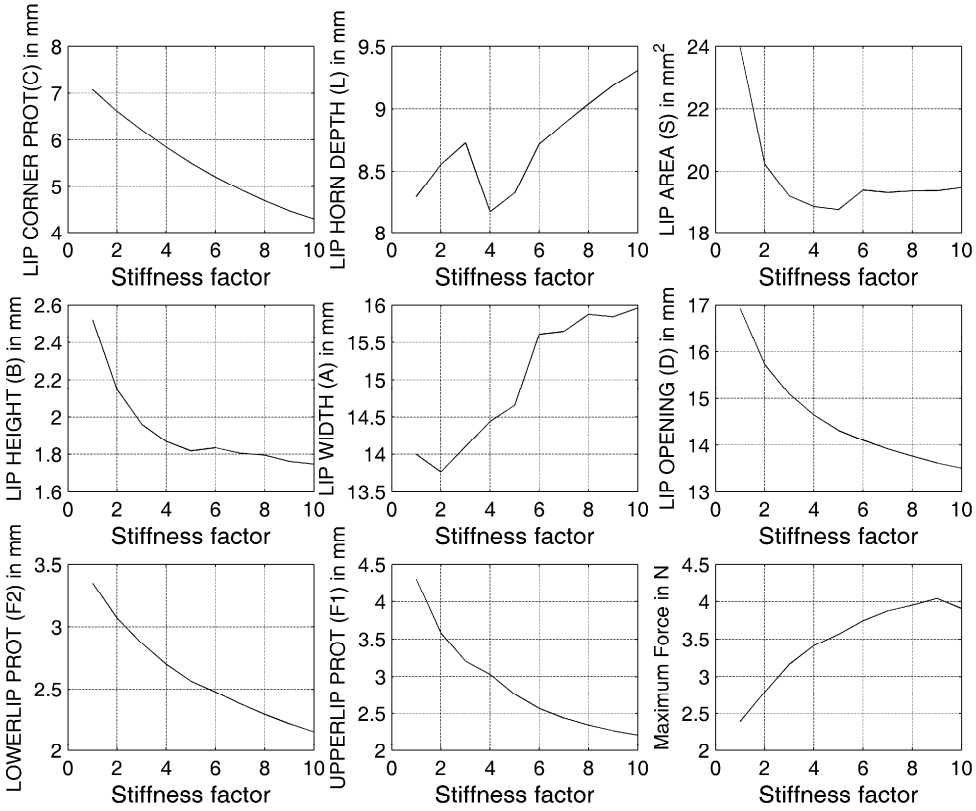

Figure 4.25 Variation in lip parameters as a function of stiffness with minimum activation.

Would a control of the activation amplitude be as efficient as the stiffening? To answer this question, the next two sets of simulations are very informative. The results, listed in Tables 4.4a and 4.4b, are plotted respectively in Figures 4.27 (no stiffening) and 4.28 (maximal stiffening). In the absence of stiffening (Figure 4.27) all the measured lip characteristics vary linearly with the activation level. No saturation is observed, even for high activation levels. For the maximum stress stiffening level (Figure 4.28) clear saturation effects are observed above the activation level 0.3 for 4 parameters, lip area, lip height, lip width and lip horn depth. In addition, the decrease in the lip area reached for a given level of activation is much larger with stiffening than in the absence of stiffening. When the stress stiffening effect is taken into account, an increase in activation is associated with a decrease in lip height. This behaviour is consistent with a prototypical protrusion/rounding gesture. In contrast, when the stress stiffening effect is not modelled, increasing the activation generates an increase in lip height, a result which is in opposition to the characteristics of a lip protrusion/rounding gesture. These results are in complete agreement with the impressionistic conclusions made from Figures 4.21 and 4.22.

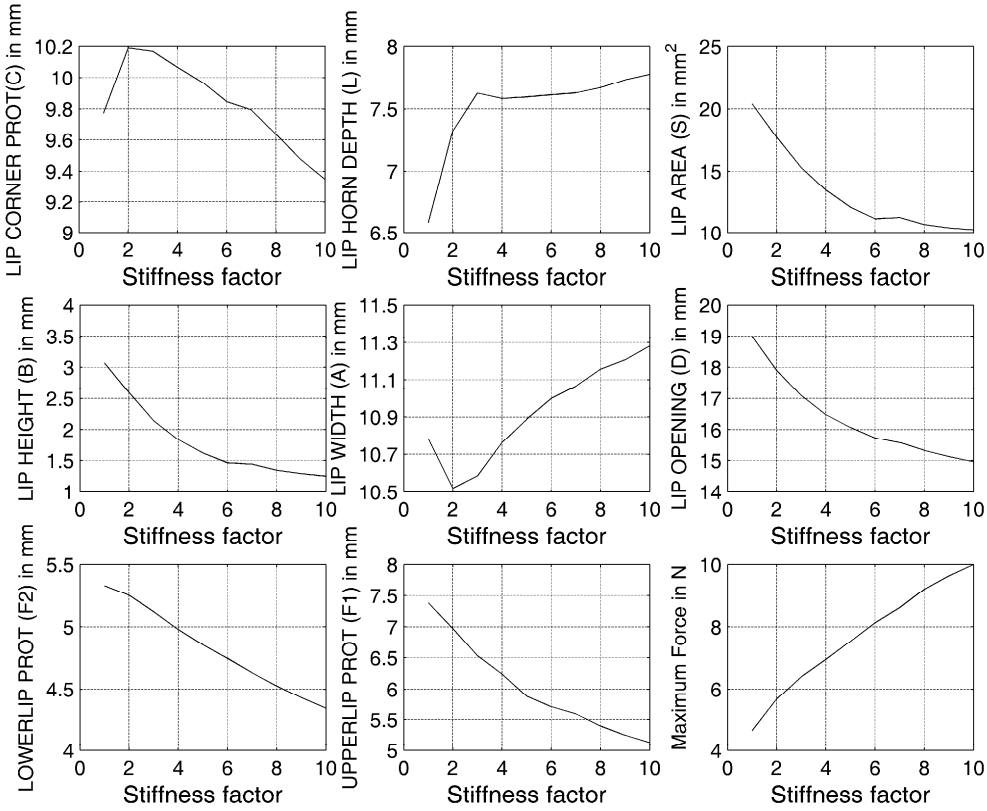

Figure 4.26 Variation in lip parameters as a function of stiffness with maximum activation.

The reduction in lip area without a saturation effect and with an increase in lip height observed in the non-stiffening conditions suggests that modelling the stress stiffening effect is extremely positive for an efficient control of lip shaping, especially regarding the rounding associated with protrusion. The increase in the activation level is "as efficient as the stiffening" only if stiffening is taken into account. The effect of stiffening on lip protrusion/rounding is confirmed.

The realism or absence of realism of the different accounts of the protrusion/rounding gesture given in the different simulation conditions can be quantitatively assessed thanks to the experimental observations provided by Abry & Boë (1986). These authors present (see Figure 3 of their paper) a law that describes how the lip area (S), lip height (B), and lip width (A) are linked with each other: S= 0.75*A*B. An additional way to evaluate our results is to test whether one of the simulation conditions gives results compatible with Abry & Boë's experimental findings. Figures 4.29 and 4.30 present the results of this evaluation. In Figure 4.29, the dashed line shows the lip area function that would result from our lip height and width measurements according to Abry & Boë's law while the solid line corresponds to the measured area function. Figure 4.30 shows the ratio between the calculated and the measured area. It can be observed that in the absence of stiffening, the ratio is significantly larger than one. Hence, the simulated lip shapes do not match the experimental observations. This ratio decreases dramatically as soon as stiffening is taken into account.

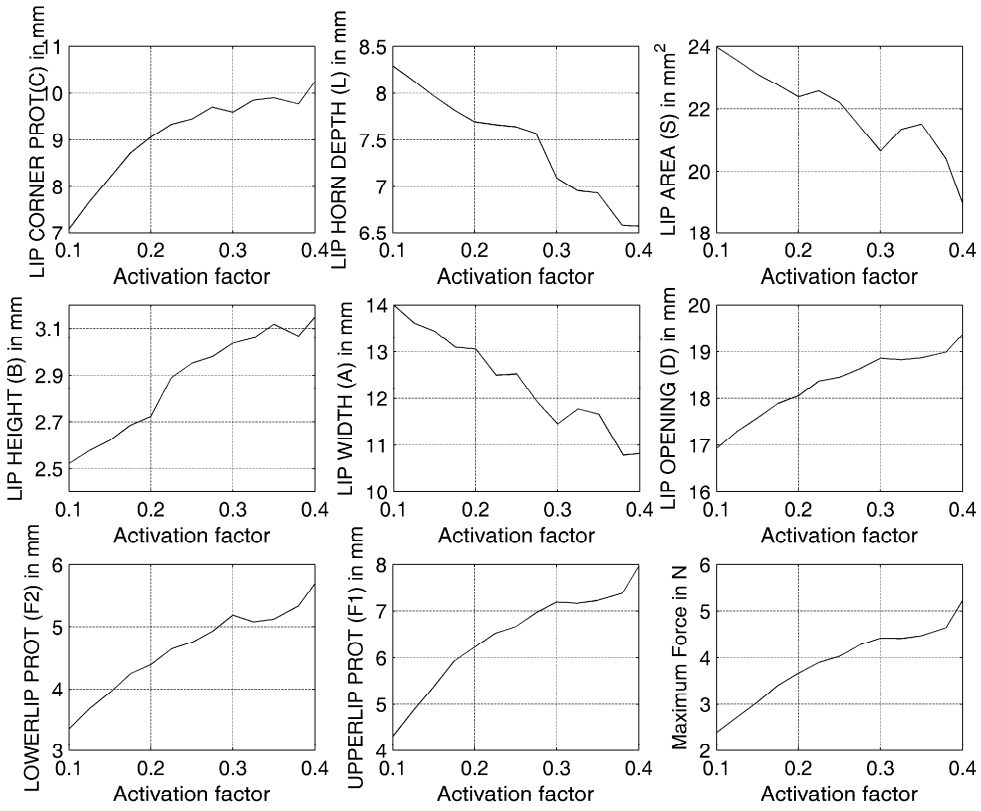

Figure 4.27 Variation in lip parameters as a function of activation with no stiffness change.

When stiffening increases, the ratio continues to decrease, almost linearly, with the multiplying factor, but significantly less strongly. The ratio becomes very close to one when the multiplying factor is equal to 10. This shows that with the inclusion of stiffening, the relation between lip parameters is in agreement with the experimental observations. Thus, including stiffening enables the generation of more natural lip shapes.

4.5.3.2 Impact of the stress stiffening effect on the spectral properties of the acoustic speech signal: The example of the vowel /u/

To study the effect of stiffening on the frequency content of the speech signal, we generated synthetic speech waves from a vocal tract in which the lip characteristics were those generated with our model in both stiffened and non-stiffened cases. The vocal tract geometry corresponded to the French vowel /u/, which is a classic example of a rounded vowel. For this purpose we took the data proposed for this vowel in Figure 1 of Apostol et al. (2004). Then we replaced the geometrical characteristics of the sections corresponding to the lips with the data extracted from our model. The addition of lip corner protrusion to lip horn depth (L in Figure 4.23) defines the length of the lip tube, and the lip area (S in Figure 4.24) is used for the cross-section of this tube. As an example an area function is show in Figure 4.31. This area function is then used as an input function for a Kelly-Lochbaum digital speech synthesis model (Kelly & Lochbaum, 1962; Story, 2005). The speech signal generated with this model (Story, 2005) is then analysed in the spectral domain. With the help of the Linear Prediction Analysis, the spectral envelope of this signal is extracted (Figure 4.32).

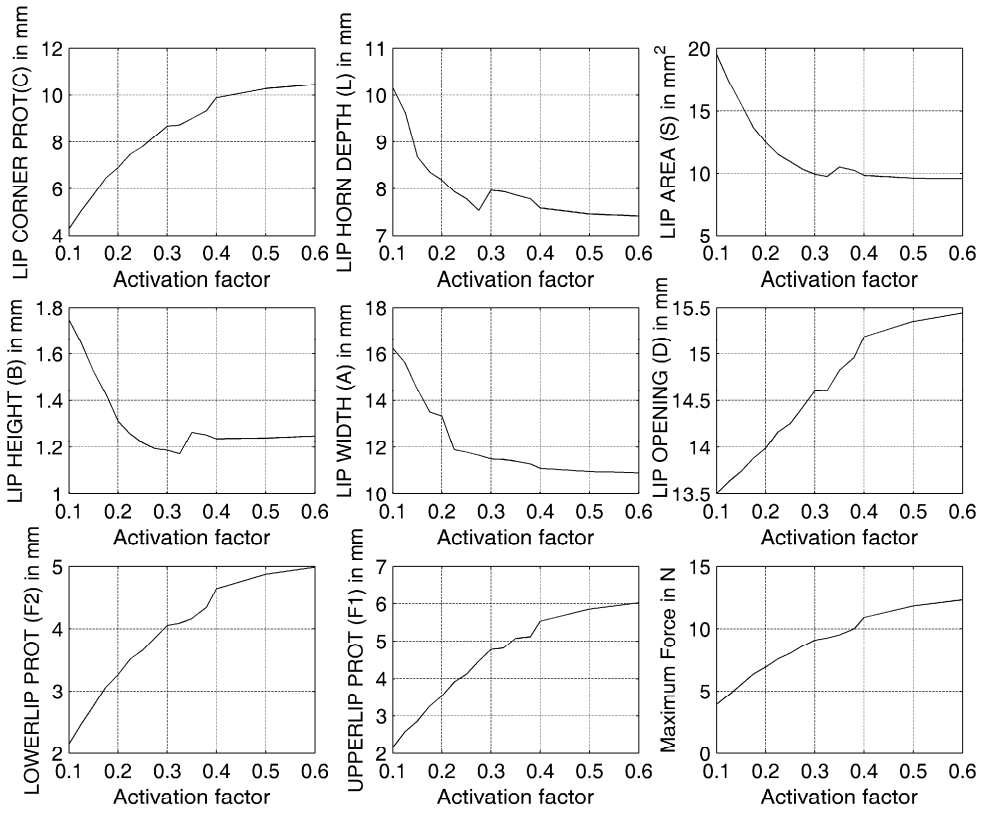

Figure 4.28 Variation in lip parameters as a function of activation with maximum stiffness change.

The spectral peaks correspond to formants, which are crucial for the perceptual quality of the vowels. For the French vowel /u/ the key spectral characteristic is that the first two formants F1 and F2 are in the low frequency domain [300 Hz 700 Hz]. Savariaux et al. (1999, Figure 3) show that the perceptual quality of this vowel improves when F2 decreases within this range to become closer to F1. In a Standard French /u/, such as the one modelled in Apostol et al. (2004), F1 mainly depends on the geometry of the back part of the vocal tract and F2 is mainly influenced by the front part and by the lips. The analysis of F1-F2 narrowing, and especially of the F2 decrease, thus provides a suitable basis to investigate acoustically the effect of stiffening in the modelled protrusion/rounding gesture.

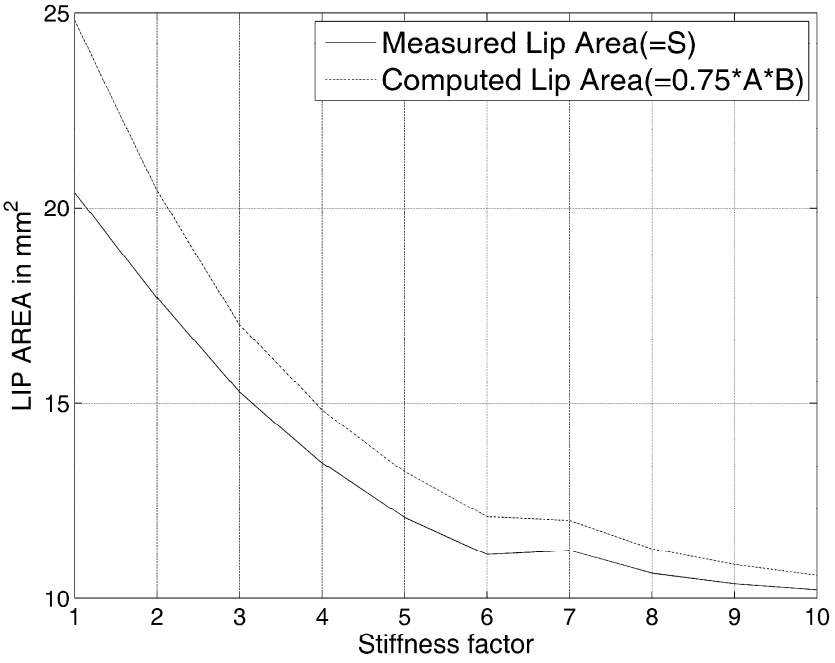

Figure 4.29 Lip area as a function of stiffness: calculated using Abry & Boë's formula (dashed line) and measured from our simulations (solid line).

The variation in the first two formants is extracted for different lip shape parameters corresponding to an increase in the stiffness level (with minimum and maximum activation levels) (Figure 4.33) and to an increase in the activation level (with minimum and maximum stiffening values) (Figure 4.34).
As Figure 4.33 shows, when the stress stiffening effect is modelled, while the activation level is kept at its maximum (bold line), the second formant decreases and converges towards the first formant, which remains fairly constant. This F2 decrease is consistent with a more rounded and protruded lip shape. It is not observed for the minimum activation level (solid line). Figure 4.34 shows that an increase in the activation level induces a decrease in F2 only if it is accompanied by stiffening (bold line). In the absence of stiffening (solid line) increasing activation has no spectral consequences.
Thus, the acoustic simulation suggests that the association of muscle activation increase and stiffening enables the production of more canonical spectral patterns for the French vowel /u/.

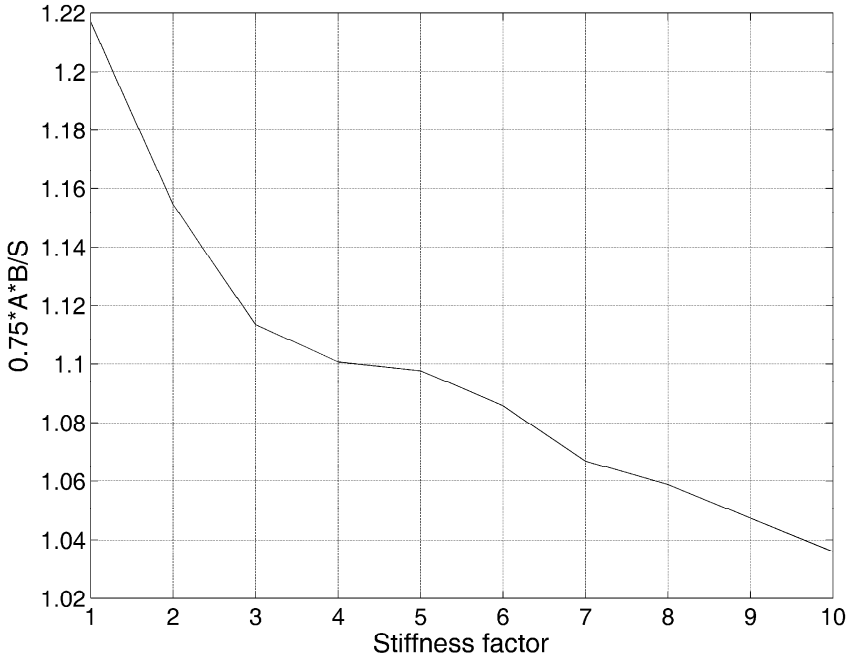

Figure 4.30 Lip area as a function of stiffness: the ratio of calculated to measured area.

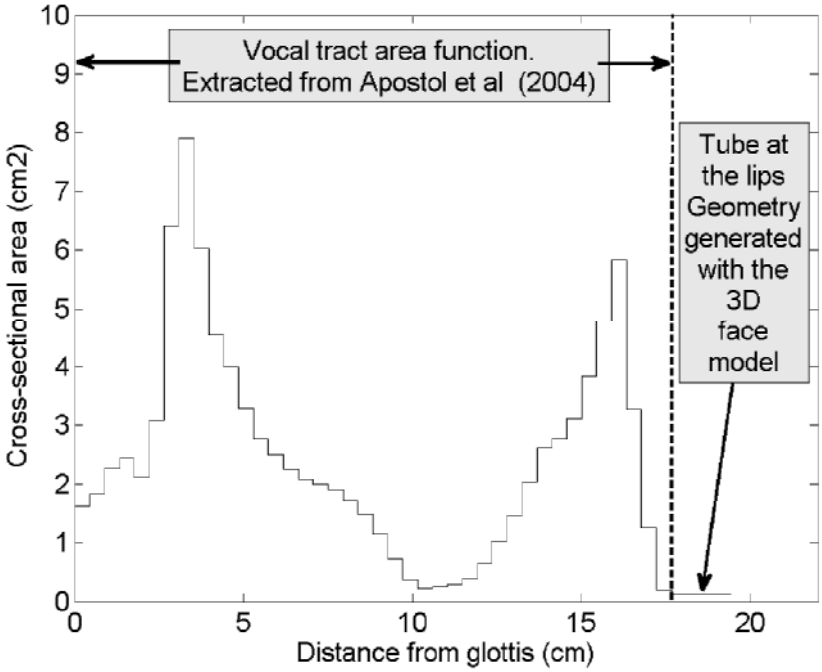

Figure 4.31 Study of spectral properties of a synthetic French vowel /u/: an example of area function.

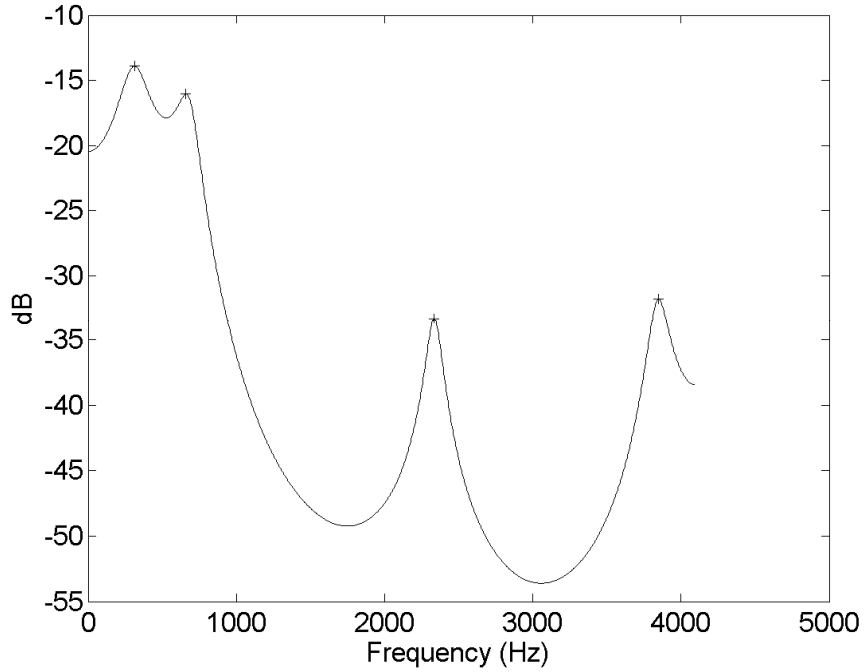

Figure 4.32 Study of spectral properties of a synthetic French vowel /u/: the spectral envelope of a signal produced from this area function computed using the Linear Prediction Analysis (the crosses show the speech formants).

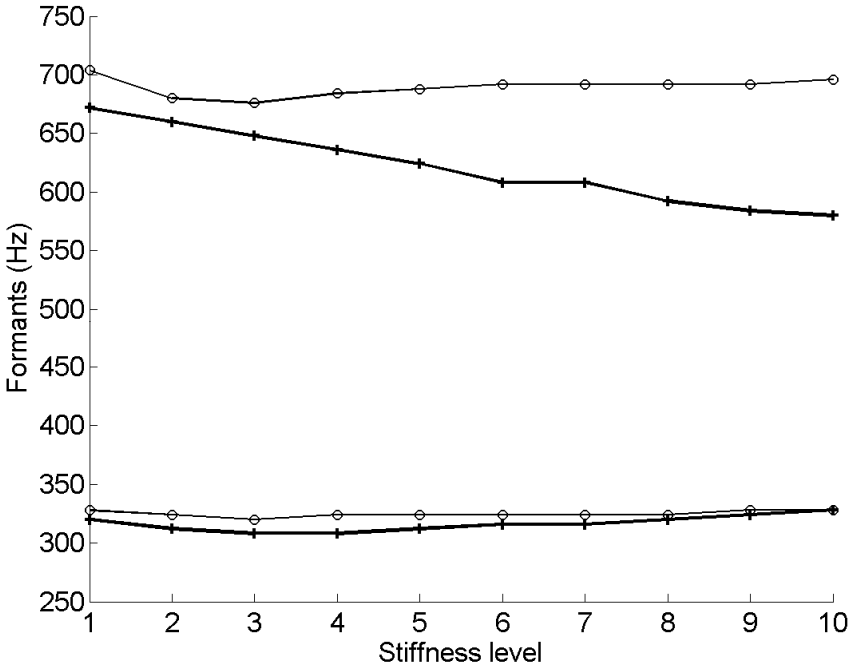

Figure 4.33 The variation in the first two speech formants (F1 and F2) corresponding to the French vowel /u/ for different stiffness levels (the bold lines correspond to maximum activation levels).

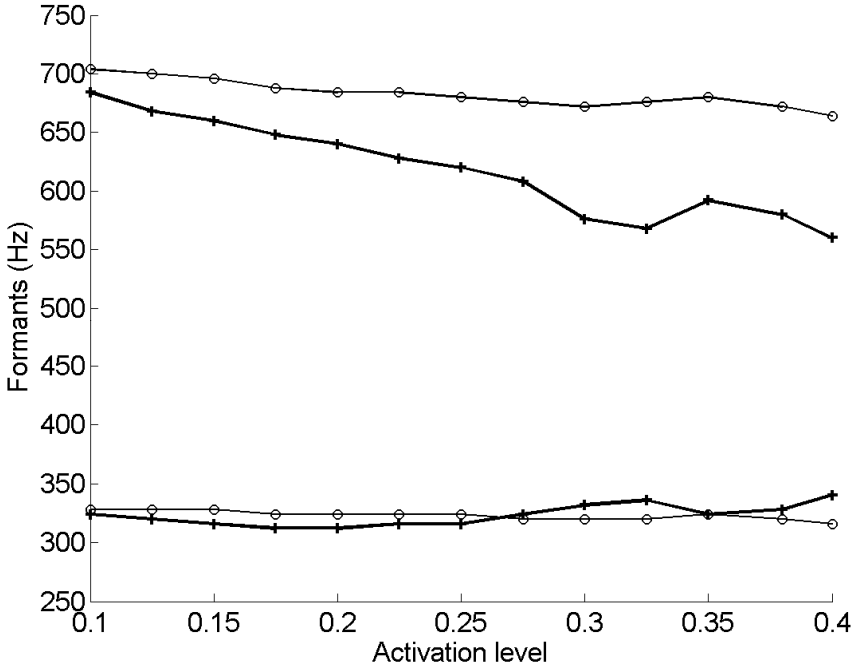

Figure 4.34 The variation in the first two speech formants (F1 and F2) corresponding to the French vowel /u/ for different activation levels (the bold lines correspond to maximum stiffening values).

4.6 Conclusion

The use of a realistic dynamical biomechanical model of the face has allowed simulating a number of facial movements comparable to those occurring during the production of speech or of facial mimics in non-verbal communication.

Studies in the literature have shown that articulatory dynamics has a major impact on the temporal patterning of speech movements. Time characteristics are important in speech perception. We have shown that lip movement patterns are indeed different in quasi-static and dynamic simulation frameworks. Interesting results, close to experimental observations, have been obtained for the dynamic framework, and not for the quasi-static one, such as the generation of curved paths and bell-shaped velocity profiles classically observed in unperturbed skilled human movements (Morasso 1981). The clear differences observed between the trajectories simulated with dynamic and static analysis demonstrate that the usage of dynamic analysis is a requirement for speech production studies. The role of dynamics has also been studied in the literature for non-speech movements. Ambadar et al. (2005) observed for example that recognition of subtle facial expressions by watching the evolution of facial gestures in time is much easier than by looking at static shots. Hence, in modelling studies, if temporal patterning of movements integrates dynamic constraints like inertia and viscosity; synthetic facial expressions will be deciphered faster and easier.

On the basis of simulations carried out with a finite element biomechanical model of the face, the impact of the stress stiffening effect (i.e. of the tissue stiffening associated with muscle activation) was studied for the protrusion/rounding gesture of the lips. The lips' protrusion/rounding gesture was generated by activating the upper and lower parts of the OOP. It was found that the stress stiffening

effect significantly influences shaping. Acoustic simulations showed that the differences in lip shaping corresponded to differences in spectral patterns.

Stiffening in the lip protrusion/rounding gesture significantly changes the shape of the lips: in the absence of stiffening, protrusion is produced and is associated with a reduction in the lip area, but the achieved lip shape does not match experimental data on rounding because of the lip height. Protrusion is associated with a clear reduction in lip height only if stiffening is taken into account. Hence, in the case of the lips, it can be concluded that *stiffening is useful for shaping*. This finding could be one explanation for the fact that, to our knowledge, the protrusion/rounding gesture has never been achieved with biomechanical models with the activation of the Orbicularis Oris alone (see for example the analysis proposed by Gomi et al. (2006) of their own simulation results).

In addition, our simulations have shown that when the stress stiffening effect is modelled, a saturation effect exists when the activation level increases. From a motor control perspective, this result is very interesting since it suggests that a simple strategy to generate protruded and rounded lips could be to activate the Orbicularis Oris while stiffening the tissues.

Chapter Five: Muscle model as a constitutive law

"People's behavior makes sense if you think about them"
"in terms of their goals, motives and needs."
Thomas Mann

Modeling the behavior of different materials is a well developed topic and covers a wide range of materials from linear elasticity to smart materials. What is usually expected from a material model is the imitation of the material's behavior as closely as it is possible. A material may behave differently depending on the level and the type of external action. Limited usage of material also limits the range of material reaction. Hence it can be said that a model imitates the behavior of a material in the range of its usage. Therefore in a process of modeling some simplifications are usually made since the coverage of the full range of material behavior is not necessary. A material model is usually called a *constitutive law*.
For muscles a two-term constitutive law is needed. The first term models the passive behavior of the muscle and the second term describes its active behavior. In context of the finite element model, its numerical implementation and the model itself will be explained in this chapter.

5.1 Muscle's constitutive law

Muscle passive behavior is generally modeled as a hyperelastic material (Fung, 1993). Hyperelastic materials are materials for which the work done by external load is independent of the load path. It is therefore possible to define a stored energy function, called the strain energy (W). According to the first and second laws of thermodynamics, the change in internal energy per unit volume ($\mathrm{d}E$) is:

$$\mathrm{d}E=\mathrm{d}W+\delta Q=\mathrm{d}W+T\mathrm{d}S \qquad (5.1)$$

where δQ is the increment in heat transferred to the body per unit volume and $\mathrm{d}W$ is the change in strain energy per unit volume. When there is no internal entropy production, the change in specific entropy $\mathrm{d}S$ (entropy per unit volume) at temperature T is equal to: $\delta Q/T$. With the definition of Helmholtz free energy (H) as $H=E-TS$, and if the entropy remains unchanged it can be concluded:

$$\mathrm{d}H=\mathrm{d}W-S\mathrm{d}T \qquad (5.2)$$

Hence we can say that the stored mechanical energy per unit volume (W) is equal to the internal energy (E) in an isentropic process (adiabatic process) or the free energy (H) in an isothermal process. This mechanical stored energy is due to the work done by external forces acting on the body. The mathematical form of the strain energy in terms of stress and strain in finite strain elasticity depends on the definition of strain and stress. In large deformation framework, various definitions of stress and strain exist. These are reviewed in the next section (for a complete discussion see among the others Holzapfel (2000); Fung and Thong (2001); Belytschko (2000)).

5.1.1 Kinematics and kinetics of finite elasticity

In this section a review of different types of strains is first presented. Then the strain rate is explained. Stress and its various types come next. Different types of stress rates are described at the end of this section.

5.1.1.1 Strain

In large deformation elasticity or as it is called "*finite elasticity*", the body before deformation at time $t=0$ is at position B and after deformation at time t it occupies the position $\phi(B)$ (Figure 5.1). The points at initial position are shown by vector **X** and in the current position by vector $\mathbf{x}=\phi(\mathbf{X},t)$.

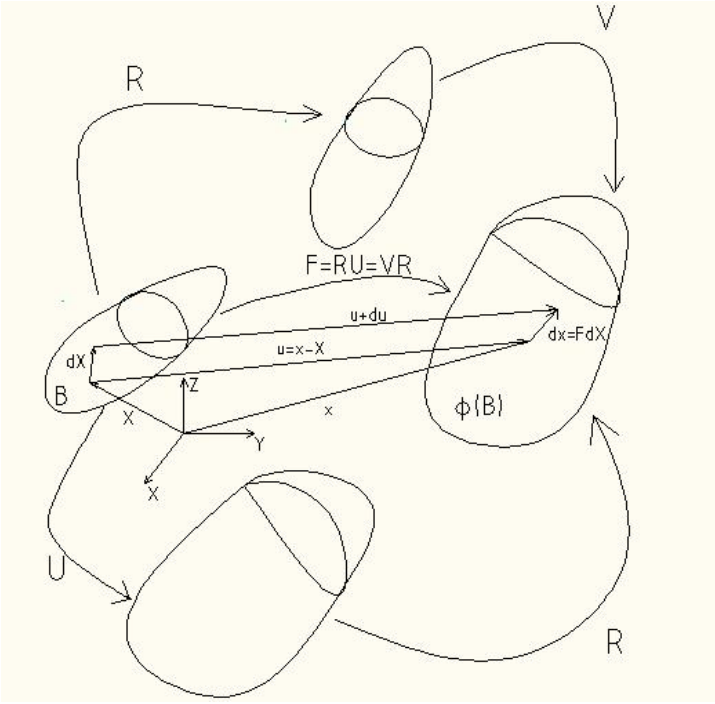

Figure 5.1 Kinematics of finite strain elasticity; polar decomposition of deformation gradient

Deformation gradient is a transformation that transforms an initial incremental material line segment d**X** to its current position (d**x**):

$$d\mathbf{x}=\mathbf{F}d\mathbf{X} \qquad (5.3a)$$

Hence

$$\mathbf{F}=\partial\mathbf{x}/\partial\mathbf{X} \qquad (5.3b)$$

With $J=det(\mathbf{F})$, an area d**A** is transformed to (Nanson's formula): $d\mathbf{a}=\mathbf{n}da=J\mathbf{F}^{-T}\mathbf{N}dA=J\mathbf{F}^{-T}d\mathbf{A}$ (with $\mathbf{F}^{-T}=(\mathbf{F}^{-1})^{T}$ and superscript T indicates transpose operation, **N** and **n** are normal unit vectors to areas dA and da respectively) and a volume dV is moved to d$v=J$dV**.**

In the large deformation framework the square of differential line segments, dx^2 and dX^2, cannot be neglected as is the case in linear analysis. These can be evaluated as:

$$dx^2=d\mathbf{x}\cdot d\mathbf{x}=\mathbf{F}d\mathbf{X}\cdot\mathbf{F}d\mathbf{X}=d\mathbf{X}\cdot\mathbf{F}^{T}\mathbf{F}d\mathbf{X} \qquad (5.4a)$$

$$dX^2=d\mathbf{X}\cdot d\mathbf{X}=\mathbf{F}^{-1}d\mathbf{x}\cdot\mathbf{F}^{-1}d\mathbf{x}=d\mathbf{x}\cdot\mathbf{F}^{-T}\mathbf{F}^{-1}d\mathbf{x} \qquad (5.4b)$$

($\cdot$ is vector dot product). With the introduction of two symmetric strain tensors $\mathbf{C}=\mathbf{F}^{T}\mathbf{F}$ and $\mathbf{B}=\mathbf{F}\mathbf{F}^{T}$, which are the right and left Cauchy-Green strain tensors respectively, equations (5.4) becomes:

$$dx^2= d\mathbf{X}\cdot\mathbf{C}d\mathbf{X} \qquad (5.5a)$$

$$dX^2=d\mathbf{x}\cdot\mathbf{B}^{-1}d\mathbf{x} \qquad (5.5b)$$

As it can be seen the Euclidean distance in a deformed/undeformed geometry, becomes a non-Euclidean one in undeformed/deformed geometry with metric tensors $\mathbf{C}/\mathbf{B}^{-1}$. In fact $\mathbf{C}$ is a Lagrangian strain tensor referring to undeformed configuration and $\mathbf{B}^{-1}$ is an Eulerian strain tensor referring to a deformed configuration. The nomenclature of these strain tensors as being left or right comes from the polar decomposition of the deformation gradient. Deformation in general can be decomposed into a rigid body rotation and a stretch tensor (Figure 5.1). The order of these two transformations can be exchanged. Showing the rotation tensor by $\mathbf{R}$, with the property $\mathbf{R}\mathbf{R}^{T}=\mathbf{R}^{T}\mathbf{R}=\mathbf{I}$, then the polar decomposition of deformation gradient gives:

$$\mathbf{F}=\mathbf{R}\mathbf{U}=\mathbf{V}\mathbf{R} \qquad (5.6)$$

where $\mathbf{U}$ and $\mathbf{V}$ are the right and left symmetric stretch tensors, respectively. Hence the Cauchy-Green strain tensors become:

$$\mathbf{C}=\mathbf{U}^2 \qquad (5.7a)$$
$$\mathbf{B}=\mathbf{V}^2 \qquad (5.7b)$$

The displacement vector field is the difference between the position vectors of the current configuration and the initial one: $\mathbf{u}=\mathbf{x}-\mathbf{X}$. A displacement vector has the same value in initial and current configurations. The increment in displacement $d\mathbf{u}$ in terms of the deformation gradient, $\mathbf{F}$, becomes:

$$d\mathbf{u}=d\mathbf{x}-d\mathbf{X}=(\mathbf{F}-\mathbf{I})d\mathbf{X} \qquad (5.8)$$

Therefore displacement gradient, $\mathbf{H}$, can be expressed as:

$$\mathbf{H}=\partial\mathbf{u}/\partial\mathbf{X}=\mathbf{F}-\mathbf{I} \qquad (5.9)$$

The right Cauchy-Green strain tensor with respect to displacement gradient becomes:

$$\mathbf{C}=\mathbf{F}^{T}\mathbf{F}=\mathbf{H}^{T}\mathbf{H}+\mathbf{H}+\mathbf{H}^{T}+\mathbf{I} \qquad (5.10)$$

Another important strain tensor is defined with respect to the difference in the square of differential line segments. From equation (5.5a) results:

$$dx^2-dX^2=d\mathbf{X}\cdot\mathbf{C}d\mathbf{X}-d\mathbf{X}\cdot d\mathbf{X}=d\mathbf{X}\cdot(\mathbf{C}-\mathbf{I})d\mathbf{X}=d\mathbf{X}\cdot 2\mathbf{E}d\mathbf{X} \qquad (5.11)$$

where $\mathbf{E}=(\mathbf{C}-\mathbf{I})/2$ is the Green strain tensor. It can be expressed with respect to displacement gradient as:

$$\mathbf{E}=(\mathbf{H}^T\mathbf{H}+\mathbf{H}+\mathbf{H}^T)/2 \qquad (5.12)$$

In the small strain framework when the displacement gradient is small, the Green strain tensor becomes the linear strain tensor, $\boldsymbol{\epsilon}$:

$$\boldsymbol{\epsilon}=(\mathbf{H}+\mathbf{H}^T)/2 \qquad (5.13)$$

Corresponding to the Green strain tensor which is a Lagrangian strain tensor, its equivalent in an Eulerian framework is called the Almansi strain tensor **e**:

$$\mathbf{e}=(\mathbf{I}-\mathbf{B}^{-1})/2 \qquad (5.14)$$

5.1.1.2 Strain rate

Velocity of a point is the derivative of its position vector with respect to time, hence:

$$\mathbf{v}=D\mathbf{x}/Dt=\partial\mathbf{x}/\partial t \qquad (5.15)$$

This velocity with the help of transformation $\mathbf{x}=\phi(\mathbf{X},t)$ can be expressed in Lagrangian description $\mathbf{v}(\mathbf{x},t)=\mathbf{V}(\mathbf{X},t)$. The velocity gradient, **L**, is the derivative of velocity with respect to Eulerian coordinates:

$$\mathbf{L}=\partial\mathbf{v}/\partial\mathbf{x} \qquad (5.16)$$

Hence from equation (5.3b) the time derivative of the deformation gradient can be expressed as[7]:

$$D\mathbf{F}/Dt=\partial\mathbf{v}/\partial\mathbf{X}=\mathbf{L}\mathbf{F} \qquad (5.17)$$

With this definition different types of strain rates can be computed. The right Cauchy-Green strain rate tensor is:

$$\partial\mathbf{C}/\partial t=\mathbf{F}^T\mathbf{L}\mathbf{F}+\mathbf{F}^T\mathbf{L}^T\mathbf{F}=\mathbf{F}^T(\mathbf{L}+\mathbf{L}^T)\mathbf{F}=2\mathbf{F}^T\mathbf{D}\mathbf{F} \qquad (5.18)$$

---

[7] The care should be taken with the time derivatives. $D(\ )/Dt$ means the derivative with respect to the time when **X** is fixed, but $\partial(\ )/\partial t$ means the derivative with respect to the time when the rest of variables, except time, are fixed. So for a scalar function like $\Gamma(\mathbf{X},t)$, we have: $D(\Gamma(\mathbf{X},t))/Dt=\partial(\Gamma(\mathbf{X},t))/\partial t$ (the same result holds for all the Lagrangian quantities), but for a function like $\gamma(\mathbf{x},t)$, we have: $D(\gamma(\mathbf{x},t))/Dt=\partial(\gamma(\mathbf{x},t))/\partial t+\partial(\gamma(\mathbf{x},t))/\partial\mathbf{x}\cdot\partial\mathbf{x}/\partial t$ and since $\mathbf{v}=\partial\mathbf{x}/\partial t$, then we obtain: $D(\gamma(\mathbf{x},t))/Dt=\partial(\gamma(\mathbf{x},t))/\partial t+\partial(\gamma(\mathbf{x},t))/\partial\mathbf{x}\cdot\mathbf{v}$. For example for the deformation gradient we have: $D\mathbf{F}/Dt=\partial\mathbf{F}/\partial t$.

where $\mathbf{D}=(\mathbf{L}+\mathbf{L}^T)/2$ is the symmetric part of the velocity gradient and is called the deformation or stretching rate tensor. The skew-symmetric part of the velocity gradient is called the spin tensor: $\mathbf{\Omega}=(\mathbf{L}-\mathbf{L}^T)/2$. From equation (5.18) the Green strain rate tensor can be found:

$$\partial \mathbf{E}/\partial t=\mathbf{F}^T\mathbf{D}\mathbf{F} \qquad (5.19)$$

This shows that the time derivative of the Green strain tensor is the pull back[8] of deformation rate tensor to initial configuration.
To compute the time derivative of quantities expressed in current configuration, a special derivative called Lie derivative (shown as $\pounds_v$) is used. In calculating the Lie derivative we first pull back the quantities expressed in the current configuration to the initial one. After taking their time derivative the result is pushed forward to the current configuration. For example the Lie derivative of the Almansi strain tensor gives:

$$\pounds_v\mathbf{e}=\mathbf{F}^{-T}(D(\mathbf{F}^T\mathbf{e}\mathbf{F})/Dt)\mathbf{F}^{-1}=\mathbf{F}^{-T}\partial \mathbf{E}/\partial t\mathbf{F}^{-1}=\mathbf{D} \qquad (5.20)$$

To get this result we used the fact that the time derivative of Lagrangian quantities is the same as their material time derivative.

5.1.1.3 Stress

Stress is used to express force distribution inside a body. The stress in large deformation is defined with respect to the current or the initial configurations. Hence various definitions of stress can be presented. Before introducing these definitions, we need to differentiate between stress vector and stress tensor. A stress vector at a point is the force density per unit of area of a plane passing through that point. It is a function of the normal (**n**) to this plane. While having the stress tensor at a point means that the state of stress at this point is completely known. This means that it is possible to find the stress vectors on all planes passing that point. Hence Cauchy stress vector ($\boldsymbol{\sigma}_\mathbf{c}$) at a point inside a body is:

$$\boldsymbol{\sigma}_\mathbf{c}=\mathrm{d}\mathbf{f}_c/\mathrm{d}a \qquad (5.21)$$

where $\mathbf{f}_\mathbf{c}$ is the force vector on area a. This stress is defined with respect to the current configuration (Figure 5.2). The Cauchy stress tensor ($\boldsymbol{\sigma}$) at a point is defined via three stress vectors with respect to the three orthogonal planes passing through the point. Cauchy stress is a symmetric tensor. Cauchy formula relates Cauchy stress vector to Cauchy stress tensor through:

---

[8] Pull-back of a quantity means expressing a physical quantity which has been defined in current configuration, back to initial configuration. Pull-back operator working on a contravariant second order tensor τ in current configuration gives: $T=F^{-1}\tau F^{-T}$ and for a covariant one: $T=F^T\tau F$. In this regard, τ is push-forward of tensor T from the initial configuration to the current one. Most of the strains are covariant tensors and most of the stresses are contravariant tensors (see Appendix A in Wriggers 2008).

$$\boldsymbol{\sigma}_c=\boldsymbol{\sigma}\mathbf{n} \qquad (5.22)$$

where **n** is a unit normal vector to the plane. Hence the force vector is:

$$d\mathbf{f}_c=\boldsymbol{\sigma}_c da=\boldsymbol{\sigma}\mathbf{n}da=\boldsymbol{\sigma}d\mathbf{a} \qquad (5.23)$$

where d**a** is area vector.

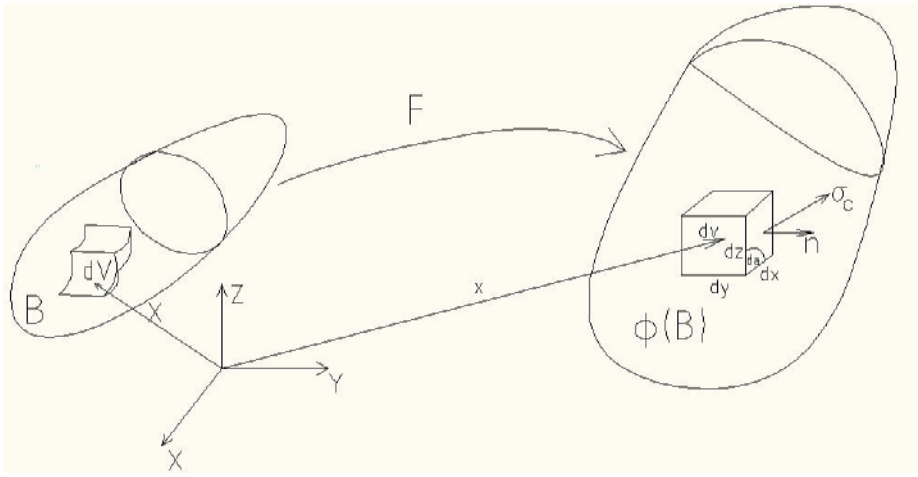

Figure 5.2 Cauchy stress representation

If we assume that the same force acts on area dA in undeformed position, this new stress is called first Piola-Kirchhoff stress tensor (**P**) and it is obtained:

$$d\mathbf{f}_c=\mathbf{P}d\mathbf{A} \qquad (5.24)$$

With the help of Nanoson's formula and equation (5.23) follows:

$$\mathbf{P}=J\boldsymbol{\sigma}\mathbf{F}^{-T} \qquad (5.25)$$

The first Piola-Kirchhoff stress tensor is not symmetric and is a mixed Lagrangian-Eulerian stress tensor since the force vector in the current configuration is applied on the original undeformed area in the initial configuration. Hence a second Piola-Kirchhoff stress tensor (**S**) is introduced in which the force vector is transformed to the initial configuration by the deformation gradient:

$$d\mathbf{F}_c=\mathbf{F}^{-1}d\mathbf{f}_c=\mathbf{S}d\mathbf{A} \qquad (5.26)$$

Hence we obtain:

$$\mathbf{S}=\mathbf{F}^{-1}\mathbf{P}=J\mathbf{F}^{-1}\boldsymbol{\sigma}\mathbf{F}^{-T} \qquad (5.27)$$

This means that **S** is a symmetric Lagrangian stress tensor. This tensor is also a pull-back (refer to footnote in section 5.1.1.2) of the Kirchhoff stress tensor defined by: $\boldsymbol{\tau}=J\boldsymbol{\sigma}$.
Another useful stress tensor is corotational stress tensor or Green-Naghdi stress tensor ($\boldsymbol{\sigma}_{co}$). This stress is obtained by expressing the Cauchy stress in a coordinate system which rotates by the rotation part (**R**) of the deformation gradient. This coordinate system is related to the global coordinate system through the rotation part of the deformation gradient as (Figure 5.3):

$$\mathbf{x}_{co}=\mathbf{R}^T\mathbf{X} \qquad (5.28)$$

The transformation equation for corotated force vector is then expressed as:

$$d\mathbf{f}_{co}=\mathbf{R}^T d\mathbf{f}_c=\mathbf{R}^T\boldsymbol{\sigma}\mathbf{n}da=\mathbf{R}^T\boldsymbol{\sigma}\mathbf{R}\mathbf{n}_{co}da \qquad (5.29)$$

In a corotated coordinate system the Cauchy stress becomes corotated stress. Equation (5.22) gives:

$$d\mathbf{f}_{co}=\boldsymbol{\sigma}_{co}\mathbf{n}_{co}da \qquad (5.30)$$

By comparing equations (5.28) and (5.29), and using (5.26) and (5.6) we obtain:

$$\boldsymbol{\sigma}_{co}=\mathbf{R}^T\boldsymbol{\sigma}\mathbf{R}=J^{-1}\mathbf{USU} \qquad (5.31)$$

Hence for a body that undergoes a rigid body motion, the stress tensor in the corotated frame remains constant.

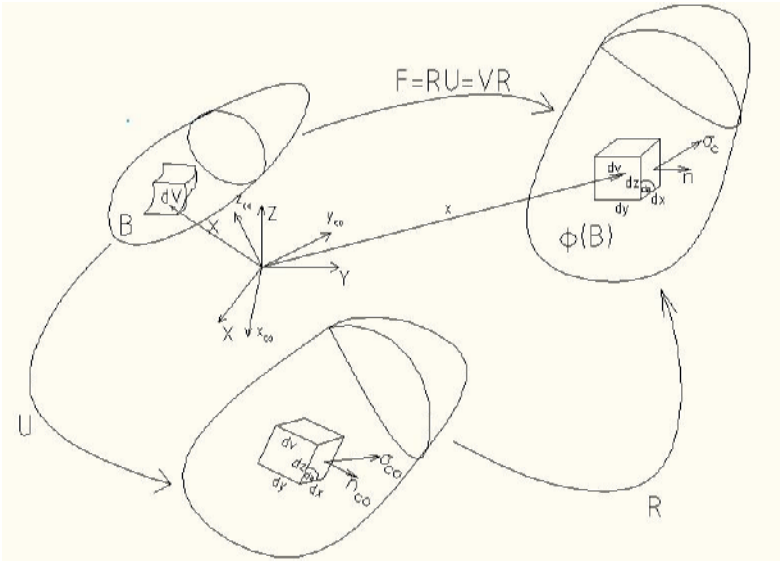

Figure 5.3 Corotated framework

5.1.1.4 Stress rate

In the incremental form of constitutive equations, the stress rate is of significance. The stress rate for the Lagrangian stress tensors (like the second Piola-Kirchhoff stress tensor) can be obtained simply by taking their derivative with respect to time. But for the Eulerian stress tensor like the Cauchy stress tensor; this derivative has to be taken while holding **X** fixed which is called material time derivative. The material time derivative of Cauchy stress gives:

$$\dot{\boldsymbol{\sigma}}=\mathrm{D}\boldsymbol{\sigma}/\mathrm{D}t=\partial\boldsymbol{\sigma}/\partial t+\partial\boldsymbol{\sigma}/\partial\mathbf{x}:\mathbf{v} \qquad (5.32)$$

where **v** is the velocity vector, and **:** denotes contraction which in this equation is between a third order tensor and a vector such that: $\partial\boldsymbol{\sigma}/\partial\mathbf{x}:\mathbf{v}=(\partial\sigma_{ij}/\partial x_k)v_k$.(summation over equal indices implied). All these material time derivatives are non-objective. Objectivity means frame indifference and is a necessary requirement for constitutive laws. To explain objectivity we consider that the coordinate system follows a rigid body transformation like $\mathbf{x_r}=\mathbf{Q}\mathbf{x}+\mathbf{c}$ with rotation matrix **Q** and translational part **c**. A physical quantity is objective when it does not change under this transformation or it transforms as follows:
for a vector quantity

$$\mathbf{v_r}=\mathbf{Q}\mathbf{v} \qquad (5.33a)$$

and for a second order tensor

$$\mathbf{G_r}=\mathbf{Q}\mathbf{G}\mathbf{Q}^T \qquad (5.33b)$$

It can be shown that the Lagrangian tensors (like the right Cauchy-Green strain tensor, the Green strain tensor and the right stretch tensor) are objective since they do not change with a rigid body transformation. The Eulerian tensors (like the left Cauchy-Green strain tensor, the Almansi strain tensor, and the left stretch tensor) are also objective tensors. For example Cauchy stress is an objective quantity because:

$$\boldsymbol{\sigma}_\mathbf{r}\mathbf{n}_\mathbf{r}\mathrm{d}a=\mathrm{d}\mathbf{f}_\mathbf{cr}=\mathbf{Q}\mathrm{d}\mathbf{f}_\mathbf{c}=\mathbf{Q}\boldsymbol{\sigma}\mathbf{n}\mathrm{d}a=\mathbf{Q}\boldsymbol{\sigma}\mathbf{Q}^T\mathbf{Q}\mathbf{Q}^T\mathbf{n}_\mathbf{r}\mathrm{d}a=\mathbf{Q}\boldsymbol{\sigma}\mathbf{Q}^T\mathbf{n}_\mathbf{r}\mathrm{d}a \qquad (5.34)$$

in which we have used the orthogonality of rotation matrix **Q** and the objectivity of the incremental force vector and unit normal vector **n**. The mixed Lagrangian-Eulerian tensors like the deformation gradient or first Piola-Kirchhoff are objective because the Lagrangian part remains unchanged and the Eulerian part changes like a vector (equation (5.33a)), so since the whole transformation is like a vector, hence we can consider them as objective. For example since for the deformation gradient we have: $\mathrm{d}\mathbf{x}=\mathbf{F}\mathrm{d}\mathbf{X}$, then following the rigid body transformation $\mathrm{d}\mathbf{x_r}=\mathbf{Q}\mathrm{d}\mathbf{x}$, the new deformation gradient becomes: $\mathbf{F_r}=\mathbf{Q}\mathbf{F}$ and we have $\mathrm{d}\mathbf{x_r}=\mathbf{F_r}\mathrm{d}\mathbf{X}$. As it can be seen it behaves like a vector and hence it is considered as an objective quantity (Holzapfel, 2000).
Velocity gradient, **L**, and spin tensor, **Ω**, are not objective whereas the stretching rate tensor, **D**, is objective. In fact it can be shown that the Lie derivative produces an objective vector. Taking the Lie derivative of the Cauchy stress tensor gives:

$$\mathcal{L}_v\boldsymbol{\sigma}=\mathbf{F}(\mathrm{D}(\mathbf{F}^{-1}\boldsymbol{\sigma}\mathbf{F}^{-T})/\mathrm{D}t)\mathbf{F}^{T} \qquad (5.35)$$

In this equation time derivative is taken with respect to the reference frame so it is a material time derivative. This equation can be expanded using time derivative of the inverse of the deformation gradient which can be found by taking time derivative of $\mathbf{F}^{-1}\mathbf{F}=\mathbf{I}$ as:

$$\partial\mathbf{F}^{-1}/\partial t=-\mathbf{F}^{-1}\mathbf{L} \qquad (5.36)$$

Hence we have:

$$\mathcal{L}_v\boldsymbol{\sigma}=\dot{\boldsymbol{\sigma}}-\mathbf{L}\boldsymbol{\sigma}-\boldsymbol{\sigma}\mathbf{L}^{T} \qquad (5.37)$$

With the help of $\mathbf{L}=\mathbf{D}+\boldsymbol{\Omega}$, this derivative can be written as:

$$\mathcal{L}_v\boldsymbol{\sigma}=\dot{\boldsymbol{\sigma}}-\mathbf{D}\boldsymbol{\sigma}-\boldsymbol{\sigma}\mathbf{D}-\boldsymbol{\Omega}\boldsymbol{\sigma}+\boldsymbol{\sigma}\boldsymbol{\Omega}=\boldsymbol{\sigma}^{\nabla J}-\mathbf{D}\boldsymbol{\sigma}-\boldsymbol{\sigma}\mathbf{D} \qquad (5.38)$$

In this equation another objective derivative is introduced, $\boldsymbol{\sigma}^{\nabla J}=\dot{\boldsymbol{\sigma}}-\boldsymbol{\Omega}\boldsymbol{\sigma}+\boldsymbol{\sigma}\boldsymbol{\Omega}$, which is called the Jaumann derivative of the Cauchy stress tensor. Taking the material time derivative of the corotational Cauchy stress, $\boldsymbol{\sigma}_{\mathbf{co}}$, gives:

$$\dot{\boldsymbol{\sigma}}_{\mathbf{co}}=\partial\boldsymbol{R}^{T}/\partial t\boldsymbol{\sigma}\mathbf{R}+\mathbf{R}^{T}\dot{\boldsymbol{\sigma}}\mathbf{R}+\mathbf{R}^{T}\boldsymbol{\sigma}\partial\boldsymbol{R}/\partial t=\mathbf{R}^{T}(\dot{\boldsymbol{\sigma}}-\boldsymbol{\omega}\boldsymbol{\sigma}+\boldsymbol{\sigma}\boldsymbol{\omega})\mathbf{R} \qquad (5.39)$$

where $\boldsymbol{\omega}=(\partial\boldsymbol{R}/\partial t)\mathbf{R}^{T}=-\mathbf{R}(\partial\mathbf{R}^{T}/\partial t)$ and it is called the skew matrix. $\dot{\boldsymbol{\sigma}}_{\mathbf{co}}$ is not an objective quantity but the term inside parenthesis introduces an objective quantity and it is called Green-Naghdi or corotational derivative:

$$\boldsymbol{\sigma}^{\nabla co}=\dot{\boldsymbol{\sigma}}-\boldsymbol{\omega}\boldsymbol{\sigma}+\boldsymbol{\sigma}\boldsymbol{\omega} \qquad (5.40)$$

For a rigid body rotation, where stretching rate tensor is zero, $\mathbf{D}=\mathbf{0}$, the spin tensor equals $\boldsymbol{\omega}$, and corotational rate of stress equals Jaumann rate of stress tensor.[9]
Now that all the mathematical foundations of finite elasticity have been introduced, the notion of *constitute law* can be better explained.

5.1.2 Constitutive law

A constitutive law relates the state of stress in the body as a function of an arbitrary deformation of that body. Since we are working with homogenous bodies, the stress is only a function of the deformation gradient, **F**, not of the position within the body, **X**. The constitutive law takes different forms depending on the behavior of the material and on the material usage. In the following the focus

[9] This fact is used in those numerical methods working with corotational stress, because in each small numerical increment step, the stretch rate can be neglected.

is on finite elasticity. In finite elasticity or finite hyperelasticity the behavior of a material is elastic but the level of the strain is not small in contrast to linear elasticity. Hyperelastic materials are materials for which the work done in a closed deformation path is zero and hence a strain energy can be defined. The energy stored in the volume dv (in the current configuration) per unit time can be computed as:

$$\delta P=(\boldsymbol{\sigma}:\mathbf{D})\mathrm{d}v=(\boldsymbol{\sigma}:(\mathbf{L}-\boldsymbol{\Omega}))\mathrm{d}v=(\boldsymbol{\sigma}:\mathbf{L})\mathrm{d}v \qquad (5.42)$$

where P is the power or the strain energy per unit of time. In equation (5.42) the symmetry of the Cauchy stress tensor and the mathematical properties of tensor contraction have been used, which for an anti-symmetric tensor $\boldsymbol{\Omega}$ yields: $\boldsymbol{\sigma}:\boldsymbol{\Omega}=\mathbf{0}$ (for a review of tensor analysis among others Lebedev & Cloud, 2003; Kintzel & Basar, 2006). Therefore this power takes the following forms for different stress definitions:
for first order Piola-Kirchhoff stress with help of equations (5.25) and (5.17):

$$\delta P=(J^{-1}\mathbf{P}\mathbf{F}^{T}:\partial\mathbf{F}/\partial t\mathbf{F}^{-1})J\mathrm{d}V=(\mathbf{P}:\partial\mathbf{F}/\partial t)\mathrm{d}V \qquad (5.43)$$

and for second order Piola-Kirchhoff stress with help of $(5.42)_1$ and equations (5.19) and (5.27):

$$\delta P=(J^{-1}\mathbf{F}\mathbf{S}\mathbf{F}^{T}:\mathbf{F}^{-T}\partial\mathbf{E}/\partial t\mathbf{F}^{-1})J\mathrm{d}V=(\mathbf{S}:\partial\mathbf{E}/\partial t)\mathrm{d}V \qquad (5.44)$$

and for corotational stress with help of equation (5.31):

$$\delta P=(\mathbf{R}\boldsymbol{\sigma}_{\mathbf{co}}\mathbf{R}^{T}:\mathbf{D})\mathrm{d}v=(\boldsymbol{\sigma}_{\mathbf{co}}:\mathbf{R}^{T}\mathbf{D}\mathbf{R})\mathrm{d}v \qquad (5.45)$$

Since for a hyperelastic material the stored energy should be independent of the path, the increment in power should be a complete differential. Noting the differential change of stored energy per unit volume as $\mathrm{d}w=\delta P\mathrm{d}t/\mathrm{d}v$, or with respect to the reference volume $\mathrm{d}W=J\mathrm{d}w=\delta PJ\mathrm{d}t/J\mathrm{d}V=\delta P\mathrm{d}t/\mathrm{d}V$, this strain energy should be a function of the deformation gradient as it can be written according to the chain rule:

$$\mathrm{d}W/\mathrm{d}t=(\partial W/\partial\mathbf{F}):\partial\mathbf{F}/\partial t \qquad (5.46)$$

It is assumed that the strain energy should be an objective quantity. Hence it should be independent of a rigid body motion. This implies that it should be independent of the rotational part of deformation gradient (in other words it should be only a function of its stretch part). Therefore it can be concluded that the strain energy is a function of the Cauchy-Green or Green strain tensors. This gives:

$$\mathrm{d}W/\mathrm{d}t=(\partial W/\partial\mathbf{E}):\partial\mathbf{E}/\partial t \qquad (5.48)$$

Therefore the first order Piola-Kirchhoff stress for a hyperelastic material can be extracted from the stored energy by comparison with equation (5.43):

$$\mathbf{P}=\partial W/\partial\mathbf{F} \qquad (5.48)$$

It can also be extracted from equation (5.44) using the definition of the Green strain tensor and the second order Piola-Kirchhoff stress tensor for a hyperelastic material:

$$\mathbf{S}=\partial W/\partial \mathbf{E}=2\partial W/\partial \mathbf{C} \qquad (5.49)$$

The Cauchy stress can be computed from equation (5.27).
A hypoelastic constitutive law is a relation in which the stress rate is expressed as a function of stretch rate or deformation rate. A general linear hypoelastic law can be stated as:

$$\boldsymbol{\sigma}^{\nabla}=\mathbb{C}:\mathbf{D} \qquad (5.50)$$

where $\mathbb{C}$ is a fourth order tensor and is called material Jacobian or elasticity tensor, $\boldsymbol{\sigma}^{\nabla}$ denotes the objective rate of the Cauchy stress tensor and **:** is the tensor contraction between a fourth order tensor and a second order tensor such that in index notation: $\mathbb{C}:\mathbf{D}=\mathbb{C}_{ijkl}D_{kl}$. This relation states that increments in stress linearly related to increments in strain and upon unloading are recovered. This relation not necessarily conserves the energy in large deformation and the work done in a closed path is not necessarily zero. The material Jacobian is stated between two objective quantities since it will be an objective quantity. The relation between different material Jacobians for different stress rates is explained below. If $\mathbb{C}^{\mathcal{L}}$, $\mathbb{C}^{\nabla J}$ and $\mathbb{C}^{\nabla Co}$ are the material Jacobian for the Lie derivative, Jaumann and corotational stress rates respectively, we have:

$$\mathcal{L}_v\boldsymbol{\sigma}=\mathbb{C}^{\mathcal{L}}:\mathbf{D} \qquad (5.51)$$
$$\boldsymbol{\sigma}^{\nabla J}=\mathbb{C}^{\nabla J}:\mathbf{D} \qquad (5.52)$$
$$\boldsymbol{\sigma}^{\nabla co}=\mathbb{C}^{\nabla co}:\mathbf{D} \qquad (5.53)$$

The relation between different material Jacobians from equations (5.38) and (5.40) and from tensor algebra (see appendix A) becomes:

$$\mathbb{C}^{\nabla J}=\mathbb{C}^{\mathcal{L}}+1/2(\mathbf{I}\odot\boldsymbol{\sigma}+\boldsymbol{\sigma}\odot\mathbf{I}+\boldsymbol{\sigma}\square\mathbf{I}+\mathbf{I}\square\boldsymbol{\sigma}) \qquad (5.54)$$
$$\mathbb{C}^{\nabla co}=\mathbb{C}^{\nabla J}+\mathbb{C}^{\omega} \qquad (5.55)$$

where $\mathbb{C}^{\nabla J}$ and $\mathbb{C}^{\nabla co}$ are the Jaumann and corotational material Jacobian respectively, and $\mathbb{C}^{\omega}:\mathbf{D}=\boldsymbol{\sigma}(\boldsymbol{\omega}\text{-}\boldsymbol{\Omega})\text{-}(\boldsymbol{\omega}\text{-}\boldsymbol{\Omega})\boldsymbol{\sigma}$, the $\odot$ and $\square$ are showing operations on second order tensors such as: $(\mathbf{a}\odot\mathbf{b})_{ijkl}=a_{il}b_{jk}$ and $(\mathbf{a}\square\mathbf{b})_{ijkl}=a_{ik}b_{jl}$ (for their properties refer to appendix A).
The material Jacobian for the second-order Piola-Kirchhoff stress is obtained from:

$$\partial\mathbf{S}/\partial t=\mathbb{C}^{S}:\partial\mathbf{E}/\partial t=\mathbb{C}^{S}:(1/2)\partial\mathbf{C}/\partial t \qquad (5.56)$$

Having $\mathbb{C}^{S}$, then material Jacobian for the Lie derivative can be computed using:

$$\partial\mathbf{S}/\partial t=D(J\mathbf{F}^{-1}\boldsymbol{\sigma}\mathbf{F}^{-T})/Dt=J\mathbf{F}^{-1}[\mathrm{tr}(\mathbf{D})\boldsymbol{\sigma}+\mathcal{L}_v\boldsymbol{\sigma}]\mathbf{F}^{-T}=J\mathbf{F}^{-1}[(\boldsymbol{\sigma}\otimes\mathbf{I}+\mathbb{C}^{\mathcal{L}}):\mathbf{D}]\mathbf{F}^{-T} \qquad (5.57)$$

where the equation (5.36) and the derivative of Jacobian ($\partial J/\partial t=Jtr(\mathbf{D})$) are used. Using equation (5.19), from the equations (5.56) and (5.57) we have:

$$\mathbf{c}:\mathbf{D}=(\boldsymbol{\sigma}\otimes\mathbf{I}+\mathbb{C}^{g}):\mathbf{D}=(1/J)\mathbf{F}(\mathbb{C}^{S}:\mathbf{F}^{T}\mathbf{D}\mathbf{F})\mathbf{F}^{T}=(1/J)(\mathbf{F}\square\mathbf{F}):(\mathbb{C}^{S}:\mathbf{F}^{T}\mathbf{D}\mathbf{F})=$$
$$(1/J)(\mathbf{F}\square\mathbf{F}):(\mathbb{C}^{S}:(\mathbf{D}:(\mathbf{F}\square\mathbf{F}))=(1/J)(\mathbf{F}\square\mathbf{F}):(\mathbb{C}^{S}:((\mathbf{F}^{T}\square\mathbf{F}^{T}):\mathbf{D}\ ) \qquad (5.58)$$

where $\mathbf{c}$ is spatial equivalent of $\mathbb{C}^{S}$ and is called Truesdell material Jacobian. In this relation the properties of $\square$ and fourth-order tensors have been used (see Appendix A). Hence we obtain:

$$\mathbf{c}=\boldsymbol{\sigma}\otimes\mathbf{I}+\mathbb{C}^{g}=(1/J)(\mathbf{F}\square\mathbf{F}):\mathbb{C}^{S}:(\mathbf{F}^{T}\square\mathbf{F}^{T}) \qquad (5.59)$$

According to (5.39) and having $\mathbf{D}=\mathbf{R}\mathbf{D}_{\mathbf{co}}\mathbf{R}^{T}$, $\dot{\boldsymbol{\sigma}}_{\mathbf{co}}$ can be written as:

$$\dot{\boldsymbol{\sigma}}_{\mathbf{co}}=\mathbb{C}^{co}:\mathbf{D}_{\mathbf{co}}=\mathbf{R}^{T}(\mathbb{C}^{\nabla co}:\mathbf{D})\mathbf{R}=\mathbf{R}^{T}(\mathbb{C}^{\nabla co}:\mathbf{R}\mathbf{D}_{\mathbf{co}}\mathbf{R}^{T})\mathbf{R} \qquad (5.60)$$

With the same way as in (5.58) we can find:

$$\mathbb{C}^{co}=(\mathbf{R}^{T}\square\mathbf{R}^{T}):\mathbb{C}^{\nabla co}:(\mathbf{R}\square\mathbf{R}) \qquad (5.61)$$

5.1.3 Hyperelastic Materials

For isotropic materials for which the material properties are independent of directions, the strain energy is insensitive to rotations and only dependents on the invariants of the Cauchy-Green strain tensors (Gurtin 1981):

$$W=W(I_1, I_2, I_3) \qquad (5.62)$$

The invariants of a second order tensor like $\mathbf{C}$ are:

$$I_1=tr(\mathbf{C})=\lambda_1+\lambda_2+\lambda_3 \qquad (5.63a)$$
$$I_2=\tfrac{1}{2}[(tr(\mathbf{C}))^2+tr(\mathbf{C}^2)]=\lambda_1\lambda_2+\lambda_2\lambda_3+\lambda_1\lambda_3 \qquad (5.63b)$$
$$I_3=det(\boldsymbol{C})=\lambda_1\lambda_2\lambda_3 \qquad (5.63c)$$

where λ_i $i=1,2,3$ show the eigenvalues of tensor $\mathbf{C}$. For a fully incompressible material the volume does not change under deformation, hence according to $dv=JdV$, the Jacobian of the deformation tensor is equal to one and hence $I_3=J^2=1$. Therefore the strain energy is not a function of I_3. For nearly incompressible materials, the deformation gradient $\mathbf{F}$ is multiplicatively split into deviatoric or distortional part (or isochoric) and volumetric or dilatational part. According to Flory (1961):

$$\mathbf{F}=\mathbf{F}_{vol}\mathbf{F}_{dev}=(J^{1/3}\mathbf{I})\bar{\mathbf{F}} \qquad (5.64)$$

With this decomposition the invariants can also be decomposed as:

$$I_i=J^{2i/3}\bar{I}_i \qquad i=1,2,3 \qquad (5.65)$$

The $\bar{I}_i$ are invariants of the deviatoric part of **C**. In a *transversely isotropic* material there is a fiber direction along which the material property is different from transverse directions. If this direction is represented at an arbitrary material point by a unit vector $\mathbf{a_0}$ in the initial configuration, and by a unit vector **a** in deformed configuration, the two vectors are related by the deformation gradient as follows:

$$\mathbf{F a_0}=\lambda \mathbf{a} \qquad (5.66)$$

where λ is the stretch ratio along fiber direction. This stretch ratio can be computed through vector inner product as:

$$\lambda^2=\mathbf{F a_0}\cdot\mathbf{F a_0}=\mathbf{a_0}\cdot\mathbf{C a_0} \qquad (5.67)$$

Spencer (1984) has shown that the invariance of strain energy to this material symmetry direction can be defined through the following two extra invariants:

$$I_4=\mathbf{a_0}\cdot\mathbf{C a_0}=\lambda^2 \qquad (5.68a)$$
$$I_5=\mathbf{a_0}\cdot\mathbf{C^2 a_0} \qquad (5.68b)$$

For a nearly incompressible material the decomposition of these invariants to their dilatational and distortional parts gives:

$$\bar{I}_4=\mathbf{a_0}\cdot\bar{\mathbf{C}}\mathbf{a_0}=\bar{\lambda}^2=J^{2/3}I_4 \qquad (5.69a)$$
$$\bar{I}_5=J^{4/3}I_5 \qquad (5.69b)$$

Hence the strain energy for a nearly incompressible transversely isotropic hyperelastic material will be in the following form:

$$W=W_{dev}(\bar{I}_1,\bar{I}_2,\bar{I}_4,\bar{I}_5)+W_{vol}(J) \qquad (5.70)$$

where W_{dev} is the strain energy corresponding to the isochoric part of deformation and W_{vol} the strain energy due to change of volume. The second Piola-Kirchhoff stress tensor for a hyperelastic material from equation (5.49) using the chain rule can be written as:

$$\mathbf{S}=2\Sigma_i(\partial W/\partial \bar{I}_i)\partial \bar{I}_i/\partial\mathbf{C}+2(\partial W_{vol}/\partial J)\partial J/\partial\mathbf{C}=\mathbf{S}_{dev}+\mathbf{S}_{vol} \qquad (5.71)$$

In this equation we need the derivatives of invariants with respect to the right Cauchy-Green strain tensor. These derivatives are (Holzapfel, 2000; Kintzel and Basar, 2006):

$$\partial I_1/\partial\mathbf{C}=\partial(tr(\mathbf{C}))/\partial\mathbf{C}=\partial(\mathbf{I}:\mathbf{C})/\partial\mathbf{C}=\mathbf{I}:\partial\mathbf{C}/\partial\mathbf{C}=\mathbf{I}:1/2(\mathbf{I}\square\mathbf{I}+\mathbf{I}\odot\mathbf{I})=\mathbf{I} \qquad (5.72a)$$
$$\partial I_2/\partial\mathbf{C}=tr(\mathbf{C})\mathbf{I}-\mathbf{C}=I_1\mathbf{I}-\mathbf{C} \qquad (5.72b)$$
$$\partial J/\partial\mathbf{C}=J\mathbf{C}^{-1}/2 \qquad (5.72c)$$
$$\partial I_4/\partial\mathbf{C}=\partial(\mathbf{a_0}.\mathbf{C a_0})/\partial\mathbf{C}=\partial((\mathbf{a_0}\otimes\mathbf{a_0}):\mathbf{C})/\partial\mathbf{C}=(\mathbf{a_0}\otimes\mathbf{a_0}):1/2(\mathbf{I}\square\mathbf{I}+\mathbf{I}\odot\mathbf{I})=\mathbf{a_0}\otimes\mathbf{a_0} \qquad (5.72d)$$

$$\partial I_5/\partial \mathbf{C}=\partial(\mathbf{a_0}.\mathbf{C}^2\mathbf{a_0})/\partial \mathbf{C}=\mathbf{a_0}\otimes\mathbf{C}\mathbf{a_0}+\mathbf{C}\mathbf{a_0}\otimes\mathbf{a_0} \qquad (5.72e)$$

For computing $\partial \bar{I}_i/\partial \mathbf{C}$, we can use the above relations simply by replacing $\mathbf{C}$ with $\bar{\mathbf{C}}$ to compute $\partial \bar{I}_i/\partial \bar{\mathbf{C}}$, using the chain rule it gives:

$$\partial \bar{I}_i/\partial \mathbf{C}=(\partial \bar{I}_i/\partial \bar{\mathbf{C}}):(\partial \bar{\mathbf{C}}/\partial \mathbf{C}) \qquad (5.73)$$

knowing that:

$$\partial \bar{\mathbf{C}}/\partial \mathbf{C}=\mathbf{C}\otimes\partial J^{2/3}/\partial \mathbf{C}+J^{2/3}/2[\mathbf{I}\square\mathbf{I}+\mathbf{I}\odot\mathbf{I}]=J^{2/3}[1/2(\mathbf{I}\square\mathbf{I}+\mathbf{I}\odot\mathbf{I})-1/3(\mathbf{C}\otimes\mathbf{C}^{-1})] \quad (5.74)$$

Combining equations (5.73) and (5.74) and using the symmetry of $\mathbf{C}$ gives:

$$\partial \bar{I}_i/\partial \mathbf{C}=J^{2/3}[\partial \bar{I}_i/\partial \bar{\mathbf{C}}-1/3(\partial \bar{I}_i/\partial \bar{\mathbf{C}}:\bar{\mathbf{C}})\bar{\mathbf{C}}^{-1}] \qquad (5.75)$$

Hence from equations (5.71), (5.72c) and (5.75), it is obtained:

$$\mathbf{S}_{dev}=2J^{2/3}\Sigma_i(\partial W/\partial \bar{I}_i)\mathrm{DEV}(\partial \bar{I}_i/\partial \bar{\mathbf{C}})=2J^{2/3}\mathrm{DEV}(\partial W/\partial \bar{\mathbf{C}}) \qquad (5.76a)$$

$$\mathbf{S}_{vol}=(\mathrm{d}W_{vol}/\mathrm{d}J)J\mathbf{C}^{-1} \qquad (5.76b)$$

where the operator DEV extracts the deviatoric part of a second order tensor ($\mathbf{O}$) is expressed in the initial configuration:

$$\mathrm{DEV}(\mathbf{O})=[\mathbf{O}-1/3(\mathbf{O}:\mathbf{C})\mathbf{C}^{-1}]=\mathbf{O}:[1/2(\mathbf{I}\square\mathbf{I}+\mathbf{I}\odot\mathbf{I})-1/3(\mathbf{C}\otimes\mathbf{C}^{-1})] \qquad (5.77)$$

In the above equation $\mathbf{C}$ can be replaced with $\bar{\mathbf{C}}$. We have $\mathbf{S}_{dev}:\mathbf{C}=0$.
The Cauchy stress from (5.17) can be written as:

$$\boldsymbol{\sigma}=J^{-1}\mathbf{F}\mathbf{S}\mathbf{F}^T=(\partial W_{vol}/\partial J)J\mathbf{I}+(2/J)\,\Sigma_i(\partial W/\partial \bar{I}_i)\,[\mathbf{F}\,\partial \bar{I}_i/\partial \bar{\mathbf{C}}\,\mathbf{F}^T-1/3(\mathbf{F}\,\partial \bar{I}_i/\partial \bar{\mathbf{C}}\,\mathbf{F}^T:\mathbf{I})\mathbf{I}]=$$
$$(\partial W_{vol}/\partial J)J\mathbf{I}+(2/J)\,\Sigma_i(\partial W/\partial \bar{I}_i)\,\mathrm{dev}[\mathbf{F}\,\partial \bar{I}_i/\partial \bar{\mathbf{C}}\,\mathbf{F}^T]=\boldsymbol{\sigma}_{vol}+\boldsymbol{\sigma}_{dev} \qquad (5.78)$$

Hereby the operator dev is like DEV but in the spatial configuration, namely:

$$\mathrm{dev}(\mathbf{o})=[\mathbf{o}-1/3(\mathbf{o}:\mathbf{I})\mathbf{I}]=\mathbf{o}:[1/2(\mathbf{I}\square\mathbf{I}+\mathbf{I}\odot\mathbf{I})-1/3(\mathbf{I}\otimes\mathbf{I})] \qquad (5.79)$$

The trace of the deviatoric stress tensor is 0, and we have: $\boldsymbol{\sigma}_{dev}:\mathbf{I}=0$.
The material Jacobian corresponding to the second-order Piola-Kirchhoff (which is not an objective quantity) can simply be computed from (5.49) by using the chain rule as:

$$\partial \mathbf{S}/\partial \mathrm{t}=(\partial^2 W/\partial \mathbf{E}\partial \mathbf{E}):\partial \mathbf{E}/\partial t=4(\partial^2 W/\partial \mathbf{C}\partial \mathbf{C}):(1/2)\partial \mathbf{C}/\partial t \qquad (5.80a)$$

$$\mathbb{C}^S=(\partial^2 W/\partial \mathbf{E}\partial \mathbf{E})=4(\partial^2 W/\partial \mathbf{C}\partial \mathbf{C}) \qquad (5.80b)$$

Therefore for a transversely isotropic nearly incompressible hyperelastic material, we have:

$$\mathbb{C}^{S}=\mathbb{C}^{S}_{vol}+\mathbb{C}^{S}_{dev} \qquad (5.81)$$

where:

$$\mathbb{C}^{S}_{vol}=2\partial\mathbf{S}_{vol}/\partial\mathbf{C}=J(J\mathrm{d}^{2}W/dJ^{2}+\mathrm{d}W_{vol}/\mathrm{d}J)\mathbf{C}^{-1}\otimes\mathbf{C}^{-1}+2(\mathrm{d}W_{vol}/\mathrm{d}J)J\partial\mathbf{C}^{-1}/\partial\mathbf{C} \qquad (5.82)$$

in which regarding symmetry of $\mathbf{C}$ we have (see Appendix A):

$$\partial\mathbf{C}^{-1}/\partial\mathbf{C}=-1/2(\mathbf{C}^{-1}\square\mathbf{C}^{-1}+\mathbf{C}^{-1}\odot\mathbf{C}^{-1}) \qquad (5.83)$$

and:

$$\mathbb{C}^{S}_{dev}=2\partial\mathbf{S}_{dev}/\partial\mathbf{C}=4[(-J^{-4/3}/3)\mathrm{DEV}(\partial W/\partial\bar{\mathbf{C}})\otimes\bar{\mathbf{C}}^{-1}+J^{-2/3}\partial\mathrm{DEV}(\partial W/\partial\bar{\mathbf{C}})/\partial\mathbf{C}] \qquad (5.84)$$

In equation (5.84) we can write:

$$\partial\mathrm{DEV}(\partial W/\partial\bar{\mathbf{C}})/\partial\mathbf{C}=\partial\mathrm{DEV}(\partial W/\partial\bar{\mathbf{C}})/\partial\bar{\mathbf{C}}:(\partial\bar{\mathbf{C}}/\partial\mathbf{C})=$$
$$[\partial^{2}W/\partial\bar{\mathbf{C}}\partial\bar{\mathbf{C}}-1/3\bar{\mathbf{C}}^{-1}\otimes(\bar{\mathbf{C}}:\partial^{2}W/\partial\bar{\mathbf{C}}\partial\bar{\mathbf{C}}+\partial W/\partial\bar{\mathbf{C}})-1/3(\partial W/\partial\bar{\mathbf{C}}:\bar{\mathbf{C}})\partial\bar{\mathbf{C}}^{-1}/\partial\bar{\mathbf{C}}]:(\partial\bar{\mathbf{C}}/\partial\mathbf{C}) \qquad (5.85)$$

In (5.85) we have:

$$\partial^{2}W/\partial\bar{\mathbf{C}}\partial\bar{\mathbf{C}}=\Sigma_{i}[\partial\bar{I}_{i}/\partial\bar{\mathbf{C}}\otimes\partial(\partial W/\partial\bar{I}_{i})/\partial\bar{\mathbf{C}}+\partial W/\partial\bar{I}_{i}(\partial^{2}\bar{I}_{i}/\partial\bar{\mathbf{C}}\partial\bar{\mathbf{C}})] \qquad (5.86)$$

where:

$$\partial(\partial W/\partial\bar{I}_{i})/\partial\bar{\mathbf{C}}=\Sigma_{j}(\partial^{2}W/\partial\bar{I}_{j}\partial\bar{I}_{i})\partial\bar{I}_{j}/\partial\bar{\mathbf{C}} \qquad (5.87)$$

and

$$\partial^{2}\bar{I}_{2}/\partial\bar{\mathbf{C}}\partial\bar{\mathbf{C}}=\mathbf{I}\otimes\mathbf{I}-1/2(\mathbf{I}\square\mathbf{I}+\mathbf{I}\odot\mathbf{I}) \qquad (5.88a)$$
$$\partial^{2}\bar{I}_{5}/\partial\bar{\mathbf{C}}\partial\bar{\mathbf{C}}=1/2[(\mathbf{a}_{0}\otimes\mathbf{a}_{0})\odot\mathbf{I}+\mathbf{I}\odot(\mathbf{a}_{0}\otimes\mathbf{a}_{0})+(\mathbf{a}_{0}\otimes\mathbf{a}_{0})\square\mathbf{I}+\mathbf{I}\square(\mathbf{a}_{0}\otimes\mathbf{a}_{0})] \qquad (5.88b)$$

5.1.4 Muscle strain energy

Fiber like structure of a muscle and its nonlinear mechanical behavior, make the transversely isotropic hyperelastic constitutive law a good candidate for modeling its passive behavior. Since water is the main constituent of a muscle, the nearly incompressible constraint is also chosen. Finding a suitable strain energy for a hyperelastic material is a complex task. This task can be less complex if the parameters of the strain energy function have a physical meaning. Criscione et al. (2001) have introduced a set of new invariants for transversely isotropic hyperelastic materials which carry a physical meaning. These invariants and their relations with respect to former invariants are as follows:

$$\beta_{1}=ln(J) \qquad (5.89a)$$
$$\beta_{2}=(3ln(I_{4})-2ln(J))/4 \qquad (5.89b)$$

$$\beta_3=ln((I_1I_4-I_5)/2\sqrt{(J^2I_4)}-\sqrt{(((I_1I_4-I_5)/2\sqrt{(J^2I_4)})^2-1))}=$$
$$ln((\bar{I}_1\bar{I}_4-\bar{I}_5)/2\sqrt{(\bar{I}_4)}-\sqrt{(((\bar{I}_1\bar{I}_4-\bar{I}_5)/2\sqrt{(\bar{I}_4)})^2-1)) \quad (5.89c)$$
$$\beta_4=\sqrt{((I_5/I_4^2)-1)}=\sqrt{((\bar{I}_5/\bar{I}_4^2)-1)} \quad (5.89d)$$

β_2 represents strain in fibers due to distortion, β_3 is related to the cross-fiber shear strain and β_4 shows the along-fiber shear strain.

The strain energy proposed for the passive behavior of a muscle is a combination of a (1) neo-Hookean term for taking into account the effect of connective tissues of a muscle and (2) the strain energy used in Blemker et al. (2005) to take into account the effect of interaction between muscle fibers and connective tissues:

$$W_{passive}=c_0(\bar{I}_1-3)+c_1(\beta_3)^2+c_2(\beta_4)^2+W_{vol}(J) \quad (5.90)$$

According to a study of convexity of different models for volumetric part of strain energy by Hartmann & Neff (2003), the following form proposed by Simo and Taylor (1985) is used:

$$W_{vol}(J)=(K/4)[(J-1)^2+(lnJ)^2] \quad (5.91)$$

To model the active behavior of the muscle, no direct energy term is introduced. The force generated in the muscle is expressed in terms of the Cauchy stress and is assumed to be driven from its corresponding strain energy (W_{active}). The Cauchy stress along the fiber direction according to (5.78) can be expressed as:

$$\boldsymbol{\sigma}_f=(2/J)(\partial W_{active}/\partial \bar{I}_4)\bar{I}_4[(\mathbf{a}\otimes\mathbf{a})-\mathbf{I}/3]=(1/J)(\partial W_{active}/\partial \bar{\lambda})\bar{\lambda}[(\mathbf{a}\otimes\mathbf{a})-\mathbf{I}/3]=(1/J)\sigma_f[(\mathbf{a}\otimes\mathbf{a})-\mathbf{I}/3] \quad (5.92)$$

The tensile stress in fiber direction is made of two components: one active and one passive component (see chapter 3). According to muscle structure the fibers can only withstand a tensile force hence the passive component models this behavior (note that this is different from the passive part due to connective tissues which is modeled through a neo-Hookean term). The value of Cauchy stress along the fiber (equation (3.4b)), is therefore expressed as (Wilhelms-Tricario, 1995; Yohansson et al., 2000; Blemker et al. 2005):

$$\sigma_f=F_{CE}/A=(F_{max}/A_{ofl})(f(\lambda,v,A)+f_{passive}))(A_{ofl}/A)=\sigma_{max}(f(\lambda,v,A_c)+f_{passive}))(A_{ofl}/A) \quad (5.93)$$

where σ_{max} is the maximum voluntary force (MVF) a muscle can produce and A is the physical cross sectional area of the muscle in its current position. The MVF of the muscle happens at the optimal fiber length (λ_{ofl}) and at the cross sectional area A_{ofl}. The ratio A_{ofl}/A is replaced with λ/λ_{ofl} to satisfy the assumption of incompressibility (see the appendix in Blemker et al., 2005):

$$\sigma_f=\sigma_{max}(f(\lambda,v,A_c)+f_{passive})(\lambda/\lambda_{ofl}) \quad (5.94)$$

The passive fiber force according to Weiss and Gardiner (2001) for collagen fibers is:

$$f_{passive}=0 \qquad \lambda \leq \lambda_{ofl} \qquad (5.95a)$$
$$f_{passive}=c_3(exp(c_4(\lambda-\lambda_{ofl}))-1) \qquad \lambda_{ofl}<\lambda<\lambda^* \qquad (5.95b)$$
$$f_{passive}=c_5\lambda+c_6 \qquad \lambda \geq \lambda^* \qquad (5.95c)$$

where λ^* is the stretch ratio at which the fibers straightened and force-stretch relationship becomes linear. c_5 and c_6 are determined so that the force at λ^* is continuous and smooth.
The active fiber force depends on the functional model of the muscle. For a Hill-type muscle model the active force is separated multiplicatively (see equation (3.5)) as:

$$f(\lambda,v,A_c)=A_c f_{active}(\lambda)g(v) \qquad (5.96)$$

Force-stretch ratio in the above equation is modeled by a polynomial curve fitting of experimental data. A parabolic curve proposed by Blemker et al. (2005) is used:

$$f_{active}(\lambda)=9((\lambda/\lambda_{ofl})^2-0.4) \qquad \lambda \leq 0.6\lambda_{ofl} \qquad (5.97a)$$
$$f_{active}(\lambda)=1-4(1-(\lambda/\lambda_{ofl})^2) \qquad 0.6\lambda_{ofl}<\lambda<1.4\lambda_{ofl} \qquad (5.97b)$$
$$f_{active}(\lambda)=9((\lambda/\lambda_{ofl})^2-1.6) \qquad \lambda \geq 1.4\lambda_{ofl} \qquad (5.97c)$$

For the Feldman model the equation (3.9) for stress in active fibers is used.

5.2 Implementation of a constitutive law in ANSYS finite element software

The muscle constitutive law in the ANSYS program has not been developed yet. But this software has the capability of implementing a new user defined constitutive law (USERMAT). In ANSYS an updated Lagrangian formulation is used, hence a user defined subroutine should provide the Cauchy stress and the corresponding material Jacobian in Voigt notation. ANSYS also uses corotational coordinates therefore the Cauchy stress provided in a USERMAT should be a corotated Cauchy stress (equation (5.31)) and the corresponding material Jacobian needs to be $\mathbb{C}^{co}$ (equation (5.61)).
With a given strain energy the Cauchy stress (equation (5.78)) and its corotated part can easily be computed from the deformation gradient that is provided by the ANSYS program. For computation of material Jacobian the numerical perturbation method proposed by Miehe (1996) and explained in detail by Sun et al. (2008) is used. In this perturbation technique the element *kl* of the deformation gradient is perturbed:

$$\mathbf{F}_{pert}=\mathbf{F}+\Delta\mathbf{F}^{kl}=\mathbf{F}+(\epsilon/2)(\mathbf{e}_k\otimes\mathbf{e}_l+\mathbf{e}_l\otimes\mathbf{e}_k) \qquad (5.98)$$

where ϵ is the perturbed value (according to Miehe (1996) this is the square root of the machine epsilon; for example of a machine epsilon of 10^{-16} this is 10^{-8}) and the vectors $\mathbf{e}_i$ are the basis vectors of spatial coordinates.
With this $\mathbf{F}_{pert}$ the perturbed value of this Cauchy stress is computed:

$$\Delta\boldsymbol{\sigma}^{kl}=\boldsymbol{\sigma}^{kl}-\boldsymbol{\sigma} \qquad (5.99)$$

And the Jaumann material Jacobian $\mathbb{C}^{\nabla}(i,j,k,l)$ is equal to:

$$\mathbb{C}^{\nabla}(i,j,k,l)=\Delta\boldsymbol{\sigma}^{kl}/\epsilon \qquad (5.100)$$

When the stretch rate tensor (**D**) is small, the spin tensor (**Ω**) is nearly equal to the skew tensor **ω** and therefore the corotational material Jacobian $\mathbb{C}^{\nabla^{co}}$ is approximated by Jaumann material Jacobian (see equation (5.55)):

$$\mathbb{C}^{\nabla^{co}} \cong \mathbb{C}^{\nabla^{J}} \qquad (5.101)$$

With this method there is no need to perform cumbersome calculations needed in equation (5.84). Within USERMAT the force-velocity dependence of a muscle cannot be implemented directly. Thus, the USERMAT implementation of the muscle constitutive law only models the force-length characteristics. The inclusion of velocity dependence is performed in the ANSYS USERELEM capability will be detailed in the next chapter.

5.3 Verification process

Within the process of construction of a new constitutive law, the existing transversely hyperelastic model of ANSYS software was modeled. The exact match between ANSYS computations and the results provided by our USERMAT implementation for one element model under uniaxial loading, shear loading and biaxial loading with USERMAT was observed (Figure 5.4).

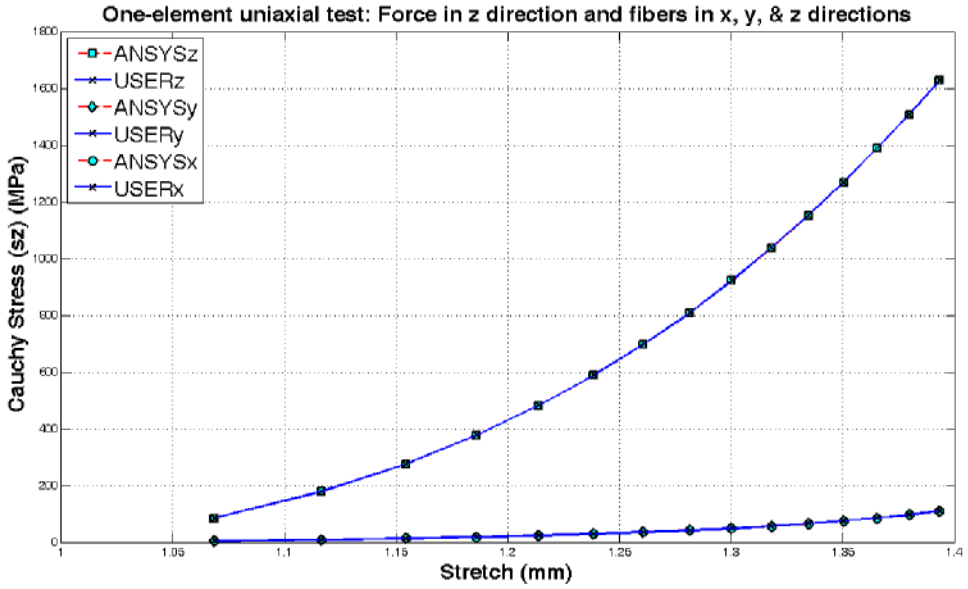

(a)

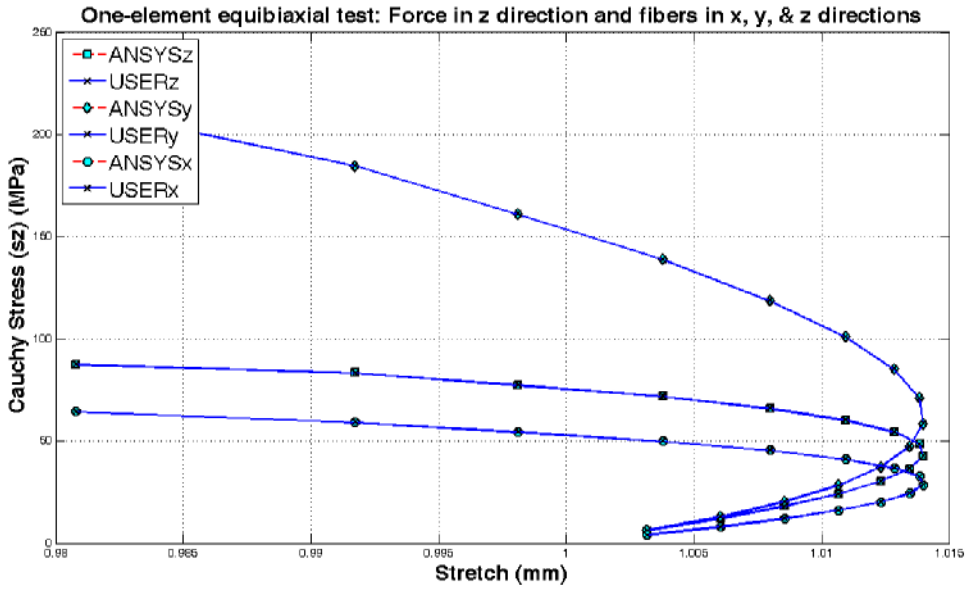

(b)

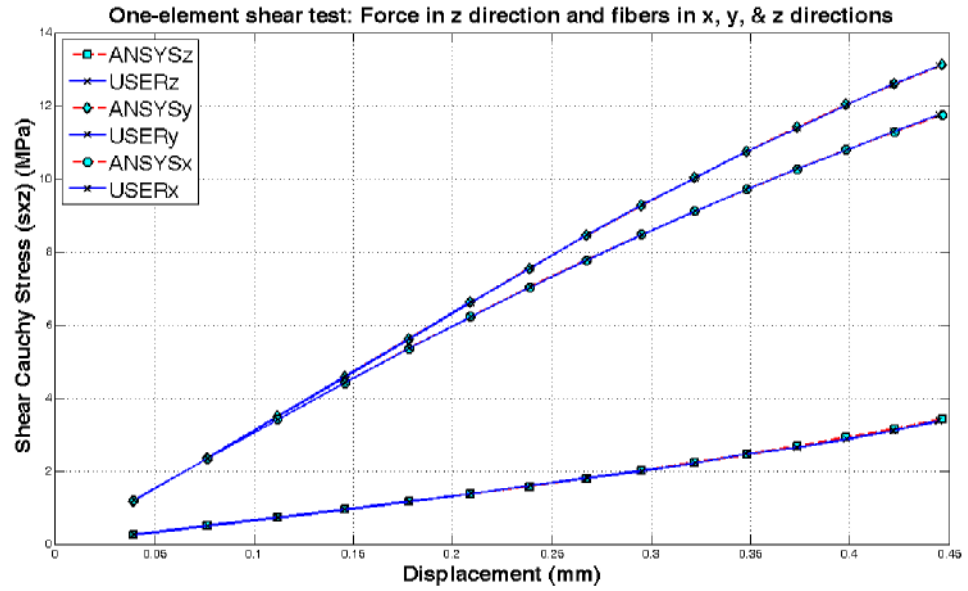

(c)

Figure 5.4- Comparison between ANSYS' transversely hyperelastic model and its equivalent USERMAT implementation for a one-element model under (a) uniaxial loading (b) biaxial loading and (c) shear loading.

Then the behavior of a muscle model was qualitatively observed. For this the deformation of a simple fixed-end bar with a row of muscle elements on top of the bar (red elements) is examined (Figure 5.5). As expected the change of muscle fiber direction from a longitudinal direction (Figure 5.5a) to a diagonal direction (Figure 5.5b) causes the twisting of the bar.

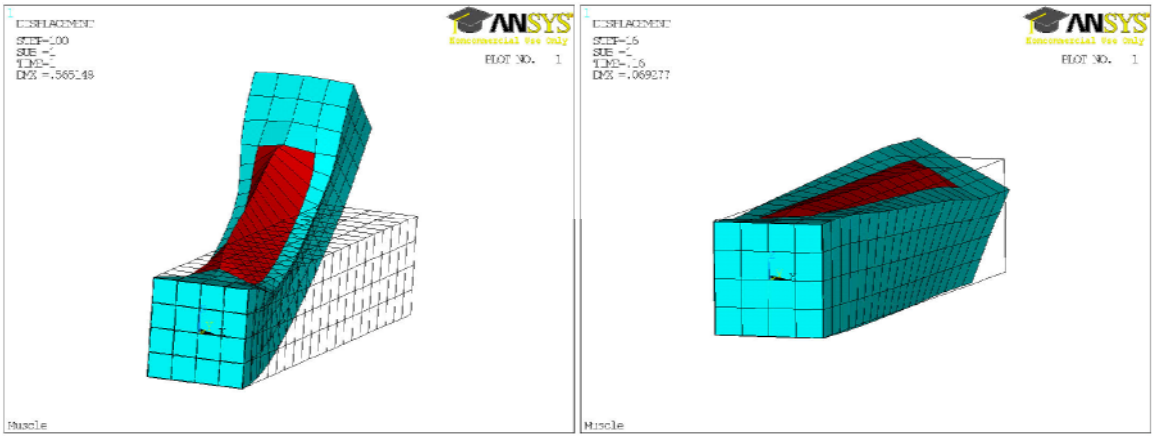

(a) (b)

Figure 5.5 The activation of muscle elements (red elements) on top of a simple fixed-end bar shows (a) a bending with muscle fibers in longitudinal direction and (b) a twisting action with muscle fibers in a diagonal direction.

5.4 Muscle constitutive law used in the face model

This active muscle constitutive law is used in the face model to produce facial gestures. In chapter 4, the focus is on the lip area and those muscles that are mostly involved in speech production. The fiber directions for each muscle element are derived from the fiber directions in the previous face model explained in chapter 4 (Figure 5.6).

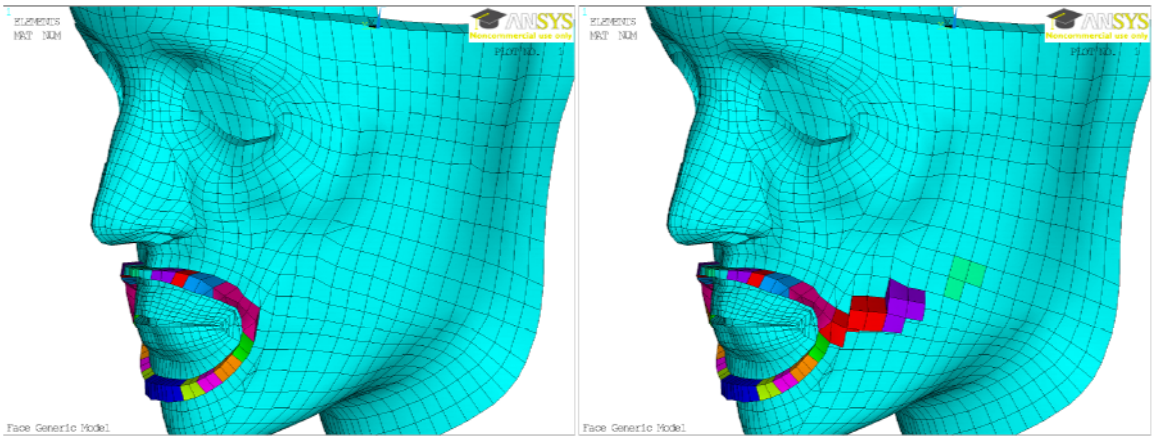

(a) (b)

Figure 5.6 Muscle mechanical properties assigned to elements to model (a) part of orbicularis oris peripheralis (OOP) and (b) OOP with part of buccinator (BUC) muscle. Different colors correspond to different fiber direction in the course of muscle.

The activation of these muscles produces facial gestures related to speech production (Figure 5.6).

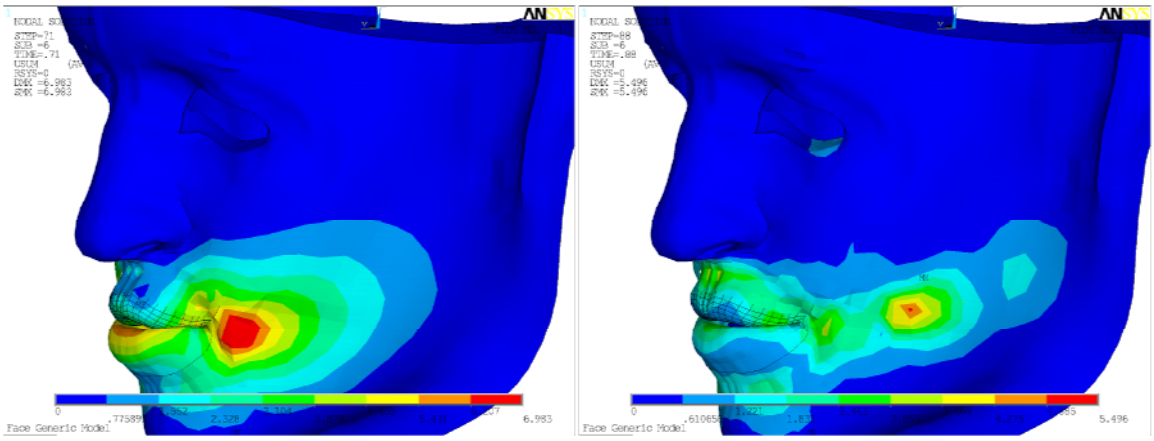

(a) (b)

Figure 5.7 The resulting deformations following the activation of muscles shown in figure 5.6. The process is a moving process and the results depend on the time pattern of activation especially when two muscles act together like in (b).

5.5 Conclusion

Assuming a transversally isotropic behavior matches well the fiber-like structure of the muscle. Nonlinear elastic behavior of the tissues can be modeled with the hyperelastic assumption. Since the main component of the tissues is water, the property of nearly incompressibility should be included in the constitutive behavior of the muscle tissue. A new strain energy for the passive behavior of the muscle is presented. This strain energy contains a neo-Hookean term for the connective tissues around the fibers in the muscle. The other terms in the passive strain energy, model the interaction between muscle fibers and connective tissues. This interaction is modeled through shear behavior along the fiber direction and cross fiber direction. This constitutive law provides a basis for inclusion of velocity dependent term in muscle model which is the subject of next chapter. The effect of this model on face and its qualitative results show stable behavior as it creates reasonable facial gestures.

Chapter Six: Muscle element: Force-Velocity Characteristics

"Slow down and enjoy life. It's not only the scenery you miss by going too fast; you also"
"miss the sense of where you are going and why."
Eddie Cantor

Damping behavior of a muscle is a major feature of a muscle especially when it moves fast. This characteristic has been first studied by Hill (1938). He investigated the relation between muscle force and shortening velocity of a tetanically simulated muscle. He modelled this property as a nonlinear viscous damping in his functional model. This property plays an important role in studying muscle fatigue, cardiac muscle and the fast and fine muscle movements as in speech production. Most of muscle models in the literature use the same force-velocity curve but with different interpolation functions (Zajac, 1989; Botinelli et al. 1996; Brown et al., 1996; Cheng et al. 2000).
In muscle modelling by finite element methods both force-length and force-velocity characteristics should be included in the muscle model. Modeling only force-length characteristics is usually performed through a constitutive law (see chapter 5) (Yucesoy, 2002; Blemker 2005) and it is useful in models which can be treated pseudo-statically. Of course modelling as a constitutive law can be used in a dynamic simulation and the damping property of the muscle can be included through a viscoelastic model (Holzapfel and Gasser, 2001; Holzapfel, 2003). Due to the nonlinear nature of damping behaviour of a muscle, finding an equivalent viscoelastic model is a difficult task, hence usually the damping behaviour of the muscle is taken into account directly through the functional muscle model and its effect as the force-velocity characteristics (Wilhelms-Tricario, 1995; Johansson et al., 2000; Lemos et al., 2004; Martins et al., 2006; Tang et al., 2009).
In this chapter we first review the differential equations of motion in finite elasticity and its equivalent variational weak form. We then explain in brief the linearization process which is essential in obtaining solutions of a nonlinear equation as for example in Newton-Raphson method. After that we review the finite element solution of equations of motion and their linearized form. (For a complete discussion see Belytschko et al., 2000 or Wriggers, 2008.)
Following that we explain how the linearization needed in the solution of finite element equations for the force velocity term in muscle model ends to a virtual time-varying damping matrix. Finally we explain how the Feldman model which includes a force-delayed velocity term creates a virtual time-dependent inertia matrix. A validation example for a Hill-type muscle model wraps up this chapter.

6.1 Equations of motion in finite elasticity and their equivalent variational form

In solid mechanics we assume that mass is conserved during deformation (Figure 6.1). This means that for an arbitrary infinitesimal mass the following equality holds for reference and deformed configuration: $\mathrm{d}m=\rho_0\mathrm{d}V=\rho\mathrm{d}v$. Since we have $\mathrm{d}v=J\mathrm{d}V$, it holds true that:

$$\rho_0=J\rho \qquad (6.1)$$

Taking the time derivative of the total mass $m=\int_B \rho_0 \mathrm{d}V$ gives:

$$J\dot{\rho}+\mathrm{D}J/\mathrm{D}t\,\rho=J\dot{\rho}+J\mathrm{div}(\mathbf{v})\rho=0 \qquad (6.2)$$

In this equation we have of the fact knowing $\partial J/\partial \mathbf{F}=J\mathbf{F}^{-T}$ from which follows that:

$$DJ/Dt=J\mathbf{F}^{-T}:D\mathbf{F}/Dt=J\mathrm{div}(\mathbf{v}) \qquad (6.3)$$

where div(**v**) is divergence operator in current configuration. In equation (6.3) the chain rule and equation (5.17) have been used. So we have:

$$\dot{\rho}+\mathrm{div}(\mathbf{v})\rho=0 \qquad (6.4)$$

Now according to the conservation of linear momentum we have:

$$\int_{\phi(B)}\rho\mathbf{v}\mathrm{d}v=\int_B\rho_0\mathbf{v}\mathrm{d}V=\int_B J\rho\mathbf{v}\mathrm{d}V \qquad (6.5)$$

The equation of motion (Newton's second law) states that the time derivative of the linear momentum is equal to external forces. External forces in general are either body forces which their intensity per unit mass is **b**, and/or traction forces with intensity **t** (force per unit area) on deformed surface $\phi(\partial B)$ (Figure 6.1). Thus, using equations (6.2), (6.3) and (5.22) we have:

$$\mathrm{D}(\int_B J\rho\mathbf{v}\mathrm{d}V)/\mathrm{D}t=\int_B J\rho\dot{\mathbf{v}}\mathrm{d}V=\int_{\phi(B)}\rho\mathbf{b}\mathrm{d}v+\int_{\phi(\partial B)}\mathbf{t}\mathrm{d}a=\int_{\phi(B)}\rho\mathbf{b}\mathrm{d}v+\int_{\phi(\partial B)}\boldsymbol{\sigma}\mathbf{n}\mathrm{d}a \qquad (6.6)$$

According to divergence theorem we have:

$$\int_{\phi(\partial B)}\boldsymbol{\sigma}\mathbf{n}\mathrm{d}a=\int_B\mathrm{div}(\boldsymbol{\sigma})\mathrm{d}v \qquad (6.7)$$

Using the above equation and $\mathrm{d}v=J\mathrm{d}V$ in (6.6), the differential equations of motion can be written as:

$$\mathrm{div}(\boldsymbol{\sigma})+\rho\mathbf{b}=\rho\dot{\mathbf{v}} \qquad (6.8)$$

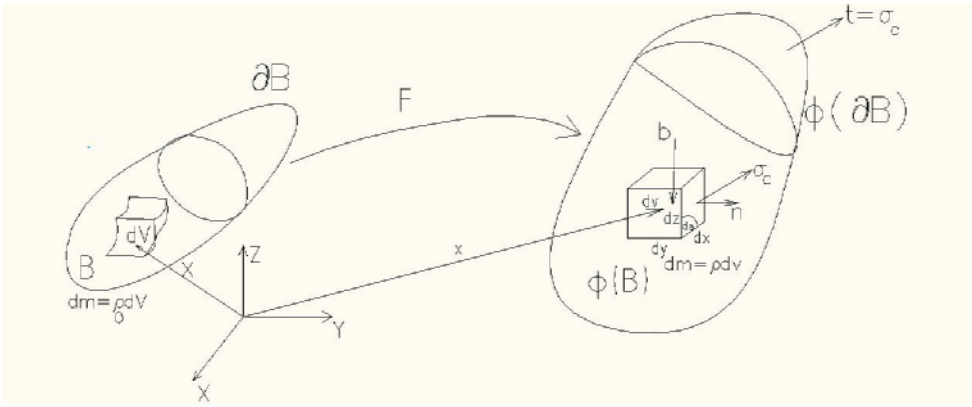

Figure 6.1 Body force b is acting through the volume and traction t on external surface

The boundary conditions for this equation is a displacement (geometric or Dirichlet) boundary condition on a displacement boundary $\phi(\partial B_u)$ as $\mathbf{u}=\mathbf{u}^{ext}$ and a force (natural or Neumann) boundary condition on a traction boundary $\phi(\partial B_\sigma)$ as $\boldsymbol{\sigma}\mathbf{n}=\mathbf{t}^{ext}$.
The equation of motion written in the initial configuration can be obtained from equation (6.6) by using equations (5.25) and (6.1), divergence theorem, using Nanosn's formula $d\mathbf{a}=\mathbf{n}da=J\mathbf{F}^{-T}\mathbf{N}dA$ and replacing $dv=JdV$, which gives:

$$\mathrm{Div}(\mathbf{P})+\rho_0\mathbf{b}=\rho_0\dot{\mathbf{v}} \qquad (6.9a)$$

where $\mathbf{P}$ is first Piola-Kirchhoff stress tensor and Div is divergence operator in initial configuration. Using $\mathbf{P}=\mathbf{FS}$ the above equation can be written in terms of the second Piola-Kirchhoff stress tensor as:

$$\mathrm{Div}(\mathbf{FS})+\rho_0\mathbf{b}=\rho_0\dot{\mathbf{v}} \qquad (6.9b)$$

The boundary equation for the equations (6.9) can be stated as: $\mathbf{u}=\mathbf{u}_0^{ext}$ on ∂B_u as displacement (geometric or Dirichlet) boundary condition and $\mathbf{PN}=\mathbf{FSN}=\mathbf{t}_0^{ext}$ on ∂B_σ as force (natural or Neumann) boundary condition.
The variational form for equations of motion can be found in different ways: by weighted residual methods or by variational principle or with Hu-Washizu principle (Washizu, 1975; Bathe, 1996). We use the weighted residual method to find the weak or variational form.
If an approximation function for body displacement ($\mathbf{u}_0^h$) is assumed, the equations of motion cannot be exactly satisfied. Inserting the assumed approximate displacement field into the equations of motion, the residual in initial configuration becomes:

$$\mathbf{R}_h=\mathrm{Div}(\mathbf{P})(\mathbf{u}_0^h)+\rho_0\mathbf{b}-\rho_0\dot{\mathbf{v}}_h=\mathrm{Div}(\mathbf{FS})(\mathbf{u}_0^h)+\rho_0\mathbf{b}-\rho_0\dot{\mathbf{v}}_h \qquad (6.10a)$$

and in current configuration we have:

$$\mathbf{r}_h=\mathrm{div}(\boldsymbol{\sigma})(\mathbf{u}^h)+\rho\mathbf{b}-\rho\dot{\mathbf{v}}_h \qquad (6.10b)$$

In a weighted residual method we multiply the residual by a weighting function and then we integrate the result over the domain of the solution and equate it to zero. Different weights create different variational methods. The weights should be differentiable to the same order as the highest order of the differential equation. In addition the weights should satisfy displacement (geometric) boundary conditions and also the homogeneous natural boundary conditions (i.e. with $\mathbf{t}_0^{ext}=\mathbf{0}$). In the Galerkin weighted residual method the weights are equal to approximation functions but we assume a Petrov-Galerkin method in which they are different (Reddy, 2002). Showing the weight function as vector $\mathbf{w}$ then the weighted residual in initial configurations becomes:

$$\int_B \mathbf{R}_h\cdot\mathbf{w}dV=\int_B(\mathrm{Div}(\mathbf{P})\cdot\mathbf{w}+\rho_0(\mathbf{b}-\dot{\mathbf{v}}_h)\cdot\mathbf{w})dV=0 \qquad (6.11)$$

The weight is called test function or virtual displacement. The integration by parts gives:

$$\int_B \mathrm{Div}(\mathbf{P})\cdot\mathbf{w}\mathrm{d}V=\int_{\partial B}\mathbf{w}\cdot\mathbf{P}\mathbf{N}\mathrm{d}A-\int_B \mathbf{P}:\mathbf{Grad}(\mathbf{w})\mathrm{d}V \qquad (6.12)$$

With replacing (6.12) in (6.11) we obtain:

$$\Psi=\int_B \mathbf{P}:\mathbf{Grad}(\mathbf{w})\mathrm{d}V-\int_B \rho_0(\mathbf{b}-\dot{\mathbf{v}}_h)\cdot\mathbf{w})\mathrm{d}V-\int_{\partial B}\mathbf{w}\cdot\mathbf{t}_0^{ext}\mathrm{d}A=0 \qquad (6.13)$$

With using $\mathbf{P}=\mathbf{F}\mathbf{S}$ the equation (6.13) can be written as:

$$\Psi=\int_B (\mathbf{S}:[\mathbf{F}^T\mathbf{Grad}(\mathbf{w})+\mathbf{Grad}(\mathbf{w})^T\mathbf{F}]/2)\mathrm{dV}-\int_B \rho_0(\mathbf{b}-\dot{\mathbf{v}}_h)\cdot\mathbf{w})\mathrm{d}V-\int_{\partial B}\mathbf{w}\cdot\mathbf{t}_0^{ext}\mathrm{d}A=0 \quad (6.14)$$

In the above equation, the symmetry of $\mathbf{S}$ is used (since the contraction of a symmetric tensor with an antisymmetric one is zero). The functional Ψ is the weak form of the equations of motion. The weak form in the current configuration can be obtained directly from equation (6.10b) or by pushing forward the equations in initial configuration (equations (6.13) or (6.14)). Using equation (6.14) and $\mathbf{S}=J\mathbf{F}^{-1}\boldsymbol{\sigma}\mathbf{F}^{-T}$ and using the push forward of gradient[10] we can write:

$$\psi=\int_{\phi(B)}\boldsymbol{\sigma}:[\mathbf{Grad}(\mathbf{w})\mathbf{F}^{-1}+\mathbf{F}^{-T}\mathbf{Grad}(\mathbf{w})^T]/2\mathrm{d}v-\int_{\phi(B)}\rho(\mathbf{b}-\dot{\mathbf{v}}_h)\cdot\mathbf{w})\mathrm{d}v-\int_{\phi(\partial B)}\mathbf{w}\cdot\mathbf{t}^{ext}\mathrm{d}a=$$
$$\int_{\phi(B)}\boldsymbol{\sigma}:[\mathbf{grad}(\mathbf{w})+\mathbf{grad}(\mathbf{w})^T]/2\mathrm{d}v-\int_{\phi(B)}\rho(\mathbf{b}-\dot{\mathbf{v}}_h)\cdot\mathbf{w})\mathrm{d}v-\int_{\phi(\partial B)}\mathbf{w}\cdot\mathbf{t}^{ext}\mathrm{d}a=0 \qquad (6.15)$$

6.2 Linearization

Solving nonlinear functions usually is performed with a linearization process. Linearization of a function like $\boldsymbol{\Gamma}(\mathbf{x})$ along a direction $\mathbf{u}$, generally can be defined as:

$$\boldsymbol{\Gamma}(\mathbf{x}+\mathbf{u})=\boldsymbol{\Gamma}(\mathbf{x})+\Delta\boldsymbol{\Gamma}+\mathbf{R}=Lin(\boldsymbol{\Gamma})+\mathbf{R} \qquad (6.16)$$

where $\Delta\boldsymbol{\Gamma}$ is called linear part of $\boldsymbol{\Gamma}$ and $\mathbf{R}$ is the residual, and $Lin(\boldsymbol{\Gamma})$ shows the linearization of $\boldsymbol{\Gamma}$. The linear part can be computed as:

$$\Delta\boldsymbol{\Gamma}=\mathrm{D}\boldsymbol{\Gamma}.\mathbf{u}=\mathrm{d}\boldsymbol{\Gamma}(\mathbf{x}+\epsilon\mathbf{u})/\mathrm{d}\epsilon|_{\epsilon=0} \qquad (6.17)$$

In the following the linear part of some important quantities is computed.

6.2.1 The deformation gradient

The linear part of the deformation gradient can be calculated as:

$$\Delta\mathbf{F}=\mathrm{D}\mathbf{F}.\mathbf{u}=\mathrm{d}\mathbf{F}(\mathbf{x}+\epsilon\mathbf{u})/\mathrm{d}\epsilon|_{\epsilon=0}=\mathrm{d}[\partial(\mathbf{x}+\epsilon\mathbf{u})/\partial\mathbf{X}]/\mathrm{d}\epsilon|_{\epsilon=0}=\mathbf{Grad}(\mathbf{u}) \qquad (6.18)$$

And for its inverse, $\mathbf{F}^{-1}$, using $\mathbf{F}\mathbf{F}^{-1}=\mathbf{I}$, it can be written as:

---

[10] The push forward of gradient of a scalar α is: $\mathrm{grad}(\alpha)=\mathbf{F}^{-T}\mathrm{Grad}(\alpha)$, and for a vector $\mathbf{w}$ is: $\mathbf{grad}(\mathbf{w})=\mathbf{Grad}(\mathbf{w})\mathbf{F}^{-1}$

$$\Delta\mathbf{F}^{-1}=\mathrm{D}\mathbf{F}^{-1}.\mathbf{u}=-\mathbf{F}^{-1}(\mathrm{D}\mathbf{F}.\mathbf{u})\mathbf{F}^{-1}=-\mathbf{F}^{-1}(\mathbf{Grad}(\mathbf{u}))\mathbf{F}^{-1}=-\mathbf{F}^{-1}\mathbf{grad}(\mathbf{u}) \qquad (6.19)$$

6.2.2 The strain tensors

From equation (6.18) and knowing that $\mathbf{C}=\mathbf{F}^T\mathbf{F}$ we have:

$$\Delta\mathbf{C}=\mathrm{D}\mathbf{C}.\mathbf{u}=\mathbf{F}^T\mathbf{Grad}(\mathbf{u})+\mathbf{Grad}(\mathbf{u})^T\mathbf{F} \qquad (6.20)$$

And for the Green strain tensor, $\mathbf{E}=(\mathbf{C}-\mathbf{I})/2$, it becomes:

$$\Delta\mathbf{E}=\mathrm{D}\mathbf{E}.\mathbf{u}=1/2[\mathbf{F}^T\mathbf{Grad}(\mathbf{u})+\mathbf{Grad}(\mathbf{u})^T\mathbf{F}]=1/2\mathbf{F}^T[\mathbf{grad}(\mathbf{u})+\mathbf{grad}(\mathbf{u})^T]\mathbf{F}=\mathbf{F}^T\nabla^s\mathbf{u}\mathbf{F} \qquad (6.21)$$

where $\nabla^s\mathbf{u}=1/2(\mathbf{grad}(\mathbf{u})+\mathbf{grad}(\mathbf{u})^T)$ shows the symmetric part of $\mathbf{grad}(\mathbf{u})$. It is interesting to note that the linearization of $\mathbf{E}$ at the origin where $\mathbf{F}=\mathbf{C}=\mathbf{I}$ gives:

$$Lin(\mathbf{E})=\mathbf{0}+1/2[\mathbf{Grad}(\mathbf{u})+\mathbf{Grad}(\mathbf{u})^T]=\epsilon \qquad (6.22)$$

which says that linearization of the Green strain tensor at the origin or within the region of small deformation is equal to the strain in linear theory.
The linear part of $\mathbf{C}^{-1}$ can be obtained from $\mathbf{C}\mathbf{C}^{-1}=\mathbf{I}$ and using the definition of $\mathbf{C}=\mathbf{F}^T\mathbf{F}$ with the definition of push forward of gradient as:

$$\Delta\mathbf{C}^{-1}=\mathrm{D}\mathbf{C}^{-1}.\mathbf{u}=-\mathbf{C}^{-1}(\mathrm{D}\mathbf{C}.\mathbf{u})\mathbf{C}^{-1}=-\mathbf{C}^{-1}[\mathbf{F}^T\mathbf{Grad}(\mathbf{u})+\mathbf{Grad}(\mathbf{u})^T\mathbf{F}]\mathbf{C}^{-1}=$$
$$=-\mathbf{F}^{-1}[\mathbf{grad}(\mathbf{u})+\mathbf{grad}(\mathbf{u})^T]\mathbf{F}^{-T} \qquad (6.23)$$

6.2.3 The Jacobian

The linearization of the Jacobian can be found with the help of chain rule and knowing that $\partial J/\partial\mathbf{F}=J\mathbf{F}^{-T}$:

$$\Delta J=\mathrm{D}J.\mathbf{u}=\partial J/\partial\mathbf{F}:(\mathrm{D}\mathbf{F}.\mathbf{u})=J\mathbf{F}^{-T}:\mathbf{Grad}(\mathbf{u})=J\mathbf{I}:\mathbf{Grad}(\mathbf{u})\mathbf{F}^{-1}=J\mathbf{I}:\mathbf{grad}(\mathbf{u})=J\mathrm{div}(\mathbf{u}) \qquad (6.24)$$

6.2.4 The strain rates: First and second order

The linear part of the derivative of the deformation gradient can be written as:

$$\mathrm{D}(\mathrm{D}\mathbf{F}/\mathrm{D}t).\mathbf{u}=\mathbf{Grad}(\dot{\mathbf{u}})=\mathbf{grad}(\dot{\mathbf{u}})\mathbf{F} \qquad (6.25)$$

And for the velocity gradient, $\mathbf{L}=(\mathrm{D}\mathbf{F}/\mathrm{D}t)\mathbf{F}^{-1}$, its linear part can be written as:

$$\mathrm{D}\mathbf{L}.\mathbf{u}=\mathbf{grad}(\dot{\mathbf{u}})-\mathbf{L}\mathbf{grad}(\mathbf{u}) \qquad (6.26)$$

The acceleration of a point of a body is the material time derivative of the velocity vector:

$$\mathbf{a}=\mathrm{D}\mathbf{v}/\mathrm{D}t=\partial\mathbf{v}/\partial t+\mathbf{L}\mathbf{v} \qquad (6.27)$$

The acceleration gradient can be written as:

$$\mathbf{A}=\partial\mathbf{a}/\partial\mathbf{x}=(D^2\mathbf{F}/Dt^2)\mathbf{F}^{-1} \qquad (6.28)$$

Now the linear part of $D^2\mathbf{F}/Dt^2$ can be written as:

$$D(D^2\mathbf{F}/Dt^2).\mathbf{u}=\mathbf{Grad}(\ddot{\mathbf{u}})=\mathbf{grad}(\ddot{\mathbf{u}})\mathbf{F} \qquad (6.29)$$

The linear part of the acceleration gradient using (6.29) becomes:

$$D\mathbf{A}.\mathbf{u}=\mathbf{grad}(\ddot{\mathbf{u}})-\mathbf{A}\mathbf{grad}(\mathbf{u}) \qquad (6.30)$$

The material time derivative of inverse of the deformation gradient is:

$$D(\mathbf{F}^{-1})/Dt=-\mathbf{F}^{-1}\mathbf{L} \qquad (6.31)$$

Therefore the material time derivative of the velocity gradient can be written as:

$$D\mathbf{L}/Dt=\mathbf{A}-\mathbf{L}^2 \qquad (6.32)$$

Hence the linearization of $\mathbf{L}^2$ and $\mathbf{A}$ can be computed as follows:

$$D\mathbf{L}^2.\mathbf{u}=\mathbf{grad}(\dot{\mathbf{u}})\mathbf{L}-\mathbf{L}\mathbf{grad}(\mathbf{u})\mathbf{L}+\mathbf{L}\mathbf{grad}(\dot{\mathbf{u}})-\mathbf{L}^2\mathbf{grad}(\mathbf{u}) \qquad (6.33)$$

$$D(D\mathbf{L}/Dt).\mathbf{u}=\mathbf{grad}(\ddot{\mathbf{u}})-\mathbf{A}\mathbf{grad}(\mathbf{u})-\mathbf{grad}(\dot{\mathbf{u}})\mathbf{L}+\mathbf{L}\mathbf{grad}(\mathbf{u})\mathbf{L}-\mathbf{L}\mathbf{grad}(\dot{\mathbf{u}})+\mathbf{L}^2\mathbf{grad}(\mathbf{u}) \qquad (6.34)$$

6.2.5 The kinematic quantities along a fiber direction

Taking the material time derivative of stretch ratio in fiber direction $\mathbf{a}_0$, i.e. $\lambda^2=\mathbf{Fa_0}.\mathbf{Fa_0}$, the velocity in the fiber direction becomes:

$$\dot{\lambda}=\lambda(\mathbf{a}\cdot\mathbf{La})=\lambda(\mathbf{a}\cdot\mathbf{Da}) \qquad (6.35)$$

where we have used this property: $\mathbf{a}.\boldsymbol{\Omega}\mathbf{a}=\mathbf{0}$. Taking the time derivative of velocity, the fiber acceleration is obtained:

$$\ddot{\lambda}=\dot{\lambda}^2/\lambda+\lambda[\mathbf{a}\cdot\mathbf{Aa}+\mathbf{a}\cdot\mathbf{L}^T\mathbf{La}-2(\mathbf{a}\cdot\mathbf{La})^2] \qquad (6.36)$$

The linear part of fiber stretch ratio can be obtained with the help of $\lambda^2=\mathbf{Fa_0}\cdot\mathbf{Fa_0}$ and $\mathbf{Fa_0}=\lambda\mathbf{a}$ and equation (6.18) as:

$$D\lambda.\mathbf{u}=(2/2\lambda)\mathbf{Grad}(\mathbf{u})\mathbf{a}_0\cdot\mathbf{Fa}_0=\lambda(\mathbf{grad}(\mathbf{u})\mathbf{a}\cdot\mathbf{a})=\lambda(\mathbf{a}\cdot\nabla^s\mathbf{ua}) \qquad (6.37)$$

where from the properties of the vector dot product we know $\mathbf{a}\cdot 1/2(\mathbf{grad}(\mathbf{u})-\mathbf{grad}(\mathbf{u})^T)\mathbf{a}=0$. Accordingly we can find:

$$D\mathbf{a}.\mathbf{u}=\mathbf{grad}(\mathbf{u})\mathbf{a}-(\mathbf{a}\cdot\nabla^s\mathbf{ua})\mathbf{a} \qquad (6.38)$$

Using the above results the linear part of the fiber velocity and fiber acceleration can be written as:

$$\mathrm{D}\dot{\lambda}\cdot\mathbf{u}=\dot{\lambda}(\mathbf{a}\cdot\nabla^{s}\mathbf{u}\mathbf{a})+\lambda[\mathbf{L}\mathbf{a}\cdot\mathbf{grad}(\mathbf{u})\mathbf{a}-2(\mathbf{a}\cdot\nabla^{s}\mathbf{u}\mathbf{a})\mathbf{L}\mathbf{a}\cdot\mathbf{a}+\mathbf{a}\cdot\nabla^{s}\dot{\mathbf{u}}\mathbf{a}] \qquad (6.39)$$

$$\begin{aligned}\mathrm{D}\ddot{\lambda}\cdot\mathbf{u}=&\ddot{\lambda}(\mathbf{a}\cdot\nabla^{s}\mathbf{u}\mathbf{a})+2\dot{\lambda}[\mathbf{L}\mathbf{a}\cdot\mathbf{grad}(\mathbf{u})\mathbf{a}-2(\mathbf{a}\cdot\nabla^{s}\mathbf{u}\mathbf{a})\mathbf{L}\mathbf{a}\cdot\mathbf{a}]+\\ &\lambda[\mathbf{a}\cdot\nabla^{s}\ddot{\mathbf{u}}\mathbf{a}+2\mathbf{L}\mathbf{a}\cdot\mathbf{grad}(\dot{\mathbf{u}})\mathbf{a}-4(\mathbf{a}\cdot\mathbf{L}\mathbf{a})(\mathbf{a}\cdot\nabla^{s}\dot{\mathbf{u}}\mathbf{a})+\\ &\mathbf{A}\mathbf{a}\cdot\mathbf{grad}(\mathbf{u})\mathbf{a}-4(\mathbf{a}\cdot\mathbf{L}\mathbf{a})(\mathbf{L}\mathbf{a}\cdot\mathbf{grad}(\mathbf{u})\mathbf{a})+(\mathbf{a}\cdot\nabla^{s}\mathbf{u}\mathbf{a})(8(\mathbf{a}\cdot\mathbf{L}\mathbf{a})^{2}-2\mathbf{a}\cdot\mathbf{L}^{T}\mathbf{L}\mathbf{a}-2\mathbf{a}\cdot\mathbf{A}\mathbf{a})]\end{aligned} \qquad (6.40)$$

6.2.6 Stress tensors

Linearization of stress tensors is dependent on the governing constitutive law. Assuming a hyperelastic material the linearization of the stress tensor is explained. The linear part of the second Piola-Kirchhoff stress tensor with the help of the equation (5.56) becomes:

$$\Delta\mathbf{S}=\mathrm{D}\mathbf{S}.\mathbf{u}=\mathbb{C}^{S}:(1/2)\mathrm{D}\mathbf{C}.\mathbf{u}=\mathbb{C}^{S}:(\mathrm{D}\mathbf{E}.\mathbf{u})=\mathbb{C}^{S}:\Delta\mathbf{E} \qquad (6.41)$$

The linear part of the first Piola-Kirchhoff stress tensor, $\mathbf{P}=\mathbf{F}\mathbf{S}$, using equation (6.18) becomes:

$$\Delta\mathbf{P}=\mathrm{D}\mathbf{P}.\mathbf{u}=(\mathrm{D}\mathbf{F}.\mathbf{u})\mathbf{S}+\mathbf{F}(\mathrm{D}\mathbf{S}.\mathbf{u})=\mathbf{Grad}(\mathbf{u})\mathbf{S}+\mathbf{F}(\mathbb{C}^{S}:\Delta\mathbf{E}) \qquad (6.42)$$

Therefore the linear part of the Kirchhoff stress tensor, $\boldsymbol{\tau}=J\boldsymbol{\sigma}=\mathbf{P}\mathbf{F}^{T}=\mathbf{F}\mathbf{S}\mathbf{F}^{T}$, using equation (5.58) can be written as:

$$\begin{aligned}\Delta\boldsymbol{\tau}=\mathrm{D}\boldsymbol{\tau}.\mathbf{u}=&\mathbf{grad}(\mathbf{u})\boldsymbol{\tau}+\mathbf{F}(\mathbb{C}^{S}:\Delta\mathbf{E})\mathbf{F}^{T}+\boldsymbol{\tau}\mathbf{grad}(\mathbf{u})^{T}=[\mathbf{grad}(\mathbf{u})\boldsymbol{\tau}+\boldsymbol{\tau}\mathbf{grad}(\mathbf{u})^{T}]+\mathbf{F}(\mathbb{C}^{S}:\mathbf{F}^{T}\nabla^{s}\mathbf{u}\mathbf{F})\mathbf{F}^{T}=\\ &[\mathbf{grad}(\mathbf{u})\boldsymbol{\tau}+\boldsymbol{\tau}\mathbf{grad}(\mathbf{u})^{T}]+J\mathbb{c}:\nabla^{s}\mathbf{u}=J[\mathbf{grad}(\mathbf{u})\boldsymbol{\sigma}+\boldsymbol{\sigma}\mathbf{grad}(\mathbf{u})^{T}+\mathbb{c}:\nabla^{s}\mathbf{u}]\end{aligned} \qquad (6.43)$$

6.2.7 Weak forms

From equation (6.13) the linear part of the weak form in initial configuration (Lagrangian point of view) can be written as:

$$\begin{aligned}\Delta\Psi=\mathrm{D}\Psi.\mathbf{u}=&\int_{B}[\mathbf{Grad}(\mathbf{u})\mathbf{S}:\mathbf{Grad}(\mathbf{w})+\mathbf{F}(\mathbb{C}^{S}:\Delta\mathbf{E}):\mathbf{Grad}(\mathbf{w})]\mathrm{d}V=\\ &\int_{B}\{\mathbf{Grad}(\mathbf{u})\mathbf{S}:\mathbf{Grad}(\mathbf{w})+(\mathbb{C}^{S}:\Delta\mathbf{E}):1/2[\mathbf{F}^{T}\mathbf{Grad}(\mathbf{w})+\mathbf{Grad}(\mathbf{w})^{T}\mathbf{F}]\}\mathrm{d}V=\\ &\int_{B}\{\mathbf{Grad}(\mathbf{u})\mathbf{S}:\mathbf{Grad}(\mathbf{w})+(\mathbb{C}^{S}:\Delta\mathbf{E}):\delta\mathbf{E}\}\mathrm{d}V\end{aligned} \qquad (6.44)$$

where the symmetry of the material Jacobian is used and $\delta\mathbf{E}=1/2[\mathbf{F}^{T}\mathbf{Grad}(\mathbf{w})+\mathbf{Grad}(\mathbf{w})^{T}\mathbf{F}]$. The linear part of weak form in current configuration (Eulerian point of view) from equations (6.15) and (6.43) and $\mathrm{d}v=J\mathrm{d}V$ may be found as:

$$\begin{aligned}\Delta\psi=\mathrm{D}\psi.\mathbf{u}=&\int_{B}(D(J\boldsymbol{\sigma}).\mathbf{u}):[\mathbf{grad}(\mathbf{w})+\mathbf{grad}(\mathbf{w})^{T}]/2\mathrm{d}V=\\ =&\int_{B}J[\mathbf{grad}(\mathbf{u})\boldsymbol{\sigma}+\boldsymbol{\sigma}\mathbf{grad}(\mathbf{u})^{T}+\mathbb{c}:\nabla^{s}\mathbf{u}]:\nabla^{s}\mathbf{w}\mathrm{d}V=\\ &\int_{\phi(B)}\{\mathbf{grad}(\mathbf{u})\boldsymbol{\sigma}:\mathbf{grad}(\mathbf{w})+(\mathbb{c}:\nabla^{s}\mathbf{u}):\nabla^{s}\mathbf{w}\}dv\end{aligned} \qquad (6.45)$$

where the symmetry of Cauchy stress and the properties of contraction is used. Please pay attention that to compute the linear part of weak form in current configuration, the domain of integral first has been changed to initial configuration and then the linearization process has been performed and after

that the domain has been changed to current configuration. Otherwise in the linearization process we should take the volume as a variable.

6.3 Finite element formulation

Usually it is not possible to obtain analytic solutions for the equations of motion (6.9a) or (6.9b), in particular if the domain of solution is geometrically complex or there are nonlinearities in the problem. Therefore we resort to the numerical approximations. Two of the most used numerical methods are the *Finite Difference Method* (FDM) and *Finite Element Method* (FEM). In these methods instead of finding the solution at all points inside the solution domain (for a continuum domain they are infinite) the problem is transformed to finding the solution at some specified points (they are called *nodes*). Then solution between these points can be interpolated from the solution at the nodes. The solution domain in the equations of motion is a space-time domain and in general it is a four dimensional domain (3D-1D). The common method to find the time history of motion is to separate discretization in space and time such that in space the FEM is used and in time domain the FDM and they are not dependent (see for example Bathe, 1996). In finite element methods the solution domain in space is discretized to small regions (called *elements*). Each element consists of a number of nodes. The solution within the element is interpolated from the solution at nodes. The type and the order of interpolation functions depend on the required precision and the number of nodes per element and the required smoothness. To extract the discretized version of equations first they are transformed to a variational or weak form. These variational forms should be integrated over the domain of solution. Due to this integration and also the derivatives with respect to spatial variables they need a presentation of geometrical space. In an isoparametric finite element method the geometry is approximated with the same order and smoothness as field variable (which in equations of motion is the displacement). For an isoparametric Lagrangian element a reference (or parent) element, Ω_0, is defined and each element in initial configuration, Ω_e; or current configuration; ω_e, is obtained from a mapping from reference element (Figure 6.2). The coordinate system in the reference element is a local orthogonal coordinate system. So for an isoparametric finite element with Lagrangian interpolation function the field and geometry discretization can be expressed as:

$$\mathbf{X}_e=N_I(\mathbf{r})\mathbf{X}_I,\ \ \mathbf{x}_e=N_I(\mathbf{r})\mathbf{x}_I,\ \ \mathbf{u}_e=N_I(\mathbf{r})\mathbf{u}_I \qquad (6.46)$$

where the Einstein's summation convention (summation over repeating indices up to total number of nodes, say q) is used. The $N_I(\mathbf{r})$ are the interpolating functions (or shape functions) and $\mathbf{u}_e$ represents the vector of field variables for a point inside an element which in our case is a displacement vector. Hence for a general 3D problem all the vectors are 3×1 vectors and $N_I(\mathbf{r})$ is a scalar function of the reference coordinates $\mathbf{r}$.

Because of the property of integration each of the equations (6.14) or (6.15) can be written as sum over the elements. A finite element method that uses equation (6.14) is called *total Lagrangian* and the one which uses the equation (6.15) is called *updated Lagrangian*. In the following only the updated Lagrangian method will be explained. The total Lagrangian method can be extended likewise. For equation (6.15) we can write:

$$\int_{\phi(B)} (\ )dv \approx \Sigma_e\left(\int_{\omega e} (\ )d\omega_e\right)=0 \qquad (6.47)$$

The summation in equation (6.47) is over elements and is not a simple summation. In fact it needs assembling of different coefficients at each node because in general each node is common between some elements.

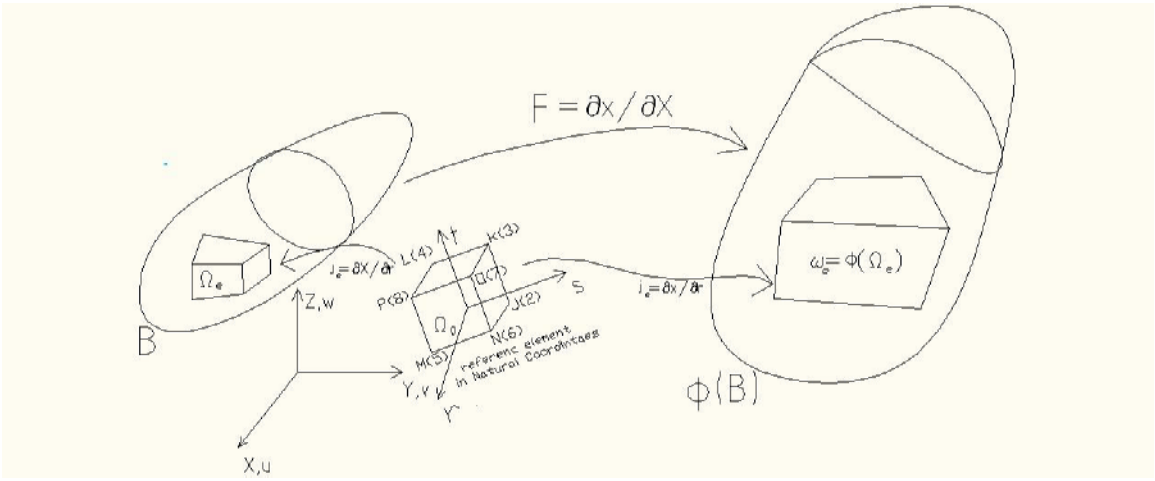

Figure 6.2 Element Ω_e in reference configuration is deformed to $\omega_e=\phi(\Omega_e)$ in current configuration. All elements in an isoparametric finite element method can be considered as a mapped elements form the reference element (Ω_0) in its coordinate system (natural coordinates).

Using the Galerkin method the weights are approximated with the same shape functions, such as:

$$\mathbf{w}_e=N_I(\mathbf{r})\mathbf{w}_I \qquad (6.48)$$

Before moving further we show how to calculate the deformation gradient and different gradients using the parent element.

Knowing from tensor analysis (for a complete discussion see Istkov,2009) and using Einstein's summation convention we have:

for a scalar α:

$$\mathbf{grad}(\alpha)=\nabla_x\alpha=\partial\alpha/\partial x_i\mathbf{e}_i \qquad (6.49a)$$

and for a vector **u**:

$$\mathbf{grad}(\mathbf{u})=\nabla_x\otimes\mathbf{u}=\partial\mathbf{u}/\partial x_i\otimes\mathbf{e}_i==\partial u_j/\partial x_i\mathbf{e}_j\otimes\mathbf{e}_i \qquad (6.49b)$$

where $\mathbf{e}_i$ are the base unit vectors in the corresponding coordinate system (here the spatial coordinates are used). Therefore the element deformation gradient can be expressed as:

$$\mathbf{F}_e=\partial\mathbf{x}_e/\partial\mathbf{X}_e=(\partial\mathbf{x}_e/\partial\mathbf{r})\partial\mathbf{r}/\partial\mathbf{X}_e=\mathbf{j}_e\mathbf{J}_e^{-1} \qquad (6.50a)$$

$$\mathbf{F}_e=\partial\mathbf{x}_e/\partial\mathbf{X}_e=\mathbf{x}_I\otimes\nabla_X N_I(\mathbf{r}) \qquad (6.50b)$$

Using the equations (6.46) and (6.49) it can be written:

$$\mathbf{j}_e=\partial\mathbf{x}_e/\partial\mathbf{r}=\nabla_r\otimes\mathbf{x}_e=\partial\mathbf{x}_e/\partial r_i\otimes\mathbf{e}_i=(\partial N_I(\mathbf{r})/\partial r_i)\mathbf{x}_I\otimes\mathbf{e}_i=\mathbf{x}_I\otimes(\partial N_I(\mathbf{r})/\partial r_i)\mathbf{e}_i=\mathbf{x}_I\otimes\nabla_r N_I(\mathbf{r}) \qquad (6.51a)$$

$$\mathbf{J}_e=\partial\mathbf{X}_e/\partial\mathbf{r}=\mathbf{X}_I\otimes\nabla_r N_I(\mathbf{r}) \qquad (6.51b)$$

This gives:

$$\mathbf{F}_e=(\mathbf{x}_I\otimes\nabla_r N_I(\mathbf{r}))\mathbf{J}_e^{-1}=\mathbf{x}_I\otimes\mathbf{J}_e^{-T}\nabla_r N_I(\mathbf{r}) \qquad (6.52)$$

Comparing (6.50b) and (6.52) it can be concluded that:

$$\nabla_X N_I(\mathbf{r})=\mathbf{J}_e^{-T}\nabla_r N_I(\mathbf{r}) \qquad (6.53a)$$

This result can also be obtained from the chain rule and using (6.49a). A similar result can be written as:

$$\nabla_x N_I(\mathbf{r})=(\partial\mathbf{r}/\partial\mathbf{X}_e)^T(\partial N_I(\mathbf{r})/\partial\mathbf{r})=\mathbf{j}_e^{-T}\nabla_r N_I(\mathbf{r}) \qquad (6.53b)$$

Accordingly the gradients of virtual displacements (or weights) for an element easily become:

$$\mathbf{Grad}(\mathbf{w}_e)=\partial\mathbf{w}_e/\partial\mathbf{X}_e=\mathbf{w}_I\otimes\mathbf{J}_e^{-T}\nabla_r N_I(\mathbf{r}) \qquad (6.54a)$$
$$\mathbf{grad}(\mathbf{w}_e)=\partial\mathbf{w}_e/\partial\mathbf{x}_e=\mathbf{w}_I\otimes\mathbf{j}_e^{-T}\nabla_r N_I(\mathbf{r}) \qquad (6.54b)$$

In order to carry out the integration in (6.47) over parent element we apply:

$$d\omega_e=\det(\mathbf{j}_e)d\Omega_0 \qquad (6.55a)$$
$$d\Omega_e=\det(\mathbf{J}_e)d\Omega_0 \qquad (6.55b)$$

which after substitution in equation (6.47) gives:

$$\Sigma_e\int_{\omega e}(\,)d\omega_e=\Sigma_e\int_{\Omega 0}(\,)\det(\mathbf{j}_e)d\Omega_0=0 \qquad (6.56)$$

The integration in (6.56) is computed numerically. The current numerical integration method in finite element softwares is the Gauss quadrature method. In this method the integral is computed with a sum of the weighted integrand evaluated at the Gauss points. So (6.56) can be written as:

$$\int_{\Omega 0}(\,)\det(\mathbf{j}_e)d\Omega_0=\Sigma\Sigma\Sigma\alpha_i\alpha_j\alpha_k((\,)\det(\mathbf{j}_e))(\xi_i,\xi_j,,\xi_k) \qquad (6.57)$$

where α_i's are weights and $(\xi_i,\xi_j,,\xi_k)$ is the coordinate of a Gauss point in natural coordinates. In one dimension a polynomial of order *(2n-1)* is integrated exactly with *n* Gauss points. In three dimensions a Gauss rule of order *n* uses n^3 points. Since the integrand in (6.57) is not a polynomial then it cannot be integrated exactly with Gauss quadrature. Full numerical integration is defined as the order which gives exact result when the element is an undistorted element (Bathe, 1996). As an example for a hexahedral element with 8 nodes a Gauss rule of 2 (with 8 Gauss points) gives the full numerical integration.

From equation (6.15) and (6.56) we have:

$$\Sigma_e\int_{\omega e}\boldsymbol{\sigma}:[\mathbf{grad}(\mathbf{w}_e)+\mathbf{grad}(\mathbf{w}_e)^T]/2\,d\omega_e+\Sigma_e\int_{\omega e}\rho\dot{\mathbf{v}}_h\cdot\mathbf{w}_e d\omega_e=\Sigma_e\{\int_{\omega e}\rho\mathbf{b}\cdot\mathbf{w}_e d\omega_e+\int_{\partial\omega e}\mathbf{w}_e\cdot\mathbf{t}^{ext}d\gamma_e\} \qquad (6.58)$$

For a hyperelastic material the stress tensor can be obtained from the deformation gradient. The first term of the left hand side of the equation (6.58) can be rewritten, using (6.54b) and (6.53b) and the properties of $\otimes$ (Istkov, 2009) as well as the symmetry of the stress tensor. This results in:

$$\Sigma_e\int_{\omega e}\boldsymbol{\sigma}:[\mathbf{grad}(\mathbf{w}_e)+\mathbf{grad}(\mathbf{w}_e)^T]/2\,d\omega_e=\Sigma_e\mathbf{w}_I\cdot\int_{\omega e}\boldsymbol{\sigma}\mathbf{j}_e^{-T}\nabla_r N_I(\mathbf{r})d\omega_e=\Sigma_e\mathbf{w}_I\cdot\int_{\omega e}\boldsymbol{\sigma}\nabla_x N_I(\mathbf{r})d\omega_e \qquad (6.59)$$

where Einstein's summation convention over I is assumed. For symmetric tensors, using Voigt notation, the components of a second order tensor can be equivalently represented as a 6×1 vector and those of a fourth order one by 6×6 matrix. The Cauchy stress in Voigt notation is: $\boldsymbol{\sigma}_e=\{\sigma_{11},\sigma_{22},\sigma_{33},\sigma_{12},\sigma_{23},\sigma_{13}\}^T$. Using this notation equation (6.59) becomes:

$$\Sigma_e\mathbf{w}_I\cdot\int_{\omega e}\boldsymbol{\sigma}\nabla_x N_I(\mathbf{r})d\omega_e=\Sigma_e\mathbf{w}_I\cdot\int_{\omega e}\mathbf{B}_I^T\boldsymbol{\sigma}_e d\omega_e=\Sigma_e\mathbf{w}_I\cdot\mathbf{f}_I^{int}=\mathbf{w}\cdot\mathbf{f}^{int} \qquad (6.60)$$

where the 6×3 matrix $\mathbf{B}_I$ is has the same form as the strain-displacement matrix in linear elasticity (Bathe, 1996) but its terms are calculated using the matrix $\nabla_x N_I(\mathbf{r})$. In (6.6) we have introduced an element internal force vector as $\mathbf{f}_I^{int}=\int_{\omega e}\mathbf{B}_I^T\boldsymbol{\sigma}_e d\omega_e$ which after assembling all elements the element vectors are assembled to global ones: $\mathbf{w}$ and $\mathbf{f}^{int}$. A global vector is an *ndof*×*1* vector, whereby *ndof* is the total number of degrees of freedom in the model. Following the same method the equation (6.58) becomes:

$$\mathbf{w}\cdot(\mathbf{f}^{int}+\mathbf{M}\dot{\mathbf{v}})=\mathbf{w}\cdot\mathbf{f}^{ext} \qquad (6.61)$$

where $\mathbf{M}$ is the mass matrix, $\dot{\mathbf{v}}$ the acceleration vector and $\mathbf{f}^{ext}$ is the global external force vector which is equal to the total body and traction forces. Since $\mathbf{w}$ is an arbitrary displacement (virtual displacement) the equation of motions for a finite element model becomes:

$$\mathbf{f}^{int}+\mathbf{M}\dot{\mathbf{v}}=\mathbf{f}^{ext} \qquad (6.62)$$

To consider a damping effect it can be implemented in two ways through a constitutive law or with a global damping matrix. The damping model with constitutive law shows its effect in the internal force. The global damping added to the equations of motions after assembling process. Hence for a global damping method the finite element equations of motion become:

$$\mathbf{f}^{int}+\mathbf{M}\dot{\mathbf{v}}+\mathbf{C}\mathbf{v}=\mathbf{f}^{ext} \qquad (6.63)$$

In a nonlinear problem the force vectors can be a function of the current displacement. In finite elasticity or large deformation analysis the internal force is a function of the current displacements. To find the solution of equations (6.63) in a nonlinear problem first these equations should be integrated in time and then the resulting equations can be solved with a method like the Newton-Raphson method.

6.4 Time integration

For the integration of equations of motion in time a finite difference method is used. There are two scheme of time integration in the finite element method. In the first group which is called the *explicit time integration method*, the equations of motion at time t are used:

$$ {}_t\mathbf{f}^{int}+\mathbf{M}\,{}_t\dot{\mathbf{v}}+\mathbf{C}\,{}_t\mathbf{v}={}_t\mathbf{f}^{ext} \qquad (6.67) $$

Then after using a numerical time integration like central difference method the displacement at time $t+\Delta t$, i.e. U_{n+1}, satisfies a relation like this:

$$ \mathbf{A}\mathbf{u}_{n+1}=\mathbf{F}(\mathbf{u}_n,\mathbf{u}_{n-1},\Delta t) \qquad (6.68) $$

and the solution of this equation can be computed easily. However, these methods suffer from the shortcoming that they are not unconditionally stable. Finding the critical time step for these problems may not be an easy task(see Belytschko et al., 2000).
In the second group, called the *implicit integration method*, the equations of motion at time $t+\Delta t$ are used:

$$ {}_{t+\Delta t}\mathbf{f}^{int}+\mathbf{M}_{t+\Delta t}\dot{\mathbf{v}}+\mathbf{C}\,{}_{t+\Delta t}\mathbf{v}={}_{t+\Delta t}\mathbf{f}^{ext} \qquad (6.69) $$

Then time integration methods like those of Houbolt, Wilson or Newmark are applied (Bathe, 1996). The Newmark method is explained here as an example. In the Newmark method the time integration formulas are:

$$ \mathbf{u}_{n+1}=\mathbf{u}_n+\Delta t\,\dot{\mathbf{u}}_n+(\Delta t^2/2)[(1-2\alpha)\ddot{\mathbf{u}}_n+2\alpha\ddot{\mathbf{u}}_n] \qquad 0\le\alpha\le0.5 \qquad (6.70a) $$

$$ \dot{\mathbf{u}}_{n+1}=\dot{\mathbf{u}}_n+\Delta t[(1-2\delta)\ddot{\mathbf{u}}_n+\delta\ddot{\mathbf{u}}_{n+1}] \qquad 0\le\delta\le1 \qquad (6.70b) $$

where ${}_{t+\Delta t}\dot{\mathbf{v}}=\ddot{\mathbf{u}}_{n+1}$ and ${}_{t+\Delta t}\mathbf{v}=\dot{\mathbf{u}}_{n+1}$. Now inserting the above equations in the equation (6.69) gives:

$$ \mathbf{M}[a_0(\mathbf{u}_{n+1}-\mathbf{u}_n)-a_2\dot{\mathbf{u}}_n-a_3\ddot{\mathbf{u}}_n]+\mathbf{C}[a_1(\mathbf{u}_{n+1}-\mathbf{u}_n)-a_4\dot{\mathbf{u}}_n-a_5\ddot{\mathbf{u}}_n]+\mathbf{f}^{int}(\mathbf{u}_{n+1})=\mathbf{f}_{n+1}{}^{ext} \qquad (6.71) $$

where $a_0=1/(\alpha\Delta t^2)$, $a_1=\delta/(\alpha\Delta t)$, $a_2=1/\alpha\Delta t$, $a_3=(1/(2\alpha))-1$, $a_4=1-\delta/\alpha$, $a_5=\Delta t(1-\delta/(2\alpha))$. This equation is a nonlinear equation and its solution can be found with a solution procedure like the Newton-Raphson method. In the Newton-Raphson method the nonlinearities are linearized and in an iteration loop the linearized equations are solved. This loop continues up to a point where the difference between the value at the first of the loop and the solution at the end of that loop becomes smaller than a tolerance value. The increment in iteration ith of this loop is:

$$ \mathbf{u}^{i+1}{}_{n+1}=\mathbf{u}^{i}{}_{n+1}+\Delta\mathbf{u}^{i+1}{}_{n+1} \qquad (6.72) $$

The only nonlinear term in equation (6.71) is $\mathbf{f}^{int}(\mathbf{u}_{n+1})$. The linearization of this term in the ith loop gives:

$$\mathbf{f}^{int}(\mathbf{u}^{i+1}{}_{n+1})=\mathbf{f}^{int}(\mathbf{u}^{i}{}_{n+1})+(\partial\mathbf{f}^{int}/\partial\mathbf{u}_{n+1})|(\mathbf{u}^{i}{}_{n+1})\Delta\mathbf{u}^{i+1}{}_{n+1}=\mathbf{f}^{int}(\mathbf{u}^{i}{}_{n+1})+\mathbf{K_T}(\mathbf{u}^{i}{}_{n+1})\Delta\mathbf{u}^{i+1}{}_{n+1} \qquad (6.72)$$

where $\mathbf{K_T}$ is the tangent matrix and it is calculated at $\mathbf{u}^{i}{}_{n+1}$. Hence the *i*th loop iteration of equation (6.71) becomes:

$$\mathbf{M}[a_0(\mathbf{u}^{i+1}{}_{n+1}-\mathbf{u}_n)-a_2\dot{\mathbf{u}}_n-a_3\ddot{\mathbf{u}}_n]+\mathbf{C}[a_1(\mathbf{u}^{i+1}{}_{n+1}-\mathbf{u}_n)-a_4\dot{\mathbf{u}}_n-a_5\ddot{\mathbf{u}}_n]+\mathbf{f}^{int}(\mathbf{u}^{i+1}{}_{n+1})=\mathbf{f}_{n+1}{}^{ext} \qquad (6.73a)$$

or:

$$[\mathbf{M}a_0+\mathbf{C}a_1+\mathbf{K_T}(\mathbf{u}^{i}{}_{n+1})]\Delta\mathbf{u}^{i+1}{}_{n+1}=\mathbf{f}_{n+1}{}^{ext}-\mathbf{M}[a_0(\mathbf{u}^{i+1}{}_{n+1}-\mathbf{u}_n)-a_2\dot{\mathbf{u}}_n-a_3\ddot{\mathbf{u}}_n]-\mathbf{C}[a_1(\mathbf{u}^{i+1}{}_{n+1}-\mathbf{u}_n)-a_4\dot{\mathbf{u}}_n-a_5\ddot{\mathbf{u}}_n]-\mathbf{f}^{int}(\mathbf{u}^{i}{}_{n+1}) \qquad (6.73b)$$

This equation is solved for $\Delta\mathbf{u}^{i+1}{}_{n+1}$ and iteration stops when $\|\mathbf{f}^{int}(\mathbf{u}^{i+1}{}_{n+1})\|\leq ftol$ or $\|\Delta\mathbf{u}^{i+1}{}_{n+1}\|\leq utol$. The above method shows the essence of using an iteration procedure in an implicit integration scheme. A large number of variations of the nonlinear procedure solution method can be found in the literature (among the others see Bathe, 1996; Belytschko et al., 2000; Wriggers 2008). In the following we describe the linearization of the internal force.

6.5 Linearization of internal force

The linear part of the internal force for an element:

$$\Delta\mathbf{f}_\mathbf{I}{}^{int}=D\mathbf{f}_\mathbf{I}{}^{int}.\Delta\mathbf{u}=\mathbf{K_T}\Delta\mathbf{u} \qquad (6.74)$$

(To be compatible with the results of previous section we have replaced in this equation **u** by Δ**u** as it was the case in section 1.2). This linearization for an element using the equation (6.45) for an updated Lagrangian formulation gives:

$$\mathbf{w}_I\cdot(D\mathbf{f}_\mathbf{I}{}^{int}.\Delta\mathbf{u})=\int_{\Omega 0}\{\mathbf{grad}(\Delta\mathbf{u})\boldsymbol{\sigma}:\mathbf{grad}(\mathbf{w})+(\mathbb{c}:\nabla^s\Delta\mathbf{u}):\nabla^s\mathbf{w}\}\det(\mathbf{j}_e)d\Omega_0=\mathbf{w}_I\cdot(\mathbf{K}_I{}^{geo}+\mathbf{K}_I{}^{mat})\Delta\mathbf{u} \qquad (6.75)$$

where $\mathbf{K}_I{}^{geo}$ is element geometric stiffness matrix and $\mathbf{K}_I{}^{mat}$ is material stiffness matrix. And we have $\mathbf{K_T}=\mathbf{K}_I{}^{geo}+\mathbf{K}_I{}^{mat}$. The specifc form of these equations can be found using the equations for gradient in an element (Wriggers, 2008).

6.6 Muscle force-velocity implementation

In general the active stress in muscle can be written as (equation (3.4b) and (5.94)):

$$\sigma_{active}=\sigma_{max}(\lambda/\lambda_{ofl})g(\lambda,\dot{\lambda},A) \qquad (6.76)$$

In the distributed Feldman model the stretch ratio λ and its time rate $\dot{\lambda}$ appear with a time delay t_d. Using a backward difference formula these delayed values can written as:

$$\lambda(t-t_d)=\lambda(t)-t_d\dot{\lambda} \qquad (6.77)$$
$$\dot{\lambda}(t-t_d)=\dot{\lambda}(t)-t_d\ddot{\lambda}(t) \qquad (6.78)$$

Hence an active force can also be a function of acceleration of stretch in the fiber directions:

$$\sigma_{active}=\sigma_{max}(\lambda/\lambda_{ofl})g(\lambda,\dot{\lambda},\ddot{\lambda},A)=f(\lambda,\dot{\lambda},\ddot{\lambda},A) \qquad (6.79)$$

The stress tensor corresponding to this stress can be written as (equation 5.92):

$$\boldsymbol{\sigma}=\sigma_{active}(\mathbf{a}\otimes\mathbf{a}) \qquad (6.80)$$

The linear part of this stress can be written as:

$$\Delta\boldsymbol{\sigma}=\mathrm{D}\boldsymbol{\sigma}.\Delta\mathbf{u}=(\mathrm{D}\sigma_{active}.\Delta\mathbf{u})(\mathbf{a}\otimes\mathbf{a})+\sigma_{active}\,\mathrm{D}(\mathbf{a}\otimes\mathbf{a}).\Delta\mathbf{u} \qquad (6.81)$$

The first term in the above equation can be written as:

$$\mathrm{D}\sigma_{active}.\Delta\mathbf{u}=\partial f/\partial\lambda\;\mathrm{D}\lambda.\Delta\mathbf{u}+\partial f/\partial\dot{\lambda}\;\mathrm{D}\dot{\lambda}.\Delta\mathbf{u}+\partial f/\partial\ddot{\lambda}\;\mathrm{D}\ddot{\lambda}.\Delta\mathbf{u} \qquad (6.82)$$

Using the linearization formulas (6.37), (6.39) and (6.40) the above equation can be expanded into known quantities. As can be seen from equations (6.39) and (6.40) can be seen the linearization of velocity and acceleration produce $\Delta\dot{\mathbf{u}}$ and $\Delta\ddot{\mathbf{u}}$. The equation (6.19) is rewritten to show this result:

$$\mathrm{D}\sigma_{active}.\Delta\mathbf{u}=\mathbf{K_T}\Delta\mathbf{u}+\mathbf{C_{vir}}\Delta\dot{\mathbf{u}}+\mathbf{M_{vir}}\Delta\ddot{\mathbf{u}} \qquad (6.83)$$

where $\mathbf{C_{vir}}$ is a virtual damping matrix and $\mathbf{M_{vir}}$ shows a virtual mass matrix (see Appendix B). Introducing this equation in the equation (6.73a) and noting that :

$$\dot{\mathbf{u}}^{i+1}{}_{n+1}=\dot{\mathbf{u}}^{i}{}_{n+1}+\Delta\dot{\mathbf{u}}^{i+1}{}_{n+1} \qquad (6.84a)$$
$$\ddot{\mathbf{u}}^{i+1}{}_{n+1}=\ddot{\mathbf{u}}^{i}{}_{n+1}+\Delta\ddot{\mathbf{u}}^{i+1}{}_{n+1} \qquad (6.84b)$$

gives:

$$[(\mathbf{M}+\mathbf{M_{vir}})a_0+(\mathbf{C}+\mathbf{C_{vir}})a_1+\mathbf{K_T}(\mathbf{u}^{i}{}_{n+1})]\Delta\mathbf{u}^{i+1}{}_{n+1}=\mathbf{f}_{n+1}{}^{ext}-(\mathbf{M}+\mathbf{M_{vir}})[a_0(\mathbf{u}^{i+1}{}_{n+1}-\mathbf{u}_n)-a_2\dot{\mathbf{u}}_n-a_3\ddot{\mathbf{u}}_n]-$$
$$(\mathbf{C}+\mathbf{C_{vir}})[a_1(\mathbf{u}^{i+1}{}_{n+1}-\mathbf{u}_n)-a_4\dot{\mathbf{u}}_n-a_5\ddot{\mathbf{u}}_n]-\mathbf{f}^{int}(\mathbf{u}^{i}{}_{n+1})+\mathbf{C_{vir}}\dot{\mathbf{u}}^{i}{}_{n+1}+\mathbf{M_{vir}}\ddot{\mathbf{u}}^{i}{}_{n+1} \qquad (6.85a)$$

The above equation can be simplified:

$$[(\mathbf{M}+\mathbf{M_{vir}})a_0+(\mathbf{C}+\mathbf{C_{vir}})a_1+\mathbf{K_T}(\mathbf{u}^{i}{}_{n+1})]\Delta\mathbf{u}^{i+1}{}_{n+1}=\mathbf{f}_{n+1}{}^{ext}-\mathbf{M}[a_0(\mathbf{u}^{i+1}{}_{n+1}-\mathbf{u}_n)-a_2\dot{\mathbf{u}}_n-a_3\ddot{\mathbf{u}}_n]-\mathbf{C}[a_1(\mathbf{u}^{i+1}{}_{n+1}-\mathbf{u}_n)-a_4\dot{\mathbf{u}}_n-$$
$$a_5\ddot{\mathbf{u}}_n]-\mathbf{f}^{int}(\mathbf{u}^{i}{}_{n+1}) \qquad (6.85b)$$

Thus, it can be seen that by introducing the force-velocity characteristics an equivalent damping is introduced in the model. This idea confirms that of the Hill's idea about the addition of a viscous damping with a nonlinear damping coefficient to his functional model. The delay introduced in the velocity in the Feldman model, introduces a virtual inertia.

6.7 Results

To investigate the effects of introducing the force-velocity relation in the muscle model, the simple example presented in chapter 5 (Figure 5.5) is revisited.
The impact of the Feldman model on OOP activation to produce lip protrusion is also studied. The same muscle is being activated using Hill-type muscle. To compare the results of these simulations, the second activation using Hill-type model is designed such that it produces approximately the same final stress as in Feldman model.

6.7.1 Qualitative assessment: The simple example

The effect of a Hill-type force-velocity on the simple bar introduced in chapter 5 (Figure 5.5) is studied. The same muscle elements are activated once without considering force-velocity relation and once with its inclusion. The activation is changing linearly and the level of activation is the same in both simulations. As it can be seen considering the force-velocity characteristics causes smaller amplitude of deflection of the tip of the beam. This result is compatible with what was expected from its effect in concentric part of force velocity relation (Figure 3.7). These results are shown in Figure 6.3 for final deformation of the beam.

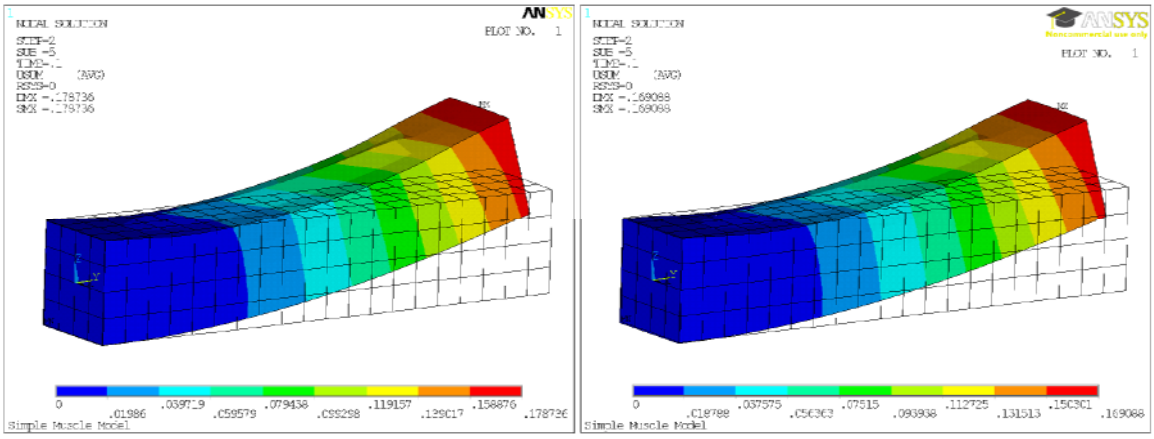

(a) (b)

Figure 6.3 Effect of force-velocity characteristics in decreasing the final amplitude of deformation (a) without the force-velocity effect (maximum deflection is 0.178m) (b) with the force-velocity effect (maximum deflection 0.169m).

6.7.2 Comparison between Hill-type model and Distributed Feldman Model (DFM) on lip protrusion

To compare the effect of a Hill-type model and DFM on muscle behaviour, the muscle elements corresponding to the part of OOP muscle (Figure 5.6a) are activated using these two models. The final shape of the face in both models is the same. The stress and stretch data in one element at the corner of lips in both simulations are compared. The stress-stretch behavior is shown in Figure 6.4.

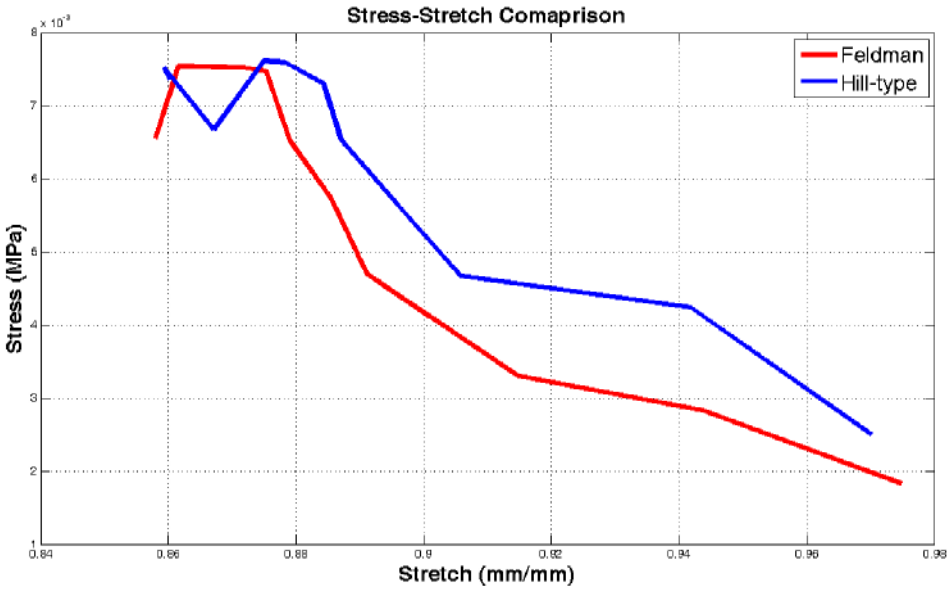

Figure 6.4 Stress-stretch curve: comparison between a Hill-type muscle model and DFM.

The time pattern of stress and stretch behavior is shown in Figure 6.5. It can be seen that in spite of the identical time variation of the stretch, in comparison to the Hill-type muscle model the level of stress during this voluntary motion is larger in DFM.

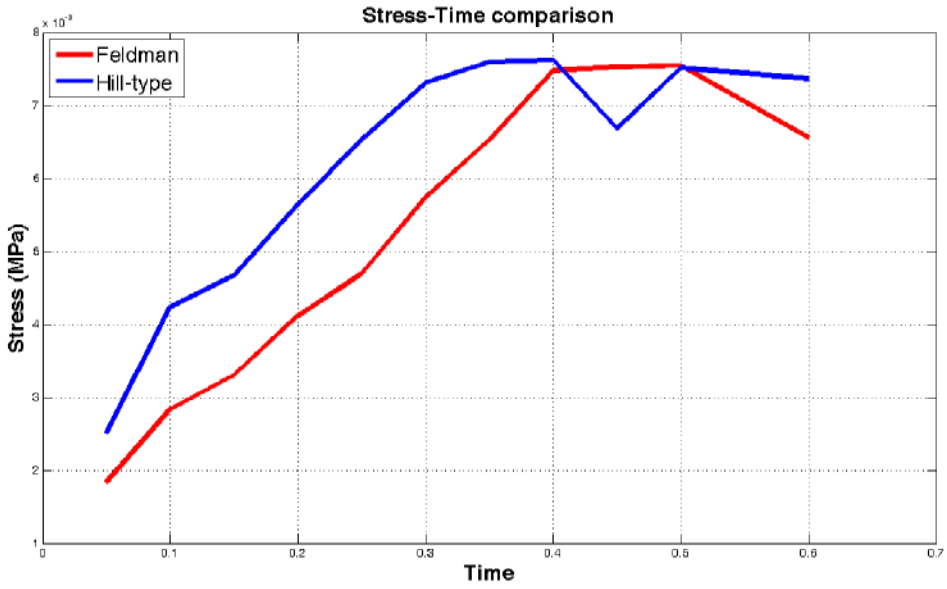

(a)

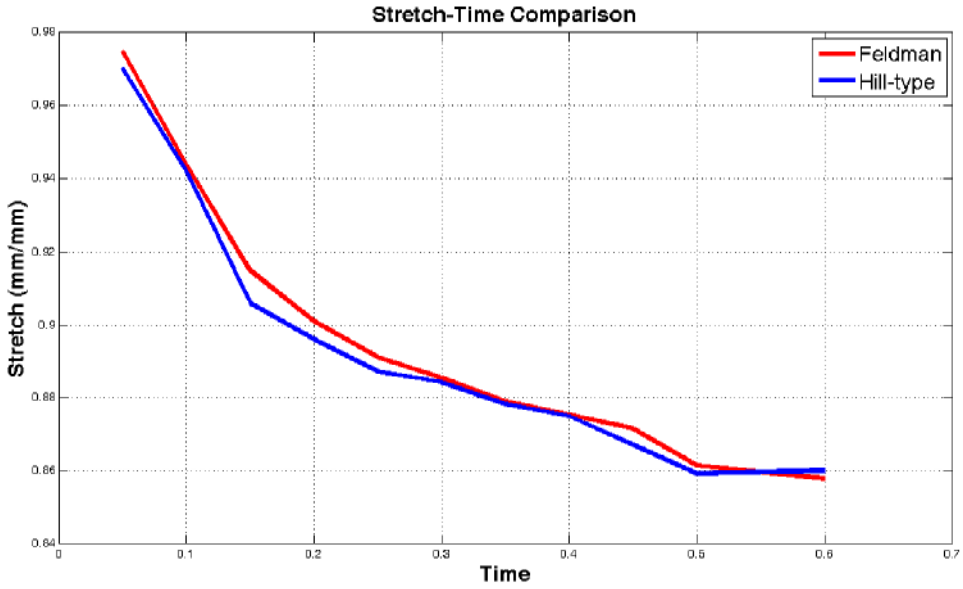

(b)

Figure 6.5 Variation of (a) stress and (b) stretch with respect to time: comparison between Hill-type muscle model and DFM.

For a final result the effect of these two models on upper and lower lip protrusion (Figure 4.23) are shown in Figure 6.6. The amount of protrusion with the Feldman muscle model is less than for the Hill-type muscle model. This data should be regarded as the total effect of muscle models and they show that the Feldman model behaves stiffer than a Hill-type muscle model.

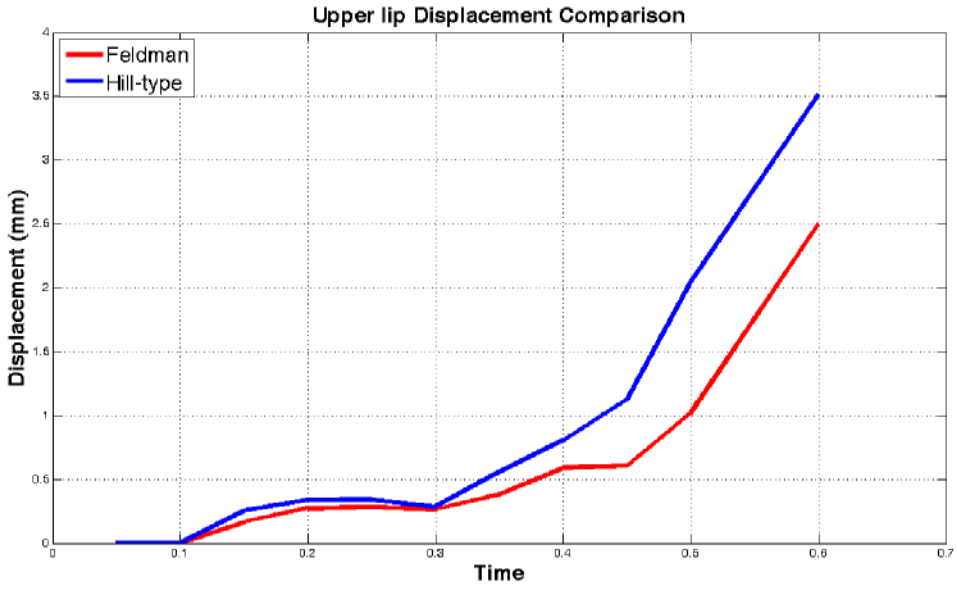

(a)

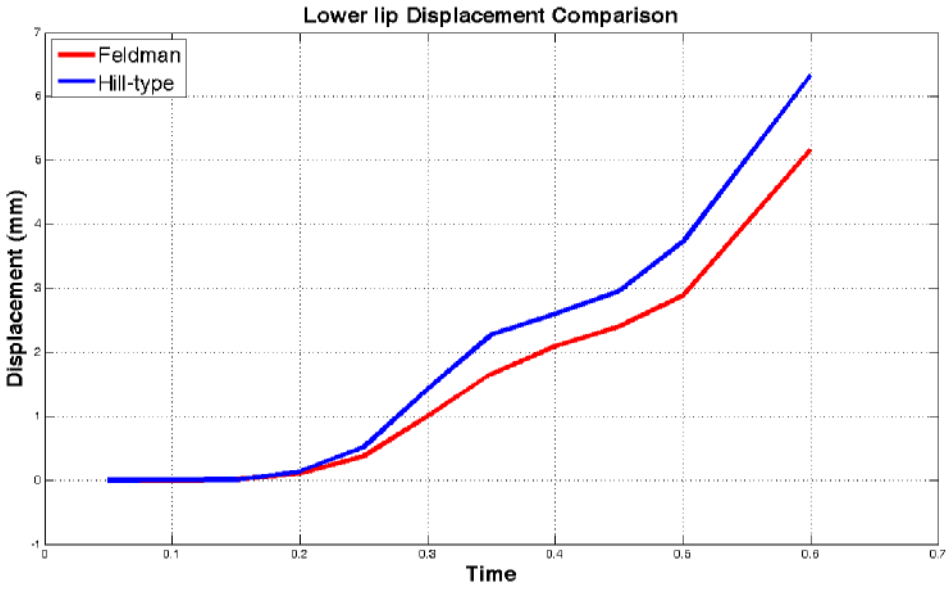

(b)

Figure 6.6 Path of point on (a) upper lip and on (b) lower lip: comparison between a Hill type muscle model and DFM.

6.8 Conclusion

In this chapter, after a general review of nonlinear finite element models, it becomes apparent that including the dependence of the muscle force on the velocity creates a virtual damping matrix. This damping in concentric contraction behaves like a nonlinear viscous damping with time dependent damping coefficients. In the eccentric part the force-velocity term acts as a booster and increases the deformations. In DFM, due to the delay in the velocity term, the force is also a function of acceleration. This creates a virtual inertia in the formulations. This result matches well with the source

of delay in the system. The comparison of Hill-type model and DFM on lip protrusion reveals that the DFM acts stiffer which can be due to exponential nature of invariant characteristics in DFM.

Chapter Seven: Conclusion

"Reasoning draws a conclusion, but does not make the conclusion certain, unless the"
"mind discovers it by the path of experience."
Roger Bacon

7.1 Main achievements of the thesis work

This work has its origins in the conviction that the signals of speech communication, i.e. the articulatory signals and the acoustic signals, are the result of a complex interaction between, on the one hand, high level motor control strategies, which aim at conveying the linguistically relevant information toward the listeners as efficiently as possible, and, on the other, physical constraints arising from the intrinsic properties of the speech organ. The final product of this interaction consists of the spatio-temporal acoustic and/or articulatory patterns that listeners are able to extract from the continuous signals in order to recover the linguistic information. How does the interaction operate? Are the physical properties learned and stored in internal models in order for the Central Nervous System to predict their influence and to determine the control signals on this basis in order to produce accurately predetermined spatio-temporal goals? Or do the physical properties largely contribute to determine the spatio-temporal patterns and to give them their final shape under the influence of a more global control from the Central Nervous System? As stated in the introduction, the debate is still open and further work is still required to delve deeper in the study of this issue. This thesis work aims at contributing to the debate (1) by providing clear and quantitative information about the potential impact of articulatory biomechanics on speech movements, and (2) by contributing to set up a research framework in which the hypotheses can be evaluated, quantitatively and systematically. This was done by designing and using a realistic dynamical biomechanical model of the face.

This model is a 3D Finite Element model. It consists of a 3-layer mesh made of isotropic nearly incompressible hyperelastic hexahedral and wedge elements. Facial muscles are represented in the mesh as subsets of contiguous elements. The main originality in this face model lies in the representation of the muscles. First, their anatomical description, which relies on subject specific medical images and anatomical landmarks, is specified independently from the finite element mesh. This approach enables to easily modify the structure of the mesh, its number or type of elements, without losing the anatomical information. The second aspect that makes our model original is the modelling of elastic muscle properties and of the impact of muscle activation on these properties. In a first stage, for sake of simplicity and in order to provide a first quantitative evaluation of the influence of oro-facial muscle activations on oro-facial gestures, a functional muscle model has been used. In this model, external fibres (in the form of cable elements) apply forces to the muscle related elements of the mesh. Any increase in muscle activation is associated to a change in the isotropic hyperelastic stress-strain relation of the muscle elements. This change corresponds to an isotropic increase in muscle tissue stiffness. This increase aims to representing functionally the stress-stiffening effect naturally associated with muscle activation.

After this first evaluation, whose results are summarized below in the next paragraph, an improvement is provided to the model, in order to propose a significantly more realistic account of the biomechanical description of a muscle. This was done by designing an active muscle element in which

the stress-strain relation contains an active component in the direction of the fibres (due to contractile parts) and a passive (tissue intrinsic) transversally isotropic component. In this element elastic properties are isotropic along the directions orthogonal to the fibre direction. Stress-stiffening arises naturally from the tension generated in the direction of muscle fibres. Two types of description of the contractile parts have also been implemented, namely the Hill type and the Feldman type model. In both models the force-velocity relation, which tends to reduce stress when contraction speed of the tissues increases, is implemented. The implementation of Feldman's model has required an adaptation of its mathematical formulation, in order to be compatible with a discretization of the muscle into a number of finite elements. This adapted representation has been called DFM, which holds for "*Distributed Feldman Model*".

The validity of the structure of the face model, i.e. of its elastic properties, of the anatomical muscle implementation, and of the muscle fibres directions, has been evaluated and testified with the functional muscle model. In doing so, a number of non-verbal facial mimics and speech movements have been simulated with the face model. It could be shown that simulated data are qualitatively comparable to those occurring during the production of speech or of facial mimics in non-verbal communication.

7.2 Soft tissues stiffening and oro-facial gestures

Results obtained with the functional model of the muscle force generation mechanisms for the lips' protrusion/rounding gesture have shown that the stress stiffening effect significantly influences lip shaping. The lips' protrusion/rounding gesture is required for the production of rounded vowels such as /u/ or /y/. It was generated in the model by activating the upper and lower parts of the Orbicularis Oris Peripheralis (OOP). Acoustic simulations showed that differences in lip shaping are associated with perceivable differences in acoustic spectral patterns. It was found that shape differences associated with tissue stiffening correspond to a facilitation of the production of accurate protrusion/rounding gestures thanks to a saturation effect in the relation between the level of muscle activation and the crucial geometrical characteristics of the lips (Nazari et al., 2010). This ensures the production of more canonical acoustic spectral patterns for the rounded vowels.

This observation raises the following question: would it be possible to control stiffening in the Orbicularis Oris Peripheralis? In the literature the classic way to increase stiffness corresponds to a coordinated increase in the agonist and antagonist muscle activations. In our simulations of lip protrusion/rounding, only the Orbicularis Oris Peripheralis is activated. This muscle consists of two parts, the Orbicularis Oris Peripheralis Superior (OOPS) and the Orbicularis Oris Peripheralis Inferior (OOPI), which actually collaborate to generate protrusion and rounding, while exerting quasi-antagonist forces on the lip corner. Hence, even if it does not correspond to the classic agonist/antagonist case, simultaneously changing the force generated by the OOPS and the OOPI seems to be an appropriate way to control stiffening. In this context, it can be concluded that controlling the intensity of the stress stiffening effect of the OO via the control of its activation could be an efficient strategy to accurately achieve lips' protrusion and rounding

Simulations with this model have also highlighted the indirect role of some face tissues stiffening on the way muscles impact lip shape. It was shown that the stiffening of the cheeks due to the activation of the buccinator induces a limitation of the amplitude of the upper lip protrusion associated with OOP

activation. The role of muscles, which are not directly involved in lip shaping, was thus demonstrated. These results, similar to those of Buchaillard et al. (2009) about the role of mouth floor muscles in tongue elevation, are encouraging for our modelling approach toward a better understanding of facial mimics and facial speech gestures generation mechanisms.

7.3 Advanced muscle model for finite element modeling

The design of an active muscle element, which accounts for the force generation mechanisms and the elastic characteristics of a muscle, includes the definition of a passive hyperelastic transversally isotropic constitutive law. This law was implemented thanks to the programming facility USERMAT of the ANSYS finite element software. Then, an active stress component was introduced in the muscle fibres direction. This active stress component takes into account the damping behaviour of muscles, i.e. the reduction of muscle force associated with an increase in speed of muscle length variation. This active stress component is applied to tissues characterized by the above mentioned hyperelastic transversally isotropic constitutive law that we implemented (see above). This was done with the USERELEM programming facility of the ANSYS finite element software.
This long lasting work has allowed a more realistic account of the mechanisms underlying muscle force generation and stress stiffening. Both with the Hill-type model and with the Feldman's model, simulations run with muscle elements embedded in simple bars of soft tissues have shown that this muscle model generates realistic patterns of strain and stress. These patterns were also shown to be independent from the number of elements in the Finite Element mesh representing the bar. In summary, the evaluation of our muscle model on simple bars of soft tissues suggested that this model works realistically.
Unfortunately, because of a lack of time, it was not possible to achieve a precise and systematic evaluation of the differences in face/lip gestures associated with the use in the face model of the functional *versus* the physical muscle model. The muscle element was integrated in the face model, and two examples of protrusion and lip closing gestures were simulated. They confirm that the associated movements are realistic, but more extensive work should be carried out for further evaluation.
A comparison of the Hill-type models with Feldman's model was possible in this context. It was done first with simple bars, and then with the face model. The results show that in the range of strain corresponding to normal conditions of movement, these models generate similar patterns of stress and strain. This suggests that criticisms of Feldman's model concerning its inability to account realistically for biomechanical facts are not justified. Hence, arguments in the debate about the weaknesses and strengths of Feldman's model should only focus on motor control issues and not on biomechanical ones.

7.4 Perspectives

Future works will first focus on a comprehensive evaluation of the differences obtained with the face model according to whether it works with the functional muscle model or with the physical one. This shall enable us to provide clear statements about the advantages of using the more realistic muscle model when evaluating the influence of biomechanical factors on movements' characteristics.

A more systematic study of the relation between facial movements and muscle activations should also be made, and in particular for lips protrusion/rounding and lips spreading. In chapter 4, we have presented simulations of lips protrusion/rounding gestures based on the activation of the Orbicularis Oris Peripheralis. We project to study more extensively the potential enhancement or perturbation of this gesture associated with the activation of other muscles surrounding the lips, more specifically of the Orbicularis Oris Marginalis, the Mentalis, the DLI, the LLS and the Risorius, This study should shed light on possible synergetic or antagonistic strategies for lips shaping in speech production. This would clarify what degrees of freedom are available for the speakers in lips protrusion or lip spreading gestures.

Lips control can strongly vary from a speaker to the next and from a language to the next. Some aspects of this variability are certainly due to cultural or social factors. However some other aspects could be associated with a variability of the anatomical distribution of the muscles in the lips region. We recently started a study along these lines in collaboration with Didier Demolin from Gipsa-lab, which aims at clarifying whether some aspects of the variability of lips shaping in speech production across languages could have anatomical origins associated with the respective size of the muscles in the lips region.

In addition, the face model will be coupled with the already existing models of the tongue (Buchaillatd et al., 2009) and of the jaw (Vogt et al., 2010). In the ANSYS finite element software, simulations using the full jaw-tongue-face model are likely to last extremely long (we estimate it close to a factor 10000 longer than real time simulations). Consequently, trying to reduce the computation time for the model is a very important challenge. This aim is at the core of the collaboration that Gipsa-lab has established a few years ago with the ArtiSynth group at the University of British Columbia in Vancouver (Canada). The ArtiSynth group develops fast algorithms for Finite Element Modeling. Our colleagues in Vancouver have thus recently implemented a full-model of the orofacial regions, which includes an original jaw model, Gipsa-lab tongue model and an adapted version of our face model. This model has not been extensively tested yet, and it does not include our recently developed muscle model. Consequently, the development of the full model in the ANSYS environment will be done in collaboration with the ArtiSynth research group.

In parallel, experimental measures of the mechanical properties of the lips and the tongue tissues will be carried out in collaboration with the 3S lab in Grenoble, The aim of this experimental study is to collect data on the stress/strain relation from cadaver's human tissues, in order to adapt the parameters of the transversally isotropic hyperelastic constitutive law to the characteristics of the main articulators of speech production.

Appendix A: Tensors: A Review

A.1 Different types of tensors

Tensors are quantities that transforms in such a way, when the coordinate system changes its position in the space, their definition remains the same in the original coordinates and in the new one. Hence all scalars that do not change when the coordinate system change, are tensors. In fact all scalars are zero-order tensors (in an n-dimensional space the scalars have $n^0=1$ component. Hereafter we use three dimensional space, so $n=3$). Vectors are first-order tensors and in a three dimensional space they have three components. The vectors are represented with a column matrix and they are written with bold lower-case letters. For example vector $\boldsymbol{a}$ represents: $\mathbf{a}=[a_1\ a_2\ a_3]^T$ ($[\ ]^T$ shows the transpose operation). When the coordinate system transforms orthogonally as: $\mathbf{x}=\mathbf{QX}+\mathbf{c}$ then vector $\mathbf{a}$ in the $\mathbf{X}$ coordinates changes to: $\hat{\mathbf{a}}=\mathbf{Q}^T\mathbf{a}+\mathbf{c}$ in the $\mathbf{x}$ coordinates. A second order tensor is a linear map from a vector space to another vector space. Second order tensor in a three dimensional space have 9 ($=3^2$) components. The second-order tensors are shown with a 3×3 matrix and by bold upper-case letters. The second order tensor $\mathbf{T}$ linearly transforms a vector $\mathbf{a}$ to a vector $\mathbf{b}$ such as:

$$\mathbf{b}=\mathbf{Ta} \qquad \text{(A.1)}$$

A special second order tensor is the tensor product or dyad of two vectors and is defined as:

$$\mathbf{Ta}=(\mathbf{u}\otimes\mathbf{v})\mathbf{a}=\mathbf{u}(\mathbf{v}\cdot\mathbf{a}) \qquad \text{(A.2)}$$

where $\cdot$ shows the dot or inner product of two vectors, which is equivalent in matrix notation to: $\mathbf{v}\cdot\mathbf{a}=\mathbf{v}^T\mathbf{a}$. Dyad tensor in matrix notation can be expressed as:

$$\mathbf{T}=\mathbf{uv}^T \qquad \text{(A.3)}$$

This corresponds, in component form, to: $T_{ij}=u_iv_j$. Using matrix notation the equation (A.2) can be verified as: $\mathbf{Ta}=\mathbf{uv}^T\mathbf{a}=\mathbf{u}(\mathbf{v}^T\mathbf{a})=\mathbf{u}(\mathbf{v}\cdot\mathbf{a})$. Trace of a dyad is: $tr(\mathbf{u}\otimes\mathbf{v})=tr(\mathbf{uv}^T)=\mathbf{u}\cdot\mathrm{v}$. The transpose of a second order tensor can be defined as the transpose of its corresponding matrix. Hence the transpose of the dyad tensor is:

$$\mathbf{T}^T=\mathbf{vu}^T=\mathbf{v}\otimes\mathbf{u} \qquad \text{(A.4)}$$

Identity second order tensor, $\mathbf{I}$, can be represented as a 3×3 identity matrix. One of the useful applications of a dyad is for projection. If a dyad is produced from a unit vector $\mathbf{a}$ as:

$$\mathbf{P}=\mathbf{a}\otimes\mathbf{a}=\mathbf{aa}^T \qquad \text{(A.5)}$$

When this special dyad tensor applies on a vector $\mathbf{b}$, it produces a vector which is collinear with $\mathbf{a}$ and its magnitude equals the projection of $\mathbf{a}$ on $\mathbf{b}$:

$$\mathbf{Pb}=(\mathbf{a}\otimes\mathbf{a})\mathbf{b}=\mathbf{aa}^T\mathbf{b}=(\mathbf{a}\cdot\mathbf{b})\mathbf{a} \qquad \text{(A.6)}$$

Hence $\mathbf{P}$ creates the projection of $\mathbf{b}$ along $\mathbf{a}$. If a physical quantity (like stress) is expressed as a dyad like $\sigma(\mathbf{a}\otimes\mathbf{a})$ (σ is a scalar) then it means that it gets its maximum value, σ, along $\mathbf{a}$ and it becomes zero in the direction normal to $\mathbf{a}$.
If the coordinate system rotates as $\mathbf{x}=\mathbf{QX}$, then according to (A.1) we have:

$$\hat{\mathbf{b}}=\hat{\mathbf{T}}\hat{\mathbf{a}} \qquad \text{(A.7)}$$

With transforming back the vectors to original coordinates we get:

$$\mathbf{Q}^T\mathbf{b}=\hat{\mathbf{T}}\mathbf{Q}^T\mathbf{a} \qquad \text{(A.8)}$$

Knowing the orthogonality of the transform, i.e. $\mathbf{Q}^T\mathbf{Q}=\mathbf{Q}\mathbf{Q}^T=\mathbf{I}$, and from (A.8) and (A.1) we obtain:

$$\hat{\mathbf{T}}=\mathbf{Q}^T\mathbf{T}\mathbf{Q} \qquad \text{(A.9)}$$

A general second order tensor can be expressed with the help of dyads of the base vectors of the coordinate system, i.e. $\mathbf{e}_i$, using Einstein summation convention over repeated indices as:

$$\mathbf{T}=T_{ij}\mathbf{e}_i\otimes\mathbf{e}_j \qquad \text{(A.10)}$$

(Here we don't make any distinction between the covariant and contravariant base vectors. In fact in an orthonormal coordinate system they are equivalent.) With this generalization, higher order tensors can be defined as:

$$\mathcal{A}=A_{ijk\ldots lmn}\mathbf{e}_i\otimes\mathbf{e}_j\otimes\mathbf{e}_k\otimes\ldots\mathbf{e}_l\otimes\mathbf{e}_m\otimes\mathbf{e}_n \qquad \text{(A.11)}$$

Now we focus on the properties of fourth-order tensors. Fourth-order tensors have $3^4=81$ components in the three-dimensional space. The fourth order tensors are shown with math blackboard upper-case letters as $\mathbb{A}=A_{ijkl}\mathbf{e}_i\otimes\mathbf{e}_j\otimes\mathbf{e}_k\otimes\mathbf{e}_l$. Like second order tensors, the fourth order tensors can be generated using tensor products of second order tensors. There are three different tensor products between the second-order tensors. These products with two second order tensors, A and B, are defined as (Kintzel and Basar, 2006):

$$\mathbb{C}=\mathbf{A}\otimes\mathbf{B}=A_{ij}B_{kl}\mathbf{e}_i\otimes\mathbf{e}_j\otimes\mathbf{e}_k\otimes\mathbf{e}_l \qquad \text{(A.12a)}$$
$$\mathbb{D}=\mathbf{A}\odot\mathbf{B}=A_{il}B_{jk}\mathbf{e}_i\otimes\mathbf{e}_j\otimes\mathbf{e}_k\otimes\mathbf{e}_l \qquad \text{(A.12b)}$$
$$\mathbb{E}=\mathbf{A}\boxdot\mathbf{B}=A_{ik}B_{jl}\mathbf{e}_i\otimes\mathbf{e}_j\otimes\mathbf{e}_k\otimes\mathbf{e}_l \qquad \text{(A.12c)}$$

Three different identity tensors of fourth order can be introduced:

$$\mathbb{I}^{\otimes}=\mathbf{I}\otimes\mathbf{I}=\delta_{ij}\delta_{kl}\mathbf{e}_i\otimes\mathbf{e}_j\otimes\mathbf{e}_k\otimes\mathbf{e}_l \qquad \text{(A.13a)}$$
$$\mathbb{I}^{\odot}=\mathbf{I}\odot\mathbf{I}=\delta_{il}\delta_{jk}\mathbf{e}_i\otimes\mathbf{e}_j\otimes\mathbf{e}_k\otimes\mathbf{e}_l \qquad \text{(A.13b)}$$
$$\mathbb{I}^{\boxdot}=\mathbf{I}\boxdot\mathbf{I}=\delta_{ik}\delta_{jl}\mathbf{e}_i\otimes\mathbf{e}_j\otimes\mathbf{e}_k\otimes\mathbf{e}_l \qquad \text{(A.13c)}$$

where δ_{ij} represents the Dirac's delta function. Different transpose operations can be defined on fourth order tensors which for brevity we consider only two of them:

$$\mathbb{A}^T=A_{jilk}\mathbf{e}_i\otimes\mathbf{e}_j\otimes\mathbf{e}_k\otimes\mathbf{e}_l \qquad \text{(A.14a)}$$
$$\mathbb{A}^t=A_{lkji}\mathbf{e}_i\otimes\mathbf{e}_j\otimes\mathbf{e}_k\otimes\mathbf{e}_l \qquad \text{(A.14b)}$$

Hence the following transpose operations on fourth order tensor products can easily be verified:

$$(\mathbf{A}\otimes\mathbf{B})^T=\mathbf{A}^T\otimes\mathbf{B}^T \qquad \text{(A.15a)}$$

$$(\mathbf{A}\odot\mathbf{B})^T=\mathbf{B}\odot\mathbf{A} \qquad \text{(A.15b)}$$
$$(\mathbf{A}\square\mathbf{B})^T=\mathbf{B}\square\mathbf{A} \qquad \text{(A.15c)}$$
$$(\mathbf{A}\otimes\mathbf{B})^t=\mathbf{B}^T\otimes\mathbf{A}^T \qquad \text{(A.15d)}$$

$$(\mathbf{A}\odot\mathbf{B})^t=\mathbf{A}^T\odot\mathbf{B}^T \qquad \text{(A.15e)}$$
$$(\mathbf{A}\square\mathbf{B})^t=\mathbf{B}^T\square\mathbf{A}^T \qquad \text{(A.15f)}$$

A.2 Contraction

Contraction means specifying two indices and sum over these indices. Contraction of two vectors is the dot product of these vectors:

$$\mathbf{u}\cdot\mathbf{v}=u_i v_i \qquad \text{(A.16)}$$

Contraction of a second order tensor and a vector has been defined in (A.1). Simple contraction of two second order tensors is obtained with multiplying their corresponding matrices:

$$\mathbf{AB}=A_{im}B_{mj}\mathbf{e}_i\otimes\mathbf{e}_j \qquad \text{(A.17)}$$

Double contraction of two second order tensors gives a scalar and is defined as:

$$\mathbf{A:B}=tr(\mathbf{A}^T\mathbf{B})=tr(\mathbf{B}^T\mathbf{A})=\mathbf{B:A}=A_{ij}B_{ij} \qquad \text{(A.18)}$$

In fact double contraction of two second order tensors is the sum of the product of their corresponding rows. Simple contraction of a dyad and a second order tensor gives: $(\mathbf{u}\otimes\mathbf{v})\mathbf{A}=\mathbf{u}\mathbf{v}^T\mathbf{A}=\mathbf{u}(\mathbf{A}^T\mathbf{v})^T=\mathbf{u}\otimes\mathbf{A}^T\mathbf{v}$ and $\mathbf{A}(\mathbf{u}\otimes\mathbf{v})=\mathbf{A}\mathbf{u}\mathbf{v}^T=(\mathbf{A}\mathbf{u})\otimes\mathbf{v}$. Double contraction of a dyad, $\mathbf{u}\otimes\mathbf{v}$ with a second order tensor gives: $(\mathbf{u}\otimes\mathbf{v})\mathbf{:A}=tr(\mathbf{u}\mathbf{v}^T\mathbf{A}^T)=tr(\mathbf{u}(\mathbf{A}\mathbf{v})^T)=\mathbf{u}\cdot\mathbf{A}\mathbf{v}$.
Simple contraction between a fourth order tensor and a second order tensor is defined as:

$$\mathbb{C}=\mathbb{A}\mathbf{B}=A_{ijkm}B_{ml}\mathbf{e}_i\otimes\mathbf{e}_j\otimes\mathbf{e}_k\otimes\mathbf{e}_l \qquad \text{(A.19a)}$$
$$\mathbb{C}=\mathbf{B}\mathbb{A}=B_{im}A_{mjkl}\mathbf{e}_i\otimes\mathbf{e}_j\otimes\mathbf{e}_k\otimes\mathbf{e}_l \qquad \text{(A.19b)}$$

The simple contraction and tensor products give:

$$(\mathbf{A}\otimes\mathbf{B})\mathbf{C}=A_{ij}B_{km}C_{ml}\mathbf{e}_i\otimes\mathbf{e}_j\otimes\mathbf{e}_k\otimes\mathbf{e}_l=\mathbf{A}\otimes\mathbf{B}\mathbf{C} \qquad \text{(A.20a)}$$
$$\mathbf{C}(\mathbf{A}\otimes\mathbf{B})=C_{im}A_{mj}B_{kl}\mathbf{e}_i\otimes\mathbf{e}_j\otimes\mathbf{e}_k\otimes\mathbf{e}_l=\mathbf{C}\mathbf{A}\otimes\mathbf{B} \qquad \text{(A.20b)}$$
$$(\mathbf{A}\odot\mathbf{B})\mathbf{C}=A_{im}B_{jk}C_{ml}\mathbf{e}_i\otimes\mathbf{e}_j\otimes\mathbf{e}_k\otimes\mathbf{e}_l=\mathbf{A}\mathbf{C}\odot\mathbf{B} \qquad \text{(A.20a)}$$
$$\mathbf{C}(\mathbf{A}\odot\mathbf{B})=C_{im}A_{ml}B_{jk}\mathbf{e}_i\otimes\mathbf{e}_j\otimes\mathbf{e}_k\otimes\mathbf{e}_l=\mathbf{C}\mathbf{A}\odot\mathbf{B} \qquad \text{(A.20b)}$$
$$(\mathbf{A}\square\mathbf{B})\mathbf{C}=A_{ik}B_{jm}C_{ml}\mathbf{e}_i\otimes\mathbf{e}_j\otimes\mathbf{e}_k\otimes\mathbf{e}_l=\mathbf{A}\square\mathbf{B}\mathbf{C} \qquad \text{(A.20a)}$$
$$\mathbf{C}(\mathbf{A}\square\mathbf{B})=C_{im}A_{mk}B_{jl}\mathbf{e}_i\otimes\mathbf{e}_j\otimes\mathbf{e}_k\otimes\mathbf{e}_l=\mathbf{C}\mathbf{A}\square\mathbf{B} \qquad \text{(A.20b)}$$

This contraction produces another fourth order tensor. Double contraction between a fourth order tensor and a second order tensor produces another second order tensor such that:

$$\mathbf{C}=\mathbb{A}\mathbf{:B}=A_{ijkl}B_{kl}\mathbf{e}_i\otimes\mathbf{e}_j \qquad \text{(A.21a)}$$
$$\mathbf{D}=\mathbf{B}:\mathbb{A}=A_{klij}B_{kl}\mathbf{e}_i\otimes\mathbf{e}_j \qquad \text{(A.21b)}$$

Using the definition of the transpose of a fourth order tensor, equations (A.14), we can write:

$$\mathbf{D}=\mathbf{B}:\mathbb{A}=\mathbb{A}^{Tr}:\mathbf{B} \qquad \text{(A.22)}$$

It is possible to define two other double contractions that won't be considered consider in this study. Now using different fourth order tensor products, we can verify the following relations[11]:

$$(\mathbf{A}\otimes\mathbf{B}):\mathbf{C}=A_{ij}B_{kl}C_{kl}\mathbf{e}_i\otimes\mathbf{e}_j=(\mathbf{B}:\mathbf{C})\mathbf{A} \qquad \text{(A.23a)}$$
$$\mathbf{C}:(\mathbf{A}\otimes\mathbf{B})=C_{kl}A_{kl}B_{ij}\mathbf{e}_i\otimes\mathbf{e}_j=(\mathbf{C}:\mathbf{A})\mathbf{B} \qquad \text{(A.23b)}$$
$$(\mathbf{A}\odot\mathbf{B}):\mathbf{C}=A_{il}B_{jk}C_{kl}\mathbf{e}_i\otimes\mathbf{e}_j=\mathbf{A}\mathbf{C}^T\mathbf{B}^T \qquad \text{(A.23c)}$$
$$\mathbf{C}:(\mathbf{A}\odot\mathbf{B})=C_{kl}A_{kj}B_{li}\mathbf{e}_i\otimes\mathbf{e}_j=\mathbf{B}^T\mathrm{C}^T\mathrm{A} \qquad \text{(A.23d)}$$
$$(\mathbf{A}\square\mathbf{B}):\mathbf{C}=A_{ik}B_{jl}C_{kl}\mathbf{e}_i\otimes\mathbf{e}_j=\mathbf{A}\mathbf{C}\mathbf{B}^T \qquad \text{(A.23e)}$$
$$\mathbf{C}:(\mathbf{A}\square\mathbf{B})=C_{kl}A_{ki}B_{lj}\mathbf{e}_i\otimes\mathbf{e}_j=\mathbf{A}^T\mathbf{C}\mathbf{B} \qquad \text{(A.23f)}$$

Using the above equations and equation (A.18) some useful relations using the fourth order identity tensors and double contraction can be extracted as[12]:

$$\mathbb{I}^{\otimes}:\mathbf{A}=(\mathbf{I}\otimes\mathbf{I}):\mathbf{A}=(\mathbf{I}:\mathbf{A})\mathbf{I}=\mathrm{tr}(\mathbf{A})\mathbf{I} \qquad \text{(A.24a)}$$
$$\mathbb{I}^{\odot}:\mathbf{A}=(\mathbf{I}\odot\mathbf{I}):\mathbf{A}=\mathbf{A}^T \qquad \text{(A.24b)}$$
$$\mathbb{I}^{\square}:\mathbf{A}=(\mathbf{I}\square\mathbf{I}):\mathbf{A}=\mathbf{A} \qquad \text{(A.24c)}$$

Double contraction between two fourth order tensors creates another fourth order tensor and there are various contraction definitions which here one form is explained:

$$\mathbb{A}:\mathbb{B}=A_{ijmn}B_{mnkl}\,\mathbf{e}_i\otimes\mathbf{e}_j\otimes\mathbf{e}_k\otimes\mathbf{e}_l \qquad \text{(A.25)}$$

Some properties of double contraction containing different tensor products are

$$(\mathbf{A}\otimes\mathbf{B}):(\mathbf{C}\odot\mathbf{D})=A_{ij}B_{mn}C_{ml}D_{nk}\mathbf{e}_i\otimes\mathbf{e}_j\otimes\mathbf{e}_k\otimes\mathbf{e}_l=\mathrm{A}\otimes(\mathbf{D}^T\mathbf{B}^T\mathbf{C}) \qquad \text{(A.26a)}$$
$$(\mathbf{A}\otimes\mathbf{B}):(\mathbf{C}\square\mathbf{D})=A_{ij}B_{mn}C_{mk}D_{nl}\mathbf{e}_i\otimes\mathbf{e}_j\otimes\mathbf{e}_k\otimes\mathbf{e}_l=\mathbf{A}\otimes(\mathbf{C}^T\mathbf{B}\mathbf{D}) \qquad \text{(A.26b)}$$
$$(\mathbf{A}\otimes\mathbf{B}):(\mathbf{C}\otimes\mathbf{D})=A_{ij}B_{mn}C_{mn}D_{kl}\mathbf{e}_i\otimes\mathbf{e}_j\otimes\mathbf{e}_k\otimes\mathbf{e}_l=(\mathbf{B}:\mathbf{C})\mathbf{A}\otimes\mathbf{D} \qquad \text{(A.26c)}$$
$$(\mathbf{A}\odot\mathbf{B}):(\mathbf{C}\odot\mathbf{D})=A_{in}B_{jm}C_{ml}D_{nk}\mathbf{e}_i\otimes\mathbf{e}_j\otimes\mathbf{e}_k\otimes\mathbf{e}_l=\mathrm{A}\mathbf{D}\square\mathbf{B}\mathrm{C} \qquad \text{(A.26d)}$$
$$(\mathbf{A}\odot\mathbf{B}):(\mathbf{C}\square\mathbf{D})=A_{in}B_{jm}C_{mk}D_{nl}\mathbf{e}_i\otimes\mathbf{e}_j\otimes\mathbf{e}_k\otimes\mathbf{e}_l=\mathrm{A}\mathbf{D}\odot\mathbf{B}\mathrm{C} \qquad \text{(A.26e)}$$
$$(\mathbf{A}\square\mathbf{B}):(\mathbf{C}\square\mathbf{D})=A_{im}B_{jn}C_{mk}D_{nl}\mathbf{e}_i\otimes\mathbf{e}_j\otimes\mathbf{e}_k\otimes\mathbf{e}_l=\mathrm{A}\mathbf{C}\square\mathbf{B}\mathbf{D} \qquad \text{(A.26f)}$$
$$(\mathbf{A}\square\mathbf{B}):(\mathbf{C}\odot\mathbf{D})=A_{im}B_{jn}C_{ml}D_{nk}\mathbf{e}_i\otimes\mathbf{e}_j\otimes\mathbf{e}_k\otimes\mathbf{e}_l=\mathrm{A}\mathbf{C}\odot\mathbf{B}\mathbf{D} \qquad \text{(A.26g)}$$

A.3 Tensor Differentiation

Differentiating a scalar α with respect to a vector $\mathbf{a}$ gives another vector: $\partial\alpha/\partial\mathbf{a}=[\partial\alpha/\partial a_1\ \partial\alpha/\partial a_2\ \partial\alpha/\partial a_3\ ]^T$. Derivative of a scalar-valued function of a second order tensor with respect to its second order tensor gives another second order tensor and each element is the derivative of that scalar with respect to the corresponding element of the tensor:

$$\partial\alpha/\partial\mathbf{T}=\partial\alpha/\partial T_{ij}\,\mathbf{e}_i\otimes\mathbf{e}_j \qquad \text{(A.27)}$$

---

[11] Equations (5.58) and (5.61) have been extracted using the equations (A.23e), (A.23f), (A.22), (A.15c) and (A.15f). Equation (5.54) has been extracted using equations (A.23c) to (A.23f) and using the definition of a symmetric tensor: $\mathbf{A}=\mathbf{A}^T$ which we can write: $\mathbf{A}=(\mathbf{A}+\mathbf{A}^T)/2$.

[12] In the literature $\mathbb{I}$ is usually used for $\mathbb{I}^{\square}$ to be consistent with the meaning of the identity tensor as in the second order tensors.

Some important scalars are the invariants of a second order tensor.

A.3.1 First Invariant

The first invariant of a second order tensor is the trace of the tensor:

$$I_1=tr(\mathbf{T})=T_{ii} \qquad \text{(A.28)}$$

The derivative of I_1 with respect to its tensor, gives:

$$\partial I_1/\partial \mathbf{T}=\partial T_{ij}/\partial T_{ii}\mathbf{e}_i\otimes\mathbf{e}_j=\mathbf{I} \qquad \text{(A.29)}$$

The derivative of a vector valued function with respect to its argument (like deformation gradient) gives a second order tensor:

$$\partial \mathbf{a}/\partial \mathbf{b}=\partial a_i/\partial b_j\mathbf{e}_i\otimes\mathbf{e}_j \qquad \text{(A.30)}$$

Differentiation of a second order tensor function with respect to another second order tensor function gives a fourth order tensor. There are different definitions. Here we present the common definition:

$$\partial \mathbf{A}/\partial \mathbf{B}=\partial A_{ij}/\partial B_{kl}\mathbf{e}_i\otimes\mathbf{e}_j\otimes\mathbf{e}_k\otimes\mathbf{e}_l \qquad \text{(A.31)}$$

We should be aware that different formulations could be used in the literature.
Now we present some important relations. We have:

$$\partial(\alpha\mathbf{A})/\partial\mathbf{C}=\partial(\alpha A_{ij})/\partial C_{kl}\mathbf{e}_i\otimes\mathbf{e}_j\otimes\mathbf{e}_k\otimes\mathbf{e}_l=[(\partial\alpha/\partial C_{kl})A_{ij}+\alpha\partial A_{ij}/\partial C_{kl}]\mathbf{e}_i\otimes\mathbf{e}_j\otimes\mathbf{e}_k\otimes\mathbf{e}_l=$$
$$\mathbf{A}\otimes\partial\alpha/\partial\mathbf{C}+\alpha\partial\mathbf{A}/\partial\mathbf{C} \qquad \text{(A.32)}$$

The derivative of the double contraction of two second order tensors based on equation (A.21b) gives:

$$\partial(\mathbf{A}:\mathbf{B})/\partial\mathbf{C}=\partial(A_{ij}B_{ij})/\partial C_{kl}\mathbf{e}_k\otimes\mathbf{e}_l=\mathbf{A}:\partial\mathbf{B}/\partial\mathbf{C}+\mathbf{B}:\partial\mathbf{A}/\partial\mathbf{C} \qquad \text{(A.33)}$$

The derivative of a second order tensor and its transpose with respect to itself, using equations (A.13), gives:

$$\partial\mathbf{A}/\partial\mathbf{A}=\partial A_{ij}/\partial A_{kl}\mathbf{e}_i\otimes\mathbf{e}_j\otimes\mathbf{e}_k\otimes\mathbf{e}_l=\delta_{ik}\delta_{jl}\mathbf{e}_i\otimes\mathbf{e}_j\otimes\mathbf{e}_k\otimes\mathbf{e}_l=\mathbf{I}\square\mathbf{I}=\mathbb{I}^{\square} \qquad \text{(A.34a)}$$
$$\partial\mathbf{A}^T/\partial\mathbf{A}=\partial\mathbf{A}/\partial\mathbf{A}^T=\partial A_{ij}/\partial A_{lk}\mathbf{e}_i\otimes\mathbf{e}_j\otimes\mathbf{e}_k\otimes\mathbf{e}_l=\delta_{il}\delta_{jk}\mathbf{e}_i\otimes\mathbf{e}_j\otimes\mathbf{e}_k\otimes\mathbf{e}_l=\mathbf{I}\odot\mathbf{I}=\mathbb{I}^{\odot} \qquad \text{(A.34b)}$$

Using $\mathbf{A}\mathbf{A}^{-1}=\mathbf{I}$, $\mathbf{A}^2=\mathbf{A}\mathbf{A}$, $\mathbf{A}^3=\mathbf{A}^2\mathbf{A}$ the derivative of $\mathbf{A}^{-1}$ and $\mathbf{A}^2$ with respect to $\mathbf{A}$ can be written as:

$$\partial\mathbf{A}^{-1}/\partial\mathbf{A}=-\mathbf{A}^{-1}\square\mathbf{A}^{-T} \qquad \text{(A.35a)}$$
$$\partial\mathbf{A}^2/\partial\mathbf{A}=\mathbf{I}\square\mathbf{A}^T+\mathbf{A}\square\mathbf{I} \qquad \text{(A.35b)}$$
$$\partial\mathbf{A}^3/\partial\mathbf{A}=\mathbf{I}\square(\mathbf{A}^2)^T+\mathbf{A}\square\mathbf{A}^T+\mathbf{A}^2\square\mathbf{I} \qquad \text{(A.35c)}$$

It should be taken care of the fact that the derivative with respect to a second order tensor has been taken in a general case. However, for symmetric and skew-symmetric tensors, the above relations should be written considering this fact that these tensors have only six independent variables. In the following the case of symmetric tensors are explained. The skew-symmetric case can be extracted in

the same way. First we should write the chain rules for the derivative with respect to a second order tensor. From equations (A.27) and (A.21b) for a scalar the chain rule can be written:

$$\partial\alpha/\partial\mathbf{T}=(\partial\alpha/\partial S_{kl})(\partial S_{kl}/\partial T_{ij})\mathbf{e}_i\otimes\mathbf{e}_j=(\partial\alpha/\partial\mathbf{S}):(\partial\mathbf{S}/\partial\mathbf{T}) \qquad \text{(A.36)}$$

And for a second order tensor using (A.25) and (A.31) we have:

$$\partial\mathbf{A}/\partial\mathbf{B}=(\partial A_{ij}/\partial C_{mn})(\partial C_{mn}/\partial B_{kl})\mathbf{e}_i\otimes\mathbf{e}_j\otimes\mathbf{e}_k\otimes\mathbf{e}_l=(\partial\mathbf{A}/\partial\mathbf{C}):(\partial\mathbf{C}/\partial\mathbf{B}) \qquad \text{(A.37)}$$

For symmetric second order tensors we can assume that the corresponding function is a function of the symmetric part of the tensor, i.e. $(\mathbf{A}+\mathbf{A}^T)/2$. Then using chain rules and equations (A.34) we can write:

$$\partial\mathbf{A}/\partial\mathbf{B}=(\partial\mathbf{A}((\mathbf{B}+\mathbf{B}^T)/2)/\partial((\mathbf{B}+\mathbf{B}^T)/2)):(\partial((\mathbf{B}+\mathbf{B}^T)/2)/\partial\mathbf{B})=(\partial\mathbf{A}/\partial\mathbf{B}):(\partial((\mathbf{B}+\mathbf{B}^T)/2)/\partial\mathbf{B})=$$
$$(\partial\mathbf{A}/\partial\mathbf{B}):(\mathbf{I}\square\mathbf{I}+\mathbf{I}\odot\mathbf{I})/2=(\partial\mathbf{A}/\partial\mathbf{B}):(\mathbb{I}^{\square}+\mathbb{I}^{\odot})/2 \qquad \text{(A.37)}$$

So we can use the results for general case and then using double contraction with the operator $(\mathbb{I}^{\square}+\mathbb{I}^{\odot})/2$ we can write the equations for the symmetric case. In fact the left double contraction of this operator on a second order tensor creates the symmetric part of that tensor (see equations (A.24b) and (A.24c)). And its left double contraction on a symmetric tensor acts as an identity tensor. Now with this introduction we write the equations (A.34) and (A.35) for a symmetric second order tensor (using equations (A.26)):

$$\partial\mathbf{A}/\partial\mathbf{A}=(\mathbf{I}\square\mathbf{I}):(\mathbf{I}\square\mathbf{I}+\mathbf{I}\odot\mathbf{I})/2=(\mathbf{I}\square\mathbf{I}+\mathbf{I}\odot\mathbf{I})/2 \qquad \text{(A.38a)}$$
$$\partial\mathbf{A}^T/\partial\mathbf{A}=\partial\mathbf{A}/\partial\mathbf{A}^T=(\mathbf{I}\odot\mathbf{I}):(\mathbf{I}\square\mathbf{I}+\mathbf{I}\odot\mathbf{I})/2=(\mathbf{I}\odot\mathbf{I}+\mathbf{I}\square\mathbf{I})/2=\partial\mathbf{A}/\partial\mathbf{A} \qquad \text{(A.38b)}$$
$$\partial\mathbf{A}^{-1}/\partial\mathbf{A}=(-\mathbf{A}^{-1}\square\mathbf{A}^{-1}):(\mathbf{I}\square\mathbf{I}+\mathbf{I}\odot\mathbf{I})/2=-(\mathbf{A}^{-1}\square\mathbf{A}^{-1}+\mathbf{A}^{-1}\odot\mathbf{A}^{-1})/2 \qquad \text{(A.38c)}^{13}$$

Following the same analogy for a skew-symmetric tensor the corresponding operator becomes: $(\mathbf{I}\square\mathbf{I}-\mathbf{I}\odot\mathbf{I})/2$.

A.3.2 Second Invariant

The second invariant of a second order tensor is defined as:

$$I_2=[(tr\mathbf{T})^2-tr(\mathbf{T}^2)]/2 \qquad \text{(A.39)}$$

The derivative of I_2 with respect to $\mathbf{T}$ using the chain rule and equations (A.29), (A.23) and (A.35b) becomes:

$$\partial I_2/\partial\mathbf{T}=(tr\mathbf{T})\mathbf{I}-\mathbf{I}:(\mathbf{I}\square\mathbf{A}^T+\mathbf{A}\square\mathbf{I})/2=(tr\mathbf{T})\mathbf{I}-\mathbf{A}^T \qquad \text{(A.40a)}$$

For a symmetric tensor this derivative becomes:

$$\partial I_2/\partial\mathbf{T}=((tr\mathbf{T})\mathbf{I}-\mathbf{A}):(\mathbf{I}\square\mathbf{I}+\mathbf{I}\odot\mathbf{I})/2=(tr\mathbf{T})\mathbf{I}-\mathbf{A} \qquad \text{(A.40b)}$$

---

[13] Equation (5.83) in the text corresponds to this equation.

A.3.3 Third Invariant

The third invariant of a second order tensor is its determinant ($I_3=det(\mathbf{A})$). According to Cayley-Hamilton equation, each square matrix satisfies its own characteristic equation (characteristic equation of a matrix is obtained with: $\det(\mathbf{A}-\lambda\mathbf{I})=0$). Hence for a second order tensor we can write:

$$\mathbf{A}^3-I_1\mathbf{A}^2+I_2\mathbf{A}-I_3\mathbf{I}=\mathbf{0} \qquad \text{(A.41)}$$

From equation (A.41) using the trace definition we can write:

$$I_3=[tr(\mathbf{A}^3)-I_1tr(\mathbf{A}^2)+I_2tr(\mathbf{A})]/3=[tr(\mathbf{A}^3)-3tr(\mathbf{A})\ tr(\mathbf{A}^2)/2+tr(\mathbf{A})^3/2]/3 \qquad \text{(A.42)}$$

Taking the derivative of I_3 with respect to **A** and using the chain rules and equations (A.35), (A.40) and (A.41) we obtain:

$$\partial I_3/\partial\mathbf{A}=(\mathbf{A}^2)^T-I_1\mathbf{A}^T+I_2\mathbf{I}=I_3\mathbf{A}^{-T} \qquad \text{(A.43)}$$

Appendix B: Virtual Damping and Virtual Inertia Matrices

In chapter 6 the linearization of the fiber stretch, its velocity and its acceleration along the muscle fibers' direction ended with relations that listed hereafter:

$$D\lambda.\mathbf{u} = \lambda\left[\mathbf{a}\cdot\nabla^{s}\mathbf{u}\mathbf{a}\right] \qquad (6.37)$$

$$D\dot{\lambda}.\mathbf{u} = \dot{\lambda}\left[\mathbf{a}\cdot\nabla^{s}\mathbf{u}\mathbf{a}\right] + \lambda\left[\mathbf{L}\mathbf{a}\cdot\mathbf{grad}(\mathbf{u})\mathbf{a} - 2(\mathbf{a}\cdot\mathbf{L}\mathbf{a})(\mathbf{a}\cdot\nabla^{s}\mathbf{u}\mathbf{a}) + \mathbf{a}\cdot\nabla^{s}\dot{\mathbf{u}}\mathbf{a}\right] \qquad (6.39)$$

$$\begin{aligned} D\ddot{\lambda}.\mathbf{u} = {} & \ddot{\lambda}\left[\mathbf{a}\cdot\nabla^{s}\mathbf{u}\mathbf{a}\right] + 2\dot{\lambda}\left[\mathbf{L}\mathbf{a}\cdot\mathbf{grad}(\mathbf{u})\mathbf{a} - 2(\mathbf{a}\cdot\mathbf{L}\mathbf{a})(\mathbf{a}\cdot\nabla^{s}\mathbf{u}\mathbf{a})\right] + \\ & \lambda\begin{bmatrix} \mathbf{a}\cdot\nabla^{s}\ddot{\mathbf{u}}\mathbf{a} + 2\mathbf{L}\mathbf{a}.\mathbf{grad}(\dot{\mathbf{u}})\mathbf{a} - 4(\mathbf{a}\cdot\mathbf{L}\mathbf{a})(\mathbf{a}\cdot\nabla^{s}\dot{\mathbf{u}}\mathbf{a}) + \mathbf{A}\mathbf{a}\cdot\mathbf{grad}(\mathbf{u})\mathbf{a} - 4(\mathbf{a}.\mathbf{L}\mathbf{a})(\mathbf{L}\mathbf{a}\cdot\mathbf{grad}(\mathbf{u})\mathbf{a}) + \\ (\mathbf{a}\cdot\nabla^{s}\mathbf{u}\mathbf{a})(8(\mathbf{a}.\mathbf{L}\mathbf{a})^{2} - 2\mathbf{a}\cdot\mathbf{L}^{T}\mathbf{L}\mathbf{a} - 2\mathbf{a}\cdot\mathbf{A}\mathbf{a}) \end{bmatrix} \end{aligned} \qquad (6.40)$$

After the linearization of the Cauchy stress along the muscle fibers' direction, we have:

$$D\boldsymbol{\sigma}_{active}.\mathbf{u} = \frac{\partial f}{\partial\lambda}D\lambda.\mathbf{u} + \frac{\partial f}{\partial\dot{\lambda}}D\dot{\lambda}.\mathbf{u} + \frac{\partial f}{\partial\ddot{\lambda}}D\ddot{\lambda}.\mathbf{u} \qquad (6.82)$$

For velocity and acceleration we consider only equations (6.39) and (6.40). Within the framework of Flory's (1961) deformation gradient decomposition (Equation (5.64)) should be written with respect to $\bar{\lambda} = J^{1/3}\lambda$. The result of this modification will produce:

$$\begin{aligned} D\dot{\bar{\lambda}}.\mathbf{u} = {} & \dot{\bar{\lambda}}\left[-\frac{1}{3}tr(\mathbf{gradu}) + \mathbf{a}\cdot\nabla^{s}\mathbf{u}\mathbf{a}\right] + \\ & \bar{\lambda}\left[-\frac{1}{3}tr(\mathbf{grad}\dot{\mathbf{u}}) + \frac{1}{3}tr(\mathbf{grad}(\mathbf{u})\mathbf{L}) + \mathbf{L}\mathbf{a}\cdot\mathbf{grad}(\mathbf{u})\mathbf{a} - 2(\mathbf{a}\cdot\mathbf{L}\mathbf{a})(\mathbf{a}\cdot\nabla^{s}\mathbf{u}\mathbf{a}) + \mathbf{a}\cdot\nabla^{s}\dot{\mathbf{u}}\mathbf{a}\right] \end{aligned} \qquad (B.1)$$

$$\begin{aligned} D\ddot{\bar{\lambda}}.\mathbf{u} = {} & \ddot{\bar{\lambda}}\left[-\frac{1}{3}tr(\mathbf{gradu}) + \mathbf{a}\cdot\nabla^{s}\mathbf{u}\mathbf{a}\right] + 2\dot{\bar{\lambda}}\begin{bmatrix} -\frac{1}{3}tr(\mathbf{gradu}) + \frac{1}{3}tr(\mathbf{graduL}) + \mathbf{L}\mathbf{a}\cdot\mathbf{grad}(\mathbf{u})\mathbf{a} \\ -2(\mathbf{a}\cdot\mathbf{L}\mathbf{a})(\mathbf{a}\cdot\nabla^{s}\mathbf{u}\mathbf{a}) + (\mathbf{a}\cdot\nabla^{s}\dot{\mathbf{u}}\mathbf{a}) \end{bmatrix} + \\ & \bar{\lambda}\begin{bmatrix} -\frac{1}{3}tr(\mathbf{grad}\ddot{\mathbf{u}}) + \frac{2}{3}tr(\mathbf{grad}\dot{\mathbf{u}}\mathbf{L}) - \frac{2}{3}tr(\mathbf{graduL}^{2}) + \frac{1}{3}tr(\mathbf{graduA}) + 2\mathbf{L}\mathbf{a}.\mathbf{grad}(\dot{\mathbf{u}})\mathbf{a} \\ -4(\mathbf{a}\cdot\mathbf{L}\mathbf{a})(\mathbf{a}\cdot\nabla^{s}\dot{\mathbf{u}}\mathbf{a}) + \mathbf{A}\mathbf{a}\cdot\mathbf{grad}(\mathbf{u})\mathbf{a} - 4(\mathbf{a}.\mathbf{L}\mathbf{a})(\mathbf{L}\mathbf{a}\cdot\mathbf{grad}(\mathbf{u})\mathbf{a}) \\ +(\mathbf{a}\cdot\nabla^{s}\mathbf{u}\mathbf{a})(8(\mathbf{a}.\mathbf{L}\mathbf{a})^{2} - 2\mathbf{a}\cdot\mathbf{L}^{T}\mathbf{L}\mathbf{a} - 2\mathbf{a}\cdot\mathbf{A}\mathbf{a}) + \mathbf{a}\cdot\nabla^{s}\ddot{\mathbf{u}}\mathbf{a} \end{bmatrix} \end{aligned} \qquad (B.2)$$

Each term in equation (6.82) should be multiplied by $\left(\mathbf{a}\otimes\mathbf{a}-\frac{\mathbf{I}}{3}\right)$, and then the result in the weak form (6.45) should be double contracted with the symmetric part of the gradient of weight which is: $\nabla^s\mathbf{w}$. The final result becomes:

$$\left(D\boldsymbol{\sigma}_{active}.\mathbf{u}\right)\left(\mathbf{a}\otimes\mathbf{a}-\frac{\mathbf{I}}{3}\right):\nabla^s\mathbf{w} \qquad \text{(B.3)}$$

The terms in equations (B.1) and (B.2), which contain **u,** participate in the tangent stiffness matrix ($\mathbf{K}_T$) (see equation (6.83)), the terms in $\dot{\mathbf{u}}$ generate the virtual damping matrix ($\mathbf{C}_{vir}$) and the terms containing $\ddot{\mathbf{u}}$ produce the virtual inertia matrix ($\mathbf{M}_{vir}$). (It should be noted that in linearization relations **u** shows increment $\Delta\mathbf{u}$.)

In the following the method used to derive these matrices is explained. There are some terms which contain trace operator. One of these terms is explained here and in analogy this method can be used for the rest. Showing $\mathbf{Q}=\mathbf{a}\otimes\mathbf{a}$, for $tr(\mathbf{grad(u)L}$ we have:

$$tr(\mathbf{grad(u)L}\left[\left(\mathbf{a}\otimes\mathbf{a}-\frac{\mathbf{I}}{3}\right):\nabla^s\mathbf{w}\right]=\left(\mathbf{L}^T:\mathbf{grad(u)}\right)\left[\left(\mathbf{a}\otimes\mathbf{a}-\frac{\mathbf{I}}{3}\right):\mathbf{grad(w)}\right]=$$
$$\sum_I\sum_K\mathbf{w}_I^{\mathbf{T}}\left[\left(\mathbf{Q}\nabla_{\mathbf{x}}N_I\otimes\mathbf{L}^T\nabla_{\mathbf{x}}N_K\right)-\frac{1}{3}\left(\nabla_{\mathbf{x}}N_I\otimes\mathbf{L}^T\nabla_{\mathbf{x}}N_K\right)\right]\mathbf{u}_K \qquad \text{(B.4)}$$

The summation is over the number of nodes in element. Each term in summation contributes to the (I,K) position in the corresponding matrices for an element. $\nabla_{\mathbf{x}}N_I$ and $\nabla_{\mathbf{x}}N_K$ are gradients of the shape function with respect to current position. Assembling all terms will give the corresponding matrices.

The terms like $\mathbf{a}\cdot\nabla^s\mathbf{ua}$ result in:

$$\left(\mathbf{a}\cdot\nabla^s\mathbf{ua}\right)\left[\left(\mathbf{a}\otimes\mathbf{a}-\frac{\mathbf{I}}{3}\right):\nabla^s\mathbf{w}\right]=\left(\mathbf{a}\otimes\mathbf{a}:\mathbf{grad(u)}\right)\left[\left(\mathbf{a}\otimes\mathbf{a}-\frac{\mathbf{I}}{3}\right):\mathbf{grad(w)}\right]=$$
$$\sum_I\sum_K\mathbf{w}_I^{\mathbf{T}}\left[\left(\mathbf{Q}\nabla_{\mathbf{x}}N_I\otimes\mathbf{Q}\nabla_{\mathbf{x}}N_K\right)-\frac{1}{3}\left(\nabla_{\mathbf{x}}N_I\otimes\mathbf{Q}\nabla_{\mathbf{x}}N_K\right)\right]\mathbf{u}_K \qquad \text{(B.5)}$$

Writing: $\mathbf{La}\cdot\mathbf{grad(u)a}=\left(\mathbf{La}\otimes\mathbf{a}\right):\mathbf{grad(u)}$ and $\mathbf{Aa}\cdot\mathbf{grad(u)a}=\left(\mathbf{Aa}\otimes\mathbf{a}\right):\mathbf{grad(u)}$, the result in (B.5) can be used easily to find their corresponding matrices.

In the above equations the quantities **a**, **L**, **A**, $\dot{\lambda}$, and $\ddot{\lambda}$ are known.

References

[1] C. Abry and L. Boë. “laws” for lips. *Speech Communication*, 5:97–104, 1986.

[2] C. Abry, L.J. Boë, P. Corsi, R. Descout, M. Gentil, and P. Graillot. Labialité et phonétique. In *Publications de l’Université des Langues et Lettres de Grenoble*. Université des Langues et Lettres de Grenoble, 1980.

[3] A.A. Ahmed and D.M. Wolpert. Transfer of dynamic learning across postures. *Journal of Neurophysiology*, 102:2816–2824, 2009.

[4] Z. Ambadar, J.W. Schooler, and J.F. Cohn. Deciphering the enigmatic face. *Psychological Science*, 16(5):403–410, 2005.

[5] ANSYS. *Theory Reference Manual, Release 11*. ANSYS Inc., 2007.

[6] L. Apostol, P. Perrier, and G. Bailly. A model of acoustic interspeaker variability based on the concept of formant-cavity affiliation. *The Journal of the Acoustical Society of America*, 115:337–351, 2004.

[7] International Phonetic Association. *Handbook of the International Phonetic Association: A Guide to the Use of the International Phonetic Alphabet*. Cambridge University Press, 1999.

[8] P. Badin, F. Elisei, G. Bailly, and Y. Tarabalka. An audiovisual talking head for augmented speech generation: Models and animations based on a real speakerâ€™s articulatory data. In Francisco Perales and Robert Fisher, editors, *Articulated Motion and Deformable Objects*, volume 5098 of *Lecture Notes in Computer Science*, pages 132–143. Springer Berlin / Heidelberg, 2008. 10.1007/978-3-540-70517-8_14.

[9] Klaus-Jurgen Bathe. *Finite Element Procedures*. Prentice Hall, Inc., 1996.

[10] L. Beldie, B. Walker, Y. Lu, S. Richmond, and J. Middleton. Finite element modelling of maxillofacial surgery and facial expressions – a preliminary study. *The International Journal of Medical Robotics and Computer Assisted Surgery*, 6:422–430, 2010.

[11] T. Belytschko, W.K. Liu, and B. Moran. *Finite Elements for Nonlinear Continua & Structures*. John Wiley and Sons, 2000.

[12] D.J. Bennett. Torques generated at the human elbow joint in response to constant position errors imposed during voluntary movements. *Experimental Brain Research*, 95:488–498, 1993.

[13] P.L. Blanton, N.L. Biggs, and R.C. Perkins. Electromyographic analysis of the buccinator muscle. *Journal of Dental Research*, 49:389–394, 1970.

[14] S.S. Blemker, P.M. Pinsky, and S.L. Delpa. A 3d model of muscle reveals the causes of nonuniform strains in the biceps brachii. *Journal of Biomechanics*, 38:657–665, 2005.

[15] R. Bottinelli, M. Canepari, M.A. Pellegrino, and C. Reggiani. Force-velocity properties of human skeletal muscle fibres: myosin heavy chain isoform and temperature dependence. *Journal of Physiology*, 495(2):573–586, 1996.

[16] I.E. Brown, E.J. Cheng, and G.E. Loeb. Measured and modeled properties of mammalian skeletal muscle. ii. the effects of stimulus frequency on force-length and force-velocity relationships. *Journal of Muscle Research and Cell Mobility*, 20:627–643, 1999.

[17] I.E. Brown, S.H. Scott, and G.E. Loeb. Mechanics of feline soleus: Ii. design and validation of a mathematical model. *Journai of Muscle Research and Cell Motility*, 17:219–232, 1996.

[18] S. Buchaillard, P. Perrier, and Y. Payan. A 3d biomechanical vocal tract model to study speech production control: How to take into account the gravity? In *Proceedings of the 7th International Seminar on Speech Production*, pages 403–410, 2006.

[19] S. Buchaillard, P. Perrier, and Y. Payan. A biomechanical model of cardinal vowel production: Muscle activations and the impact of gravity on tongue positioning. *The Journal of the Acoustical Society of America*, 126(4):2033–2051, 2009.

[20] E. Burdet, R. Osu, D.W. Franklin, T.E. Milner, and M. Kawato. The central nervous system stabilizes unstable dynamics by learning optimal impedance. *Nature*, 414:446–449, 2001.

[21] M. Chabanas, V. Luboz, and Y. Payan. Patient specific finite element model of the face soft tissues for computer-assisted maxillofacial surgery. *Medical Image Analysis*, 7:131–151, 2003.

[22] E.J. Cheng, I.E. Brown, and G.E. Loeb. Virtual muscle: a computational approach to understanding the effects of muscle properties on motor control. *Journal of Neuroscience Methods*, 101:117–130, 2000.

[23] J.C. Criscione, A.S. Douglas, and W.C. Hunter. Physically based strain invariant set for materials exhibiting transversely isotropic behavior. *Journal of the Mechanics and Physics of Solids*, 49:871–879, 2001.

[24] J.C. Criscione and W.C. Hunter. Kinematics and elasticity framework for materials with two fiber families. *Continuum Mech. Thermodyn. (2003) 15: 613–628*, 15:613–628, 2003.

[25] P.R. Davidson and D.M. Wolpert. Motor learning and prediction in a variable environment. *Current Opinion in Neurobiology*, 13:1–6, 2003.

[26] J. Delaire, J. R. Fève, J.P. Chateau, D. Courtay, and J.F. Tulasne. Anatomie et physiologie des muscles et du frein médian de la lèvre supérieure premiers résultats de l'électromyographie sélective. *Revue de Stomatologie*, 2:93–103, 1977.

[27] M. Epstein and W. Herzog. Aspects of skeletal muscle modelling. *Phil. Trans. R. Soc. Lond. B*, 358:1445–1452, 2003.

[28] A.G. Feldman. Functional tuning of the nervous system with control of movement or maintenance of a steady posture - ii. controllable parameters of the muscles. *Biophysics 11:565-578*, 11:565–578, 1966.

[29] A.G. Feldman. Once more on the equilibrium-point hypothesis (lambda model) for motor control. *Journal of Motor Behavior*, 18(1):17–54, 1986.

[30] A.G. Feldman, S.V. Adamovich, D.J. Ostry, and J.R. Flanagan. The origin of electromyograms - explanations based on the equilibrium point hypothesis. In J.M. Winters and S.L-Y. Woo, editors, *Multiple Muscle Systems: Biomechanics and Movement Organization*, chapter 12. Springer-Verlag, 1990.

[31] P.J. Flory. Thermodynamic relations for high elastic materials. *Transactions of the Faraday Society*, 57:829–838, 1961.

[32] C. A. Fowler. Coarticulation and theories of extrinsic timing control. *Journal of Phonetics*, 8:113–133, 1980.

[33] S. Fuchs, P. Perrier, and M. Hartinger. A critical evaluation of gestural stiffness estimations in speech production based on a linear second-order model. *Journal of Speech Language & Hearing Research*, 54:1067-1076, 2011.

[34] Y.C. Fung. *Biomechanics: Mechanical properties of living tissues*. Sprinegr-Verlag New-York, Inc., 1993.

[35] Y.C. Fung and P. Tong. *Classical And Computational Solid Mechanics*. World Scientific Publishing Co. Pte. Ltd., 2001.

[36] A.W.J. Gielen, C.W.J. Oomens, P.H.M. Bovendeerd, T. Arts, and J.D. Janssen. A finite element approach for skeletal muscle using a distributed moment model of contraction. *Computer Methods in Biomechanics and Biomedical Engineering*, 3:231–244, 2000.

[37] E. Gladilin, A. Ivanov, and V. Roginsky. A framework for biomechanical simulation of cranio-maxillofacial surgery interventions. In S. Cotin and D. Metaxas, editors, *Proc of International Symposium on Medical Simulation, ISMS 2004*, pages 287–294, 2004.

[38] H. Gomi and M. Kawato. Equilibrium-point control hypothesis examined by measured arm stiffness during multijoint movement. *Science*, 272:117–120, 1996.

[39] H. Gomi, J. Nozoe, J. Dang, and K. Honda. A physiologically based model of perioral dynamics for various lip deformations in speech articulation. In J. Harrington and M. Tabain, editors, *Speech Production: Models, Phonetic Processes and Techniques*, pages 119–134. Psychology Press, 2006.

[40] J.M. Gérard, J. Ohayon, V. Luboz, P. Perrier, and Y. Payan. Non-linear elastic properties of the lingual and facial tissues assessed by indentation technique, application to the biomechanics of speech production. *Medical Engineering & Physics*, 27:884–892, 2005.

[41] P.L. Gribble and D.J. Ostry. Origins of the power law relation between movement velocity and curvature: Modeling the effects of muscle mechanics and limb dynamics. *Journal of Neurophysiology*, 76(5):2853–2860, 1996.

[42] P.L. Gribble and D.J. Ostry. Independent coactivation of shoulder and elbow muscles. *Experimental Brain Research*, 123:355–360, 1998.

[43] P.L. Gribble, D.J. Ostry, V. Sanguineti, and R. Laboissiere. Are complex control signals required for human arm movement? *Journal Of Neurophysiology*, 79:1409–1424, 1998.

[44] E.S. Grood, R.E. Mates, and H. Falsetti. A model of cardiac muscle dynamics. *Circulation Research*, 35:184–196, 1974.

[45] M.E. Gurtin. *An Introduction to Continuum Mechanics*. Academic Press, 1981.

[46] Wolfgang Happak, Ji Liu, Georg Burggasser, Amanda Flowers, Helmut Gruber, and Gerhard Freilinger. Human facial muscles: Dimensions, motor endplate distribution, and presence of muscle fibers with multiple motor endplates. *The Anatomical Record*, 249(2):276–284, 1997.

[47] W.J. Hardcastle. *Physiology of Speech Production*. Academic Press, London., 1976.

[48] S. Hartmann and P. Neff. Polyconvexity of generalized polynomial-type hyperelastic strain energy functions for near-incompressibility. *International Journal of Solids and Structures*, 40:2767–2791, 2003.

[49] S. Hedenstierna, P. Halldin, and K. Brolin. Evaluation of a combination of continuum and truss finite elements in a model of passive and active muscle tissue. *Computer Methods in Biomechanics and Biomedical Engineering*, 11(6):627–639, 2008.

[50] A.V. Hill. The heat of shortening and the dynamic constants of muscle. *Proceedings of the Royal Society B: Biological Sciences*, 126(126):136–195, 1938.

[51] M.R. Hinder and T.E. Milner. The case for an internal dynamics model versus equilibrium point control in human movement. *Journal of Physiology*, 549(3):953–963, 2003.

[52] J.A. Hoffer and S. Andreassen. Factors affecting the gain of the stretch reflex and soleus stiffness in premammillary cats. *The Society for Neuroscience Abstracts*, 4:935, 1978.

[53] G.A. Holzapfel. *Nonlinear Solid Mechanics: A Continuum Approach for Engineering*. John Wiley & Sons, Chichester, 2000.

[54] G.A. Holzapfel. Structural and numerical models for the (visco)elastic response of arterial walls with residual stresses. In G.A. Holzapfel and R.W. Ogden, editors, *Biomechanics of Soft Tissue in Cardiovascular Systems*, pages 109–184. Springer: Wien, New York, 2003.

[55] G.A. Holzapfel and T.C. Gasser. A viscoelastic model for fiber-reinforced composites at finite strains: Continuum basis, computational aspects and applications. *Computer Methods in Applied Mechanics and Engineering*, 190:4379–4430, 2001.

[56] S. Hooper. Motor control: The importance of stiffness. *Current Biology*, 16:283–285, 2006.

[57] J.C. Houk and W.Z. Rymer. Neural control of muscle length and tension. In V.B. Brooks, editor, *Handbook of physiology-nervous system*, volume II, pages 257–323. American Physiological Society, Bethesda, MD, 1981.

[58] J.D. Humphrey and F.C.P. Yin. Constitutive relations and finite deformations of passive cardiac tissue ii: Stress analysis in the left ventricle. *Circulation Research*, 65:805–817, 1989.

[59] A.F. Huxley and R. Niedergerke. Structural changes in muscle during contraction. interference microscopy of living muscle fibers. *Nature*, 173(173):971–973, 1954.

[60] H.E. Huxley and J. Hansonn. Changes in the cross-striations of muscle during contraction and stretch and their structural interpretation. *Nature*, 173(173):973–976, 1954.

[61] M. Itskov. *Tensor Algebra and Tensor Analysis for Engineers: With Applications to Continuum Mechanics*. Springer-Verlag Berlin Heidelberg, 2009.

[62] V.G. Ivancevic and T.T. Ivancevic. *Human-like biomechanics: a unified mathematical approach to human- Biomechanics and Humanoid Robotics*. Springer, 2006.

[63] T. Johansson, P. Meier, and R. Blickhan. A finite-element model for the mechanical analysis of skeletal muscles. *Journal of Theoretical Biology*, 206:131–149, 2000.

[64] E.R. Kandel, J.H. Schwartz, and T.M. Jessell. *Principles of Neural Science*. McGraw-Hill, New York, 4th edition, 2000.

[65] B. Katz. The relation between force and speed in muscular contraction. *Journal of Physioloy*, 96:45–64, 1939.

[66] M. Kawato, Y. Maeda, Y. Uno, and R. Suzuki. Trajectory formation of arm movement by cascade neural network model based on minimum torque-change criterion. *Biological Cybernetics*, 62:275–288, 1990.

[67] J.L. Kelly and C.C. Lochbaum. Speech synthesis. In *Proceedings of the Fourth Int. Congress on Acoustics, Copenhagen, Denmark '62*, pages 1–4, 1962.

[68] J.A.S. Kelso. *Dynamic Patterns: the self-organization of brain and behavior.* MIT Press, Cambridge, Massachusetts, 1995.

[69] J.A.S. Kelso, P. Holt, K.G. andRubin, and P.N. Kugler. Patterns of human interlimb coordination emerge from the properties of non-linear oscillatory processes: Theory and data. *Journal of Motor Behavior*, 13:226–261, 1981.

[70] W.M. Kier and J.L. Van Leeuwen. A kinematic analysis of tentacle extension in the squid loligo pealei. *The Journal of Experimental Biology*, 200:41–53, 1997.

[71] K. Kim and H. Gomi. Model-based investigation of control and dynamics in human articulatory mortion. *Journal of System, Design and Dynamics*, 1(3):558–569, 2007.

[72] O. Kintzel. Fourth-order tensors – tensor differentiation with applications to continuum mechanics. part ii: Tensor analysis on manifolds. *Zeitschrift für Angewandte Mathematik und Mechanik (ZAMM: Z. Angew. Math. Mech.) (Applied Mathematics and Mechanics)*, 86(4):312–334, 2006.

[73] O. Kintzel and Y. Basar. Fourth-order tensors – tensor differentiation with applications to continuum mechanics. part i: Classical tensor analysis. *Zeitschrift für Angewandte Mathematik und Mechanik (ZAMM) (Applied Mathematics and Mechanics)*, 86(4):291–311, 2006.

[74] B.G. Lapatki, R. Oostenveld, J.P. Van Dijk, I.E. Jonas, M.J. Zwarts, and D.F. Stegeman. Topographical characteristics of motor units of the lower facial musculature revealed by means of high-density surface emg. *Journal Neurophysiology*, 95:342–354, 2006.

[75] L.P. Lebedev and M.J. Cloud. *Tensor Analysis*. World Scientific Publishing Co. Pte. Ltd., 2003.

[76] Y. Lee, D. Terzopoulos, and K. Waters. Realistic modeling for facial animation. In S.G. Mair and R. Cook, editors, *SIGGRAPH'95*, pages 55–62. ACM Press, New York, 1995.

[77] J.L. Van Leeuwen and W.M. Kier. Functional design of tentacles in squid: Linking sarcomere ultrastructure to gross morphological dynamics. *Philosophical Transactions: Biological Sciences*, 352(1353):551–571, 1997.

[78] R.R. Lemos, E. Epstein, W. Herzog, and B. Wyvill. A framework for structured modeling of skeletal muscle. *Computer Methods in Biomechanics and Biomedical Engineering*, 7(6):305–317, 2004.

[79] M. Van Loocke, C.G. Lyons, and C. Simms. The three-dimensional mechanical properties of skeletal muscle: experiments and modelling. In P.J. Prendergast and P.E. McHugh, editors, *Topics in Bio-Mechanical Engineering*, chapter VIII, pages 216–234. Trinity Centre for Bioengineering & National Centre for Biomedical Engineering Science, 2004.

[80] M. Van Loocke, C.G. Lyons, and C.K. Simms. A validated model of passive muscle in compression. *Journal of Biomechanics*, 39:2999–3009, 2006.

[81] M. Van Loocke, C.G. Lyons, and C.K. Simms. Viscoelastic properties of passive skeletal muscle in compression: Stress-relaxation behaviour and constitutive modelling. *Journal of Biomechanics*, 41:1555–1566, 2008.

[82] J.C. Lucero and K.G. Munhall. A model of facial biomechanics for speech production. *The Journal of the Acoustical Society of America*, 106(5):2834–2842, 1999.

[83] J.C. Lucero, S.T.R. Maciel, D.A. Johns, and K. G. Munhall. Empirical modeling of human face kinematics during speech using motion clustering. *The Journal of the Acoustical Society of America*, 118(1):405–409, 2005.

[84] A. Marchal. *From Speech Physiology to Linguistic Phonetics*. ISTE Ltd and John Wiley & Sons, Inc., 2009.

[85] E.N. Marieb and K. Hoehn. *Human Anatomy and Physiology*. Pearson/Benjamin Cummings, CA, 2007.

[86] J.A.C. Martins, M.P.M. Patob, and E.B. Pires. A finite element model of skeletal muscles. *Virtual and Physical Prototyping*, 1(3):159–170, 2006.

[87] J.A.C. Martins, E.B. Pires, R. Salvado, and P.B. Dinis. A numerical model of passive and active behavior of skeletal muscles. *Computer Methods in Applied Mechanical Engineering*, 151:419–433, 1998.

[88] A.J. McComas. Oro-facial muscles: internal structure, function and ageing. *Gerodontology*, 15(1):3–14, 1998.

[89] H. McGurk and J. MacDonald. Hearing lips and seeing voices. *Nature*, 264(5588):746–748, December 1976.

[90] T.A. McMahon. *Muscles, Reflexes, and Locomotion*. Princeton University Press, 1984.

[91] C. Miehe. Numerical computation of algorithmic (consistent) tangent moduli in large-strain computational inelasticity. *Computer Methods in Applied Mechanics and Engineering*, 134:223–240, 1996.

[92] T.S. Miles and M.A. Nordstrom. Fatigue of jaw muscles and speech mechanisms. *Advances in Experimental Medicine and Biology*, 384:415–426, 1995.

[93] T.E. Milner. Adaptation to destabilizing dynamics by means of muscle cocontraction. *Experimental Brain Research*, 143:406–416, 2002.

[94] T.E. Milner and C. Cloutier. Damping of the wrist joint during voluntary movement. *Experimental Brain Research*, 122:309–317, 1998.

[95] T.E. Milner and D.W. Franklin. Impedance control and internal model use during the initial stage of adaptation to novel dynamics in humans. *Journal of Physiology*, 567.2:651–664, 2005.

[96] M. Mooney. A theory of large elastic deformation. *Journal of Applied Physics*, 11(9):582–592, 1940.

[97] P. Morasso. Spatial control of arm movements. *Experimental Brain Research*, 42:223–227, 1981.

[98] K.G. Munhall and E. Vatikiotis-Bateson. The moving face during speech communication. In R. Campbell, B. Dodd, and D. Burnham, editors, *Hearing By Eye II : Advances in the Psychology of Speechreading and Auditory-visual Speech*, chapter 6, pages 123–142. Taylor & Francis Routledge, 1998.

[99] S. Murtada, M. Kroon, and G.A. Holzapfel. A calcium-driven mechanochemical model for prediction of force generation in smooth muscle. *Biomechanics and Modeling in Mechanobiology*, 9:749–762, 2010.

[100] S. Murtada, M. Kroon, and G.A. Holzapfel. Modeling the dispersion effects of contractile fibers in smooth muscles. *Journal of the Mechanics and Physics of Solids*, 58:2065–2082, 2010.

[101] M.A. Nazari, P. Perrier, M. Chabanas, and Y. Payan. Simulation of dynamic orofacial movements using a constitutive law varying with muscle activation. *Computer Methods in Biomechanics and Biomedical Engineering*, 13(4):469–482, 2010.

[102] M.A. Nazari, P. Perrier, M. Chabanas, and Y. Payan. Shaping by stiffening: A modeling study for lips. *Motor Control*, 15:141–168, 2011.

[103] V. Ng Thow Hing and E. Fiume. Application-specific muscle representations. In W. Sturzlinger and M. McCool, editors, *Proc. of Gr. Inter*, pages 107–115, 2002.

[104] C.W.J. Oomens, M. Maenhout, C.H. Van Oijen, M.R. Drost, and F.P. Baaijens. Finite element modelling of contracting skeletal muscle. *Philosophical Transactions of RoyalSociety, London B*, 358(1437):1453–1460, 2003.

[105] D. O'Shaughnessy. A study of french vowel and consonant durations. *Journal of Phonetics*, 9:385–406, 1981.

[106] R. Osu, N. Kamimura, H. Iwasaki, E. Nakano, C.M. Harris, Y. Wada, and M. Kawato. Optimal impedance control for task achievement in the presence of signal-dependent noise. *Journal of Neurophysiology*, 92:1199–1215, 2004.

[107] Y. Payan and P. Perrier. Synthesis of v-v sequences with a 2d biomechanical tongue model controlled by the equilibrium point hypothesis. *Speech Communication*, 22:185–205, 1997.

[108] P. Perrier, H. Lœvenbruck, and Y. Payan. Control of tongue movements in speech: The equilibrium point hypothesis perspective. *Journal of Phonetics*, 24:53–75, 1996.

[109] P. Perrier, Y. Payan, M. Zandipour, and J. Perkell. Influences of tongue biomechanics on speech movements during the production of velar stop consonants: A modeling study. *The Journal of the Acoustical Society of America*, 114(3):1582–1599, 2003.

[110] J.E. Pessa, V.P. Zadoo, K.A.J. Earl, C.H. Yuan, J. Aydelotte, and J.R. Garza. Variability of the midfacial muscles: Analysis of 50 hemifacial cadaver dissections. *Plastic & Reconstructive Surgery*, 102(6):1888–1893, 1998.

[111] J.E. Pessa, V.P. Zadoo, P.A. Garza, K.A.J. Earl, C.H. Yuan, A.I. Dewitt, and J.R. Garza. Double or bifid zygomaticus major muscle. *Clinical Anatomy*, 11:310–313, 1998.

[112] M. Pitermann and K.G. Munhall. An inverse dynamics approach to face animation. *The Journal of the Acoustical Society of America*, 110(3):1570–1580, 2001.

[113] J.N. Reddy. *Energy Principles and Variational Methods in Applied Mechanics*. John Wiley & Sons, Inc., 2002.

[114] R.S. Rivlin. Large elastic deformations of isotropic materials. iv. further developments of the general theory. *Philosophical Transactions of the Royal Society of London. Series A, Mathematical and Physical Sciences*, 241(835):379–397, 1948.

[115] R.Laboissière, D.J. Ostry, and A.G. Feldman. The control of multi-muscle systems: human jaw and hyoid movements. *Bilogical Cybernetics Biol. Cybern.*, 74:373–384, 1996.

[116] O. Rohrle and A.J. Pullan. Three-dimensional finite element modelling of muscle forces during mastication. *Journal of Biomechanics*, 40(15):3363–3372, 2007.

[117] E. Saltzman. Task dynamic coordination of the speech articulators: A preliminary model. In H. Heuer and C. Fromm, editors, *Experimental Brain Research Series 15*, pages 129–144. Springer-Verlag, New York, 1986.

[118] C. Savariaux, P. Perrier, J.P. Orliaguet, and J.L. Schwartz. Compensation strategies for the perturbation of french [u] using a lip tube. ii. perceptual analysis. *The Journal of the Acoustical Society of America*, 106(1):381–393, 1999.

[119] K.L. Schmidt and J.F. Cohn. Human facial expressions as adaptations: Evolutionary questions in facial expression research. *American Journal of Physical Anthropology*, 44:3–24, 2001.

[120] C.Y. Scovil and J.L. Ronsky. Sensitivity of a hill-based muscle model to perturbations in model parameters. *Journal of Biomechanics*, 39:2055–2063, 2006.

[121] R. Shadmehr and M. Arbib. A mathematical analysis of the force-stiffness characteristics of muscles in control of a single joint system. *Bilogical Cybernetics*, 66:463–477, 1992.

[122] R. Shadmehr and Z.M.K. Moussavi. Spatial generalization from learning dynamics of reaching movements. *Journal of Neuroscience*, 20(20):7807–7815, 2000.

[123] S. Shaiman, S.G. Adams, and M.D.Z. Kimelman. Velocity profiles of lip protrusion across changes in speaking rate. *Journal of Speech, Language, and Hearing Research*, 40:144–158, 1997.

[124] M.B. Shapiro and R.V. Kenyon. Control variables in mechanical muscle models: A mini-review and a new model. *Motor Control*, 4:329–349, 2000.

[125] D.M. Shiller, R. Laboissière, and D.J. Ostry. The relationship between jaw stiffness and kinematic variability in speech. *Journal of Neurophysiology*, 88:2329–2340, 2002.

[126] T. Siebert, C. Rode, W. Herzog, O. Till, and R. Blickhan. Nonlinearities make a difference: comparison of two common hill-type models with real muscle. *Bilogical Cybernetics*, 98:133–143, 2008.

[127] E. Sifakis, I. Neverov, and R. Fedkiw. Automatic determination of facial muscle activations from sparse motion capture marker data. In *ACM Transactions on Graphics (SIGGRAPH Proceedings)*, volume 24, pages 417–425, 2005.

[128] E. Sifakis, A. Selle, A. Robinson-Mosher, and R. Fedkiw. Simulating speech with a physics-based facial muscle model. In M.P. Cani and J. O'Brien, editors, *Eurographics/ ACM SIGGRAPH Symposium on Computer Animation*, 2006.

[129] J.C. Simo and T.J.R. Hughes. *Computational Inelasticity*. Springer-Verlag, New York, 1998.

[130] J.C. Simo and R.L. Taylor. Penalty function formulations for incompressible nonlinear elastostatics. *Computer Methods in Applied Mechanics and Engineering*, 35:107–118, 1982.

[131] A.J.M. Spencer. *Continuum Theory of the Mechanics of Fibre-Reinforced Composites*. Springer-Verlag, New York, 1984.

[132] S. Standring, editor. *Gray's Anatomy: The Anatomical Basis of Clinical Practice*. Elsevier Ltd., 39th edition, 2005.

[133] P. Stål, P.-O. Eriksson, A. Eriksson, and L.-E. Thornell. Enzyme-histochemical and morphological characteristics of muscle fibre types in the human buccinator and orbicularis oris. *Archives of Oral Biology*, 35(6):449 – 458, 1990.

[134] B. H. Story. A parametric model of the vocal tract area function for vowel and consonant simulation. *The Journal of the Acoustical Society of America*, 117:3231–3254, 2005.

[135] W. Sun, E.L. Chaikof, and M.E. Levenston. Numerical approximation of tangent moduli for finite element implementations of nonlinear hyperelastic material models. *Journal of biomechanical engineering*, 130(6):061003–1–061003–7, 2008.

[136] M. Suzuki, D.M. Shiller, P.L. Gribble, and D. J. Ostry. Relationship between cocontraction, movement kinematics and phasic muscle activity in single-joint arm movement. *Experimental Brain Research*, 140:171–181, 2001.

[137] C.Y. Tang, G. Zhang, and C.P. Tsui. A 3d skeletal muscle model coupled witha ctive contrac tion of muscle fibres and hyperelastic behaviour. *Journal of Biomechanics*, 42:856–872, 2009.

[138] J. Teran, E. Sifakis, Blemker. S., V. Ng Thow Hing, C. Lau, and R. Fedkiw. Creating and simulating skeletal muscle from the visible human data set. *IEEE Transactions on Visualization and Computer Graphics (IEEE TVCG)*, 11:317–328, 2005.

[139] P. Tracqui and J. Ohayon. Transmission of mechanical stresses within the cytoskeleton of adherent cells: a theoretical analysis based on a multi-component model. *Acta Biotheoretica*, 52:323–341, 2004.

[140] C.A. Truesdell and W. Noll. *The Non-linear Field Theories of Mechanics*. Springer-Verlag, Berlin, 2004.

[141] K. Washizu. *Variational Methods in Elasticity and Plasticity (Monographs in Aeronautics & Astronautics)*. Pergamon Press, 1975.

[142] J.A. Weiss and J.C. Gardiner. Computational modeling of ligament mechanics. *Critical Reviews in Biomedical Engineering*, 29(4):1–70, 2001.

[143] J.A. Weiss, B.N. Maker, and S. Govindjee. Finite element implementation of incompressible, transversely isotropic hyperelasticity. *Computer Methods in Applied Mechanical Engineering*, 135:107–128, 1996.

[144] R. Wilhelms-Tricarico. Physiological modeling of speech production: Methods for modeling soft-tissue articulators. *Journal of the Acoustical Society of America*, 97(5):3085–3098, 1995.

[145] J.M. Winters. Hill-based muscle models: A systems engineering perspective. In J.M. Winters and S.L-Y. Woo, editors, *Multiple Muscle Systems: Biomechanics and Movement Organization*, chapter 5. Springer-Verlag, 1990.

[146] J.M. Winters and L. Stark. Analysis of fundamental human movement patterns through the use of in-depth antagonistic muscle models. *IEEE TRANSACTIONS ON BIOMEDICAL ENGINEERING*, BME-32(10):826–839, 1985.

[147] J.M. Winters and L. Stark. Muscle models: What is gained and what is lost by varying model complexity. *Bilogical Cybernetics*, 55:403–420, 1987.

[148] S.P. Wise and R. Shadmehr. Motor control.(2002). In V.S. Ramachandran, editor, *Encyclopedia of the Human Brain*, volume 3, pages 137–157. Academic Press: San Diego, CA, 2002.

[149] J. Wong, E. T. Wilson, N. Malfait, and P. L. Gribble. Limb stiffness is modulated with spatial accuracy requirements during movement in the absence of destabilizing forces. *Journal of Neurophysiology*, 101:1542–1549, 2009.

[150] P. Wriggers. *Nonlinear Finite Element Methods*. Springer-Verlag Berlin Heidelberg, 2008.

[151] C.A. Yucesoy, B.H.F.J.M. Koopman, P.A. Huijing, and H.J. Grootenboera. Three-dimensional finite element modeling of skeletal muscle using a two-domain approach: linked fiber-matrix mesh model. *Journal of Biomechanics*, 32:1253–1262, 2002.

[152] G.I. Zahalak. Modeling muscle mechanics (and energetics). In J.M. Winters and S.L-Y. Woo, editors, *Multiple Muscle Systems: Biomechanics and Movement Organization*, chapter 1. Springer-Verlag, 1990.

[153] F.E. Zajac. Muscle and tendon: Properties, models, scaling, and application to biomechanics and motor control. *Critical Reviews in Biomedica/ Engineering*, 17(4):359–411, 1989.

Abstract

To address motor control issues in speech production a 3D finite element model of the face has been constructed. This model is made of a mesh that consists of hexahedral and wedge elements. The mesh has three distinctive layers and is symmetrical about the mid-sagittal plane. Face muscles are anatomically represented in the mesh as subsets of contiguous elements. The elements of the mesh have elastic properties described by an isotropic nearly incompressible hyperelastic constitutive law. In order to study the global effects of muscles on facial mimics and lips gestures, and more specifically on speech gestures like protrusion and rounding, a simple linear muscle model has been first designed. The impact on facial gestures of stiffness changes in soft tissues is studied. Stiffening in soft tissues is indeed concomitant with muscle activation due to stress stiffening effect. This effect is accounted for in the muscle model through a variation of the hyperelastic constitutive law. Special attention is also devoted to the production of protruded and rounded lips which are required for the production of rounded vowels particularly in French. It is shown that stiffening helps the achievement of an accurate protrusion/rounding gesture thanks to the existence of a saturation effect in the relation between the muscle activations and the acoustically relevant geometrical characteristics of the lips.
The result shows the importance of the dynamical properties of the articulators in the achievement of speech production gestures. Having been incited to improve the modeling of the main source of the force in speech movements, namely the muscles, a more realistic muscle model including a new constitutive law corresponding to a transversely isotropic nearly incompressible hyperelastic material and a Hill-type muscle model is designed in the ANSYS® finite element software thanks to the USERMAT programming facilities of this software. To account for a full Hill-type muscle model a force-velocity characteristic is then included in the new muscle element, thanks to the USERELEM facilities of ANSYS®. The implementation of this force-velocity characteristic introduces a damping effect on muscle movement due to a decrease of the muscle force when muscle compression velocity increases.
The designed structure of the muscle element is general enough to enable studying other muscle models. Hence, Feldman's muscle model, which has been extensively used in former modelling works at Gipsa-lab, is implemented. In a bid to integrate the Feldman's model in a finite element structure a distributed formulation of this model has been proposed. The Hill-type and the Feldman-type muscle element are included in the face model to replace the first simple linear muscle model. The first simulations of lips protrusion/rounding gesture show realistic results. A comparison of the results obtained with the Hill-type model with those obtained with the Feldman's model is also conducted which shows that the final face shapes are very similar to those of these two models.

Keywords: speech production; muscle biomechanics; Feldman's muscle model; large deformation elasticity; nonlinear finite element method; motor control; biomechanical face modeling

Résumé

Un modèle tridimensionnel du visage a été élaboré, dans la perspective de contribuer à l'étude de questions importantes sur le contrôle moteur de la production de la parole. Ce modèle est construit sur un maillage constitué d'éléments hexahédraux et de clavettes, qui comporte 3 couches distinctes et est symétrique par rapport au plan medio-sagittal. Les muscles faciaux sont représentés dans le maillage par un sous-ensemble d'éléments contigus. Les propriétés élastiques des éléments du maillage sont décrites par une loi de comportement de type isotrope quasi incompressible et hyperélastique. Dans une première phase de ce travail, pour étudier les conséquences globales de l'activation des muscles oro-faciaux sur les mimiques faciales et les gestes labiaux, et plus particulièrement sur les gestes labiaux en parole, un modèle linéaire de muscle a été élaboré. L'influence des variations de la raideur des tissus mous sur les gestes faciaux a été étudiée. En effet, l'activation des muscles entraîne un raidissement des tissus mous musculaires concernés. Cet effet est pris en compte dans le modèle de muscle par un changement de la loi de comportement hyperélastique avec l'activation musculaire. Une attention particulière a été portée dans cette étude à la production du geste de protrusion/arrondissement des lèvres qui est un geste fondamental dans la production des voyelles arrondies, en particulier en Français. Nous montrons que le raidissement des tissus mous musculaires facilite la production précise de ce geste grâce à l'existence d'un effet de saturation dans la relation entre les activations musculaires et les paramètres géométriques des lèvres qui sont pertinents acoustiquement.
Ce résultat souligne l'importance des propriétés dynamiques des articulateurs dans la production des gestes de la parole, et il nous a incités à améliorer encore la modélisation de la source principale de force en production de la parole, c'est-à-dire les muscles. C'est pourquoi, un modèle de muscles plus réaliste a été élaboré qui se fonde sur une loi de comportement transversalement isotrope quasi incompressible et hyperélastique et sur un modèle de muscle de type Hill. Ce modèle a été implémenté dans le logiciel éléments finis ANSYS® grâce à sa fonction de programmation USERMAT. La prise en compte supplémentaire d'une loi caractéristique force-vitesse a permis la modélisation complète d'un modèle de muscle de type Hill. Ceci a été fait sous ANSYS® grâce à sa fonction de programmation USERELEM. Cette loi caractéristique force-vitesse introduit un effet d'amortissement dans le mouvement du muscle du fait d'une atténuation croissante de la force musculaire lorsque la vitesse de compression du muscle augmente.
Ce nouvel élément de type muscle a été conçu de manière telle qu'il est possible d'implémenter d'autres modèles de muscles que le modèle de type Hill. C'est pourquoi nous avons aussi implémenté le modèle de Feldman, qui a été utilisé de manière importante à Gipsa-lab dans les dernières années. L'intégration du modèle de Feldman dans une structure à éléments finis a nécessité une reformulation de façon à le rendre compatible avec une modélisation distribuée. Les modèles de Hill et de Feldman ont ensuite été incorporés dans le modèle de visage pour remplacer le modèle linéaire initial. Dans ces conditions les premières simulations du geste de protrusion/arrondissement labial ont donné des résultats réalistes. Finalement une comparaison des résultats obtenus avec le modèle de Hill avec ceux qui génère le modèle de Feldman montrent que les formes labiales finales sont très similaires pour les deux modèles.